



UNIVERSITÀ DEGLI STUDI DI MILANO

FACOLTÀ DI SCIENZE DEL FARMACO

Department of Pharmaceutical Sciences

PhD Course in Pharmaceutical Sciences

XXIX Cycle

**Novel functional hydrophilic polymers and hydrogels for  
microanalytical systems**

Tutor: Dr. Marcella Chiari

Co-Tutor: Prof. Marina Carini

Coordinator: Prof. Marco De Amici

**Chiara Finetti**

**R10496-R29**

Academic year 2015/2016

# List of Contents

<b>List of abbreviations</b>	vi
<b>OBJECTIVES AND OVERVIEW</b>	viii
<b>PART A</b>	
<b>CHAPTER 1   INTRODUCTION TO NANOTECHNOLOGY AND NANOPARTICLES</b>	1
1.1 WHAT IS A NANOPARTICLE?	2
1.2 NANOPARTICLES PREPARATION	5
1.3 NANOPARTICLES CHARACTERIZATION	6
1.4 BIBLIOGRAPHY	10
<b>CHAPTER 2   NANOPARTICLES SURFACE MODIFICATION</b>	13
2.1 PHASE TRANSFER AND BIOCONJUGATION WITH POLYMERS	14
2.2 CLICK CHEMISTRY AND “CLICKED” NANOPARTICLES	18
2.3 BIBLIOGRAPHY	23
<b>CHAPTER 3   NANOPARTICLES IN BIOSENSING</b>	27
3.1 MICROARRAY TECHNOLOGY: OVERVIEW	27
3.2 POLYMER COATING FOR MICROARRAY SUPPORTS	31
3.3 SILICON SURFACES FOR MICROARRAY	33
3.4 MICROARRAY DETECTION METHODS	35
3.4.1 Label-based detection methods	35
3.4.1.1 Chromogenic labels	35
3.4.1.2. Chemiluminescent label	36
3.4.1.3. Fluorescent label	36
3.4.2 Label-free detection methods	37
3.5 BIBLIOGRAPHY	39

<b>CHAPTER 4   INNOVATIVE STRATEGIES FOR NANOPARTICLES SURFACE MODIFICATION WITH FUNCTIONAL COPOLYMERS: ONE-POT PHASE TRANSFER AND BIOCONJUGATION OF QUANTUM DOTS</b>	42
4.1 N,N –DIMETHYLACRYLAMIDE (DMA) BASED COPOLYMERS	44
4.2 ONE-POT PHASE TRANSFER AND BIOCONJUGATION OF QDs USING POLY (DMA-NAS-MAPS)	47
4.2.1 MATERIALS AND METHODS	49
4.2.1.1 <i>Reagents</i>	49
4.2.1.2 <i>Synthesis of poly(DMA-NAS-MAPS) and poly(DMA-PMA-MAPS)</i>	49
4.2.1.3 <i>QDs phase transfer and bioconjugation</i>	50
4.2.1.4 <i>QDs characterization</i>	50
4.2.1.5 <i>Bioassay: coating procedure and microarray experiments</i>	52
4.2.2 RESULTS AND DISCUSSION	54
4.2.2.1 <i>One-Pot phase transfer procedure</i>	54
4.2.2.2 <i>Characterization of coated and functionalized QDs</i>	55
4.2.2.3 <i>Application of functionalized QDs in a microarray experiment</i>	63
4.2.3 CONCLUSIONS	64
4.3 BIBLIOGRAPHY	65
<b>CHAPTER 5   USE OF QUANTUM DOTS AS MASS AND FLUORESCENCE LABELS IN A HIGH-PERFORMING MICROARRAY PLATFORM</b>	67
5.1 LABEL FREE DETECTION: ADVANTAGES AND LIMITATIONS	67
5.2 MATERIALS AND METHODS	71
5.2.1 Reagents	71
5.2.2 IRIS Detection Setup	71
5.2.3 $\beta$ -Lactoglobulin assay	72
5.3 RESULTS AND DISCUSSION	74
5.3.1 Interferometric Reflectance Imaging Sensor (IRIS)	74
5.3.2 QDs as mass tag and fluorescent labels in b-Lactoglobulin assay	77
5.3.3 Calculation of QDs monolayer	81
5.4 CONCLUSIONS	82
5.5 BIBLIOGRAPHY	83

<b>CHAPTER 6   CLICK-CHEMISTRY FUNCTIONALIZATION OF POLYMER-COATED NANOPARTICLES</b>	<b>85</b>
6.1 MATERIALS AND METHODS	87
6.1.1 Reagents	87
6.1.2 Synthesis of Silica Gold Nanoparticles	87
6.1.3 Nanoparticles Coating	88
6.1.4 Antibody derivatization	88
6.1.5 Functionalization of Gold Nanoparticles	89
6.1.6 Nanoparticles characterization	89
6.1.7 Bioassay: microarray experiments	90
6.2 RESULTS AND DISCUSSION	92
6.2.1 Coating of Silica Gold Nanoparticles	92
6.2.2 Characterization of coated and functionalized AuNPs	95
6.2.3 Application of antibody-labeled AuNPs in a novel digital platform: Single Particle Interferometric Reflectance Imaging System (SP-IRIS)	99
6.3 CONCLUSIONS	104
6.4 BIBLIOGRAPHY	105

## **PART B**

<b>CHAPTER 7   INTRODUCTION TO DNA GEL ELECTROPHORESIS</b>	<b>107</b>
7.1 DNA SEPARATION MECHANISM	110
7.2 WHAT IS A HYDROGEL?	111
7.3 GENERAL CHARACTERISTICS OF COMMON GEL MATRICES	112
7.3.1 Agarose gels	112
7.3.2 Polyacrylamide gels	113
7.4 ELECTROPHORESIS COMPONENTS	115
7.4.1 DNA detection: fluorescent dyes	115
7.4.2 Electrophoretic buffer system	116
7.4.3 Voltage/current applied	117
7.4.4 Loading buffer	118
7.5 FROM SLAB GEL TO CAPILLARY ELECTROPHORESIS	118
7.6 FROM CAPILLARY ELECTROPHORESIS TO MICROCHIP BASED-GEL ELECTROPHORESIS	122
7.7 BIBLIOGRAPHY	125

<b>CHAPTER 8   DEVELOPMENT OF A NOVEL SIEVING MATRIX THROUGH <i>CLICK CHEMISTRY</i> FOR HIGH PERFORMANCE DNA ELECTROPHORESIS</b>	128
<b>8.1 MATERIALS AND METHODS</b>	134
8.1.1 Reagents	134
8.1.2 Synthesis of poly(DMA-PMA-MAPS) ,poly(DMA-NAS-MAPS) and Copoly Alkyne	134
8.1.3 Click gel preparation and polymerization conditions	135
8.1.4 ScreenTape store conditions	136
8.1.5 DNA Ladder preparation	136
8.1.6 Preparation of DNA sample	136
8.1.7 FT-IR spectra analysis	137
8.1.8 Fluorescence assay	137
8.1.9 Swelling test	137
8.1.10 Electrophoresis conditions and data analysis	138
<b>8.2 RESULTS AND DISCUSSION</b>	139
8.2.1 Development of a novel hydrogel with preformed polymers through click chemistry	139
8.2.2 Optimization of the dye in the gel matrix and the key role of THPTA	142
8.2.3 Comparison between “in-gel stain” and “prestain” approaches	145
8.2.4 Development of a “clickable” polymer through a post modification approach	147
8.2.5 Comparison between click hydrogel and acrylamide-based gel	151
8.2.6 Click hydrogel formulations with different polymer concentrations	154
8.2.7 Shelf-life studies and dye stability	157
8.2.8 Characterization of click gel: swelling test	168
<b>8.3 CONCLUSIONS</b>	170
<b>8.4 BIBLOGRAPHY</b>	171
<b>CHAPTER 9   FINAL CONCLUSIONS AND FUTURE PERSPECTIVES</b>	173
<b>APPENDIX A</b>	174

## **List of abbreviations**

**NPs:** nanoparticles

**AuNPs:** gold nanoparticles

**QDs:** Quantum Dots

**PEG:** poly(ethylene glycol)

**TOPO:** trioctylphosphine oxide

**TPP:** triphenylphosphine oxide

**DDT:** dodecanethiol

**TOAB:** tetraoctylammonium bromide

**OA:** oleic acid

**DLS:** Dynamic Light Scattering

**NTA:** Nanoparticle Tracking Analysis

**TEM:** Transmission Electron Microscopy

**HDA:** hexadecylamine

**EDC:** 1-Ethyl-3-(3-dimethylaminopropyl)carbodiimide

**NHS:** N-hydroxysuccinimid

**CuAAC:** Cu(I)-Catalyzed Huisgen Azide–Alkyne 1,3-Dipolar Cycloaddition Reaction

**THPTA:** tris(3-hydroxypropyltriazolylmethyl)amine

**AAC:** ascorbic acid

**DMA:** *N,N*-Dimethylacrylamide

**NAS:** N-acryloyloxy succinimide

**MAPS:** 3-(Trimethoxysilyl)propyl methacrylate

**SPR:** Surface Plasmon Resonance

**IRIS:** Interferometric Reflectance Imaging Sensor

**SP-IRIS:** Single Particle Interferometric Reflectance Imaging Sensor

**LOD:** Limit of detection

**DPI:** Dual Polarization Interferometry

**TEMED:** *N,N* Tetramethylethylenediamine

**EB:** Ethidium Bromide (EB)

**SG:** SYBR Green I

**dsDNA:** double stranded DNA

**ssDNA:** single stranded DNA

**CE:** capillary electrophoresis

**PAA:** linear polyacrylamide

**PVA:** poly(vinylalcohol)

**DMSO:** dimethylsulfoxide

**TPAOH:** tetrapentylammonium hydroxide

## OBJECTIVES AND OVERVIEW

This thesis focuses on the use of hydrophilic polymers for bioanalytical applications, including several microanalytical techniques encompassing nanotechnology, microarray technology and DNA gel electrophoresis.

The dissertation is divided in two parts, which share the employment of dimethylacrylamide-based copolymers, developed at the laboratory of Analytical Microsystems of the Institute of Chemistry for Molecular Recognition (National Research Council of Italy) where the thesis has been carried out.

What follows is a brief overview of the dissertation with the main objectives of each part.

**PART A** introduces a novel approach for surface modification of quantum dots and gold nanoparticles, based on physi-/chemisorption of two different functional dimethylacrylamide copolymers. The main goals of this part are the development of innovative strategies for the functionalization of these two kinds of nanoparticles and demonstrate their application in highly sensitive immunoassays based on microarray technology.

**Chapter 1** provides a general overview on the use of nanoparticles in nanotechnology and presents the methods of synthesis employed to tailor their characteristics. It also discusses how the behaviour of nanoparticles is determined by a number of properties, such as size, surface area and charge, fluorescence that require careful characterization.

**Chapter 2** provides an overview of the methods, most commonly used, to modify the surface of nanoparticles through polymeric coatings. It also introduces *Click-chemistry* reactions that have gained increasing interest in nanoparticles functionalization.

**Chapter 3** discusses the pivotal role of nanoparticles to enhance detection sensitivity and selectivity in biosensing, specifically in microarray technology, one of the most important techniques to perform high-throughput, multiplexed biorecognition analysis. The principles of microarray technology are presented, and the importance of polymeric coatings for an efficient and homogeneous microarray support derivatization are discussed. Furthermore, Chapter 3 gives an overview of the different detection modalities used in microarray technology, and analyses pros and cons of label and label-free detection techniques.

**Chapter 4** presents an innovative, robust and user-friendly procedure to transfer QDs from organic solvents into an aqueous solution that employs the functional copolymer poly(DMA-NAS-MAPS). A one-pot process for phase transfer and functionalization of QDs with biomolecules is presented in this chapter.

**Chapter 5** illustrates the use of coated semiconductor nanocrystals (QDs) as protein mass labels and their use to enhance sensitivity in a novel interferometric detection platform, called Interferometric Reflectance Imaging Sensor (IRIS). Furthermore, we discuss the versatility of coated QDs in dual, fluorescent and mass, detection modality and demonstrate that they overcome the limitations of traditional fluorophores.

**Chapter 6** describes a simple and robust procedure to stabilize and functionalize Gold Nanoparticles through an efficient *click chemistry* approach that employs poly(DMA-PMA-MAPS), an evolution of the aforementioned polymer poly(DMA-NAS-MAPS). The Chapter discusses the application of the functionalized gold nanoparticles as biomolecule tags in a novel sensing platform, called Single Particle Interferometric Reflectance Imaging System (SP-IRIS) that provides digital detection of single molecules, immunocaptured on the surface of a silicon/silicon oxide layered chip.

**PART B** of the dissertation presents the results of an activity, conducted in collaboration with the company Agilent Technology (UK), aimed at improving the

performance provided by the commercial acrylamide-based gel matrices. The main goal is thus the development of an innovative gel sieving matrix for high performance DNA electrophoresis.

We introduce in the following Chapters, 7 and 8, a new hydrogel obtained by cross-linking an alkyne modified polymer with an azide one, exploiting a copper catalysed click chemistry reaction. The alkyne functionalized polymer is based on poly(dimethylacrylamide) and it was obtained by a post-polymerization modification approach from the parent copolymer poly(DMA-NAS-MAPS), extensively used in the first part of this dissertation. The azide polymer is a polyethyleneglycol terminated with azide groups at both ends, and is commercially available.

**Chapter 7** introduces the principles of DNA electrophoresis and discusses the characteristics of the commonly used gel matrices. It also provides a comparison between standard slab gel electrophoresis and Capillary Electrophoresis and discusses the integration of microchip-electrophoresis in lab-on-a-chip applications.

**Chapter 8** describes the synthesis and characterization of the novel hydrogel and its application in DNA electrophoresis. The chapter illustrates how using *click chemistry* it is possible to form a hydrogel that does not require UV-initiated radical polymerization. It also discusses the numerous advantages of the new gelation procedure that allows to add fluorescent dyes in the gel before cross-linking. At the same time, it clarifies that the new gel does not involve the use of toxic and unstable monomers, such as acrylamide, that are replaced by nontoxic preformed polymers. Furthermore, the chapter shows comparison of the performance of the novel gel with standard commercial polyacrylamide gel and demonstrates remarkable improvements in the DNA separation performance in the new hydrogel. A considerable part of this Chapter is devoted to the optimization of the characteristics of the new hydrogel, in particular to the extension of its *shelf-life*, an important parameter in view of its industrial application.

# *Part A*



# **Chapter 1**

## **INTRODUCTION TO NANOTECHNOLOGY AND NANOPARTICLES**

Nanotechnology is a field of science and engineering based on understanding and knowledge of the properties of materials, whose dimensions are in the order of 100 nm or less<sup>1</sup>. The physicist Richard Feynman, Nobel Prize for Physics in 1965, was the first who forecasted the enormous potential of nanotechnology. Feynman, in a famous conference, said a phrase passed into history: "There is plenty of room at the bottom", i.e.: there is a lot of space down there. "Bottom" refers to the size of atoms and to the fact that the matter can be manipulated atom by atom, molecule by molecule, aggregate of molecules by aggregate of molecules. He realized that the key for future technology and advancement would have been scaling down to nanolevel and starting from the bottom<sup>2</sup>. Nowadays, some experts consider nanotechnology a proper revolution: "Every nation in the world is looking at nanotechnology as a future technology that will drive its competitive position in the world economy"<sup>3</sup>. In fact, in recent years, several industrial sectors like biotechnology<sup>4</sup>, electronics<sup>5</sup>, magnetic and optical systems<sup>6</sup> as well as a set of scientific disciplines such as physics, chemistry, especially the chemistry of the materials and disciplines related to engineering such as robotics, chemical engineering, mechanical engineering, have embraced nanotechnology. This impact of nanotechnology in a number of human activities is due to the unique, size-dependent, properties of nanomaterials. In fact, at the nanometer scale, the behavior and characteristics of matter change dramatically, exhibiting different and extraordinary physical properties. Nanotechnology realizes objects with properties that matter "in bulk" does not possess. In particular, the size and the high surface-to-volume ratio are the properties that make the nanomaterials excellent candidates for many applications. As mentioned above, a vast field of interest concerns the application of nanotechnology in biology and medicine. Nanomaterials are promising in the field of: biosensing, study of molecular interactions (see *Chapter*

3), human diagnostics as well as in therapeutic applications, regenerative medicine and tissue engineering.

## 1.1 WHAT IS A NANOPARTICLE?

Nanoparticles (NPs), which range in size from 1-100 nm, are the most fundamental component in the fabrication of a nanostructure and, for this reason they have a central role for any significant advances in nanomaterial based applications. They are attractive multifunctional materials because they represent effectively a bridge between bulk materials and atomic or molecular structures. As a matter of fact, NPs employment has opened up the door to several original applications in many different fields including engineering, nanomedicine, biomedical sciences. In particular, within biomedical context, they have gained increasing interest because of their tremendous potential resulting from their easy synthesis, resistance to oxidation, interesting physical and optical properties and highly tolerance by human organs when functionalized with biomolecules, allowing the communication with cells surface.

There are several approaches for the classification of nanoparticles. One of the most common is based on one, two and three dimensions<sup>7</sup>. Briefly, *thin films or monolayer* belong to one dimension class, whereas *carbon nanotubes* are defined as two dimensions NPs<sup>8</sup>. The class of three dimensions nanoparticles is extremely vast and it is the object of this PhD thesis. Some examples of three dimensions NPs are *Fullerenes and Dendrimers*. Fullerenes have a spherical structure containing from 28 to more than 100 carbon atoms. Since they have electrical properties, they are generally used in electronics but, thanks to their empty structures, they can be filled with different substances and exploited in medical applications<sup>9</sup>.

*Dendrimers* (1-100nm) are micelles formed by amphiphilic copolymers. In aqueous solutions these molecules self-assemble to hide the hydrophobic region while the hydrophilic portion interacts with the solvent. For this reason they can be used as drug delivery systems and in the field of imaging<sup>10</sup>. In addition, they are widely employed in pharmaceutical applications<sup>11</sup>.

One of the most famous example of three dimensions NPs are **Quantum Dots (QDs)**, which have been the focus of the first part of this work. They are colloidal particles

ranging in size from 2 to 10 nm, generally called colloidal semiconductor nanocrystals because they are synthesized from semiconductor materials, such as cadmium selenide (CdSe), indium arsenide (InAs), cadmium telluride (CdTe) and indium phosphide (InP). When semiconductors are made of extremely small particles, these have particular properties. A phenomenon called "*quantum confinement*"<sup>12</sup> is responsible of many properties of these particles. In fact, semiconductor nanocrystals absorb and emit light whose colour varies essentially according to their size. Consequently, for a given semiconductor material, it is possible to set its colour by varying the size of the QD. Because of their unique photophysical properties including photostability, wide excitation bands, narrow emission peaks, tunable spectral range and brightness, QDs are promising candidates for biomedical application, such as in vivo multicolour imaging and tissue engineering<sup>13</sup>. As a matter of fact, the use of semiconductor nanocrystals as fluorescent labels has gained considerable interest and their use as fluorescent probes will be widely discussed in *Chapter 4*.

Beside Quantum Dots, many kinds of nanoparticles have been developed from different materials, such as magnetic materials, metallic oxides and metals. Among different types of metal nanoparticles including magnetic nanoparticles (iron oxide), silver nanoparticles, copper nanoparticles, **gold nanoparticles (AuNPs)** have been used since ancient times to make stained glass for decorative purpose<sup>14</sup>. In 1857 Michael Faraday discovered that the color of a colloidal solution was due to the dimension of the gold particles while he was synthesizing the first sample of pure gold colloid. Depending on particle size, the colloidal gold solution can have an intense red color (for particles less than 100 nm ) or a purple/violet color (for particles larger than 100 nm ), (**Figure 1**). The amazing optical properties of gold nanoparticles are related to their unique interaction with the light<sup>15</sup>. In particular, the gold free electrons undergo a resonant oscillation when the light is present and absorbed by AuNPs. This phenomenon is called *Localized Surface Plasmon Resonance (LSPR)*<sup>15</sup>. For instance, in aqueous solution, gold nanoparticles around 10 nm have an absorption peak around 520 nm due to the LSPR phenomenon.

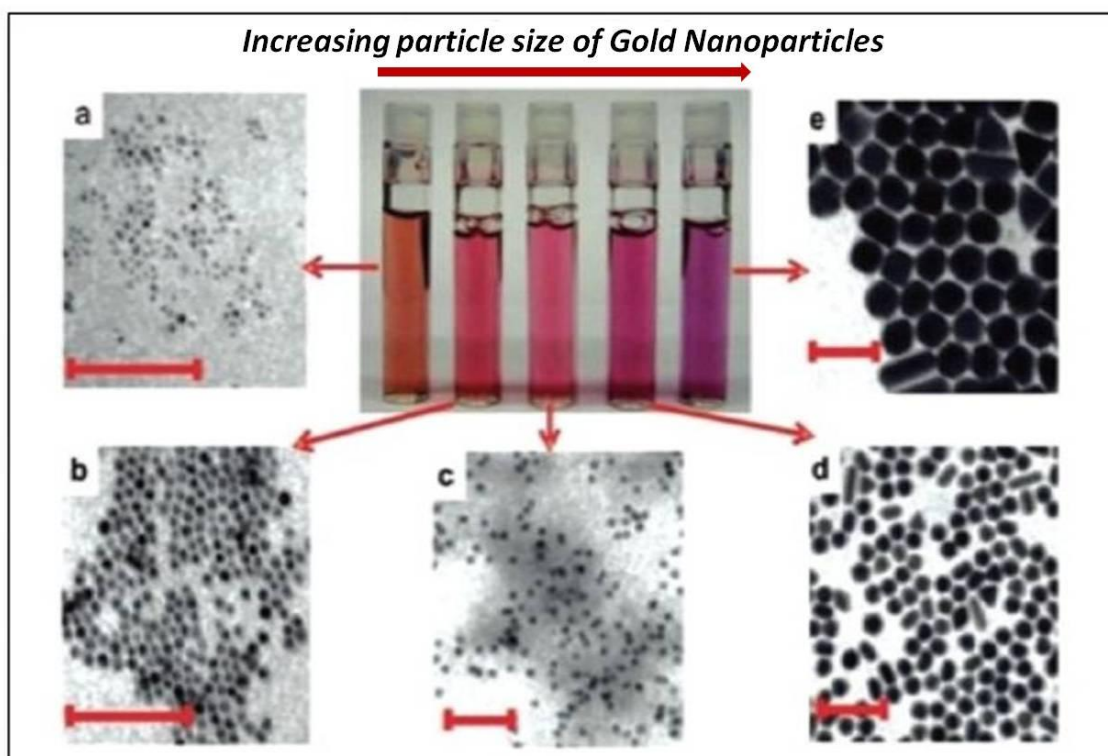


**Figure 1.** Color size-dependent of gold nanoparticles

When molecules are immobilized on the surface of gold nanoparticles, a shift of the absorption peak is expected. This means that LSPR is useful to confirm the presence of molecules on the NPs surface and thus their derivatization<sup>16</sup>. Moreover, the shape of gold nanospheres influences the optical properties, because, for example, rod-shaped nanoparticles have two Plasmon oscillation Resonances: one along the short axis and the other along the long axis<sup>17</sup>. Thanks to their unique physicochemical properties gold nanoparticles are object of intense research and their application in several fields, including biosensing, material science, biomedical imaging and electronics, is widely reviewed<sup>18</sup>. In particular, in *Chapter 6*, their key role in the development of a novel biosensing platform will be extensively discussed.

## 1.2 NANOPARTICLES PREPARATION

Nowadays, many kinds of nanoparticles which differ in composition, size, shape and physical or chemical properties can be synthesized<sup>19</sup>. Colloidal nanoparticles can be dispersed either in aqueous solutions or in organic solvents for hydrophilic or hydrophobic particles respectively, while amphiphilic nanoparticles can be dispersed in both kinds of solvents. The synthesis of metal nanoparticles is extensively reviewed and depending on the required nanoparticle material, such as gold NPs<sup>20</sup>, silver NPs<sup>21</sup>, quantum dots or magnetic NPs<sup>22,23</sup>, different preparation methods have been optimized. In particular, in this work, gold nanoparticles synthesized in aqueous solution are employed and the preparation method developed by our collaborators, the research group of Fondazione Don Gnocchi, will be illustrated in *Chapter 6*<sup>24</sup>.

One of the key points of the synthesis of nanoparticles is the *stabilization against aggregation*. In general, nanoparticle preparations require surfactant molecules bound to the surface to provide stabilization and prevent aggregation by repulsive forces. Moreover, surfactants control the growth of the nanospheres, defining their size and geometric shape. The solubility of a nanoparticles results from the interaction between the ligand molecule and the solvent. In particular, polar or charged surfactants confer solubility in polar or aqueous solvents, while apolar ligand molecules, like hydrocarbon chains, provide solubility in apolar organic solvents. Nanoparticles which have amphiphilic surfactants, e.g. poly(ethylene) glycol (PEG), possess amphiphilic properties and, therefore, are soluble in many solvents with intermediate polarity. Examples of hydrophobic ligands molecules that cover nanoparticles surface in organic solvents are trioctylphosphine oxide (TOPO), triphenylphosphine (TPP), dodecanethiol (DDT), tetraoctylammonium bromide (TOAB) and oleic acid (OA). The stabilizing surfactant plays a significant role because its desorption, caused by several reasons<sup>25</sup>, may induce aggregation of the particles<sup>25</sup>. In fact, even though hydrophilic nanoparticles are stabilized by electrostatic repulsion, the presence of high salt concentrations can shield the electric field causing particles agglomeration. An effective strategy for the stabilization of the particles is based on the use of

polymers<sup>26,27,28</sup>. In this thesis, the significant role of polymeric coatings in the context of nanoparticle stabilization will be extensively discussed in *Chapter 2*.

### 1.3 NANOPARTICLES CHARACTERIZATION

The characterization of nanoparticles is a fundamental step during their preparation<sup>7</sup> since NPs behaviour is strictly correlated to several nanoparticles properties, such as particle size, surface area, surface charge, spectrophotometric and fluorescent features. Therefore, the characterization is a pivotal point in order to predict the behaviour of NPs.

In general, the characterization of NPs includes size, morphology and surface charge determinations. These properties influence NPs physical stability and their in vivo performance by affecting NPs toxicity.

#### **Particle size:**

The most important parameters of NPs are the size and morphology. These properties can dramatically influence many applications of nanoparticles, like drug release. Since small particles have a large surface area, the drug release is faster from these particles than from large particles. However small particles tend to aggregate more. This means that there is a compromise between the stability of NPs and their size<sup>29</sup>.

***Dynamic light scattering (DLS)*** is an optical spectroscopy technique, widely used to determine the size of NPs colloidal suspensions. A solution of particles in Brownian motion is shined by a light laser. When light hits particles, it scatters in all directions, changing the wavelength of the incoming light. This change is correlated to the hydrodynamic radius of the particles. Thus, DLS measurements allow to acquire information on particle motion, size and shape. The results are generally presented as a graph of intensity of the scattered light over the dimensions of the particles. This technique is very sensitive to the presence of large particles<sup>30</sup>. This can be an

advantage if the purpose is to detect small amounts of large particles, but it can be a major drawback for accurate size determination.

**Nanoparticle tracking analysis (NTA)**, is a method for visualizing and analyzing particles in liquids. It relates the rate of Brownian motion to particle size. Unlike in DLS technique, the presence of few large particles in a sample has a little impact on sizing accuracy. This technique gives a more precise size distribution than DLS; it enables the visualization and recording of nanoparticles in solution, and provides particles concentration values and size information. Moreover, when used in conjunction with fluorescence, the technique provides differentiation of labeled or naturally fluorescent particles.

**Transmission electron microscopy (TEM)** provides data related to the size of the core. The technique allows to estimate the molecular weight and to obtain information of the shape and of the size distribution interval of the nanoparticles. The sample preparation onto support grids or films for TEM is cumbersome and time consuming because the specimen must be ultra thin for the electron transmittance. Transmission Electronic Microscope uses an electron beam which interacts with the sample as it passes through<sup>31</sup>. This technique can be exploited for inorganic particles but it is less suitable for organic NPs, as they provide poor contrast in TEM analysis due to their small electron density.

### **Surface Charge**

The colloidal stability of NPs is extremely influenced by the surface charge that determines their interaction with bioactive compounds and with the biological environment. So, it is very important to assess the nature and the intensity of the surface charge in order to predict the behaviour of NPs *in vitro* and *in vivo*.

**Zeta potential ( $\zeta$ -potential)**: the surface charge is analyzed through measurements of the  $\zeta$ -potential of nanoparticles. This parameter corresponds to the electric potential difference across the ionic layer around a charged colloid ion, which is the nanoparticle in this case. With this measurement it is possible to predict the storage stability of a

colloidal dispersion. High zeta potential values, either positive or negative, (i.e.  $<-30\text{mV}$  e  $>+30\text{mV}$ ) avoid aggregation of the particles. Through this technique it is also possible to collect information about the nature of the material encapsulated in the nanospheres or coated onto the surface<sup>32</sup>.

***Gel Electrophoresis:*** it is a powerful technique that provides interesting information about the surface of nanoparticle. Since the electrophoretic mobility of molecules in a gel matrix depends on the ratio between its charge and its size, it is possible to exploit this technique for analyzing the attachment of ligands onto NPs surface. In fact, in the presence of a polymeric coating and/or biomolecules, the mobility of NPs is altered. As a matter of fact, gel electrophoresis is a high sensitive detection technique. An example of its high resolving power was demonstrated by Pellegrino et al, who were able to resolve with this technique even monoconjugate DNA-nanoparticle<sup>33</sup>.

### **Raman Spectroscopy**

It is a non-destructive vibrational spectroscopy able to provide the chemical composition of the analyzed sample, collecting the light inelastically scattered by a sample after a laser excitation. Raman spectroscopy is not affected by the presence of water and therefore biomolecules in aqueous solution can be analyzed without any problem. It is a label free technology, highly specific and it requires low amounts of sample and minimal sample preparation. Thanks to its high sensitivity and specificity it is possible to exploit it to reveal very little changes on nanoparticles surface.

### **Fluorescence spectroscopy**

It is a type of electromagnetic spectroscopy that analyzes the fluorescence of a sample. It uses a light beam, usually ultraviolet light, that excites the electrons in molecules of certain compounds and causes them to emit light; typically, but not necessarily, visible light. A complementary technique is absorption spectroscopy. Fluorescence spectroscopy is extremely suitable for the characterization of fluorescent nanoparticles, Quantum Dots in particular, because it is possible to monitor their fluorescence properties in a very precise way thanks to their narrow emission spectra.

### **UV-Vis-NIR spectrometry**

It is one of the most useful methods for the characterization of metallic nanoparticles. The technique measures the light adsorbed by a sample at different wavelengths in the ultraviolet, visible and near infrared spectra. Upon irradiation of the sample with a light of known wavelength and intensity, the transmitted light is measured. In the case of metallic nanoparticles absorption peaks at the wavelengths corresponding to plasmon excitation are detected. In general, gold nanoparticles have an absorption peak in the 500-600 nm range, which can be shifted due to size variations. The technique can be used to evaluate the quality of a NPs preparation, because through the analysis of the UV spectrum it is possible to reveal the presence of agglomerates or aggregates.

## 1.4 BIBLIOGRAPHY

- (1) Salata, O.; Feynman, R.; Murray, C.; Kagan, C.; Bawendi, M.; Mazzola, L.; Paull, R.; Wolfe, J.; Hebert, P.; Sinkula, M.; et al. Applications of Nanoparticles in Biology and Medicine. *J. Nanobiotechnology* 2004 21 **2004**, 2 (1), 1300–1301.
- (2) APPENZELLER, T. The Man Who Dared to Think Small. *Science (80-. )*. **1991**, 254 (5036).
- (3) Swiss Reinsurance Company. Nanotechnology: Small Matter, Many Unknowns. *Chem. Eng. News* **2004**, No. August, 56.
- (4) Pankhurst, Q. A.; Connolly, J.; Jones, S. K.; Dobson, J.; D, J.; H, M. A.; L, N.; Jr, B. W. F.; R, G.; M, Z.; et al. Applications of Magnetic Nanoparticles in Biomedicine. *J. Phys. D. Appl. Phys.* **2003**, 36 (13), 12.
- (5) Young Soo Kang, †,§; Subhash Risbud, †; John F. Rabolt, ‡ and; Pieter Stroeve\*, †. Synthesis and Characterization of Nanometer-Size Fe<sub>3</sub>O<sub>4</sub> and γ-Fe<sub>2</sub>O<sub>3</sub> Particles. **1996**.
- (6) Catherine J. Murphy, \*; Tapan K. Sau; Anand M. Gole; Christopher J. Orendorff; Jinxin Gao; Linfeng Gou; Simona E. Hunyadi, and; Li, T. Anisotropic Metal Nanoparticles: Synthesis, Assembly, and Optical Applications. **2005**.
- (7) Gayatri, K.; Lakshmi, G.; Preeti, K. Nanoparticles—An Overview of Preparation and Characterization. *Nov. Sci. Int. J. ...* **2012**, 1 (8), 557–562.
- (8) Khler, M.; Fritzsche, W. *Nanotechnology*; Wiley-VCH Verlag GmbH & Co. KGaA: Weinheim, Germany, 2004.
- (9) Partha, R.; Conyers, J. L. Biomedical Applications of Functionalized Fullerene-Based Nanomaterials. *Int. J. Nanomedicine* **2009**, 4, 261–275.
- (10) Wiener, E. C.; Brechbiel, M. W.; Brothers, H.; Magin, R. L.; Gansow, O. A.; Tomalia, D. A.; Lauterbur, P. C. Dendrimer-Based Metal Chelates: A New Class of Magnetic Resonance Imaging Contrast Agents. *Magn. Reson. Med.* **1994**, 31 (1), 1–8.
- (11) Cheng, Y.; Wang, J.; Rao, T.; He, X.; Xu, T. Pharmaceutical Applications of Dendrimers: Promising Nanocarriers for Drug Delivery. *Front. Biosci.* **2008**, 13, 1447–1471.
- (12) Wise, F. W. Lead Salt Quantum Dots: The Limit of Strong Quantum Confinement. **2000**.

- (13) Larson, D. R.; Zipfel, W. R.; Williams, R. M.; Clark, S. W.; Bruchez, M. P.; Wise, F. W.; Webb, W. W. Water-Soluble Quantum Dots for Multiphoton Fluorescence Imaging in Vivo. *Science* **2003**, *300* (5624), 1434–1436.
- (14) Ruivo, A.; Gomes, C.; Lima, A.; Botelho, M. L.; Melo, R.; Belchior, A.; Pires de Matos, A. Gold Nanoparticles in Ancient and Contemporary Ruby Glass. *J. Cult. Herit.* **2008**, *9*, e134–e137.
- (15) Jain, P. K.; Huang, X.; El-Sayed, I. H.; El-Sayed, M. A. Noble Metals on the Nanoscale: Optical and Photothermal Properties and Some Applications in Imaging, Sensing, Biology, and Medicine. *Acc. Chem. Res.* **2008**, *41* (12), 1578–1586.
- (16) Kneipp, K.; Moskovits, M.; Kneipp, H. *Surface-Enhanced Raman Scattering Physics and Applications*; 2006; Vol. 103.
- (17) S. Link; M. B. Mohamed, and; El-Sayed\*, M. A. Simulation of the Optical Absorption Spectra of Gold Nanorods as a Function of Their Aspect Ratio and the Effect of the Medium Dielectric Constant. **1999**.
- (18) Tiwari, P.; Vig, K.; Dennis, V.; Singh, S. Functionalized Gold Nanoparticles and Their Biomedical Applications. *Nanomaterials* **2011**, *1* (1), 31–63.
- (19) Murray, C. B.; Kagan, C. R.; Bawendi, M. G. Synthesis and Characterization of Monodisperse Nanocrystals and Close-Packed Nanocrystal Assemblies. *Annu. Rev. Mater. Sci.* **2000**, *30* (1), 545–610.
- (20) Hedkvist, O. Synthesis and Characterization of Gold Nanoparticles.
- (21) Abou El-Nour, K. M. M.; Eftaiha, A.; Al-Warthan, A.; Ammar, R. A. A. Synthesis and Applications of Silver Nanoparticles. *Arabian Journal of Chemistry*. 2010, pp 135–140.
- (22) Grieve, K.; Mulvaney, P.; Grieser, F. Synthesis and Electronic Properties of Semiconductor Nanoparticles/quantum Dots. *Curr. Opin. Colloid Interface Sci.* **2000**, *5* (1–2), 168–172.
- (23) Lu, A. H.; Salabas, E. L.; Sch??th, F. Magnetic Nanoparticles: Synthesis, Protection, Functionalization, and Application. *Angewandte Chemie - International Edition*. 2007, pp 1222–1244.
- (24) Picciolini, S.; Mehn, D.; Morasso, C.; Vanna, R.; Bedoni, M.; Pellacani, P.; Marchesini, G.; Valsesia, A.; Prospero, D.; Tresoldi, C.; et al. Polymer Nanopillar–Gold Arrays as Surface-Enhanced Raman Spectroscopy Substrate for the Simultaneous Detection of Multiple Genes. *ACS Nano* **2014**, *8* (10), 10496–10506.

- (25) Clarke, S. J.; Hollmann, C. A.; Aldaye, F. A.; Nadeau, J. L. Effect of Ligand Density on the Spectral, Physical, and Biological Characteristics of CdSe/ZnS Quantum Dots. *Bioconjug. Chem.* **2008**, *19* (2), 562–568.
- (26) Finetti, C.; Colombo, M.; Prosperi, D.; Alessio, G.; Morasso, C.; Sola, L.; Chiari, M. One-Pot Phase Transfer and Surface Modification of CdSe-ZnS Quantum Dots Using a Synthetic Functional Copolymer. *Chem. Commun.* **2014**, *50* (2), 240–242.
- (27) Sola, L.; Finetti, C.; Gagni, P.; Chiari, M.; Cretich, M.; Nazionale, C.; Molecolare, R. Surface Modifications by Polymers for Biosensing Applications.
- (28) Finetti, C.; Sola, L.; Pezzullo, M.; Prosperi, D.; Colombo, M.; Riva, B.; Avvakumova, S.; Morasso, C.; Picciolini, S.; Chiari, M. Click Chemistry Immobilization of Antibodies on Polymer Coated Gold Nanoparticles. *Langmuir* **2016**, *32* (29), 7435–7441.
- (29) Redhead, H. M.; Davis, S. S.; Illum, L. Drug Delivery in Poly(lactide-Co-Glycolide) Nanoparticles Surface Modified with Poloxamer 407 and Poloxamine 908: In Vitro Characterisation and in Vivo Evaluation. *J. Control. Release* **2001**, *70* (3), 353–363.
- (30) Hawe, A.; Hulse, W. L.; Jiskoot, W.; Forbes, R. T. Taylor Dispersion Analysis Compared to Dynamic Light Scattering for the Size Analysis of Therapeutic Peptides and Proteins and Their Aggregates. *Pharm. Res.* **2011**, *28* (9), 2302–2310.
- (31) Molpeceres, J.; Aberturas, M. R.; Guzman, M. Biodegradable Nanoparticles as a Delivery System for Cyclosporine: Preparation and Characterization. *J. Microencapsul.* *17* (5), 599–614.
- (32) Ramala, S. K.; Manivasagam, G. A. Updated Review of Nanoparticles. *5* (7), 1622–1637.
- (33) Pellegrino, T.; Sperling, R. A.; Alivisatos, A. P.; Parak, W. J. Gel Electrophoresis of Gold-DNA Nanoconjugates. *J. Biomed. Biotechnol.* **2007**, *2007*, 26796.

## **Chapter 2**

### **NANOPARTICLES SURFACE MODIFICATION**

The key factor for every possible employment of nanoparticles is the proper surface modification, which determines their interaction with the environment. The characteristics of the surface influence their colloidal stability, water solubility, chemical reactivity and biocompatibility, all features that ultimately affect their application in biomedicine.

Thanks to their advantageous properties, such as biodegradability, biocompatibility in physiological systems, NPs have been widely exploited in nanomedicine. A number of surface modification and functionalization strategies have been recently reviewed<sup>1</sup>.

Surface coatings protect NPs against agglomeration and confer them compatibility in solvents different from those in which they were synthesised<sup>2</sup>. Furthermore, through modification of the surface, the physical, chemical and mechanical properties of NPs can be tailored<sup>3</sup> so to improve delivery properties and pharmacokinetic profiles. For instance, NPs, properly modified, permeate deeper into tissues, through thin blood vessels, i.e. capillaries, allowing efficient delivery of therapeutic agents to target sites<sup>4</sup>. Thus, functionalized nanoparticles are promising devices for overcoming the limits of traditional therapeutics<sup>5</sup>.

## 2.1 PHASE TRANSFER AND FUNCTIONALIZATION WITH POLYMERS

In general, several types of colloidal nanoparticles are synthesized in organic solvents. Therefore, in many cases, mostly for biomedical applications, a phase transfer of NPs to aqueous solutions is required in order to confer them the compatibility with biological systems. Within this context, the challenge is to develop strategies to manipulate their surface chemistry keeping their properties identical to those that they have in the organic solvents where they were synthesized.

For instance, even though semiconductor nanocrystals can be synthesized either in aqueous solution starting from various materials such as Au<sup>6</sup>, CdTe, CdSe and Fe<sub>3</sub>O<sub>4</sub><sup>7</sup>, synthetic approaches in organic solvents are preferable as, at high temperature, it is easier to control size and shape<sup>8</sup> and to obtain highly crystalline and monodisperse nanocrystals. The surface of nanoparticles grown in an organic solvent must be coated with different hydrophobic surfactant molecules, such as trioctylphosphine oxide (TOPO) or hexadecylamine (HDA) that confer them hydrophobicity and prevent from further growth.

Even particles that are synthesized in aqueous solution may require phase transfer, if they cannot be synthesized with the desired surfactant on the surface; many strategies already exist for phase transfer in both directions. Sperling et al<sup>1</sup> discussed the three most common strategies to transfer nanoparticles from organic solvents into aqueous solutions: molecular exchange, use of amphiphilic molecules, and polymer coating<sup>9</sup>.

1) *MOLECULAR EXCHANGE*. It is the simplest approach to transfer NPs in aqueous solution<sup>10 11</sup>. This method is based on the competition for binding sites onto the nanoparticle surface between the original surface ligand (e.g., TOPO or HDA) and another molecule (e.g. mercaptoacetic acid), which is added to a solution of nanoparticles in a specific solvent, such as chloroform. In this way the displacement of the surface ligand by the external molecule occurs and the surface chemistry and the polarity of the nanoparticles are changed, conferring them hydrophilicity. In addition, surface reactive groups (e.g. carboxylic acid groups), useful for conjugation, are

provided. However, this method has some drawbacks: nanoparticles aggregation can occur if the surface ligand desorbs from the surface, compromising the stability of the particles and, moreover, the choice of the ligand has to be done considering the core material. The complexity of this approach is reflected by the numerous protocols reported in the literature.

2) *AMPHIPHILIC MOLECULES*. An alternative approach employs, amphiphilic molecule (e.g., phospholipids). On one site, the hydrophobic portion interacts with the nanoparticle surface, on the other site the hydrophilic functionalities extend in solution<sup>12 13</sup>. Coating NPs with this kind of molecules leads to the desired polarity and functionality<sup>14 15</sup>, but the size of NPs could be increased.

3) *POLYMER COATING*. The use of amphiphilic polymeric shell to coat hydrophobic nanoparticles is advantageous compared to the two strategies described above. In fact, since the nanoparticles are simply wrapped in a polymeric shell, this strategy can be used regardless of the type of inorganic core material and the type of surfactant. Thus, it is possible to apply this procedure to many different types of hydrophobic nanoparticles. Moreover, the phase transfer from organic solvents into an aqueous solution using polymeric coatings confers long-term colloidal stability to NPs. At the same time NPs retain most of their physical and optical properties (such as, the fluorescence of CdSe/ZnS QDs and the magnetic properties for Fe<sub>2</sub>O<sub>3</sub> nanoparticles). Lastly, using amphiphilic polymers, many contact points between ligand molecules and polymer are present, which minimize the desorption of the polymer molecule from the particle. It is also possible to further improve the stability by cross-linking the polymer shell<sup>16 12</sup>. Basically, this approach is mostly based on hydrophobic interactions and van der Waals forces between the alkyl chains of the surfactant molecule and the hydrophobic regions of the polymer. This sort of interdigitation of the polymer hydrophobic portions with the surfactants on the nanoparticle surface provides the solubility of the nanoparticle in aqueous solution thanks to the exposure of the polar polymer backbone to the environment. Pellegrino et al.<sup>12</sup> described a general method that allows the phase transfer of hydrophobic nanocrystals from organic to aqueous solution by enclosing the particles in an amphiphilic polymer, poly(maleic anhydride

alt-1-tetradecene). **Figure 2** depicts the scheme of the coating procedure: in the first step the intercalation of the hydrophobic alkyl chains of the polymer with the surfactant molecule plays a significant role. In a second step, the amino group of the cross-linker, bis(6 aminoethyl)amine, reacts with the anhydride ring of the polymer cross-linking individual polymer chains. In this way, a negative charge is conferred to the surface of the nanoparticles that become stable in aqueous solution thanks to electrostatic repulsion.

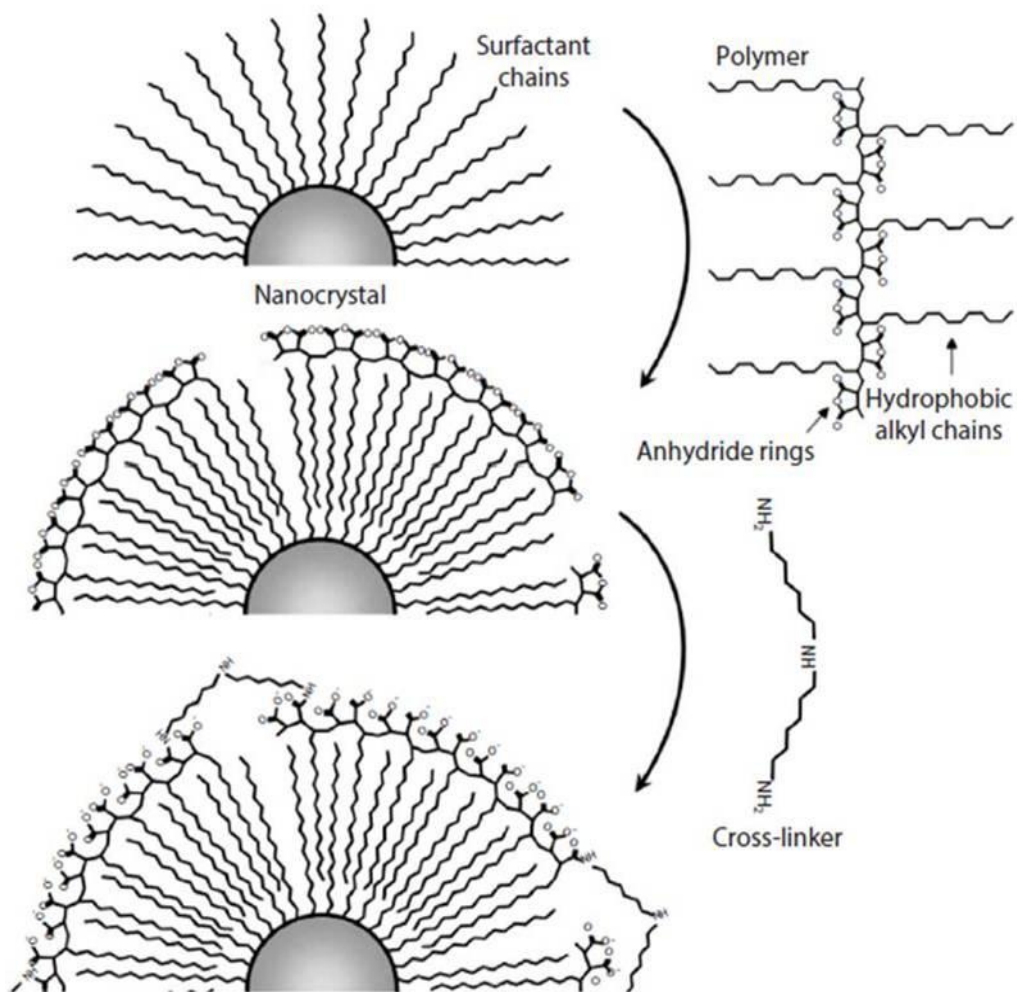


**Figure 2.** Scheme of the phase transfer with an amphiphilic polymer.  
 Reproduced, with permission, from<sup>12</sup>

Through this simple and general protocol, different kind of nanopartilces, such as magnetic, semiconductor, and metallic nanoparticles have been phase transferred<sup>17 18</sup>. Block copolymers are another family of amphiphilic polymers currently used. They include polystyrene-*b*-poly(acrylic acid)<sup>19</sup>, poly(methyl methacrylate)–poly(ethyleneoxide)<sup>20</sup> and amphiphilic hyperbranched polyethylenimine<sup>21</sup>. As underlined in a number of publications, QDs coated with amphiphilic polymers possess high integrity and stability, maintain their optical properties, especially quantum yield and have reduced sensitivity to oxygen and light<sup>22</sup>. In fact it is fundamental that the manipulation of the surface chemistry of semiconductor nanocrystals preserves their optical properties in biological imaging applications.

Amphiphilic NPs coatings, not only allow phase transfer of nanoparticles from organic solvents to aqueous solution, but also acts as a flexible platform for chemical modification and bioconjugation<sup>23</sup>. In fact, the chemical reactive groups, such as carboxylic acids and amines, included in the polymer, are used for the attachment of biomolecules, thus consenting to employ polymer-coated and biofunctionalized nanoparticles in a variety of biomedical applications.

In most functionalization methods, a post-modification of the polymer coating in aqueous solution is needed in order to introduce functionalities on the particle surface<sup>1</sup>. For instance, the introduction of linkers, for example EDC (1-ethyl-3-(3-dimethylamino propyl-carbodiimide), provides activated carboxylic groups that are unstable intermediates, that can undergo two different chemical reactions: hydrolysis or formation of a stable amide bond by reacting with a primary amino group. EDC activated acids can react with NHS (*N*-hydroxysuccinimide) or sulpho-NHS, which have a longer half-life and may react in a second stage with primary amines. Even though the functionalization via EDC/NHS is extensively exploited and quite efficient, as most post-modification approaches, this process can affect the stability of the surfactant layer. For this purpose, Lin et al.<sup>24</sup> describe a strategy where functional groups such as poly-ethylen glycol (PEG), sugar, flurophore, biotin are directly embedded in the polymeric coating, avoiding any additional reagents for the post-bioconjugation chemistry. Basically, the coupling of the functional molecules to the polymer is done in organic solvent before coating the particles.

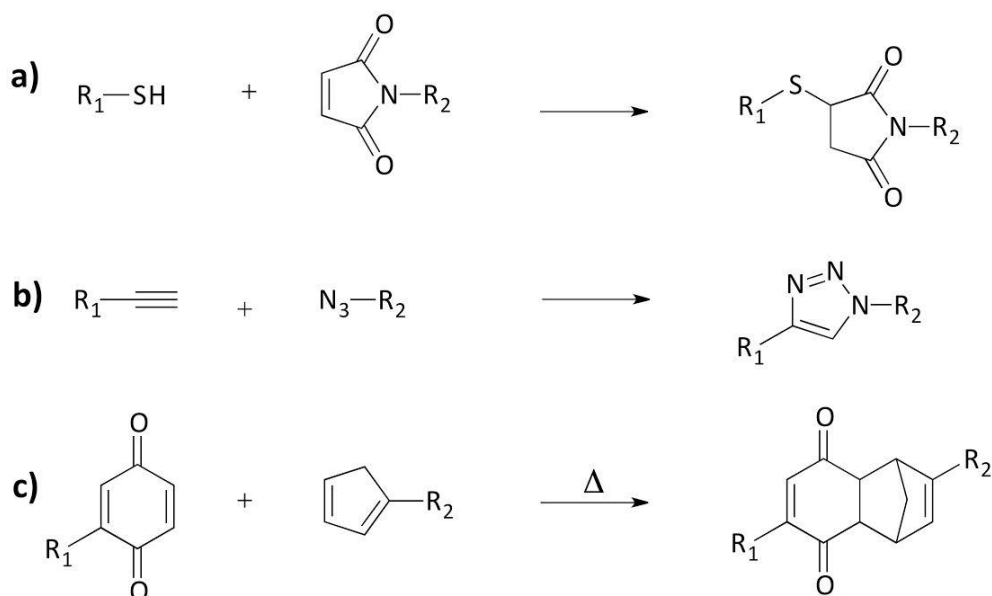
## 2.2 CLICK CHEMISTRY AND “CLICKED” NANOPARTICLES

The click chemistry concept was introduced by Sharpless and co-workers in 2001<sup>25</sup> and it involves a large number of reactions for the universal linkage of molecules avoiding the use of highly reactive or cross-reactive intermediates. This class of chemical reactions are characterized by fast kinetics, (“Click”), high yield, high selectivity and efficiency (often the reactions are quantitative), limited or zero residual by-products and biocompatibility, reactivity in mild conditions i.e. aqueous solvents, room temperature and near physiological pH. Furthermore, several “click” reactions are orthogonal to each other, meaning that they can happen in a one-pot approach or in a sequential manner. This property makes them an efficient toolbox to obtain the synthesis of bioconjugates in a selective way and a suitable approach to successfully modify numerous surfaces and interfaces<sup>26 27</sup>.

“Click reactions” involve the reaction of many different functional groups, for example thiols and maleimides (**Figure 3a**), azides and alkynes (**Figure 3b**) or Diels-Alder reactions (**Figure 3c**).

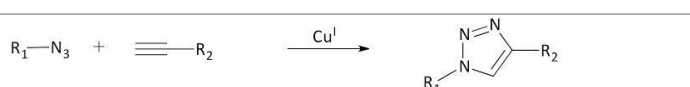
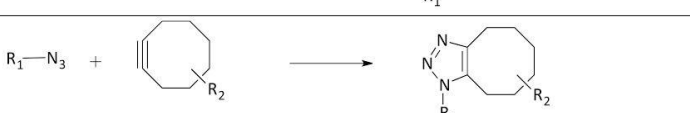
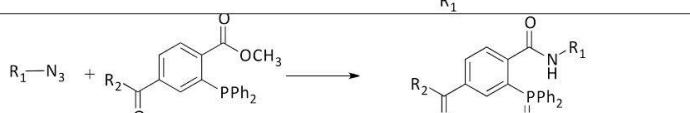
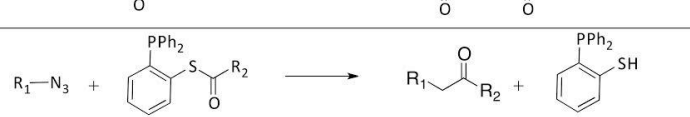
In the panorama of *clickable* reactions, those that involves azide groups are summarized in **Table 1**. In particular, the copper-catalyzed 1,3-dipolar cycloaddition (CuAAC) between azide and alkyne (**Table 1, Figure a**) has gained remarkable attention thanks to the dramatic acceleration rate obtained with the catalyst (Copper, Cu) and the beneficial effects of water, used as solvent<sup>28</sup>.

This reaction process does not require protecting the functionalities naturally present in biomolecules. The formation of 1,4- disubstituted-1,2,3-triazole, **see Table 1 Figure a** proceeds with complete conversion and selectivity with surprising insensitivity to solvent type and solution pH.



**Figure 3.** General scheme of click reactions

**Table 1.** Click reactions which involve azide groups

a) CuAAC	
b) SPAAC	
c) Non- Traceless Staudinger Ligation	
d) Traceless Staudinger Ligation	

Huisgen<sup>29</sup> was the first who developed a thermally initiated cycloaddition between an azide and a linear alkyne which led to the formation of the stable triazole mentioned above. Terminal alkynes are not very reactive towards azides, but the efficiency of this reaction is exponentially increased by the presence of the metal catalyst copper in its +1 oxidation state (Cu(I)) formed in situ by reduction of Cu(II) with ascorbic acid (AAC), the preferred reducing agent used in many applications to provide copper in the required oxidation state. However, the use of Cu(I) as catalyst has some drawbacks, including cytotoxicity, denaturation of proteins<sup>30</sup> and, when used with quantum dots, reduction of their quantum yield<sup>31</sup>. Copper toxicity is related to its oxidation from Cu(I)

to Cu(II), which may damage some biomolecules. In fact, some examples of in vitro copper-induced degradation of viruses or oligonucleotide strands have been reported<sup>32 33</sup>. In order to overcome the problems related to the use of copper catalysis, a copper-free azide-alkyne cycloaddition (SPAAC) strategy was developed by Bertozzi and co-workers in 2007<sup>34</sup>. It requires the use of strained cycloalkynes differently substituted, instead of linear alkynes (**Table 1 Figure b**). The cycloalkynes react towards azide moieties at room temperature with high yield; they do not require any catalysts. As a drawback, the high reactivity of these compounds reduces the chemoselectivity of the click reaction and the cycloaddition kinetics is slower if compared with copper-mediated click reaction (CuAAC).

For these reasons, to maintain all the advantages related to copper-mediated cycloaddition but without damaging biological scaffolds, complexing agents such as tris[(1-benzyl-1H-1,2,3-triazol-4-yl)methyl]amine, (THPTA) and tris-[(1-benzil-1H-triazol-4-il)metil]ammina (TBTA)(**Figure 4**), have been used to enhance the role of copper catalyzed reactions. The most efficient ligand, THPTA, has a dual important role: it increases the reaction kinetics and protects the Cu(I) from oxidation avoiding damages to biomolecules.<sup>35 28</sup>.

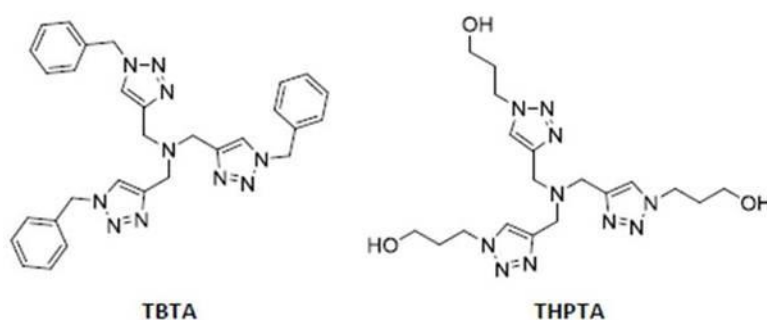


**Figure 4.** Structures of two ligands reported in literature for the acceleration of click-chemistry

In the last few years, click-chemistry reactions have been used to modify the surface of nanoparticles, providing an efficient tool for their functionalization. In particular, nanoparticles derivatization through *click chemistry* was demonstrated either in

organic<sup>36</sup> or in aqueous solution<sup>37</sup> on polymer nanoparticles<sup>38</sup> and carbon nanotubes<sup>39</sup>. Click chemistry is suitable for gold nanoparticles since they are usually stabilized with alkanethiol ligands to prevent aggregation. Thus, through a simple *ligand exchange* approach, such as the one described in *Section 2.1*, it is possible to replace alkanethiol molecules with the desired azide or alkyne functional ligand, providing the nanoparticle with the reactive moiety for CuAAC click reaction<sup>40</sup>. Moreover, AuNPs coated with water-soluble ligands, such as azido-PEG moieties, can be clicked in aqueous solvent. For instance, Gole and co-workers attached alkyne-functionalized *Thermomyces Lanuginosus* lipase to azide-functionalized water-soluble gold nanoparticles<sup>37</sup>.

The application of “clicked” NPs is widespread and, in particular, their potentiality in sensors and bioprobes is enormous. In fact, using the CuAAC reaction, many kinds of nanoscale probes such as gold NPs<sup>41</sup>, semiconductor quantum dots<sup>42</sup>, polymer conjugates, and magnetofluorescent NPs<sup>43</sup> have been developed. Functional metal NPs, especially Au and Ag NPs, have been exploited as labels in colorimetric immunoassays without using sophisticated equipment, thanks to their high extinction coefficient and optical properties.

Azide and alkyne-functionalized AuNPs were used for the detection of Cu<sup>2+</sup> ions in aqueous solution<sup>41</sup>: the addition of CuSO<sub>4</sub> and sodium ascorbate to a colloidal solution of azide and alkyne-functionalized AuNPs induces the cross-linking of NPs: bleaching of the red solution confirms the aggregation. With this method it is possible to detect a concentration as low as 50 nM of Cu<sup>2+</sup> ions just by naked eye-assay (**Figure 5**).

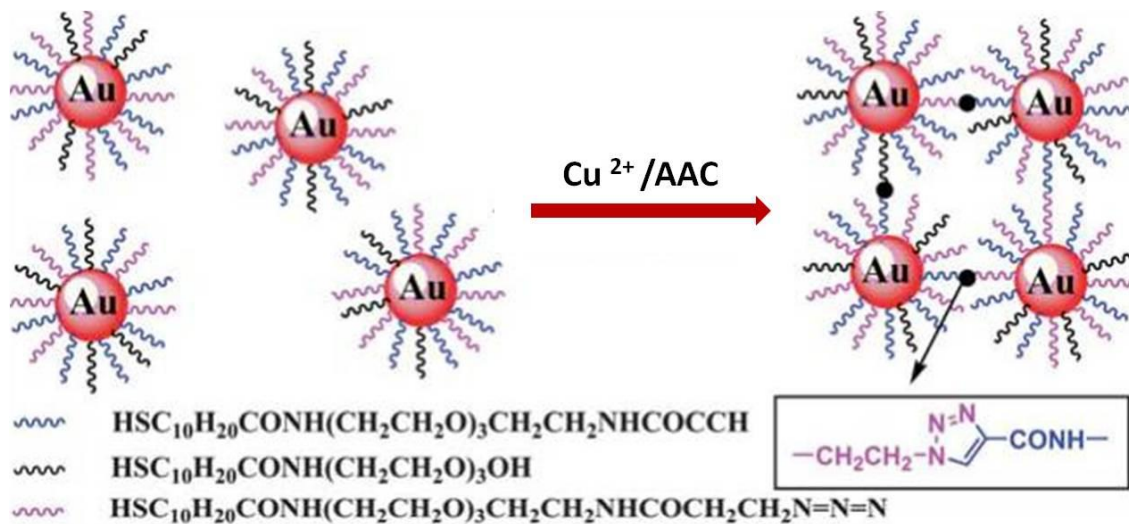


**Figure 5.** The detection of  $\text{Cu}^{2+}$  ions using CuAAC reaction for crosslinking

Another example of colorimetric sensor, which exploits NPs triazole rings as binding sites for many metal cations, detects lead ions in drinking water, where in the presence of  $\text{Pb}^{2+}$  ions, AuNPs aggregation occurs<sup>44</sup>.

## 2.3 BIBLIOGRAPHY

- (1) Sperling, R. A.; Parak, W. J.; Ackerson, C. J.; Jadzinsky, P. D.; Kornberg, R. D.; Akerman, M. E.; Chan, W. C. W.; Laakkonen, P.; Bhatia, S. N.; Ruoslahti, E.; et al. Surface Modification, Functionalization and Bioconjugation of Colloidal Inorganic Nanoparticles. *Philos. Trans. A. Math. Phys. Eng. Sci.* **2010**, *368* (1915), 1333–1383.
- (2) R. Christopher Doty, †,‡; T. Robert Tshikhudo, †; Mathias Brust, † and; David G. Fernig\*, ‡. Extremely Stable Water-Soluble Ag Nanoparticles. **2005**.
- (3) Moon, J. H.; Shul, Y. G.; Hong, S. Y.; Choi, Y. S.; Kim, H. T. A Study on UV-Curable Adhesives for Optical Pick-up: II. Silane Coupling Agent Effect. *Int. J. Adhes. Adhes.* **2005**, *25* (6), 534–542.
- (4) Panyam, J.; Labhasetwar, V. Biodegradable Nanoparticles for Drug and Gene Delivery to Cells and Tissue. *Adv. Drug Deliv. Rev.* **2003**, *55* (3), 329–347.
- (5) Zhang, L.; Gu, F. X.; Chan, J. M.; Wang, A. Z.; Langer, R. S.; Farokhzad, O. C. Nanoparticles in Medicine: Therapeutic Applications and Developments. *Clin. Pharmacol. Ther.* **2008**, *83* (5), 761–769.
- (6) Schmid, G.; Lehnert, A. The Complexation of Gold Colloids. *Angew. Chemie Int. Ed. English* **1989**, *28* (6), 780–781.
- (7) Berger, P.; Adelman, N. B.; Beckman, K. J.; Campbell, D. J.; Ellis, A. B.; Lisensky, G. C. Preparation and Properties of an Aqueous Ferrofluid. *J. Chem. Educ.* **1999**, *76* (7), 943.
- (8) Liberato Manna; Erik C. Scher, and; Alivisatos\*, A. P. Synthesis of Soluble and Processable Rod-, Arrow-, Teardrop-, and Tetrapod-Shaped CdSe Nanocrystals. **2000**.
- (9) Zns-, S.; Anderson, R. E.; Chan, W. C. W. Systematic Investigation of Preparing Capped CdSe Quantum Dots with Amphiphilic Polymers. *ACS Nano* **2008**, *2* (7), 1341–1352.
- (10) Chan, W. C.; Nie, S. Quantum Dot Bioconjugates for Ultrasensitive Nonisotopic Detection. *Science* **1998**, *281* (5385), 2016–2018.
- (11) Freeman, R. G.; Grabar, K. C.; Allison, K. J.; Bright, R. M.; Davis, J. A.; Guthrie, A. P.; Hommer, M. B.; Jackson, M. A.; Smith, P. C.; Walter, D. G.; et al. Self-Assembled Metal Colloid Monolayers: An Approach to SERS Substrates. *Science* **1995**, *267* (5204), 1629–1632.

- (12) Pellegrino, T.; Manna, L.; Kudera, S.; Liedl, T.; Koktysh, D.; Rogach, A. L.; Keller, S.; Rädler, J.; Natile, G.; Parak, W. J. Hydrophobic Nanocrystals Coated with an Amphiphilic Polymer Shell: A General Route to Water Soluble Nanocrystals. *Nano Lett.* **2004**, *4* (4), 703–707.
- (13) Dubertret, B.; Skourides, P.; Norris, D. J.; Noireaux, V.; Brivanlou, A. H.; Libchaber, A. In Vivo Imaging of Quantum Dots Encapsulated in Phospholipid Micelles. *Science* (80-. ). **2002**, *298* (5599).
- (14) Masih Darbandi; Ralf Thomann, and; Nann\*, T. Single Quantum Dots in Silica Spheres by Microemulsion Synthesis. **2005**.
- (15) Han, M.; Gao, X.; Su, J. Z.; Nie, S. Quantum-Dot-Tagged Microbeads for Multiplexed Optical Coding of Biomolecules. *Nat. Biotechnol.* **2001**, *19* (7), 631–635.
- (16) Wen Jiang; Sawitri Mardiyani; Hans Fischer, and; Chan\*, W. C. W. Design and Characterization of Lysine Cross-Linked Mercapto-Acid Biocompatible Quantum Dots. **2006**.
- (17) Elena V. Shevchenko; Dmitri V. Talapin; Andrey L. Rogach; Andreas Kornowski; Markus Haase, and; Weller\*, H. Colloidal Synthesis and Self-Assembly of CoPt3 Nanocrystals. **2002**.
- (18) John Fink, †,‡; Christopher J. Kiely, †; Donald Bethell, ‡ and; David J. Schiffrin\*, ‡. Self-Organization of Nanosized Gold Particles. **1998**.
- (19) Schabas, G.; Yusuf, H.; Moffitt, M. G.; Sinton, D. Controlled Self-Assembly of Quantum Dots and Block Copolymers in a Microfluidic Device. *Langmuir* **2008**, *24* (3), 637–643.
- (20) Smith, A. M.; Duan, H.; Rhyner, M. N.; Ruan, G.; Nie, S. A Systematic Examination of Surface Coatings on the Optical and Chemical Properties of Semiconductor Quantum Dots. *Phys. Chem. Chem. Phys.* **2006**, *8* (33), 3895–3903.
- (21) Nann, T. Phase-Transfer of CdSe@ZnS Quantum Dots Using Amphiphilic Hyperbranched Polyethylenimine. *Chem. Commun.* **2005**, No. 13, 1735–1736.
- (22) Nida, D. L.; Nitin, N.; Yu, W. W.; Colvin, V. L.; Richards-Kortum, R. Photostability of Quantum Dots with Amphiphilic Polymer-Based Passivation Strategies. *Nanotechnology* **2008**, *19* (3), 35701.
- (23) Yu, W. W.; Chang, E.; Falkner, J. C.; Zhang, J.; Al-Somali, A. M.; Sayes, C. M.; Johns, J.; Drezek, R.; Colvin, V. L. Forming Biocompatible and Nonaggregated Nanocrystals in Water Using Amphiphilic Polymers. *J. Am. Chem. Soc.* **2007**, *129* (10), 2871–2879.

- (24) Lin, C. A. J.; Sperling, R. A.; Li, J. K.; Yang, T. Y.; Li, P. Y.; Zanella, M.; Chang, W. H.; Parak, W. J. Design of an Amphiphilic Polymer for Nanoparticle Coating and Functionalization. *Small* **2008**, *4* (3), 334–341.
- (25) Kolb, H. C.; Finn, M. G.; Sharpless, K. B. Click Chemistry: Diverse Chemical Function from a Few Good Reactions. *Angew. Chem. Int. Ed. Engl.* **2001**, *40* (11), 2004–2021.
- (26) Such, G. K.; Quinn, J. F.; Quinn, A.; Tjipto, E.; Caruso, F. Assembly of Ultrathin Polymer Multilayer Films by Click Chemistry. *J. Am. Chem. Soc.* **2006**, *128* (29), 9318–9319.
- (27) *Click Chemistry for Biotechnology and Materials Science*; Lahann, J., Ed.; John Wiley & Sons, Ltd: Chichester, UK, 2009.
- (28) Presolski, S. I.; Hong, V. P.; Finn, M. G. Copper-Catalyzed Azide-Alkyne Click Chemistry for Bioconjugation. *Curr. Protoc. Chem. Biol.* **2011**, *3* (4), 153–162.
- (29) Proceedings of the Chemical Society. October 1961. *Proc. Chem. Soc.* **1961**, No. October, 357.
- (30) Brewer, G. J. Iron and Copper Toxicity in Diseases of Aging, Particularly Atherosclerosis and Alzheimer's Disease. *Exp. Biol. Med. (Maywood)*. **2007**, *232* (2), 323–335.
- (31) Bernardin, A.; Cazet, A.; Guyon, L.; Delannoy, P.; Vinet, F.; Bonnaffé, D.; Texier, I. Copper-Free Click Chemistry for Highly Luminescent Quantum Dot Conjugates: Application to in Vivo Metabolic Imaging. *Bioconjug. Chem.* **2010**, *21* (4), 583–588.
- (32) Gierlich, J.; Burley, G. A.; Gramlich, P. M. E.; Hammond, D. M.; Carell, T. Click Chemistry as a Reliable Method for the High-Density Postsynthetic Functionalization of Alkyne-Modified DNA. *Org. Lett.* **2006**, *8* (17), 3639–3642.
- (33) Qian Wang; Timothy R. Chan; Robert Hilgraf; Valery V. Fokin, \*; K. Barry Sharpless, \* and; Finn\*, M. G. Bioconjugation by Copper(I)-Catalyzed Azide-Alkyne [3 + 2] Cycloaddition. **2003**.
- (34) Jewett, J. C.; Bertozzi, C. R. Cu-Free Click Cycloaddition Reactions in Chemical Biology. *Chem. Soc. Rev.* **2010**, *39* (4), 1272–1279.
- (35) Uttamapinant, C.; Tangpeerachaikul, A.; Grecian, S.; Clarke, S.; Singh, U.; Slade, P.; Gee, K. R.; Ting, A. Y. Fast, Cell-Compatible Click Chemistry with Copper-Chelating Azides for Biomolecular Labeling. *Angew. Chem. Int. Ed. Engl.* **2012**, *51* (24), 5852–5856.

- (36) Binder, W. H.; Petraru, L.; Sachenhofer, R.; Zirbs, R. Synthesis of Surface-Modified Nanoparticles via Cycloaddition-Reactions. *Monatshefte für Chemie - Chem. Mon.* **2006**, *137* (7), 835–841.
- (37) Jennifer L. Brennan, †,⊥; Nikos S. Hatzakis, ‡; T. Robert Tshikhudo, †; Nijole Dirvianskyte, §; Valdemaras Razumas, §; Shamkant Patkar, ||; Jesper Vind, ||; Allan Svendsen, ||; Roeland J. M. Nolte, ‡; Alan E. Rowan, \*,‡ and; et al. Bionanoconjugation via Click Chemistry: The Creation of Functional Hybrids of Lipases and Gold Nanoparticles. **2006**.
- (38) Rachel K. O'Reilly, †,‡; Maisie J. Joralemon, †; Karen L. Wooley, \*,† and; Craig J. Hawker\*, ‡,§. Functionalization of Micelles and Shell Cross-Linked Nanoparticles Using Click Chemistry. **2005**.
- (39) Voggu, R.; Suguna, P.; Chandrasekaran, S.; Rao, C. N. R. Assembling Covalently Linked Nanocrystals and Nanotubes through Click Chemistry. *Chem. Phys. Lett.* **2007**, *443* (1–3), 118–121.
- (40) Li, H.; Yao, Y.; Han, C.; Zhan, J.; Tang, X. L.; Peng, X. H.; Dou, W.; Mao, J.; Zheng, J. R.; Qin, W. W.; et al. Triazole-Ester Modified Silver Nanoparticles: Click Synthesis and Cd<sup>2+</sup> Colorimetric Sensing. *Chem. Commun.* **2009**, *10* (32), 4812.
- (41) Zhou, Y.; Wang, S.; Zhang, K.; Jiang, X. Visual Detection of copper(II) by Azide- and Alkyne-Functionalized Gold Nanoparticles Using Click Chemistry. *Angew. Chem. Int. Ed. Engl.* **2008**, *47* (39), 7454–7456.
- (42) Lee, J. Y.; Kim, J. S.; Park, J. C.; Nam, Y. S. Protein-Quantum Dot Nanohybrids for Bioanalytical Applications. *Wiley Interdiscip. Rev. Nanomedicine Nanobiotechnology* **2016**, *8* (2), 178–190.
- (43) Lv, X.; Weng, J. Ternary Composite of Hemin, Gold Nanoparticles and Graphene for Highly Efficient Decomposition of Hydrogen Peroxide. *Sci. Rep.* **2013**, *3*, 3285.
- (44) Yao, Y.; Tian, D.; Li, H. Cooperative Binding of Bifunctionalized and Click-Synthesized Silver Nanoparticles for Colorimetric co(2+) Sensing. *ACS Appl. Mater. Interfaces* **2010**, *2* (3), 684–690.

# Chapter 3

## NANOPARTICLES IN BIOSENSING

### 3.1 MICROARRAY TECHNOLOGY: OVERVIEW

Beside being widely used in many fields of nanomedicine<sup>1 2</sup>, nanoparticles find wide application in biosensing. In 1992 IUPAC defined biosensors as “devices that use specific biochemical reactions mediated by isolated enzymes, immune systems, tissues, organelles or whole cells to detect chemical compounds usually by electrical, thermal or optical signals”<sup>3</sup>.

Due to their unique physicochemical properties and high surface area, nanoparticles have a pivotal role in the construction and development of novel sensing devices thanks to their ability to enhance detection sensitivity and selectivity<sup>4</sup>. Their use as transducers in electrochemical and optical biosensors, in diagnostic applications as nanoprobe for in vivo imaging/cell tracking in biomedical research, has been extensively reported<sup>5 6</sup>. Nanoparticles are used in biosensing for the immobilization of biomolecules, as catalysis of electrochemical reactions or to enhance electron transfer and labelling of biomolecules, such as antigens, antibodies and DNA. Their role as transducers of the interaction between two biomolecules is widely exploited in **microarray technology**. This technology allows to detect molecular interactions between biomolecules of known identity (*probes*), immobilized with an orderly arrangement on a solid support, and their complementary counterparts (*targets*) contained in a liquid sample. The first step in the realization of a microarray involves the immobilization of probes on the surface. This is a very critical step which requires high accuracy and reproducibility: using a robot (*spotter*) it is possible to dispense few pico-litres of probe solution at a precise position, creating onto the surface small circular spots (diameter < 250 microns). An *array* is an orderly set of spots which can be divided in distinct regions called *subarrays* (**Figure 6**).

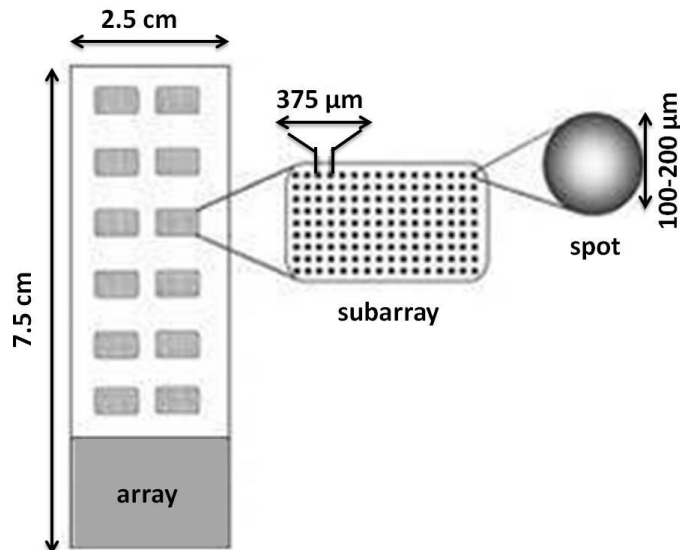


**Figure 6.** Traditional microarray format. Many subarrays can be printed on a conventional support. Many replicate spots can constitute each subarray

After washing and blocking the unreacted sites on the surface, the array is incubated with a sample containing the *target* analytes, that interact specifically with the probe depending on the molecular recognition event under study. If the interaction between probe and target occurs, the molecular complex is revealed on the surface by a *transducer*, which converts the biological interaction in a quantifiable physical signal, that in most cases is fluorescence (**Figure 7**). The variety of detection techniques will be extensively described in *Section 3.4*.

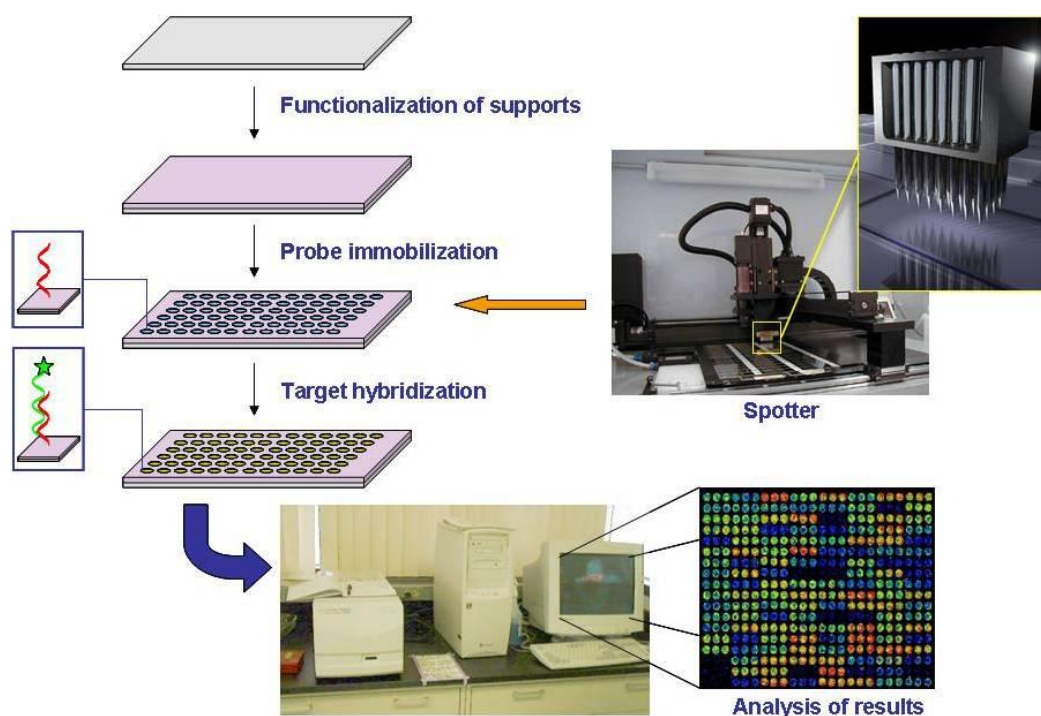


**Figure 7.** General scheme of a microarray experiment

There are different types of microarrays depending on the biomolecules used as probes (DNA, protein or peptide probes). Microarray technology was first developed for DNA analysis. The technique was widely used for genotyping, gene expression and DNA mutation detection. In the last years, protein microarrays have gained increased acceptance in proteomics. Over the last ten years, the major technique in proteomics has been the combination of two-dimensional gel electrophoresis with mass spectrometry (MS). Even though classical proteomic techniques provide excellent resolution of protein isoforms and optimal performance in biomarker discovery, they are not suitable for *high-throughput screening* of protein biomarkers. Protein microarray technology has great potential as tool for biomarker validation and screening. In particular, multiplexing capability, low sample volume consumption, process automation and ability to carry out different analysis in parallel (*high-throughput screening*), make protein microarrays effective tools for multicomponent biomarker diagnostics. A microarray can be seen as the evolution of a conventional Enzyme Linked ImmunoSorbent Assays (ELISA). Thanks to its miniaturization and

multiplexing capability, the amount of data that can be obtained per volume of biological sample has dramatically increased compared to traditional approaches.

Microarray technology can be easily implemented into *Lab on a Chip* (LoC) systems, hybrid micro analytical devices aimed at containing onto a single platform of various process that typically require an entire biochemical laboratory<sup>7</sup>. They basically integrate fluidic and electronic constituents on the same chip. Microchannels, microvalves, sensing components, microelectrodes, thermal elements, optical apparatuses and/or micro-mixers are integrated on the same device where a series of processes or, in some cases, an entire experiment, are conducted.

LoC have been used in several applications, including *high-throughput* medical and biochemical analysis<sup>8</sup>, environmental monitoring and food quality assessment<sup>9</sup>. They have also gained importance in drug discovery<sup>10</sup>, for example in clinical trial studies, drug synthesis, pharmaceutical formulation and in evaluating synergic effect of co-administrated medicines. LoC systems offer significant advantages over standard benchtop systems in terms of compactness of size, portability, process automation, limited power consumption, minimal use of samples and reagents, and reduced risk of contamination. Besides these practical advantages, there is a gain in terms of performance and sensitivity: molecular and thermal diffusion times, for example, are incredibly reduced. LoC systems support a variety of processes, such as sampling, dispensing, mixing, concentrating, amplification, separation, detection and allow parallel sample processing. In order to reach a real clinical impact, the ultimate goal of LoC-based technologies is their evolution into Point-of-care tests (POCT)<sup>11</sup>, defined as medical test performed close to the patient: in the doctor's office, by the hospital bed, or at home, e.g. glucose tests, rapid streptococcal tests and pregnancy tests. They usually require sensitivity and specificity equivalent or better than centralised laboratory tests, as well as self-contained, disposable and low-cost cartridges, which is why LoC are easily applied to POCT.

## 3.2 POLYMER COATING FOR MICROARRAY SUPPORTS

A microarray analysis requires the immobilization of probe-molecules on functionalized surfaces in an ordered matrix. Within this context, the chemistry used for the arrangement of probe molecules on the surface plays a pivotal role in any experiment as the final performance of a microarray biochip is strongly related to the immobilization process itself<sup>12</sup>. Proteins are highly sensitive to the immobilization procedure. The tendency of polypeptides is to bind to the surfaces in a nonspecific manner and this binding mechanism can alter their biological activity<sup>13</sup>. Therefore, the surface chemistry of the support has to:

- 1) keep the integrity, the native conformation and the biological function of ligands (*probes*)
- 2) provide an optimal binding capacity of capture ligands
- 3) ensure accessibility of the ligand to the counterpart (*target*)
- 4) minimize the non-specific interactions; this is extremely difficult when a complex matrix, such as serum, has to be analyzed.

Polymer coatings, usually referred to as tri-dimensional coatings, if properly designed, satisfy all these requirements, assuring homogenous surface derivatization and high concentration of reactive groups for capturing the ligand. Furthermore, they act as linkers, also distributing the bound probe in an axial position, thus causing a faster reaction with the target involved in the biomolecular recognition.

One of such 3-D coatings was developed by Dr. Chiari's group, at the Institute of Chemistry of Molecular Recognition of the National Research Council of Italy in Milan (ICRM-CNR). A copolymer made of three different monomers: *N,N*-dimethylacrylamide (DMA), *N*-acryloyloxysuccinimide (NAS), and 3(trimethoxysilyl)propyl methacrylate (MAPS), which will be referred as poly(DMA-NAS-MAPS) for the remainder of the dissertation, was synthesized by random radical polymerization in an organic solvent. This polymer, illustrated in **Figure 8**, was employed for the first time for the

preparation of low-density DNA microarrays on glass surfaces<sup>14</sup>. Each monomer has a specific role in the correct interaction between the polymer and the surface in the adsorption step and between the polymer and the probes in the immobilization and the incubation steps. The presence of a *N,N*-dimethylacrylamide (DMA) backbone promotes polymer adsorption on the surface through hydrogen bond and Van der Waals interactions. The silanizing moiety, (MAPS), reinforces surface interactions with covalent bonds, whereas the *N*-acryloyloxysuccinimide (NAS) is the reactive monomer that provides anchors for binding amino-modified probes (DNA, proteins and peptides).

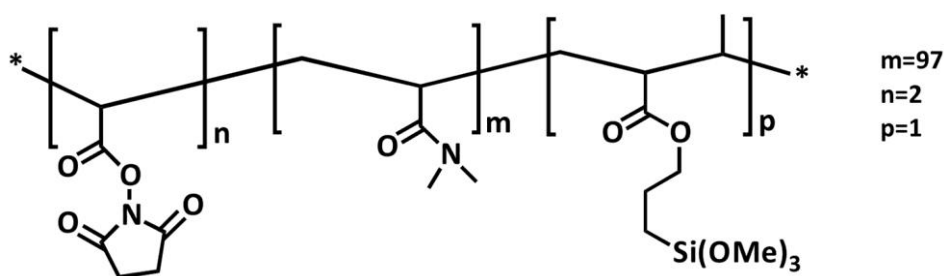


**Figure 8.** Chemical structure of poly(DMA-NAS-MAPS). The molar fraction of the three monomers is 97%DMA, 2% NAS, 1% MAPS

A simple, fast and inexpensive coating procedure was developed using this copolymer that self-adsorbs onto glass, or other materials, such as plastic, PDMS, nitrocellulose and gold, very quickly just by deeping the substrate in its diluted aqueous solution. This robust “*dip and rinse*” coating method avoids time consuming glass pre-treatments and multi-step processes.

### 3.3 SILICON SURFACES FOR MICROARRAY

Glass slides are the favoured surfaces for microarrays because of their availability, cost, flatness, rigidity, transparency, amenability of the surface to chemical modification and non-porosity<sup>15</sup>. However, materials with more favorable optical properties can be employed to enhance fluorescence signals detected on the surface of the substrate: for example, Cretich et al.<sup>16</sup> have introduced silicon substrates coated with a layer of silicon oxide. The principle exploited to enhance fluorescence signals is constructive optical interference, a phenomenon in which light waves, reflected by the upper and lower boundaries of a thin film, interfere with one another to form a new wave. When the thickness of the film is a half-multiple of the wavelength used for the detection, reflections at various interfaces of the layered substrate interfere to build each other up, increasing the reflected wave and reducing the transmission. In order to induce this phenomenon, substrate layered materials with different refractive index are required as substrates<sup>17</sup>. The optimized thickness for the oxide layer is 100 nm. The thermally grown silicon oxide (SiO<sub>2</sub>) coating of the slides, introduced by Cretich et al., has low roughness and low fluorescence background. The phenomenon of constructive interference between the incident and reflected waves of the fluorescence radiation is depicted in **Figure 9**.

This innovative type of microarray slide has demonstrated to provide a 5 to 10-fold enhancement of fluorescence signals in comparison to commercial glass slides<sup>18</sup>, leading to significant improvements in detection sensitivity. Furthermore, the optical properties of the silicon oxide are not altered by the nanometric poly(DMA-NAS-MAPS) coating.

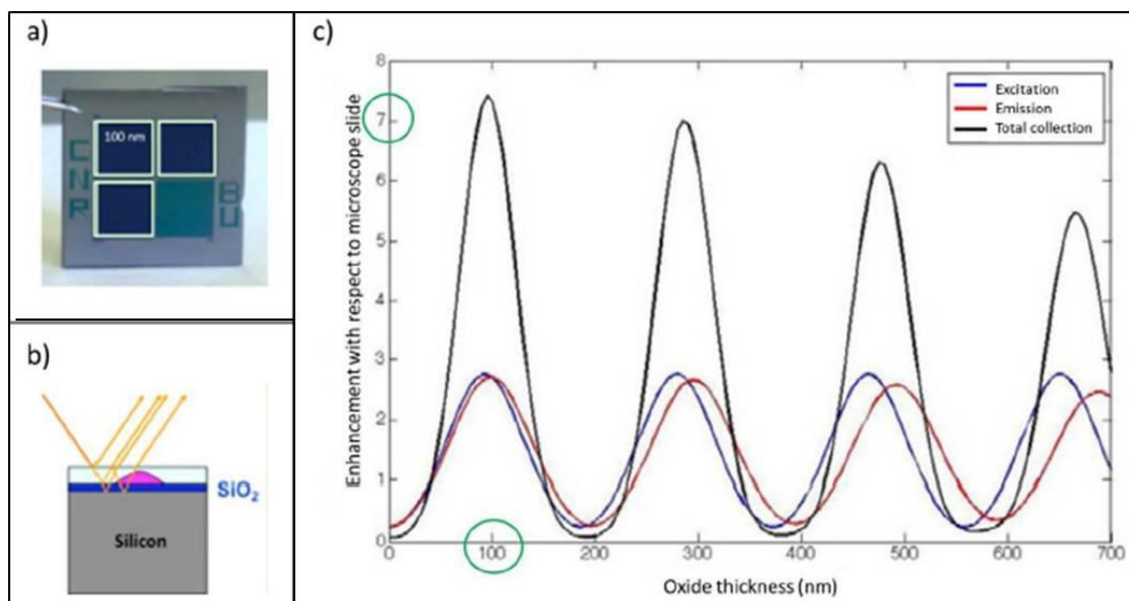


**Figure 9.** With Si/SiO<sub>2</sub> chips, with a top layer of 100 nm oxide, it is possible to obtain a 5 to 10-fold enhancement of the fluorescence signals in comparison to commercial glass slides, thus providing higher sensitivity in analytes detection. **a)** Silicon chip employed for fluorescence detection: white squares mark the 100 nm silicon oxide layer thickness. **b)** Layers of well defined thickness act as interference layers and reflect, towards the detector, the light that would be otherwise absorbed by the substrate. **c)** Fluorescence enhancement on reflecting substrates at normal incidence of excitation and collection. The simulations for excitation (**blu line**), emission (**red line**) and total collected intensity enhancement (**black line**), via utilization of the layered reflecting substrate for varying thickness of the top transparent oxide layer are shown. Monochromatic excitation at 543nm, and collection in the 550-600nm range are assumed<sup>19</sup>

Through variation of the thickness of the SiO<sub>2</sub> layer, it is possible to enhance the emission of any fluorophore of choice by constructive interference with significant improvements in detection sensitivity<sup>16</sup>.

In addition, silicon oxide layered substrates are currently used in the Interferometric Reflectance Imaging Sensor (IRIS), a sensing platform which enables label-free multiplexed detection<sup>20</sup>. This technique will be extensively described in *Chapter 5*.

### **3.4 MICROARRAY DETECTION METHODS**

Microarrays are powerful analytical tools for the simultaneous analyses of thousands of biomolecules, DNA or proteins, in a single experiment. However, their application for analytical and diagnostic purposes is still limited by several challenges which can be overcome by advances in detection methods allowing to improve sensitivity and reliability in signal detection. The wide range of methods of detection includes magnetic and electronic devices<sup>21</sup>, metallic and semiconductor electrodes for electrochemical (amperometric, voltametric) detection<sup>22</sup> and, more rarely, acoustic detection method approaches<sup>23</sup>. Optical methods of detection for biomolecular interaction have gained increasing interest and, nowadays, this strategy is widely employed in microarray technology. Available optical methods can be divided in two categories: label-based and label-free detection methods.

#### **3.4.1 LABEL-BASED DETECTION METHODS**

Label-based sensing represents the standard approach for microarray detection due to the availability of reagents and instruments dedicated to this detection mode that requires fluorescently labeled, chromogenic or chemiluminescent labels in order to detect analytes bound to the surface.

##### ***3.4.1.1 Chromogenic labels***

Chromogen labels are a class of compounds that can be converted to a pigment or a dye through enzymatic reactions (e.g. oxidation). In microarray technologies, they are used as substrate of enzymes covalently bound to detection antibodies. The most commonly employed enzymes are the alkaline phosphatase (AP) and horseradish peroxidase.

The signal intensity depends on the chromogen employed. However, in all cases the coloured product precipitates in correspondence of the spot and is often visible by

naked eye. The higher is the colour intensity, the higher is the concentration of target biomolecule in the sample.

#### **3.4.1.2 Chemiluminescent labels**

Microarrays detection methods based on chemiluminescence reactions are adapted from *Western blotting* protocols. Like chromogenic label, detection antibodies are covalently bound to enzymes (e.g. HRP or AP), but a different substrate, such as luminal is oxidated, eliciting a prolonged light emission. Emitted photons can be captured by Xray films, phosphorous plates or more commonly by a CCD camera. Non-specific signals are minimized thanks to opportune buffer solutions, usually prepared with diluted bovine serum albumin (BSA) or casein. Even though they are very sensitive, chemiluminescence microarrays detection methods have low resolution due to small spot size and limited dynamic range<sup>24</sup>.

#### **3.4.1.3 Fluorescent labels**

Nowadays, fluorescent labels have become the gold standard for microarray detection. A lot of fluorochromes have been developed in order to enhance brightness and stability. Many fluorochromes are available on the market, such as Fluorescein, Cyanine, AlexaFluor, Rodamine, Acridine, Ficobiliproteins and Bodipy. The property that determines the success of a fluorophore, beside its quantum yield, is its stability in a large range of pH values. The choice of the fluorescent molecules is based on the sample properties, spectra emission and kind of support used. In fact, due to auto-fluorescence phenomena, not all supports are compatible with fluorescence detection. Furthermore, molecules that interfere with the signal emission can be contained in the sample itself. An example is represented by the case of flavoproteins whose emitted light has the same wavelength range of fluorescein dye.

Cyanine-3 (Cy3) and Cyanine-5 (Cy5) are the most commonly used fluorochromes. Since they absorb and emit light at two different wavelengths (Cy3 absorbs green light at 550 nm and emits at 570 nm, while Cy5 absorbs red light at 649nm and emits at 670

nm), they can be used for the simultaneous detection of two different targets without any overlapping in emission spectra. Derivatized with *N*-hydroxysuccinimide (NHS) esters, these dyes react with amines on biomolecules rendering them fluorescent.

### 3.4.2 LABEL-FREE DETECTION METHODS

It is well known that the effect of labels on molecular conformation is still a major problem. In fact, labeling approaches often alter surface characteristics and natural activities of the labelled molecule. Furthermore, the labelling procedure is laborious and it is difficult to find an appropriate label equally applicable to all molecules. These limitations provide strong arguments in favor of label-free detection methods, which are gaining a lot of interest and would greatly simplify assay development. They are based on the direct detection of target molecules by means of their intrinsic effect on some of the physical properties of the sensing surface as they interact with immobilized probes. In addition to being insensitive to *photobleaching* and self quenching, label-free methods are compatible with kinetic measurements which are not possible with fluorescence detection. However, sophisticated and expensive equipments are required for label-free approaches. In addition, up to now, label-based detection has still higher sensibility than label-free methods.

Many label free techniques have been successfully integrated with microarrays and represent a potential complement to label-based methods. The label-free techniques for microarrays are extensively reviewed by Sandipan et al.<sup>25</sup>. The most widely employed method is based on Surface Plasmon Resonance (SPR), whose principle is the optical reflectance of a surface coated with a thin layer of gold modified by the presence of biomolecules<sup>26</sup>. The efficiency of SPR is improved by SPR imaging (SPRi), facilitating analysis of multiple interactions simultaneously. This technique represents a potential alternative to label-based detection approaches.

Although SPR methods are the most commonly used, other optical label-free techniques have gained a lot of interest: nanophotonic devices, such as ring resonators, are in full expansion as they perform quantitative label-free, multiplexed analyses of clinically relevant protein biomarkers<sup>27</sup>. A novel multiplexed, label-free

detection method called Reflective Phantom Interface (RPI) was developed by Giavazzi et al<sup>28</sup>. This is a simple, potentially low-cost and multiplex detection method based on measuring the weak intensity of the light reflected by the functionalized surface of a plastic material whose refractive index is very close to that of water. This system provides the direct detection of the target molecules, which interact with the probes immobilized on the sensing surface and their quantification on the basis of the local increase in optical reflectivity.

The group of Professor Selim Ünlü at Boston University (MA, USA), has introduced a label-free imaging technique that can be applied to both DNA and protein microarrays<sup>29</sup>. This innovative label-free technique is called Interferometric Reflectance Imaging Sensor (IRIS<sup>30</sup>) and it is based on a simple interferometric method: the optical phase-shift resulting from the surface accumulation of biological mass at different binding sites is monitored to investigate molecular interactions. A detailed description of this novel technique and its potential as label-free approach will be presented in the next Chapter.

### 3.5 BIBLIOGRAPHY

- (1) Alivisatos, P.; Barbara, P. F.; Castleman, A. W.; Chang, J.; Dixon, D. A.; Klein, M. L.; McLendon, G. L.; Miller, J. S.; Ratner, M. A.; Rossky, P. J.; et al. From Molecules to Materials: Current Trends and Future Directions. *Adv. Mater.* **1998**, *10* (16), 1297–1336.
- (2) Efros, A. L.; Rosen, M. The Electronic Structure of Semiconductor Nanocrystals <sup>1</sup>. *Annu. Rev. Mater. Sci.* **2000**, *30* (1), 475–521.
- (3) Brandenburg, A.; Curdt, F.; Sulz, G.; Ebling, F.; Nestler, J.; Wunderlich, K.; Michel, D. Biochip Readout System for Point-of-Care Applications. *Sensors Actuators B Chem.* **2009**, *139* (1), 245–251.
- (4) Ye, B.-C.; Yin, B.-C. Highly Sensitive Detection of Mercury(II) Ions by Fluorescence Polarization Enhanced by Gold Nanoparticles. *Angew. Chemie Int. Ed.* **2008**, *47* (44), 8386–8389.
- (5) Jain, K. K. Applications of Nanobiotechnology in Clinical Diagnostics. *Clin. Chem.* **2007**, *53* (11).
- (6) Jain, K. K. Nanomedicine: Application of Nanobiotechnology in Medical Practice. *Med. Princ. Pract.* **2008**, *17* (2), 89–101.
- (7) Martinez Vazquez, R.; Osellame, R.; Cretich, M.; Chiari, M.; Dongre, C.; Hoekstra, H. J. W. M.; Pollnau, M.; Van Den Vlekkert, H.; Ramponi, R.; Cerullo, G. Optical Sensing in Microfluidic Lab-on-a-Chip by Femtosecond-Laser-Written Waveguides.
- (8) Yager, P.; Edwards, T.; Fu, E.; Helton, K.; Nelson, K.; Tam, M. R.; Weigl, B. H. Microfluidic Diagnostic Technologies for Global Public Health. *Nature* **2006**, *442* (7101), 412–418.
- (9) Gardeniers, J. G. E.; van den Berg, A. Lab-on-a-Chip Systems for Biomedical and Environmental Monitoring. *Anal. Bioanal. Chem.* **2004**, *378* (7), 1700–1703.
- (10) Neuži, P.; Giselbrecht, S.; Länge, K.; Huang, T. J.; Manz, A. Revisiting Lab-on-a-Chip Technology for Drug Discovery. *Nat. Rev. Drug Discov.* **2012**, *11* (8), 620–632.
- (11) Chin, C. D.; Linder, V.; Sia, S. K. Commercialization of Microfluidic Point-of-Care Diagnostic Devices.
- (12) Sola, L.; Finetti, C.; Gagni, P.; Chiari, M.; Cretich, M.; Nazionale, C.; Molecolare,

R. Surface Modifications by Polymers for Biosensing Applications.

- (13) Chiari, M.; Cretich, M.; Corti, A.; Damin, F.; Pirri, G.; Longhi, R. Peptide Microarrays for the Characterization of Antigenic Regions of Human Chromogranin A. *Proteomics* **2005**, *5* (14), 3600–3603.
- (14) Pirri, G.; Damin, F.; Chiari, M.; Bontempi, E.; Depero, L. E. Characterization of A Polymeric Adsorbed Coating for DNA Microarray Glass Slides. *Anal. Chem.* **2004**, *76* (5), 1352–1358.
- (15) Holloway, A. J.; van Laar, R. K.; Tothill, R. W.; Bowtell, D. D. L. Options Available—from Start to Finish—for Obtaining Data from DNA Microarrays II. *Nat. Genet.* **2002**, *32* (Supp), 481–489.
- (16) Cretich, M.; Monroe, M. R.; Reddington, A.; Zhang, X.; Daaboul, G. G.; Damin, F.; Sola, L.; Unlu, M. S.; Chiari, M. Interferometric Silicon Biochips for Label and Label-Free DNA and Protein Microarrays. *Proteomics* **2012**, *12* (19–20), 2963–2977.
- (17) Fouqué, B.; Schaack, B.; Obeïd, P.; Combe, S.; Gétin, S.; Barritault, P.; Chaton, P.; Chatelain, F. *Multiple Wavelength Fluorescence Enhancement on Glass Substrates for Biochip and Cell Analyses*; 2005; Vol. 20.
- (18) Cretich, M.; Di Carlo, G.; Longhi, R.; Gotti, C.; Spinella, N.; Coffa, S.; Galati, C.; Renna, L.; Chiari, M. High Sensitivity Protein Assays on Microarray Silicon Slides. *Anal. Chem.* **2009**, *81* (13), 5197–5203.
- (19) Yalçm, A.; Cretich, M.; Di Carlo, G.; Sola, L.; Monroe, M.; Ünlü, M. S.; Chiari, M. Fluorescence Enhancement on Reflecting Substrates for Microarray Applications. In *Conference Proceedings - Lasers and Electro-Optics Society Annual Meeting-LEOS*; 2009; pp 465–466.
- (20) Monroe, M. R.; Reddington, A. P.; Collins, A. D.; LaBoda, C.; Cretich, M.; Chiari, M.; Little, F. F.; Ünlü, M. S. Multiplexed Method to Calibrate and Quantitate Fluorescence Signal for Allergen-Specific IgE. *Anal. Chem.* **2011**, *83* (24), 9485–9491.
- (21) Albisetti, E.; Petti, D.; Damin, F.; Cretich, M.; Torti, A.; Chiari, M.; Bertacco, R. Photolithographic Bio-Patterning of Magnetic Sensors for Biomolecular Recognition. *Sensors Actuators B Chem.* **2014**, *200*, 39–46.
- (22) Dill, K.; Ghindilis, A. Electrochemical Detection on Microarrays. *Microarrays Prep. Microfluid. Detect. Methods, Biol. Appl.* **2009**, 25–35.
- (23) Cular, S.; Branch, D. W.; Bhethanabotla, V. R.; Meyer, G. D.; Craighead, H. G. Removal of Nonspecifically Bound Proteins on Microarrays Using Surface

Acoustic Waves. *IEEE Sens. J.* **2008**, *8* (3), 314–320.

- (24) Schweitzer, B.; Predki, P.; Snyder, M. Microarrays to Characterize Protein Interactions on a Whole-Proteome Scale. *Proteomics* **2003**, *3* (11), 2190–2199.
- (25) Ray, S.; Mehta, G.; Srivastava, S. Label-Free Detection Techniques for Protein Microarrays: Prospects, Merits and Challenges. *Proteomics* **2010**, *10* (4), 731–748.
- (26) Surface Plasmon Resonance (SPR) and Other Options for Label-free Detection | Biocompare Editorial Article <http://www.biocompare.com/Editorial-Articles/41803-Surface-Plasmon-Resonance-SPR-and-Other-Options-for-Label-free-Detection/>.
- (27) Washburn, A. L.; Gunn, L. C.; Bailey, R. C. Label-Free Quantitation of a Cancer Biomarker in Complex Media Using Silicon Photonic Microring Resonators. *Anal. Chem.* **2009**, *81* (22), 9499–9506.
- (28) Giavazzi, F.; Salina, M.; Cerbino, R.; Bassi, M.; Prosperi, D.; Ceccarello, E.; Damin, F.; Sola, L.; Rusnati, M.; Chiari, M.; et al. Multispot, Label-Free Biodetection at a Phantom Plastic-Water Interface. *Proc. Natl. Acad. Sci. U. S. A.* **2013**, *110* (23), 9350–9355.
- (29) Ozkumur, E.; Yalçın, A.; Cretich, M.; Lopez, C. a; Bergstein, D. a; Goldberg, B. B.; Chiari, M.; Ünlü, M. S. Quantification of DNA and Protein Adsorption by Optical Phase Shift. *Biosens. Bioelectron.* **2009**, *25*, 167–172.
- (30) Avci, O.; Ünlü, N. L.; Özkumur, A. Y.; Ünlü, M. S. Interferometric Reflectance Imaging Sensor (IRIS)--A Platform Technology for Multiplexed Diagnostics and Digital Detection. *Sensors (Basel)*. **2015**, *15* (7), 17649–17665.

## **Chapter 4**

# **INNOVATIVE STRATEGIES FOR NANOPARTICLES SURFACE MODIFICATION WITH FUNCTIONAL COPOLYMERS: ONE-POT PHASE TRANSFER AND BIOCONJUGATION OF QUANTUM DOTS**

In the literature, terms such as modification, functionalization or stabilization are used to define the processes that alter surface properties of nanoparticles. This diversity in terms reflects the different motivations for using a coating or for its intended function. The properties of nanomaterials are selectively changed by surface coatings as, often, it is the shell, rather than the core of the nanoparticles, that determines their main final properties.

Compared to larger particles, nanoparticles possess a large surface to volume ratio surface properties, especially if they are smaller than 10 nm. These properties dictate the behaviour of the particles during production, processing and final application(s). As already extensively discussed in *Section 2.1*, coating the surface of nanoparticles with a polymer provides one of the most efficient methods to influence their properties<sup>1</sup>. Polymeric coating can confer to NPs all the features that allow their use in medical applications such as colloidal stability, biocompatibility, water-solubility and biofunctionalization. This latter characteristic is essential for the targeted transport of NPs to certain cells or organs. By binding appropriate antibodies to the surface, the coated particles can be directed to target organs and cells like tumour cells or inflamed areas. Another application that requires binding the nanoparticle to a biomolecule is biosensing where the nanoparticles are used as signal transducers.

Biomolecules are immobilized commonly on nanoparticles either passively, through hydrophobic or ionic interactions (physical adsorption), or covalently by a chemical reaction with a reactive surface group. The second option provides significant advantages over physical adsorption, the most important being the higher stability of

the bioconjugate. The common strategies, which allow the covalent binding of biomolecules, require the introduction on the NPs surface of a chemical group that is reactive towards primary amines or carboxylic acids present on the surface of protein. An example of this approach is the EDC/NHS strategy described in *Section 2.1*. However, poor stability of nanoparticles can often compromise an efficient bioconjugation. During the modification, nanoparticles are used in suspension having been dispersed in a (aqueous) medium. To stabilise such suspension, and to prevent sedimentation or agglomeration, the use of functional polymers, which, at the same time, provide stabilization or functionalization with anchoring points to bind biomolecules, is advantageous.

The purpose of this study was to devise an innovative, robust and user-friendly one-step procedure by employing a synthetic, functional poly-*N,N*-dimethylacrylamide based copolymer to provide stabilization and functionalization of nanoparticles.

## 4.1 *N,N* –DIMETHYLACRYLAMIDE (DMA) BASED COPOLYMERS

The development of three-dimensional hydrophilic coatings, suitable for the functionalization of different kinds of surfaces, is one of the most important fields of research in our laboratory. For this purpose, the research group has developed a family of *N,N*-dimethylacrylamide based copolymers, whose basic structure is represented in **Figure 10**. The parent polymer of the family is obtained by radical copolymerization<sup>2</sup> of three different monomers, two of which are always present: *N,N*-dimethylacrylamide, DMA, (**Figure 10, green box**), the major component, which provides the adhesivity to a variety of materials by hydrogen and van der Waals interactions and the silane monomer, MAPS, (**Figure 10, blue box**), which reinforces the stability of the polymer to the surfaces through condensation with hydroxyl or silanol groups. In addition, a third moiety, which is a functional monomer, (**Figure 10, letter “R”**) is included into the basic structure of poly(DMA-MAPS), giving to this polymer an incredible versatility. In fact, this third monomer provides active groups whose reactivity is related to the characteristic of molecules that have to be immobilized. Examples of various monomers that have been used include active ester, oxirane<sup>3</sup> and ionizable groups<sup>4</sup>.

As already mentioned in *Section 3.2 (“Polymer Coating for Microarray Supports”)*, the first DMA-based copolymer of this family was developed by Pirri et al in 2004 and it is called poly(DMA-NAS-MAPS)<sup>2</sup>. Its chemical structure is shown in **Figure 10a**. The polymer backbone bears a succinimidyl ester (NHS ester) that is the functional monomer highly reactive towards nucleophiles such as amino groups present in proteins and easily insertable in oligonucleotides. NHS is thus exploited for covalent immobilization of biomolecules thanks to the stable amide bond it forms by reaction with amino groups.

This copolymer has been firstly employed for the preparation of low-density DNA microarrays on glass<sup>2</sup>; then, its use has also been extended to protein and peptides microarrays. Besides its use for the coating of glass microarray supports (*see Section 3.2*), this polymer provides a stable functional coating through a simple, fast and inexpensive coating procedure for different materials, including, silicon oxide, gold,

nitrocellulose, thermoplastics, expanding its use in many application in the field of biosensing<sup>5</sup>. This copolymer satisfies all the key requirements for an efficient surface derivatization (in terms of binding capacity of capture ligands, minimization of non-specific interaction, probe accessibility etc.). In order to exploit the coating forming properties of this polymer in the field of click chemistry, Zilio and co-workers in 2014 synthesized a new copolymer similar to poly(DMA-NAS-MAPS), with the only difference that the succinimidyl ester was replaced with an alkyne functionality.

The new copolymer, copoly(*N,N*-dimethylacrylamide (DMA)-3-trimethylsilyl-prop-2-ynyl methacrylate (PMA)-3-(Trimethoxysilyl)propyl methacrylate (MAPS)), Poly(DMA-PMA-MAPS), see **Figure 10b**, was produced by random radical copolymeration of the three monomer, by a synthetic approach similar to that used for the parent copolymer, and allows the conjugation of biomolecules derivatized with azide groups that react with the alkyne monomer through a well known click reaction: the copper-catalyzed 1,3-dipolar cycloaddition (CuAAC) (see Section 2.2). This polymer was developed to take advantage from *Click Chemistry*, defined as a synthetic approach introduced by K. B. Sharpless in 2001. *Click chemistry* are reactions that are high yielding, wide in scope, create only byproducts that can be removed without chromatography, are stereospecific, simple to perform, and can be conducted in easily removable or benign solvent<sup>6</sup> (see Section 2.2).

The “clickable” poly(DMA-PMA-MAPS) was initially employed in glycan microarray for the immobilization of a variety of different carbohydrates on the same surface, with proper spacing and orientation<sup>7</sup>.

Replacing NAS with PMA did not cause any change in the coating procedure already optimized for the parent copolymer poly(DMA-NAS-MAPS). Poly(DMA-PMA-MAPS) preserved both the simplicity of the coating procedure and the advantages of the nanometric coating of the parent copolymer from which it originates, such as low level of non-specific adsorption<sup>8</sup>, homogenous surface derivatization and high concentration of reactive groups for the capture ligands.

In this chapter and in *Chapter 6*, the purpose of work was to demonstrate the use of these functional copolymers in functionalization and stabilization of two different types of nanoparticles: Quantum Dots and gold nanoparticles. Poly(DMA-NAS-MAPS)

was used for the phase transfer and the functionalization of semiconductor nanocrystals CdSe/ZnS (see Section 4.2), whereas poly(DMA-PMA-MAPS) was employed for the functionalization of gold nanoparticles surrounded by a thin silicon oxide layer through a click chemistry approach (see Chapter 6).

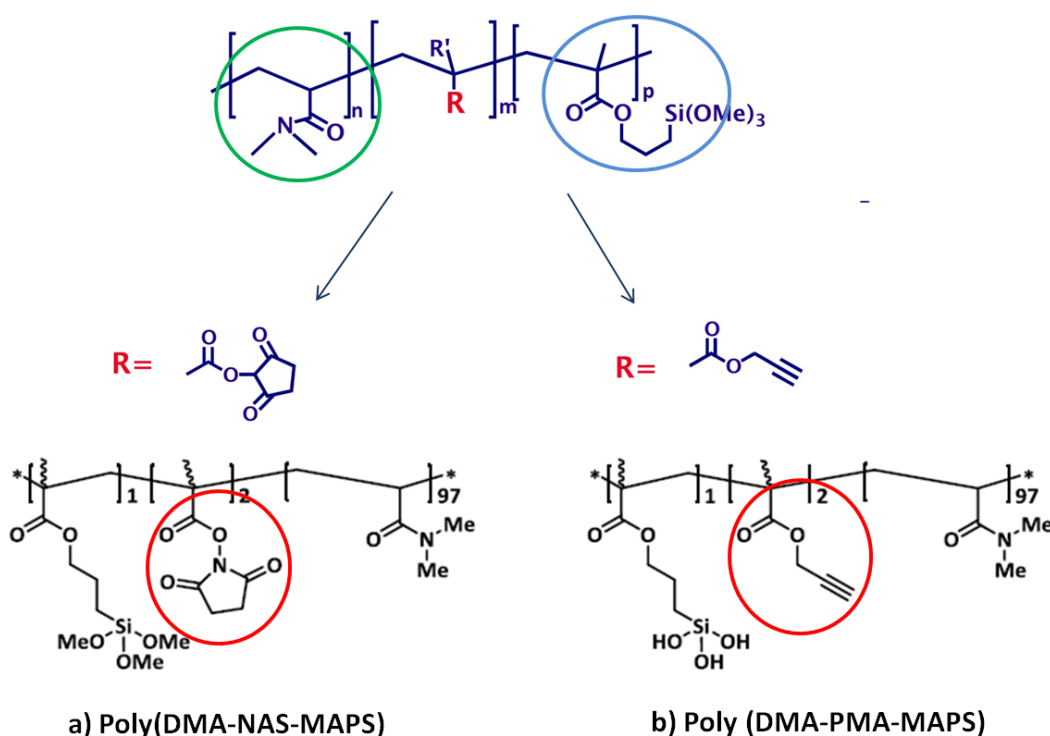


**Figure 10.** Structure of *N,N*-dimethylacrylamide copolymers. The basic structure is composed of dimethylacrylamide portion (**green**) 97%, which confers the adhesivity to a variety of materials, and the silane monomer, 1%, that reinforces the stability of the polymer to the surfaces (**blue**). Adding functional monomers (2%; **red**) two different kinds of functional copolymer were developed. In particular, poly(DMA-NAS-MAPS) (**a**) is obtained when the functional portion is a succinimidyl ester (NHS ester), whereas poly(DMA-PMA-MAPS) (**b**) includes an alkyne functionality.

## 4.2 ONE-POT PHASE TRANSFER AND BIOCONJUGATION OF QDs USING POLY (DMA-NAS-MAPS)

In this work, organic CdSe-ZnS core-shell QDs (emission peak at 655nm) were employed. QDs nanocrystals are nanometer-scale atom clusters comprising a core and a shell. The core is made up of a few hundred to a few thousand atoms of a semiconductor material, cadmium selenide (CdSe). A semiconductor shell (zinc sulfide, ZnS) surrounds and stabilizes the core, improving both the optical and physical properties of the material. The core-shell assembly is extremely hydrophobic because QDs are mostly synthesized in organic solvent<sup>9</sup>.

Thus, the phase transfer process through an amphiphilic coating is one of the most efficient approaches to render them stable in water, biocompatible and easily derivatizable. Coatings are required to use these nanoparticles in biological applications as fluorophores or as multifunctional nanoscaffolds. As detailed in *Section 2.1* a number of amphiphilic polymers including Poly(maleic anhydride-alt-1-octadecene)<sup>10</sup>, block copolymers (e.g., polystyrene-bpoly(acrylic acid))<sup>11</sup>, poly(methyl methacrylate), poly(ethyleneoxide)<sup>12</sup> and amphiphilic hyperbranched polyethylenimine<sup>13</sup> have been used to this aim. The solubilization process involves an interdigitation of the polymer hydrophobic portions with the surfactant ligands on the QD surface (TOPO and/or HDA) while the polar polymer backbone is exposed to the environment with the hydrophilic groups protruding from the surface.

An efficient phase transfer process maintains the optical properties of the QDs identical to that of the original organic-soluble QDs. A procedure that allows the manipulation of the surface chemistry of nanocrystals without altering their key features is highly desirable.

In this thesis, we present a facile procedure for the transfer of QDs from organic solvents into aqueous solution employing, for the first time, the functional copolymer poly(DMA-NAS-MAPS)<sup>14</sup>. Moreover, the proposed method permits the functionalization of QDs by a one pot procedure: proteins can be directly coupled to the active ester groups of the polymer by means of a peptide bond formed during the solubilization phase. In particular, in this work, the biofunctionalization with

Streptavidin (SAv), was carried out. This protein, chosen as model, is capable of binding biotin or biotinylated molecules with extremely high affinity. In fact, streptavidin-immobilized particles have shown great potential due to the stability of the biotin-streptavidin interaction and the resulting ability to bind to target molecules specifically and efficiently. However, this novel NPs functionalization approach can be exploitable to conjugate QDs to any kind of biomolecules, since the ester groups of poly(DMA-NAS-MAPS) are highly reactive towards nucleophiles such as amino groups present in proteins, peptides and easily insertable in oligonucleotides.

## 4.2.1 MATERIAL AND METHODS

### 4.2.1.1. Reagents

Chloroform ( $\text{CHCl}_3$ ), methanol (MeOH), isopropanol (iPrOH), phosphate saline buffer (PBS), trizma base (Tris), HCl, ethanolamine ( $\text{NH}_2\text{CH}_2\text{CH}_2\text{OH}$ ), NaCl, sodium bicarbonate ( $\text{NaHCO}_3$ ), boric acid ( $\text{H}_3\text{BO}_3$ ), ethylenediaminetetraacetic acid (EDTA) disodium salt dehydrate, sodium phosphoric acid ( $\text{Na}_3\text{PO}_4$ ), sodium hydroxide (NaOH), Triton X-100, Tween 20, ammonium sulfate ( $\text{NH}_4\text{SO}_4$ ), *N,N*-dimethylacrylamide (DMA), 3-(trimethoxysilyl)propyl methacrylate (MAPS), azoisobutyronitrile (AIBN), streptavidin from *Streptomyces avidinii* (lyophilized powder), dialysis tubing cellulose membrane (12KDa), were purchased from Sigma-Aldrich (St. Louis, MO, USA). *N*-acryloyloxysuccinimide (NAS) was synthesized as reported elsewhere<sup>2</sup>. Hi-res standard agarose from Bioproducts Ltd, 655 ITKTM Organic Quantum Dots purchased from Life Technologies, Biotin-SP-conjugated AffiniPure Goat Anti-Rabbit IgG, AffiniPure Goat Anti-Rabbit IgG, Cyanine 5 labeled with AffiniPure Goat Anti-Human IgG were obtained from Jackson, ImmunoResearch. X- Spin-X UF Concentrator (100 kDa filter cut off) were bought by VWR. Silicon oxide chips with a thermal oxide layer of 100 nm were bought from Silicon Valley Microelectronics (Santa Clara, CA, USA).

### 4.2.1.2 Synthesis of poly(DMA-NAS-MAPS) and poly(DMA- PMA-MAPS)

The copolymers poly(DMA-NAS-MAPS) and poly(DMA-PMA-MAPS) were obtained by free radical polymerization of DMA and MAPS with NAS or protected PMA, as reported in ref<sup>2</sup>. The total monomer concentration in the feed was 20% w/v, while the molar fraction of the three monomers in both polymers, was 97%, 1% for DMA and MAPS and 2% for NAS or protected PMA. Briefly, for the synthesis of poly(DMA-NAS-MAPS), the three monomers were diluted in anhydrous tetrahydrofuran, together with a thermocatalyst (AIBN); the reaction flask was heated to 65 °C to initiate the polymerization process, and after 2 h the polymer was precipitated in petroleum ether and collected as a white powder. The synthetic process of poly(DMA-PMA-MAPS) required two separate steps: (a) the synthesis of polymer which contains 3-

trimethylsilyl-prop-2-yn methacrylate, a protected form of prop-2-ynyl prop-2-enoate (PMA) and (b) removal of the protective trimethylsilyl groups. The first step was similar to that used for the synthesis of poly(DMA-NAS-MAPS), while the deprotection was achieved by dissolving the polymer in a basic solution containing potassium carbonate. After a 3 h reaction, the polymer was dialyzed and lyophilized<sup>7</sup>.

#### **4.2.1.3 Quantum dots phase-transfer and bioconjugation**

Commercial CdSe/ZnS QDs were precipitated from decane according to the protocol suggested by the manufacturer and dispersed in chloroform at 1  $\mu\text{M}$  concentration. Water phase transfer and streptavidin conjugation were performed in a one-pot reaction: 56 mg of poly(DMA-NAS-MAPS) were solubilized in 1,750 mL of chloroform and added to 250  $\mu\text{L}$  of 1  $\mu\text{M}$  QDs chloroform colloidal solution. The mixture was homogenized and the solvent was evaporated at reduced pressure. The precipitate, was suspended in 150 mM phosphate buffer, pH 8.5, triton x-100 0.001% (v/v), containing streptavidin (0.625 mg mL<sup>-1</sup>) and provided a clean and stable dispersion. The colloidal solution was sonicated for 30 min and stirred overnight at room temperature. The nanoparticles were centrifuged several times on a Spin-X UF Concentrator (100 kDa filter cutoff), at 2000 rpm to remove soluble salts and copolymer/streptavidin excess. The streptavidin modified QDs (SAv-QDs) stock solution was then stored at 5 °C in the Incubation Buffer, Tris 0.05 M, NaCl 0,15M, pH 7,6, Tween 20 0,02% (v/v).

#### **4.2.1.4 Nanoparticles Characterization**

##### ***Morphological Analysis***

Transmission electron microscopy (TEM) images of Quantum Dots coated with poly(DMA-NAS-MAPS), Copoly-QDs, were obtained with a Zeiss EM-109 microscope (Oberkochen, Germany) operating at 80 kV. The nanoparticles were dispersed under sonication in water (50  $\mu\text{g mL}^{-1}$ ) and a drop of the resulting solution was placed on a formvar/carbon-coated copper grid and air-dried.

A TEM image of the commercial QDs that were phase transferred in this work is shown in **Figure 14b** of *Section 4.2.2.2 (Results and Discussion Section)*.

The shape and morphology of the QDs reported in the manufacturer datasheet, available online at the following link: <http://www.lifetechnologies.com/it/en/home/references/molecular-probes-the-handbook/ultrasensitive-detection-technology/qdot-nanocrystal-technology.html>, are similar to those shown in **Figure 14a** of *Section 4.2.2.2 (Results and Discussion Section)*.

#### ***Particle size and $\zeta$ -potential analyses***

Dynamic light scattering (DLS) measurements were performed at 90° with a 90Plus Particle Size Analyzer from Brookhaven Instrument Corporation (Holtsville, NY) working at 15 mW of a solid-state laser ( $\lambda = 661$  nm). Zeta-potential measurements were elaborated on the same instrument equipped with AQ-809 electrode and data were processed by ZetaPlus software. The final sample concentration used for measurements was typically 0.4 nM. At this concentration the QDs are fully dispersed. All measurements (accepted PDI below 0.3) were performed in triplicate and the average values were taken.

#### ***Nanoparticle tracking analysis (NTA)***

Nanoparticle tracking analysis, NanoSight, enables the visualization and recording of nanoparticles in solution, providing information on particle size and concentration based on the Brownian motion of individual particles.

Sight distribution spectra were collected using NanoSight LM10 from NanoSight Limited (Amesbury, UK) and analyzed with Nanoparticle Tracking Analysis (NTA) software, version 2.2 Build 0363; the samples were in a range of concentration around  $10^8$  to  $10^9$  nanoparticles mL<sup>-1</sup> working at a temperature of 23 °C. All measurements were performed in triplicate and the average values were taken.

Nanoparticle tracking analysis (NTA) enables the visualization and recording of nanoparticles in solution, providing information on particle size and concentration based on the Brownian motion of individual particles.

### ***Optical properties***

*The optical properties of polymer (Copoly-QDs) and streptavidin coated QDs (SAv-QDs) were assessed by fluorescence spectrometry (Fluorimeter VP-750, Jasco) and UV visible spectrometry (Spectrophotometer VP -650, Jasco). Before collecting UV-Vis and fluorescence spectra all sample solutions were sonicated for 5 minutes in order to minimize aggregation. The concentration of QDs solution was calculated using an absorption (450nm wavelength) calibration curve using solutions of CdSe/ZnS QDs of known concentration, assuming a quantitative transfer from chloroform to aqueous solution. The concentration values were consistent with those estimated with NanoSight analysis.*

### ***Raman spectroscopy***

Raman spectra were recorded with an Aramis Horiba Jobin-Yvon micro-Raman spectrometer, using a solid state 500 mW near-infrared laser operating at 785 nm, and equipped with a liquid sample holder.

#### **4.2.1.5 Bioassay: coating procedure and microarray experiments**

To demonstrate the functionalization of QDs with Streptavidin, biotinylated and non-biotinylated antibodies (Biotin-SP-conjugated AffiniPure Goat Anti-Rabbit IgG, Jackson, ImmunoResearch and AffiniPure Goat Anti-Rabbit IgG, Jackson, ImmunoResearch) were patterned on silicon chips coated with poly(DMA-NAS-MAPS) by means of SciFlexArrayer S5 spotter from Scienion (Berlin, Germany), together with a reference antibody labeled with Cyanine 5 (AffiniPure Goat Anti-Human IgG, Jackson, ImmunoResearch).

The silicon chips, 15x15 mm substrates were coated before spotting by immersion for 30 minutes in a 0.9 M ammonium sulfate solution containing poly(DMA-NAS-MAPS) at 1% w/v concentration. The chips were left for 20 minutes immersed in the polymer solution and then rinsed with water, dried with nitrogen and finally cured under vacuum at 80°.

The antibodies were spotted in PBS in 84 replicates on the chips in order to create two different subarrays. In the experimental conditions used, the volume of the spotted

drop was 400 pL. The chips were placed in a humid chamber immediately after the spotting and stored overnight at room temperature. After immobilization, the residual active esters on the chip were blocked with 50 mM ethanolamine solution in 1 M Tris/HCl, pH 9, for 1 h, washed with water and dried by a stream of nitrogen. The spotted chips were incubated with a 20 nM solution of QDs conjugated with Streptavidin for 2 hours in dynamic incubation conditions (in a petri dish on a horizontal shaker at 50 rpm), washed with the Washing Buffer (Tris/HCl 0.05 M pH 9, NaCl 0.25 M, Tween 20 0.05% v/v) for 10 min under stirring and finally rinsed with water. As negative control, a spotted chip was incubated with a 20 nM Copoly-QDs solution. Scanning for fluorescence evaluation was performed with a ProScanArray scanner from Perkin Elmer (Boston, MA); silicon chips were analyzed using 70% or 90% Photomultiplier (PMT) gain and laser power ( $\lambda_{em} = 633$  nm). The fluorescence intensities of 84 replicated spots were averaged.

## 4.2.2. RESULTS AND DISCUSSION

### 4.2.2.1. ONE-POT PHASE TRANSFER PROCEDURE

The QDs coating procedure is depicted in **Figure 11**: the nanocrystals are phase transferred and functionalized by a one-pot procedure. Thanks to the amphiphilic character of the copolymer backbone (polyDMA), the colloidal suspension of QDs coated with poly(DMA-NAS-MAPS), Copoly-QDs, is stable in both water and THF. MAPS, with its negative charges, contributes to QDs solubilisation in water, while NAS confers to the QD a reactivity towards biomolecules. Unlike other amphiphilic polymers<sup>15</sup>, the use of poly(DMA-NAS-MAPS) is advantageous as it does not lead to formation of micelles during the phase transfer process.

During the solvent/water phase transfer process, streptavidin is directly conjugated to the active ester groups of the polymer, forming streptavidin functionalized Quantum Dots (SAv-QDs). In fact, coated QDs are extremely reactive towards proteins, thanks to the multiple *N*-hydroxysuccinimidyl ester groups on the polymer chain. Thus, the protein is efficiently immobilized on Copoly-QDs by simple incubation of the nanoparticles with the protein dissolved in phosphate buffer saline. The buffer solution shows a good dispersion ability: a clear and transparent colloidal suspension is obtained, indicating a good QD dispersion during phase transfer and purification.

Commercial CdSe/ZnS QDs of known concentration are precipitated from decane and quantitatively dispersed in chloroform. Lastly, they are phase transferred from chloroform into buffer solution containing streptavidin as described above. The concentration of the semiconductor nanocrystals, after the various steps, is evaluated using a calibration curve obtained with nanoparticles suspension of known concentration. The transfer from chloroform into aqueous solution is assumed to be quantitative. The concentration values determined in this way are perfectly in accordance with NanoSight analysis (*see Materials and Methods, Section 4.2.1.4*), which confirms the assumption of the quantitative phase transfer.

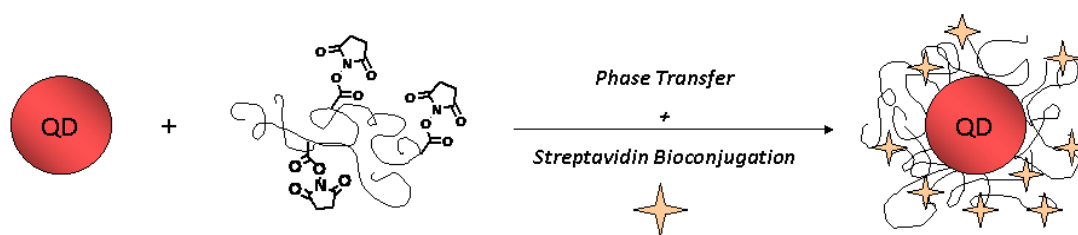


**Figure 11.** Schematic representation of one-pot phase transfer with poly(DMA-NAS-MAPS) of the QDs and their derivatization.

#### **4.2.2.2 CHARACTERIZATION OF COATED AND FUNCTIONALIZED QDs**

The presence of the copolymer on the surface of the nanocrystals is validated by Raman spectroscopy (see Section 1.3); in fact, thanks to the high sensitivity and specificity of this technique, it is possible to reveal little changes on nanoparticles surface. **Figure 12** shows Raman spectra of Copoly-QDs dispersed in water (**A**) and of a solution of the polymer in water (**B**). The spectrum of the polymer coated-QDs shows the characteristic peaks corresponding to the chemical structure of the polymer: amide I band at  $1635\text{ cm}^{-1}$ ;  $\text{CH}_3$  stretching at  $1416\text{ cm}^{-1}$ ; amide III band at  $1348\text{ cm}^{-1}$  and C–C stretching at  $987\text{ cm}^{-1}$

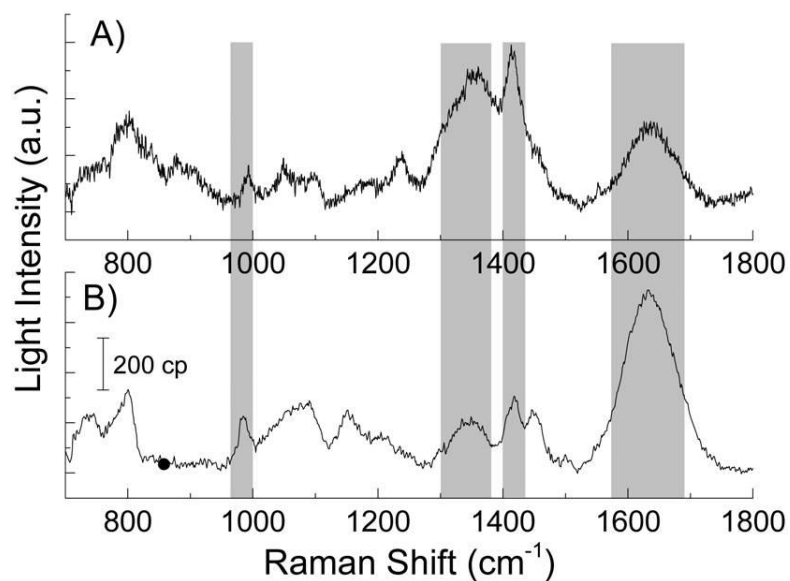


**Figure 12.** Raman spectra of Copoly QDs dispersed in water (A) and of a solution 10 mg/ml of poly(DMA-NAS-MAPS) in water (B). The bands of the chemical groups of the poly(DMA-NAS-MAPS) are shown in **grey**: amide I band at  $1635\text{ cm}^{-1}$ ;  $\text{CH}_3$  stretching at  $1416\text{ cm}^{-1}$ ; amide III band at  $1348\text{ cm}^{-1}$  and C–C stretching at  $987\text{ cm}^{-1}$

### **Optical properties**

Following phase transfer process, functionalization and purification, an extensive physical characterization of the obtained QDs was carried out.

The fluorescence spectra confirms that CdSe/ZnS polymer coated QDs maintain high fluorescence in water, half of the initial fluorescence in chloroform, as shown in **Figure 13a**.

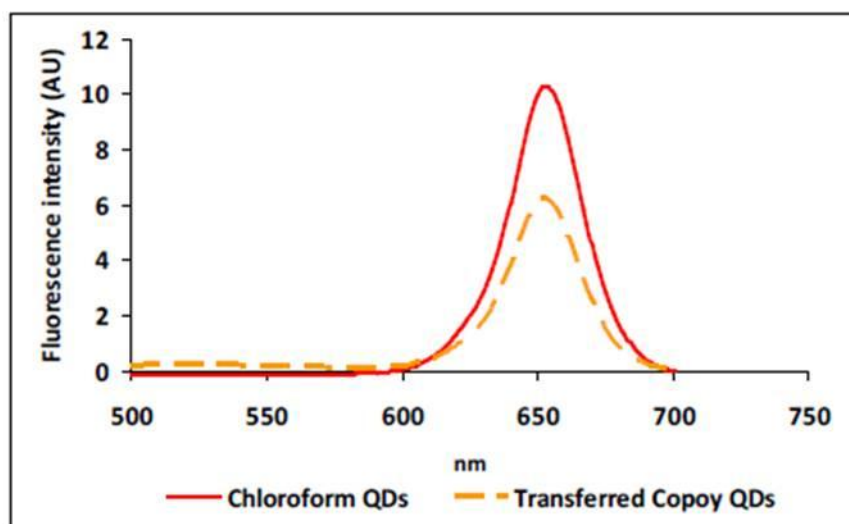


**Figure 13a.** Fluorescence spectra of QDs before (**solid line**) and after (**dotted line**) the phase transfer ( $\lambda_{ex}=475$ ). The coating procedure and the functionalization with streptavidin do not cause a broadening of the emission peak ( $\lambda_{em}=651$ ) and a narrow size distribution is maintained.

A comparison with commercial QDs derivatized with streptavidin, shows that the absorption and emission spectra of polymer coated SAV-QDs are similar to those of commercial streptavidin conjugate QDs. In **Figure 13b**, the absorption and emission spectra of commercial and Copoly-QDs, both functionalized with streptavidin, are shown. Moreover, as it is depicted in **Figure 13c**, only minor changes are observed before and after the protein conjugation to QDs.

The value of the full-width at half maximum (FWHM) of the emission band is  $28 \pm 2$  nm for SAV-QDs, emitting at 651 nm, indicating a narrow size distribution of colloidal suspension. The stability of SAV-QDs is demonstrated by the fact that a good fluorescence is kept over a period of three months (stored at 4 °C), proving that the copolymer coating does not degrade or detach over time.

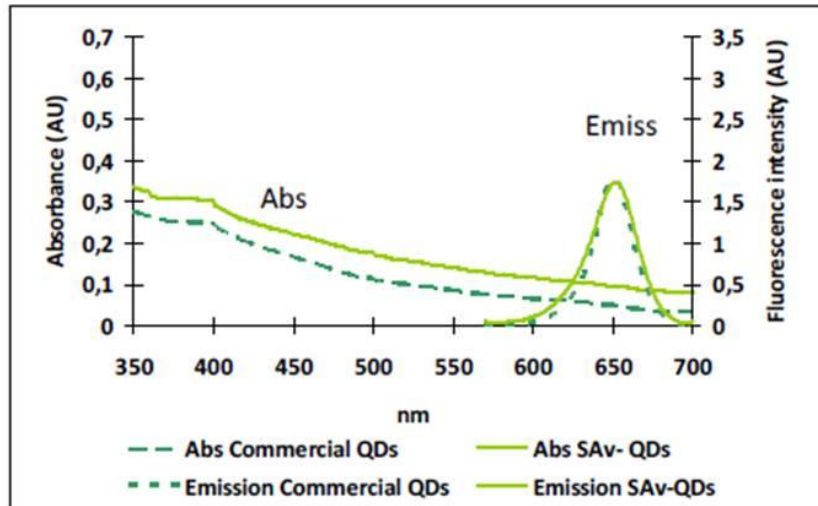


**Figure 13b.** Absorbance spectrum of commercial QDs (**dotted line**) and Copoly-QDs (**solid line**), both coated with streptavidin. The spectra show a weak shoulder at 450nm. Fluorescence spectra of commercial QDs (**dotted line**) and SAV-QDs (**solid line**) are very similar ( $\lambda_{ex}=475$ ). For Sav-QDs only a negligible broadening of the emission peak is shown, proving that QDs CopolyStrep have a narrow size distribution. Solutions are at pH 7 in Incubation Buffer

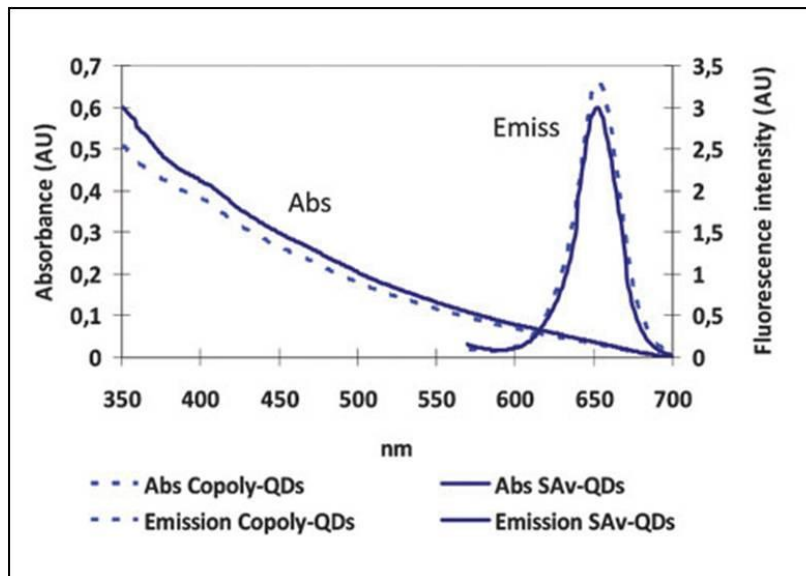


**Figure 13c.** Absorbance spectrum of functionalized QDs (**solid line**) and non functionalized (**dotted line**). No significant differences are detected before and after functionalization. Solutions are at pH 7.0 in Incubation Buffer.

### **Morphology and particle size**

The morphology of coated QDs particles is investigated through Transmission Electron Microscopy (TEM).

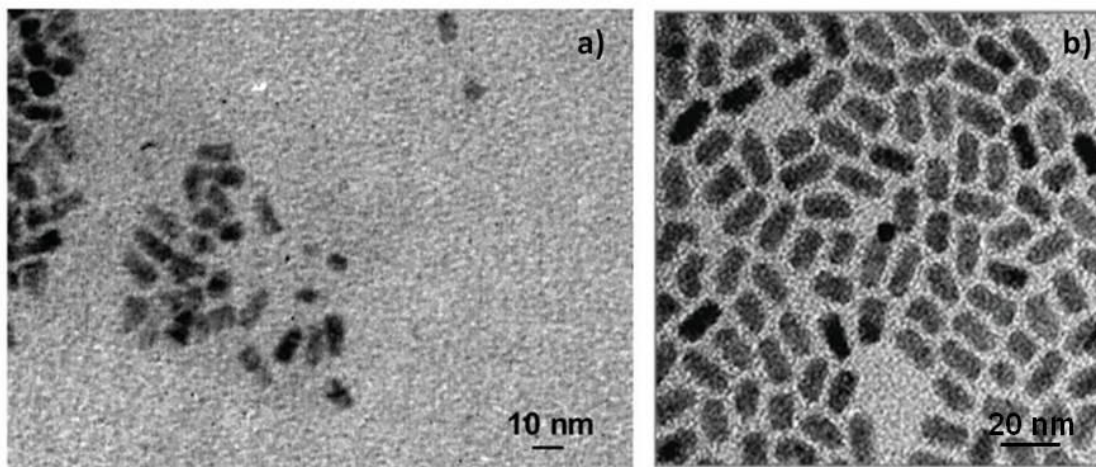


**Figure 14.** (a) TEM analysis of phase transferred QDs reveals a rod-like shape with an average size of about 10 nm, maintaining size and shape similar to that of the organic-soluble QDs (b)

As it is clearly visible in **Figure 14a**, phase transferred QDs have approximately a rod-like shape (aspect ratio 2:1), with an average size of about 10 nm in the longer dimension, maintaining size and shape similar to that of the organic-soluble QDs (**Figure 14b**).

Dynamic Light Scattering (DLS) measurements demonstrate the absence of aggregates, showing a narrow size distribution. The hydrodynamic diameter of SAV-QDs is  $42.7 \pm 2.9$  nm, while that of non-functionalized Copoly-QDs is  $40.4 \pm 8.9$  nm (**Figure 15**). These data suggest that the functionalization does not significantly increase the dimension of the nanocrystals. In addition, the influence of salts concentration on stability is tested by DLS analysis. Also in this case, a narrow distribution is obtained indicating good stability of the colloidal suspension (**Figure 15**).

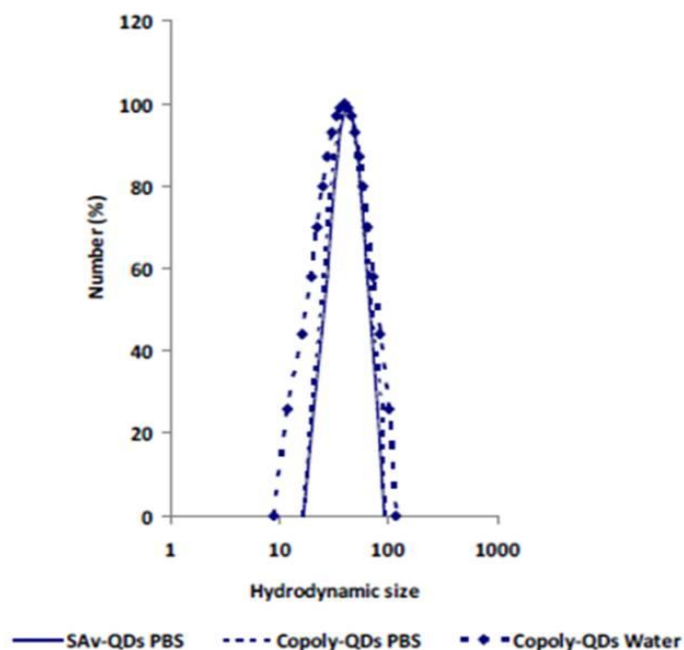


**Figure 15.** DLS of semiconductor nanocrystals in water and buffer solution

Even though Nanoparticle Tracking Analysis (NTA) does not provide absolute values of size for very small nanoparticles, such as those analyzed here, we exploited this technique just to confirm the narrow distribution of SAV-QDs, simply comparing the profile of the commercial functionalized nanoparticles. The size distribution of SAV-QDs is shown in **Figure 16a**. The diameter is  $120 \pm 4,24$  nm (**Figure 16a**), while the commercial QDs show a diameter of  $118 \pm 2.82$  nm (**Figure 16b**): in both cases a similar narrow size distribution is obtained.

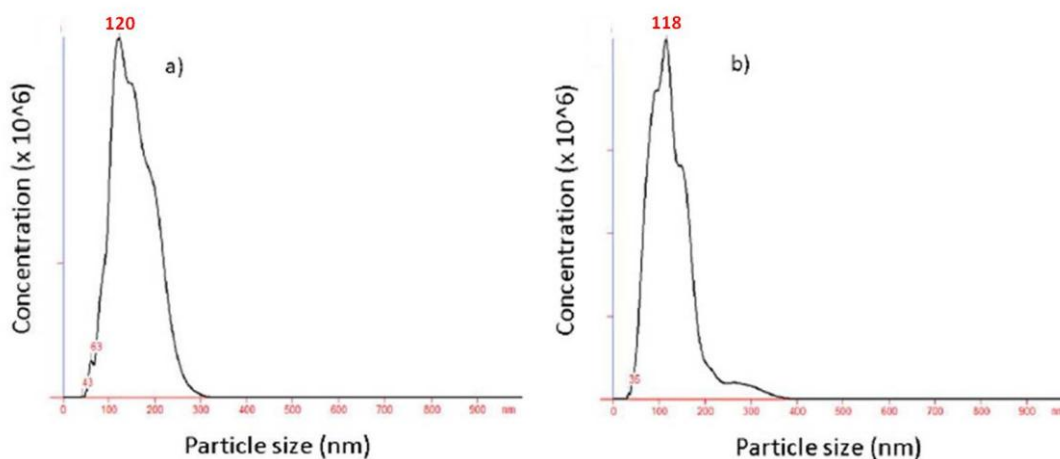


**Figure 16:** Size distribution from NTA measurements of QDs: **a)** in house functionalized QDs and **b)** commercial QDs functionalized with streptavidin.

Since the electrophoretic mobility of molecules in a gel matrix depends on the ratio between the charge and the size of the compounds, it is possible to exploit gel electrophoresis (See *Section 1.3*) to analyze the attachment of ligands onto NPs surface. In fact, the mobility of NPs is altered by the presence of a polymeric coating and/or biomolecules. The mobility of polymer coated QDs (**Figure 17, lane 3**) is compared to those of additionally functionalized with streptavidin (**Figure 17, lane 2**) and of commercial QDs (**Figure 17, lane 1**): SAv-QDs migrate towards the cathode, leading to the formation of a sharp and pronounced band. On the contrary, coated-QDs do not migrate at all.

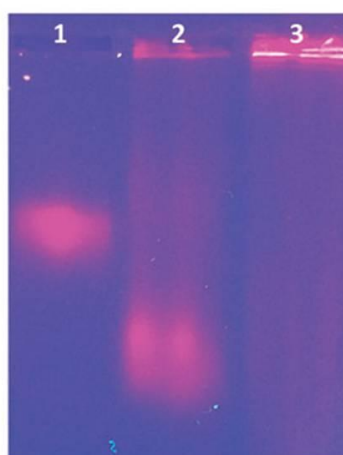


**Figure 17:** Gel electrophoresis of QDs samples in 0.8% agarose. QDs are visualized under UV light. Lane **(1)**: Commercial QDs; lane **(2)**: streptavidin QDs; lane **(3)**: polymer coated QDs.

These data confirm the presence of the protein, bound to the polymeric coating, conferring to QDs a charge and thus electrophoretic mobility. Moreover, the bands of functionalized QDs are isolated and electrophoresed a second time, generating a narrower size distribution and proving the efficient conjugation of the protein to QDs surface.

The good stability and the minimal aggregation of the preparation are confirmed by the zeta potential analysis ( $\zeta$ ) at pH 7. For the functionalized QDs, z-potential value is  $15.25 \pm 6.94$  mV, whereas for the coated particles is  $41.89 \pm 7.72$  mV. Combining these data, we conclude that the protein bound to the polymer contributes to decrease the surface charges of functionalized QDs, resulting in a higher value of  $\zeta$ -potential.

#### 4.2.2.3 APPLICATION OF FUNCTIONALIZED QDs IN A MICROARRAY EXPERIMENT

In order to evaluate the potential of the proposed QDs functionalization method, a simple bioassay experiment is carried out. In this experiment, functionalized QDs are used as fluorescent labels. Two silicon slides are coated with poly(DMA-NAS-MAPS) as illustrated in *Material and Method section*. Then, biotinylated and non-biotinylated (control) Anti-Rabbit IgG antibodies are immobilized in two different subarrays on the coated silicon slides.

The first chip (**Figure 18a**) is incubated with SAV-QDs, whereas the second chip (**Figure 18b**) is incubated just with polymer-coated QDs (non functionalized). Spots of non-biotinylated antibody, in the **bottom frame**, represent additional negative controls. **Figure 18** illustrates a fluorescence image of 84 replicates surrounded by a frame of Cy5 labeled streptavidin (reference spots). An intense fluorescent signal (Relative Fluorescence Intensity (RFI):  $20.156 \pm 1743$ ) is appreciable from the spots of the chip incubated with SAV-QDs (**Figure 18a, upper frame**), whereas no fluorescence signal is detected on the spots of non-biotinylated antibodies (**Figure 18a, bottom frame**), proving a specific interaction of functionalized QDs with biotinylated antibodies. The slide incubated with non-functionalized QDs (just coated) reveals a negligible fluorescence signal (RFI:  $1954 \pm 123$ ) for both subarrays (**Figure 18b**).

The sensitivity and the accuracy of this microarray-based immunoassay are enhanced by the minimisation of non-specific binding between the capture antibodies and QDs.

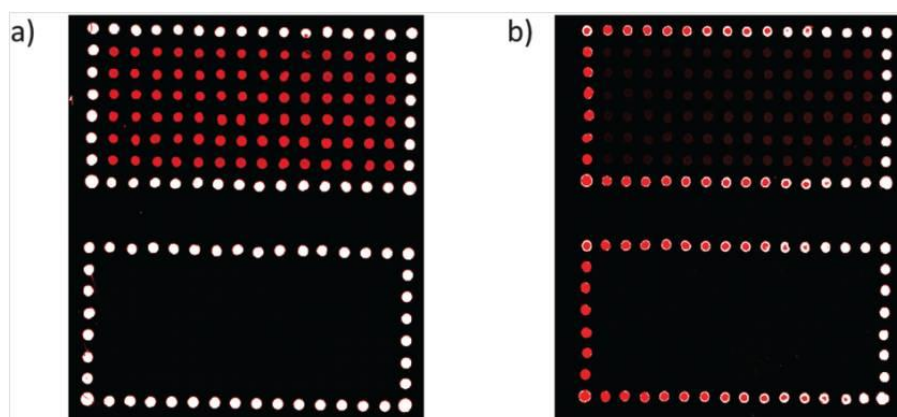


**Figure 18.** Biotinylated antibody (upper subarray) and non-biotinylated antibody (lower subarray) incubated with functionalized QDs (**a**) and QDs coated with the poly(DMA-NAS-MAPS) (**b**). Laser power and PMT were set at 70% of their power.

### 4.2.3. CONCLUSIONS

In conclusion, CdSe/Zns Quantum Dots are successfully phase transferred and functionalized under mild conditions via a robust and efficient one-pot strategy using the functional copolymer poly(DMA-NAS-MAPS). The use of this polymer for this purpose is new, although its application in the field of microarray and microfluidics has been reported previously. Exploiting the active ester groups (NAS) of this polymer, proteins (streptavidin in this case) can be directly bound during QDs phase transfer process. Unlike most of the published methods, the functionalization approach proposed in this thesis does not require coupling agents and/or multistep reactions, which are needed in other common conjugation strategies<sup>16 17</sup>. The extensive physical and functional characterization of the streptavidin-QDs has demonstrated that the phase transfer process leads to a homogeneous and stable QDs preparation that can be exploited as fluorophorescent tags in bioassay experiments, after conjugation with antibodies. Moreover, this robust and simple strategy of conjugation can be extended to the stabilization and functionalization of other kind of nanoparticles, as it will be demonstrated in the next chapter.

### 4.3. BIBLIOGRAPHY

- (1) Sola, L.; Finetti, C.; Gagni, P.; Chiari, M.; Cretich, M.; Nazionale, C.; Molecolare, R. Surface Modifications by Polymers for Biosensing Applications.
- (2) Pirri, G.; Damin, F.; Chiari, M.; Bontempi, E.; Depero, L. E. Characterization of A Polymeric Adsorbed Coating for DNA Microarray Glass Slides. *Anal. Chem.* **2004**, *76* (5), 1352–1358.
- (3) Sola, L.; Chiari, M. Modulation of Electroosmotic Flow in Capillary Electrophoresis Using Functional Polymer Coatings. *J. Chromatogr. A* **2012**, *1270*, 324–329.
- (4) Sola, L.; Chiari, M. Tuning Capillary Surface Properties by Charged Polymeric Coatings. *J. Chromatogr. A* **2015**, *1414*, 173–181.
- (5) Giavazzi, F.; Salina, M.; Cerbino, R.; Bassi, M.; Prospero, D.; Ceccarello, E.; Damin, F.; Sola, L.; Rusnati, M.; Chiari, M.; et al. Multispot, Label-Free Biodetection at a Phantom Plastic-Water Interface. *Proc. Natl. Acad. Sci. U. S. A.* **2013**, *110* (23), 9350–9355.
- (6) Hein, C. D.; Liu, X.-M.; Wang, D. Click Chemistry, A Powerful Tool for Pharmaceutical Sciences. *Pharm. Res.* **2008**, *25* (10), 2216–2230.
- (7) Zilio, C.; Bernardi, A.; Palmioli, A.; Salina, M.; Tagliabue, G.; Buscaglia, M.; Consonni, R.; Chiari, M. New “clickable” Polymeric Coating for Glycan Microarrays. *Sensors Actuators B Chem.* **2015**, *215*, 412–420.
- (8) Platt, G. W.; Damin, F.; Swann, M. J.; Metton, I.; Skorski, G.; Cretich, M.; Chiari, M. Allergen Immobilisation and Signal Amplification by Quantum Dots for Use in a Biosensor Assay of IgE in Serum. *Biosens. Bioelectron.* **2014**, *52*, 82–88.
- (9) B. O. Dabbousi, †; J. Rodriguez-Viejo, ‡; F. V. Mikulec, †; J. R. Heine, §; H. Mattoussi, §; R. Ober, ⊥; K. F. Jensen, ‡,§ and; M. G. Bawendi\*, †. (CdSe)ZnS Core–Shell Quantum Dots: Synthesis and Characterization of a Size Series of Highly Luminescent Nanocrystallites. **1997**.
- (10) Di Corato, R.; Quarta, A.; Piacenza, P.; Ragusa, A.; Figuerola, A.; Buonsanti, R.; Cingolani, R.; Manna, L.; Pellegrino, T. Water Solubilization of Hydrophobic Nanocrystals by Means of Poly(maleic Anhydride-Alt-1-Octadecene). *J. Mater. Chem.* **2008**, *18* (17), 1991.
- (11) Schabas, G.; Yusuf, H.; Moffitt, M. G.; Sinton, D. Controlled Self-Assembly of

- Quantum Dots and Block Copolymers in a Microfluidic Device. *Langmuir* **2008**, *24* (3), 637–643.
- (12) Smith, A. M.; Duan, H.; Rhyner, M. N.; Ruan, G.; Nie, S.; Dubertret, B.; Skourides, P.; Norris, D. J.; Noireaux, V.; Brivanlou, A. H.; et al. A Systematic Examination of Surface Coatings on the Optical and Chemical Properties of Semiconductor Quantum Dots. *Phys. Chem. Chem. Phys.* **2006**, *8* (33), 3895.
- (13) Nann, T. Phase-Transfer of CdSe@ZnS Quantum Dots Using Amphiphilic Hyperbranched Polyethylenimine. *Chem. Commun.* **2005**, No. 13, 1735–1736.
- (14) Finetti, C.; Colombo, M.; Prosperi, D.; Alessio, G.; Morasso, C.; Sola, L.; Chiari, M. One-Pot Phase Transfer and Surface Modification of CdSe-ZnS Quantum Dots Using a Synthetic Functional Copolymer. *Chem. Commun.* **2014**, *50* (2), 240–242.
- (15) Nida, D. L.; Nitin, N.; Yu, W. W.; Colvin, V. L.; Richards-Kortum, R. Photostability of Quantum Dots with Amphiphilic Polymer-Based Passivation Strategies. *Nanotechnology* **2008**, *19* (3), 35701.
- (16) Medintz, I. L.; Uyeda, H. T.; Goldman, E. R.; Mattoussi, H. Quantum Dot Bioconjugates for Imaging, Labelling and Sensing. *Nat. Mater.* **2005**, *4* (6), 435–446.
- (17) Xing, Y.; Chaudry, Q.; Shen, C.; Kong, K. Y.; Zhau, H. E.; Chung, L. W.; Petros, J. A.; O'Regan, R. M.; Yezhelyev, M. V.; Simons, J. W.; et al. Bioconjugated Quantum Dots for Multiplexed and Quantitative Immunohistochemistry. *Nat. Protoc.* **2007**, *2* (5), 1152–1165.

## Chapter 5

# USE OF QUANTUM DOTS AS MASS AND FLUORESCENCE LABELS IN A HIGH-PERFORMING MICROARRAY PLATFORM

### 5.1. LABEL FREE DETECTION: ADVANTAGES AND LIMITATIONS

In the last decade, the amount of information available in the field of medicine and biology has grown exponentially. While the entire human genomic information is readily available, scientists continue to try to understand the vast interconnectivity of gene and regulatory networks. Quantification of multiple biomolecular expression profiles can better illuminate complex biological functions and highly parallel analysis can provide economic advantages. The need for *high-throughput* analysis can be met by combinatorial advancements in computing power, statistical analyses, and multiplexed detection platforms. Multiplex and *high-throughput* methods for detection of protein biomarkers that provide high selectivity and low limits of detection (LOD), are required. (LOD is defined as the minimum concentration of the analyte that the sensor can detect).

Luminescence techniques can present a number of complications caused by labeling. Direct labeling process of the target analyte can be laborious and costly. Furthermore, the presence of the labels can interfere with the target-probe interaction altering the binding affinity from its native state. Although fluorescent labels are widely employed as transducers allowing LODs in the order of  $\text{pM}^{1,2}$  the direct, label free detection of biomarkers is preferable in several applications. A schematic representation of the concept of direct label-free and sandwich label-based assay formats is shown in **Figure 19**.

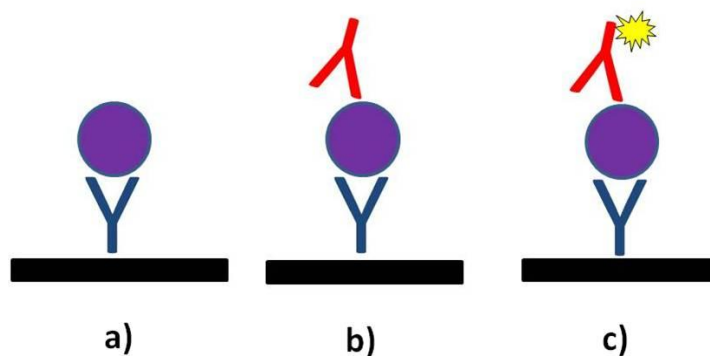


**Figure 19.** Schematic representation of three different detection modalities in traditional sandwich assay format. **a)** Direct analyte label-free capture. The analyte (**purple**) is bound by the capture antibody (**blue**) and directly detected. **b)** Analyte-specific second antibody label-free signal. The analyte is detected through a second antibody (**red**), called detection antibody, which recognizes a different epitope of the analyte captured by the primary antibody. **c)** Label-based detection. The detection antibody is labeled with a fluorophore, enabling the detection by fluorescence.

Ideally, label-free approaches facilitate the simultaneous detection of a high number of biomarkers. However, in the real world, the assay is complicated by the fact that not only the species of interest bind to the biosensor, but also other biomolecules, present in the sample matrix, interact non specifically with the probe on the surface, thus generating a "noise floor" which considerably reduces the sensitivity, an important parameter in developing label-free biosensors to successfully compete with the well-established luminescence-based detection techniques.

Sensitivity of a biosensor can be defined as the magnitude of the signal changes provided by the transduction/detection element in response to changes in the amount of analyte interacting with the biological recognition element. Typically, sensitivity of a sensor is expressed by the limit of detection of the sensor. As mentioned above, LOD is the minimum resolvable signal, e.g. the minimum concentration of the analyte that the sensor can detect, with less than 1 % false positive error. This minimum detectable concentration is a particularly useful parameter because of its clinical relevance. It does not contain any information on the detection mechanism of the sensor and only reports the biological parameter that all sensors are subjected to. Therefore, LOD defined in this manner can be used to compare the performances of different sensors independently of their sensing mechanisms. For example, the minimum detectable

concentration of the analyte can be used to compare a fluorescence-based detection method (**Figure 19, case c**) to a label-free detection method (**Figure 19, case a**).

The performance of a biosensor largely depends on the sensitivity of the sensor. Highly sensitive biosensors are particularly desirable when the amount of analyte is limited. Luminescence-based detection techniques are the gold-standards in biological and medical research fields for biosensing, as they offer very high sensitivity. While label-free sensors present a number of merits over the labeling approach, as mentioned above, their sensitivity is lower than that of luminescence-based detection techniques. Thus, much of the efforts to improve label-free sensors have focused on increasing the sensitivity. Within this context, mass labels can help to overcome the lack of sensitivity of label free methods. In fact, a tag with a large mass, indirectly enhances the mass accumulated on the sensor surface and consequently the intensity of the signal measured by any optical detector, whose functioning principle is the detection of surface refractive index variations. For example, by labeling with a “mass tag” an antibody that recognizes a different epitope of an antigen captured by a primary antibody, an approach similar to traditional sandwich immunoassay is applied, but the final labeling step is eliminated (**Figure 19, case b**). Although in this configuration the technique cannot be defined *label free* anymore, the assay does not require fluorescence detection and all the complications connected with the detection of fluorescence are eliminated. As it will be demonstrated in the next paragraphs, this detection modality offers significant advantages. Inspired by a previous work carried out at CNR, which demonstrated sensitivity enhancement in label free protein detection by using Quantum Dots as mass labels in a technology, called Dual Polarization Interferometry (DPI)<sup>3</sup>, we propose to extend the use of these nanoparticles in another bio-mass detection platform, called Interferometric Reflectance Imaging Sensor (IRIS). As stated by IRIS inventors<sup>4</sup>, this platform lacks of the sensitivity required to measure surface mass variations induced by antigens due to the small molecular weight of these proteins in comparison to antibodies. An example of optimization of label free detection sensing was given by Ahn et al. who showed that cytokine detection by IRIS, requires the use of a secondary antibody that recognizes a different epitope of the cytokine<sup>4</sup>. When the secondary antibody was used as a mass tag, a 7-fold sensitivity enhancement was obtained.

In this thesis we demonstrate the efficacy of a QD mass label strategy to further enhance sensitivity in IRIS and discuss the advantages of this label when used with an interferometric detection platform as well as in fluorescence detection. In fact, it is well known that Quantum Dots are suitable labels, which can be employed instead of the common fluorophores. Ute Resch-Genger et al.<sup>5</sup> describes exhaustively the properties of organic dyes and QDs, remarking the unique physical properties of these nanocrystals such as photostability, wide excitation band, narrow emission peak, tunable spectral range and brightness, characteristics that can be exploited to overcome the limitations of traditional fluorophores. For instance, common fluorophores lose fluorescence quickly when irradiated by a laser due to the well known *photobleaching phenomenon*, whereas QDs possess photochemical stability. The use of QDs in microarray technology has become widespread<sup>6 7</sup>. Morales-Narvaez et al.<sup>8</sup> compared the performance of CdSe/ZnS QDs with the fluorescent dye Alexa 647 as fluorescent tags in a sandwich immunoassay microarray to detect ApoE, a potential biomarker of Alzheimer's disease. The authors compare their results with those provided by a conventional ELISA assay and they obtained a seven-fold enhancement in the limit of detection employing QDs. Moreover, in comparison with Alexa 647 five-fold enhancement was reached.

In this study, we demonstrate that commercial Streptavidin-conjugated QDs can be employed in a dual, label and label free, detection platform, where the QDs act simultaneously as mass and fluorescent labels. Their ability to enhance assay sensitivity, when bound to biotin-modified antibody, is explored in an exemplar assay of  $\beta$ -Lactoglobulin<sup>9</sup>.

## 5.2. MATERIALS AND METHODS

### 5.2.1. Reagents

Phosphate-buffered saline (PBS), Trizma base (Tris), HCl, ethanolamine, sodium chloride, potassium chloride, calcium chloride, magnesium chloride 6-hydrate, sodium bicarbonate, sodium phosphate, bovine serum albumin (BSA), biotin-labeled bovine serum albumin (Bio-BSA), Tween 20, ammonium sulphate, *N*-dimethylacrylamide (DMA), 3-(trimethoxysilyl)propyl methacrylate (MAPS), azoisobutyronitrile (AIBN),  $\beta$ -lactoglobulin from bovine milk,  $\alpha$ -lactalbumin from bovine milk, and streptavidin from *Streptomyces avidinii* (lyophilized powder) were all purchased from Sigma-Aldrich (St. Louis, MO, USA). *N*-acryloyloxysuccinimide (NAS) was synthesized as reported elsewhere<sup>10</sup>. 655 ITK TM Organic Quantum Dots (QD-655) were purchased from Life Technologies.  $\alpha$ -Lactalbumin antibody, bovine  $\beta$ -lactoglobulin antibody, biotin-SP-conjugated AffiniPure Goat Anti-Rabbit IgG, AffiniPure Goat Anti-Rabbit IgG, and Cyanine 3-labeled streptavidin (SA-Cy3), were all obtained from Jackson ImmunoResearch (West Grove, PA, USA). Silicon oxide chips with a 100 nm thermal oxide layer were bought from Silicon Valley Microelectronics (Santa Clara, CA, USA), and IRIS chips patterned with four 500 nm thermal oxide layer subregions were a kind gift from Prof. Selim M. Unlu, Boston University.

### 5.2.2. IRIS Detection Setup

LED-based Interferometric Reflectance Imaging Sensor (IRIS) has been well described as a method to detect accumulated biomass using the shift in spectral reflectance<sup>11</sup>. In summary, the spectral reflectance of biomass on an SiO<sub>2</sub> surface is sequentially sampled at four specific wavelengths, illuminated by an ACULED VHL surface-mount LED package (Perkin-Elmer), which has four independently driven LEDs with peak emission wavelengths of 455nm, 518nm, 598nm, and 635nm. At each wavelength, intensity of reflected light is measured, pixel by pixel, from images taken with a CCD camera. The position of each LED's emission peak, at key positions along the specified SiO<sub>2</sub> reflectance curve (which is thickness-dependent), is critical for detecting a shift in

this curve due to a change in the thickness, i.e. added material. After acquiring images of the substrate for each of the four wavelengths, each pixel of the CCD image provides a measurement of the reflective interference intensity at all four wavelengths. Pixels from the entire sensor are then fitted to a curve derived using the Fresnel equation, which describes the reflection and refraction of light through layers with different refractive index<sup>12</sup>. Fluctuations in light intensity are monitored with an on-chip reference region that is just bare silicon, a non-interfering surface<sup>13</sup>. After fitting every pixel in the image, the surface topography of the sensor's surface is presented in a greyscale image, where brighter regions indicate greater thickness on the surface. To determine optical spot heights, the average value from pixels in a background region around the spot is subtracted from the average value of pixels inside the spot. To eliminate dirt and other particles from averages, pixels more than one standard deviation are automatically eliminated from the calculations<sup>4</sup>. This optical spot height has been calibrated for several common microarray materials to convert the data into a surface density information. Previously reported values demonstrate that 1 nm of optical thickness correlate to 1.21 ng/mm<sup>2</sup> of BSA, 1.28 ng/mm<sup>2</sup> of IgG, and 0.8 ng/mm<sup>2</sup> of DNA<sup>14</sup>.

### 5.2.3. $\beta$ -Lactoglobulin assay

In label-free IRIS and fluorescence assays, all proteins were spotted by means of a SciFlexArrayer S5 spotter from Scienion (Berlin, Germany) on 15 X 15 mm silicon chips, coated before spotting with poly(DMA-NAS-MAPS) as reported in the previous Chapter (**Section 4.2.1.5**). A 500 nm oxide layer was patterned so to define four sub-regions on the chips surface as shown in Figure 21. Four hundred  $\mu$ L of each species were spotted from recommended buffers with at least 7 replicates on each chip. Ahn et al.<sup>4</sup> recommend PBS as the best buffer for sensitive mass measurements, as it promotes protein binding while minimizing etching of the SiO<sub>2</sub> surface. For oligomer spots, the authors recommend 150 mM phosphate buffer. Printed chips were placed in a humid chamber and incubated at room temperature overnight. The chips were then blocked with 50 mM ethanolamine solution in 1M TRIS/HCl, pH 9, for 1h, rinsed with distilled water, and dried under a stream of nitrogen gas.

$\beta$ -Lactoglobulin,  $\alpha$ -lactalbumin (negative control), both at 1 mg/mL, and Cyanine 3-labeled streptavidin at 2  $\mu$ g/mL concentration were patterned, as described above, in 14 spot replicates per protein. The chips were then incubated with anti bovine  $\beta$ -lactoglobulin antibody at varying concentrations in the incubation buffer (Tris/HCl 0.05M pH 7.6, NaCl 0.15M, Tween 20 0.02%). For detection limit experiments, 6 chips were incubated for 2h in dynamic conditions with anti- $\beta$ -lactoglobulin antibody at 10, 5, 2, 1, 0.5 and 0 ng/mL in incubation buffer (Tris/HCl 0.05M pH 7.6, NaCl 0.15M, Tween 20 0.02%) with 1% (w/v) BSA. These antibody concentrations were optimized to simulate a clinical range of relevance.

After incubation with the primary antibody, the chips were washed with the washing buffer (0.05 M Tris/HCl pH 9, 0.25 M NaCl, 0.05% v/v Tween 20) for 10 min on a lab shaker, rinsed with water, and incubated for 2h in dynamic conditions with the biotin-labeled secondary antibody (biotin-SP-conjugated AffiniPure Goat Anti-Rabbit IgG) at 1  $\mu$ g/ml in PBS for 1h. Chips were then washed with PBS (pH 7.2) and water for 10min each and, finally, incubated with 100  $\mu$ L of a non limiting concentration of 15 nm Quantum Dots conjugated with Streptavidin (SAv-QDs) in PBS to saturate the bound probes. Chips were washed again with PBS for 10 min each then dip rinsed in water and dried under N<sub>2</sub> gas.

Fluorescence was determined by a ProScanArray scanner (PerkinElmer, Boston, MA), and silicon chips were analysed with a 633 nm laser at constant laser power and photomultiplier gain. The fluorescence intensities as well as the mass signals of 14 replicate spots were averaged.

IRIS images were acquired and fitted with Zoiray Acquire software (Zoiray, Boston USA). For each protein, signals from 6 to 14 replicate spots were averaged using MGrid spot finding software provided as a kind gift by Prof. Selim Ünlü.

In order to determine the limit of detection (LOD), the concentrations of antibody used were plotted versus the intensities of the corresponding detected fluorescence and mass signal, respectively. The values were fitted with a linear regression and the limit of detection (LOD) was taken to be three standard deviations above the blank signal, i.e. at zero analyte concentration. The corresponding analyte concentration was interpolated from the slope of the linear regression corresponding to this value. T-test and Anova were performed to confirm the linear regression.

## 5.3. RESULTS AND DISCUSSION

### 5.3.1 INTERFEROMETRIC REFLECTANCE IMAGING SENSOR (IRIS)

The laboratory of ICRM-CNR, which has hosted this project, has established a collaboration with the group of Professor Selim Ünlü at Boston University. This group has introduced a label free technology called Interferometric Reflectance Imaging Sensor (IRIS), for the high-throughput screening of biomolecular interactions on a solid surface. As it is illustrated in **Figure 20**, this technique is based on the principle of optical interference. In particular, the technique quantifies the shifts in the spectral reflectance signature to measure the added biomass gathered on each spot, by sampling light reflections at four different wavelengths, using a multiple discrete LED sources and collecting the characteristic reflection intensities using a CCD camera<sup>12</sup>. In fact, by adding biomass on the surface (e.g. biomolecules), the LED-IRIS quantifies the optical thickness increase (nm), indirectly providing the actual surface-adsorbed mass density ( $\text{ng}/\text{mm}^2$ ). (For the details see Section: 5.2.2 “IRIS Detection Setup”).

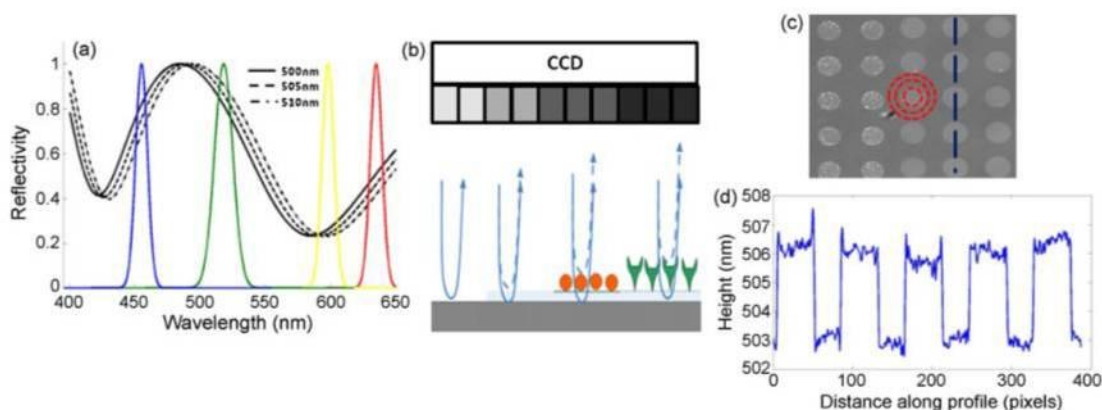


**Figure 20.** Method of detection: (a) shift of the reflectivity curve due to 5 nm step increases in thickness on the surface. The colored Gaussians represent the 4 LEDs used to sample the curve. (b) Scheme of the sensor's imaging path illustrating biomass accumulation dependent grayscale intensity changes. (c) Example of the sensor's surface with an array of protein spots. (d) Height profile along the dashed line in (c) across spots.

IRIS technique requires a specific support for *high-throughput* and multiplexed detection: a thermally grown 500 nm silicon oxide, ( $\text{SiO}_2$ ) layered biochip (**Figure 21, a**). To keep the simplicity of the system without sacrificing sensitivity, a non-interfering region, i.e. a region etched to the bare silicon (**b**), is included on the support and used as reference <sup>13</sup>.

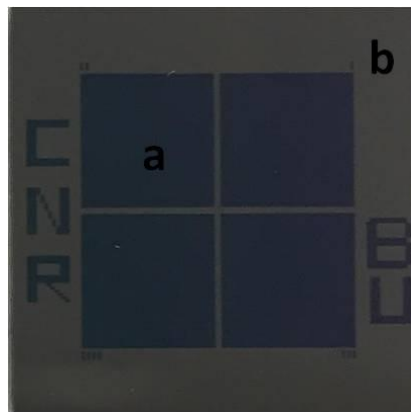


**Figure 21.** Silicon chip used for IRIS detection: **a**) region of 500 nm silicon oxide layer thickness **b**) non-interfering reference region

Furthermore, as it has been anticipated in *Section 3.3 (“Silicon Surface for microarray”)*, the silicon technology and the modulation of the oxide layer provide the possibility to manufacture supports with areas bearing both 100 and 500 nm silicon oxide layers. This platform, called Calibrated Fluorescence Enhancement (CaFE), illustrated in **Figure 22**, provides the sensitivity of fluorescence combined with the quantitative accuracy of label-free detection through the quantification of the amount of biomass accumulated on the surface. In particular, the 100 nm silicon oxide area allows to enhance fluorescence detection by constructive interference, whereas the 500 nm provides the optimal thickness for label-free detection (**Figure 22**). Through the constructive interference between the incident and reflected waves of the

fluorescence radiation, a 5 to 10-fold enhancement of surface fluorescence signal is achieved on the 100 nm oxide region, providing higher sensitivity in analytes detection, compared to those of commercial glass slides.

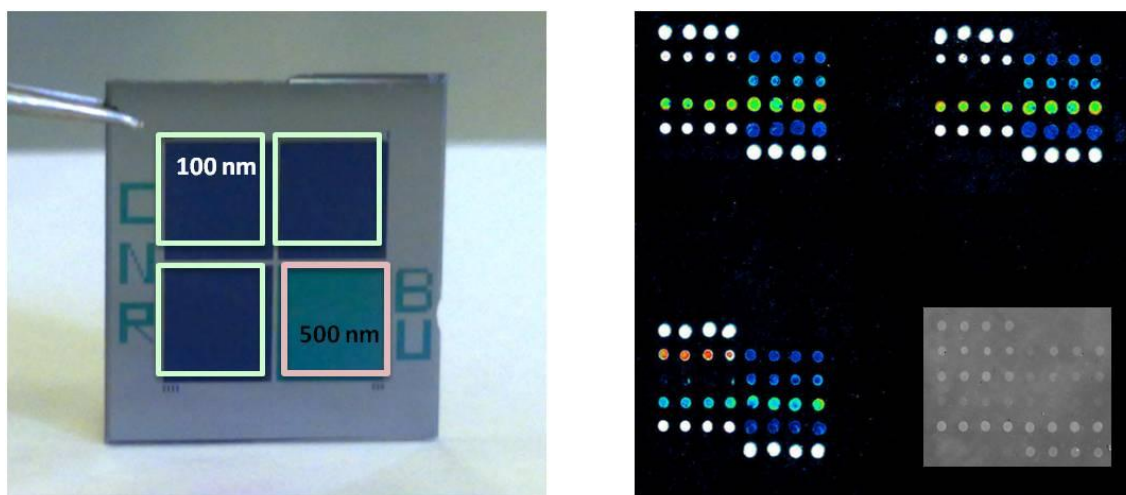


**Figure 22.** Dual-detection scheme. Each quarter of the chip is spotted with the same protein array within the same spotting session. The 100 nm silicon oxide area enables the fluorescence detection, while the 500 nm square allows the label-free modality detection.

The optical properties of the silicon/silicon oxide layered chips are not appreciably altered by polymeric coatings with nanometric thickness, such as the poly(DMA-NAS-MAPS), which confers to the surfaces optimal binding specificity, thus leading to a high signal-to noise ratio<sup>15</sup>. In addition, the techniques chosen for both substrate production and surface modification are simple, cheap and amenable to mass production.

The dual, label and label-label free detection scheme is extremely advantageous during assay development allowing to determine spot morphology and surface probe density in a single experiment. Generally, glass microarrays do not provide this information, which is decisive for studying the quality of the spotted array.

### 5.3.2 QUANTUM DOTS AS MASS TAG AND FLUORESCENT LABELS IN $\beta$ -LACTOGLOBULIN IMMUNOASSAY

In this work, streptavidin conjugated Quantum Dots (SAv-QDs) with a fluorescent emission peak at 655 nm were employed. They have an ellipsoidal shape with major axis of 15 nm and minor axis of 8 nm. In the presence of a protein coating their overall diameter can be approximately 20 nm. QDs are useful labels in biosensing as they provide a large detectable mass as well as an intense fluorescent emission peak at 655 nm. They have been used in microarrays to extend the dynamic range of the technique and increase assay sensitivity<sup>8 16</sup>. In this study, SAv-QDs are used as high-powered labels for the detection of antibodies against  $\beta$ -lactoglobulin, a common milk allergen, chosen as an example of immunoassay microarray. The assay is schematically represented in **Figure 23**.

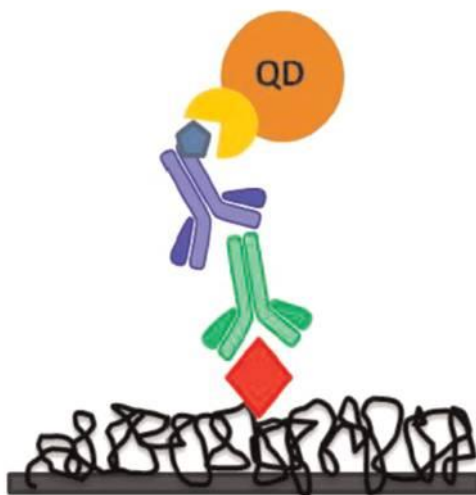


**Figura 23.**  $\beta$ -lactoglobulin (red) is spotted on IRIS coated chip (black). Then, the chip was incubated with the antibody against  $\beta$ -lactoglobulin (primary antibody, Ab 1°, green). The incubation of the Ab 1° was followed by an incubation with a secondary biotinylated antibody (Ab 2°, blue) and finally with streptavidin-conjugated QDs (SA-QDs, orange).

In particular,  $\beta$ -lactoglobulin and  $\alpha$ -lactalbumin (negative control) are immobilized on poly(DMA-NAS-MAPS) coated Si/SiO<sub>2</sub> of 500 nm slides, and the chips are blocked as described in the *Materials and Methods Section*. As illustrated in **Figure 24**, IRIS images are taken at each assay step. A first incubation of the spotted chip with different concentrations of the primary antibody (anti  $\beta$ -lactoglobulin IgG) is carried out; the incubation of the primary antibody is followed by the incubation with a secondary antibody (biotinylated anti IgG) and, finally, with SA-QDs.

IRIS provides information on the mass increase. At the same time, the specificity of the antibody signals is demonstrated by the absence of mass increase on the negative control  $\alpha$ -lactalbumin antigen (not shown). The immobilized allergen is incubated with solutions containing four concentrations of the primary antibody (0 ng/mL as negative control, 0.5, 2, 20 and 200 ng/mL). As shown in **Figure 24**, the incubation with the secondary antibody does not provide a detectable signal up to a concentration of 200 ng/mL (**Figure 24, image a**) unless a QD mass tag is used as label. In fact, the amplification effects of the SA-QDs is clearly observable in **Figure 24, image b**. The mass on the surface increases up to 4-fold for certain concentrations, compared to the negligible enhancement due to the biotinylated antibody.

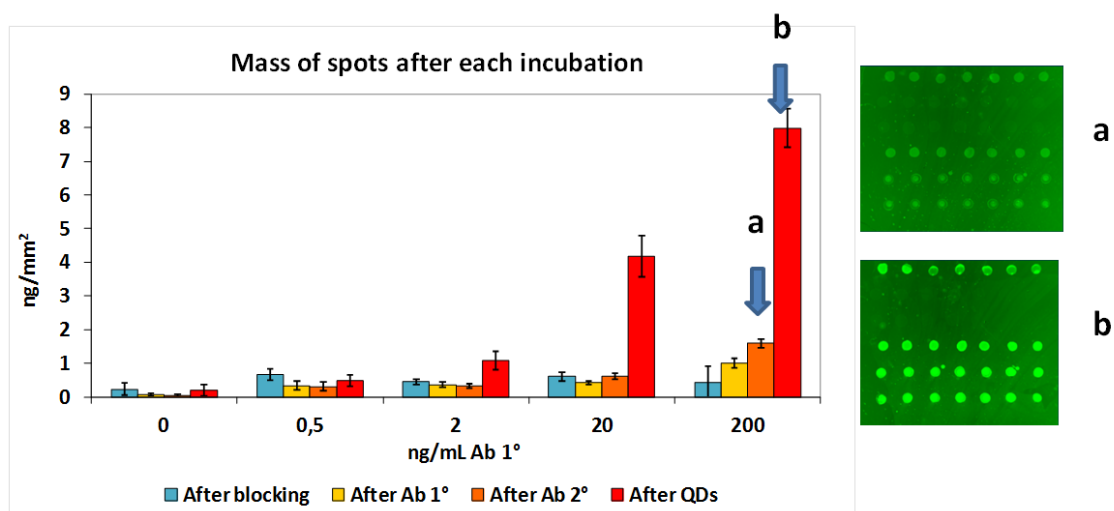


**Figure 24:** Several concentration of the primary antibody are tested. IRIS images are taken after each incubation step, and each addition of biomass is recorded. The mass of the SA-QD layer is taken as the difference between the mass after the secondary antibody and the mass after SA-QD incubation. **Image a** is taken after the incubation with the secondary antibody, **Image b** is taken after the incubation of QDs. In this case, the fluorescence signal from the spots has considerably increased by the addition of the particles.

Thanks to this amplification step, the LOD (limit of detection) of the primary antibody is significantly reduced: plotting detected mass signal versus antibody concentration (10, 5, 2, 1, 0.5 and 0 ng/mL) and fitting the values with a linear regression, a LOD of 10.6 ng/mL is obtained, in label-free conditions, using only the secondary antibody as mass tag. This value is reduced to 0.81 ng/mL with SAV-QD mass tags. The advantage of employing QDs as mass label over only the secondary antibody is clearly demonstrated by the gained sensitivity.

One of the reasons of the failure of the assay to detect low concentrations of antibody in its pure label free format, could be the desorption of antigen probes from the surface when they are incubated with antibodies during the incubation phase. This undesirable phenomenon is discussed by Ahn et al.<sup>4</sup> The authors of this study suggest to use secondary antibodies as tags to enhance the mass signal. Suitable sensitivity in the detection of cytokines is achieved in Ahn's work simply using a secondary antibody as mass tag<sup>4</sup>. However, in that work, the measurement is carried out in real time in a flow cell. Therefore, the authors are able to take into account the mass loss, due to desorption, during the incubation step, normalizing each spot density to its original mass. The majority of microarray platform are not able to establish desorption kinetics, because measurements are conducted end point in dry conditions. In this work, it is possible to avoid elaborate desorption calculations thanks to the large detectable mass of QDs, which compensate for the possible loss of material from the surface.

In this first part of the work, the efficacy of a Quantum Dot mass label strategy to enhance sensitivity in the interferometric technique IRIS is demonstrated.

In order to assess the potential of QDs in fluorescent detection, the same chips are imaged with a fluorescence scanner and the specific interaction of SAV-QDs with biotinylated antibodies is demonstrated by the absence of fluorescence signal on spots of  $\alpha$ -Lactalbumin allergen. Regarding sensitivity, it is demonstrated that QDs are advantageous fluorescent tags in microarray technology. Even though they are not excited at their ideal wavelength (633 nm), since commercial scanners are optimized for cyanine dyes, a LOD of 0.020 ng/mL is obtained indeed. Combining the two modes,

the dynamic range of this assay is therefore extended from 0.02 ng/ml to 10 ng/mL.

**Figure 25** reports the calibrations curves obtained with mass and fluorescence labels.

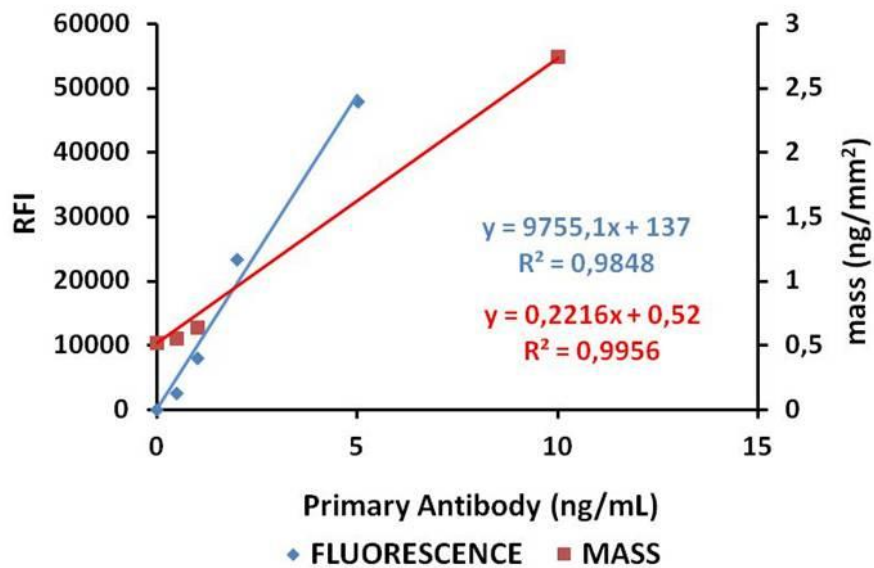


**Figure 25.** Dose-response curves for fluorescence and IRIS immunoassay used to extrapolate the LODs in the two detection modes.

### **5.3.3. CALCULATION OF QUANTUM DOTS MONOLAYER**

Since, in microarray experiments, mass accumulation is limited by the available binding sites on the surface, it is desirable for each binding event to capture a large mass. Platt et al.<sup>3</sup> demonstrate the efficacy of Streptavidin-conjugated QDs-655 as mass labels in the detection of biomolecules using Analight Bio200 (Farfield, UK), a commercial platform based on Dual Polarization Interferometry (DPI), which allows to detect the mass that accumulates on the surface, measuring refractive index changes. In particular, they calculate that the surface density of a saturated monolayer of SAV-QDs is  $6.19 \text{ ng/mm}^2$ , while that of a saturated monolayer of streptavidin is  $2.30 \text{ ng/mm}^2$ . Therefore, starting from the information provided in Platt's article about the mass needed to form a monolayer, we have calculated the percentage of surface occupancy for each surface densities measured. In **Figure 26**, the concept is schematically shown: a 50% decrease in surface accumulation yields 50%, i.e. half of a SAV-QD monolayer. From the mass accumulation due to QDs, a density is calculated for each concentration of secondary antibody. At  $200 \text{ ng/mL}$ , a surface density of  $6.40 \text{ ng/mm}^2$  is found. This value indicates the formation of a monolayer of QDs closely agreeing with Platt's. It is worth noting that, although these methods are based on similar principals, DPI measures biomass accumulation in wet conditions, whereas the mass change is measured here in dry conditions, which corroborates the two techniques.

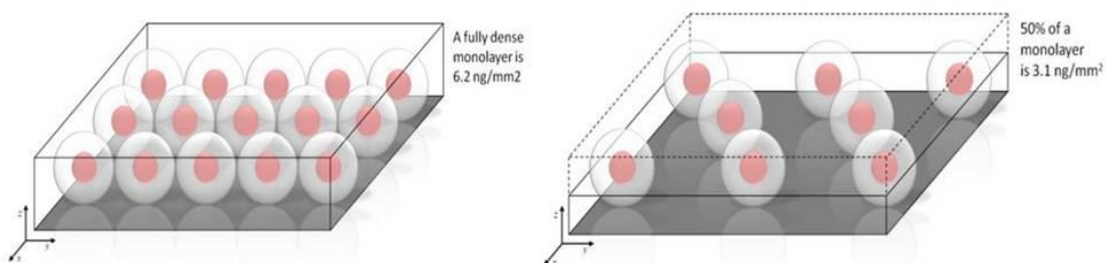


**Figure 26.** At high concentrations of analyte, SAV-QDs saturate the surface, generating a monolayer with a surface density of  $6.2 \text{ ng/mm}^2$ . At lower concentrations, it is possible to calculate a percentage of a monolayer.

## 5.4 CONCLUSIONS

The possibility of using QDs as mass and fluorescent label at the same time to enhance sensitivity in both label and label-free technology is demonstrated. This is possible thanks to the development of a label-free technique, called IRIS, which requires Si/SiO<sub>2</sub> chips as supports. IRIS chips can be employed for a dual detection modality: the quantification of the mass (label-free) and the fluorescence of detection. Combining the two modes, the dynamic range of the assay is considerably expanded. Moreover, in accordance with Platt et al., who measured the mass accumulation of QDs that leads to formation of a fully saturated monolayer using DPI, we calculated the maximum enhancement in mass that can be reached in IRIS and we obtained 6.2 ng/mm<sup>2</sup>, a value that corresponds to the mass of a SAV-QDs monolayer found by Platt and co-workers.

## 5.5 BIBLIOGRAPHY

- (1) Schweitzer, B.; Kingsmore, S. F. Measuring Proteins on Microarrays. *Curr. Opin. Biotechnol.* **2002**, *13* (1), 14–19.
- (2) Lashkari, D. A.; DeRisi, J. L.; McCusker, J. H.; Namath, A. F.; Gentile, C.; Hwang, S. Y.; Brown, P. O.; Davis, R. W. Yeast Microarrays for Genome Wide Parallel Genetic and Gene Expression Analysis. *Proc. Natl. Acad. Sci. U. S. A.* **1997**, *94* (24), 13057–13062.
- (3) Platt, G. W.; Damin, F.; Swann, M. J.; Metton, I.; Skorski, G.; Cretich, M.; Chiari, M. Allergen Immobilisation and Signal Amplification by Quantum Dots for Use in a Biosensor Assay of IgE in Serum. *Biosens. Bioelectron.* **2014**, *52*, 82–88.
- (4) Ahn, S.; Freedman, D. S.; Massari, P.; Cabodi, M.; Ünlü, M. S. A Mass-Tagging Approach for Enhanced Sensitivity of Dynamic Cytokine Detection Using a Label-Free Biosensor. *Langmuir* **2013**, *29* (17), 5369–5376.
- (5) Resch-Genger, U.; Grabolle, M.; Cavaliere-Jaricot, S.; Nitschke, R.; Nann, T. Quantum Dots versus Organic Dyes as Fluorescent Labels. *Nat. Methods* **2008**, *5* (9), 763–775.
- (6) Nichkova, M.; Dosev, D.; Davies, A. E.; Gee, S. J.; Kennedy, I. M.; Hammock, B. D. Quantum Dots as Reporters in Multiplexed Immunoassays for Biomarkers of Exposure to Agrochemicals. *Anal. Lett.* **2007**, *40* (7), 1423–1433.
- (7) Sapsford, K. E.; Spindel, S.; Jennings, T.; Tao, G.; Triulzi, R. C.; Algar, W. R.; Medintz, I. L. Optimizing Two-Color Semiconductor Nanocrystal Immunoassays in Single Well Microtiter Plate Formats. *Sensors (Basel)*. **2011**, *11* (8), 7879–7891.
- (8) Morales-Narváez, E.; Montón, H.; Fomicheva, A.; Merkoçi, A. Signal Enhancement in Antibody Microarrays Using Quantum Dots Nanocrystals: Application to Potential Alzheimer’s Disease Biomarker Screening. *Anal. Chem.* **2012**, *84* (15), 6821–6827.
- (9) Finetti, C.; Plavisch, L.; Chiari, M. Use of Quantum Dots as Mass and Fluorescence Labels in Microarray Biosensing. *Talanta* **2016**, *147*, 397–401.
- (10) Pirri, G.; Damin, F.; Chiari, M.; Bontempi, E.; Depero, L. E. Characterization of A Polymeric Adsorbed Coating for DNA Microarray Glass Slides. *Anal. Chem.* **2004**, *76* (5), 1352–1358.
- (11) Daaboul, G. G.; Vedula, R. S.; Ahn, S.; Lopez, C. A.; Reddington, A.; Ozkumur, E.; Ünlü, M. S. LED-Based Interferometric Reflectance Imaging Sensor for Quantitative Dynamic Monitoring of Biomolecular Interactions. *Biosens. Bioelectron.* **2011**, *26* (5), 2221–2227.
- (12) Avci, O.; Ünlü, N. L.; Özkumur, A. Y.; Ünlü, M. S. Interferometric Reflectance

Imaging Sensor (IRIS)--A Platform Technology for Multiplexed Diagnostics and Digital Detection. *Sensors (Basel)*. **2015**, *15* (7), 17649–17665.

- (13) Vedula, R.; Daaboul, G.; Reddington, A.; Özkumur, E.; Bergstein, D. A.; Ünlü, M. S. Self-Referencing Substrates for Optical Interferometric Biosensors. *J. Mod. Opt.* **2010**, *57* (16), 1564–1569.
- (14) Ozkumur, E.; Needham, J. W.; Bergstein, D. A.; Gonzalez, R.; Cabodi, M.; Gershoni, J. M.; Goldberg, B. B.; Unlü, M. S. Label-Free and Dynamic Detection of Biomolecular Interactions for High-Throughput Microarray Applications. *Proc. Natl. Acad. Sci. U. S. A.* **2008**, *105* (23), 7988–7992.
- (15) Cretich, M.; Di Carlo, G.; Longhi, R.; Gotti, C.; Spinella, N.; Coffa, S.; Galati, C.; Renna, L.; Chiari, M. High Sensitivity Protein Assays on Microarray Silicon Slides. *Anal. Chem.* **2009**, *81* (13), 5197–5203.
- (16) Ludwig, S. K. J.; Tokarski, C.; Lang, S. N.; van Ginkel, L. A.; Zhu, H.; Ozcan, A.; Nielen, M. W. F. Calling Biomarkers in Milk Using a Protein Microarray on Your Smartphone. *PLoS One* **2015**, *10* (8), e0134360.

## Chapter 6

### **CLICK CHEMISTRY FUNCTIONALIZATION OF POLYMER COATED GOLD NANOPARTICLES**

The conjugation of proteins and other biomolecules to the surface of gold nanoparticles (AuNPs) has gained increasing attention in the last years. Several strategies of surface AuNPs functionalization are reported in the literature<sup>1</sup>. Non-covalent modes have several major weaknesses; these include the necessity of a high concentration of antibodies for the preparation of antibody–gold particle conjugates, random orientation of antibodies at the gold nanoparticle surface, and due to their electrostatic attraction they are making the biological response difficult to control; the binding is impressed by changes in pH, and ultimately because antibodies are non-covalently conjugated to nanoparticles; they can be replaced by other molecules in biological samples.

Covalent modes are also used to bind functionalized groups to gold nanoparticle surface. The most direct covalent approach involves strong Au-S bonds with organothiols, disulfides and cysteine groups. The conjugation with thiol group-containing bio-molecules such as antibodies, and other biomolecules is a well-established route: the covalent bond occurs between the gold nanoparticle and free sulfhydryl groups of the antibody<sup>1</sup>. The attachment of biomolecules via thiol linkage to gold nanoparticles is much stronger than direct adsorption described above.

Another commonly adopted strategy implies the coating of NPs with polymers. Thiolated PEGs, modified with a carboxyl group and activated via EDC/NHS reaction, are widely used to this purpose, however they suffer from several drawbacks. In fact, PEG chains have only one carboxyl group per chain which can be activated to provide terminal *N*-hydroxysuccinimide ester groups. Thus, it is difficult to achieve a high immobilization density of biomolecules. Furthermore, these kinds of coupling reactions are often performed in aqueous solutions (pH 6-9) and, under these conditions, the amidization process and the hydrolysis of the ester group are in competition, compromising the efficiency of the reaction. Lastly, chemical reactions between amino

groups and active esters are not regiospecific and do not provide oriented and controlled immobilization of the biomolecules. Click chemistry reactions can overcome all these limitations enabling easy and robust functionalization of nanoparticles (*Section 2.2*).

The advantages of employing synthetic functional copolymers to carry out stabilization and functionalization of nanoparticles have been already discussed in *Section 4.2.*, where poly(DMA-NAS-MAPS) was used for the straightforward phase transfer and functionalization of QDs in a one-pot procedure<sup>2</sup>.

The use of the “clickable” polymer, poly(DMA-PMA-NAS), described in *Chapter 4*, allows to combine the simplicity and robustness of NPs coating process with the advantages of the click chemistry reactions. As described in *Section 4.1*, this copolymer represents an evolution of the parent polymer poly(DMA-NAS-MAPS). Thanks to the replacement of NAS with an alkyne group, the polymer reacts regioselectively with azido modified molecules by Cu(I)-catalyzed azide/alkyne 1,3-dipolar cycloaddition (CuAAC, click chemistry).

In this work, an anti-mouse IgG antibody, modified with azido functionalities, is bound to the surface of gold nanoparticles surrounded by a silica layer. This surface modification approach is used for the covalent binding of antibodies to gold NPs. Antibodies labeled with gold nanoparticles are then used in biosensing<sup>3</sup>.

## 6.1 MATERIAL AND METHODS

### 6.1.1 Reagents

Phosphate-buffered saline (PBS), tris-(hydroxymethyl)aminomethane (Tris), HCl, sodium hydroxide (NaOH), ethanolamine, N,N-dimethylformamide (DMF), sodium chloride (NaCl), sodium phosphate (Na phosphate), bovine serum albumin (BSA), copper(II) sulfate pentahydrate ( $\text{CuSO}_4$ ), L-ascorbic acid (AAC), tris(3-hydroxypropyltriazolylmethyl)amine (THPTA), agarose low gelling temperature, ethylenediaminetetraacetic acid (EDTA), boric acid, Tween20, ammonium sulfate ( $(\text{NH}_4)_2\text{SO}_4$ ), N,N-dimethylacrylamide (DMA),  $\gamma$ -methacryloxypropyltrimethoxysilane (MAPS), azoisobutyronitrile (AIBN), and goat anti-mouse polyclonal IgG (whole molecule) antibody were all purchased from Sigma-Aldrich (St. Louis, MO). N-Acryloyloxy-succinimide (NAS) and 3-trimethylsilyl-prop-2-ynyl methacrylate (protected PMA) were synthesized as reported elsewhere<sup>4</sup>. Rabbit anti-bovine betalactalbumin was purchased from Jackson Immuno Research (West-Grove, PA); purified anti-mouse CD63 was purchased from BioLegend; azido-PEG<sub>8</sub>-N-hydroxysuccinimide ( $\text{N}_3$ -PEG-NHS) ester was purchased from Jena Bioscience (Jena, Germany). Silicon oxide chips with a 100 nm thermal oxide layer were bought from Silicon Valley Microelectronics (Santa Clara, CA); 30 kDa centrifugal filters were purchased from Amicon.

poly(DMA-NAS-MAPS) and poly(DMA-PMA-MAPS) were synthesized as reported in *Chapter 4, Section 4.2.1.2*.

### 6.1.2 Synthesis of Silica Gold Nanoparticles.

A solution (200 mL) of tetrachloroauric(III) acid (0.01% w/v) in water was heated to reflux. Next, 700  $\mu\text{L}$  of trisodium citrate (2%) was added to the solution and left under stirring at 100 °C for a few minutes until the appearance of a deep red color indicated the formation of the nanoparticles. The suspension was left under stirring at 100 °C for further 20 min and then slowly cooled down to room temperature. A very thin layer of

silicon oxide was grown on the surface according to the protocol described by Li et al.<sup>5</sup> A volume of 30 mL of a gold nanoparticles suspension was mixed with 400  $\mu$ L of APTES (1 mM) and left under stirring. After 15 min, 3.2 mL of a sodiumsilicate solution (0.54% w/v), acidified until the pH was <11, was added to the gold nanoparticles. The suspension was left under stirring for 3 min at room temperature and for 35 min in a water bath at 70 °C. To stop the reaction, the gold nanoparticles were moved in a water bath at 4 °C. At last, gold nanoparticles were centrifuged at 3000g for 20 min at 15 °C and resuspended in water.

### **6.1.3 Nanoparticles Coating**

Poly(DMA-PMA-MAPS) was dissolved in DI water to a final concentration of 1%; to this solution, a suspension of AuNPs (0.1 mg/mL) was added and the mixture was gently stirred for 1 h in the dark on a shaker. To remove the polymer excess, the AuNPs suspension was washed two times with DI water and the particles were recovered by centrifugation (10 min at 7000 rpm). After the second washing cycle, the supernatant was discarded and replaced by sodium phosphate buffer (pH 7.4, 50 mM) and the suspension stored at 4 °C.

### **6.1.4 Antibody Derivatization**

An anti-mouse IgG antibody was dissolved in PBS to a final concentration of 5 mg/mL; to this solution, azido-PEG<sub>8</sub>-NHS ester was added to a final concentration of 0.5 mM. The mixture was stirred for 2 h at room temperature. Once the reaction was completed, the azido modified IgG was washed three times by centrifugation on 30 kDa centrifugal filters (10 min at 7000 rpm) to remove residual traces of unreacted azido ester.

### 6.1.5 Functionalization of Gold Nanoparticles

Polymer coated AuNPs were spun down and resuspended in Na phosphate buffer (50 mM pH 7.4); to this suspension, the azido modified antibody (1 mg/ mL), CuSO<sub>4</sub> (100 μM), THPTA (400 μM), and ascorbic acid (6.25 mM) were added. The mixture was then stirred overnight. The antibody-AuNPs suspension was washed three times by centrifugation (10 min at 7000 rpm) to remove residual traces of unreacted azido antibody. To prove that the covalent binding was promoted by the CuSO<sub>4</sub>/THPTA/AAC assisted click reaction, the same procedure was performed without addition of the click catalysts. In this case, the antimouse antibody could only be adsorbed on the polymer coated AuNPs.

### 6.1.6 Nanoparticles Characterization

#### *Morphology*

Transmission electron microscopy (TEM) images of AuNPs were obtained on a “FEI Tecnai G” Spirit BioTWIN microscope (Hillsboro, OR) operating at 120 kV. The samples were prepared by evaporating a drop of nanoparticles onto carbon-coated copper grid (200 mesh) and allowing it to dry on the air. Nanoparticles were sonicated prior to analysis. The histograms of the particle size distribution and the average particle diameter were obtained by measuring about 150–200 particles by using Measure IT Olympus Software.

#### *Particle Size and ζ-Potential Analyses*

Dynamic light scattering (DLS) measurements were performed at 173° with a Zetasizer Nano ZS ZEN3600 from Malvern Instruments Ltd. (Worcestershire, UK) working at 4 mW of a He–Ne laser ( $\lambda = 632.8$  nm). A disposable cuvette with 1 cm optical path length was used for the measurements. The samples were prepared by dilution with Milli-Q water containing 1 mM citrate. Each sample was allowed to equilibrate for 30 s prior to starting measurement. The measurements were performed at 25 °C. The calculations of hydrodynamic diameter were performed using Mie scattering theory, considering absolute viscosity and refractive index values of the medium to be 0.8872

cP and 1.334, respectively. The results are reported in Intensity.  $\zeta$ -Potential measurements were elaborated on the same instrument by electrophoretic light scattering;  $\zeta$ -potential values were automatically calculated from electrophoretic mobility using Zetasizer Software (Malvern Instruments Ltd., Malvern, UK). A viscosity of 0.8872 cP, a dielectric constant of 78.5, and a Henry function of 1.5 were used for the calculations. All measurements were performed in triplicate, and the average values were calculated.

### ***Gel Electrophoresis***

In order to characterize the particles after each derivatization step, 100  $\mu$ L of functionalized and non functionalized gold NPs were loaded on a 0.7% agarose gel in 0.5 $\times$  Tris-borate-EDTA buffer pH 8.8 (TBE: 67 mM tris-(hydroxymethyl)aminomethane, 37 mM boric acid, 1.6 mM EDTA). The separation was run for 60 min at a constant voltage of 100 V.

### ***Optical Properties***

The optical properties of AuNPs, polymer coated AuNPs, and AuNPs functionalized with antibody were assessed by UV-visible spectrometry (spectrophotometer VP-650, Jasco). Before collecting UV-vis spectra (400–700 nm), all sample solutions were sonicated for few seconds in order to minimize aggregation. The plasmon band shift due to the polymer layers deposited on AuNPs and to the subsequent antibody linking was evaluated keeping in consideration the maximum absorption peak of bare AuNPs is 525 nm. The concentration of the AuNPs suspension is expressed in optical density (OD), measured at the maximum absorption peak (525 nm).

### **6.1.7 Bioassay: microarray experiments**

To demonstrate the binding between the antibody and AuNPs, an anti-CD63 mouse antibody, and an anti- $\beta$ -lactoglobulin rabbit antibody (negative control) were patterned on two silicon chips coated with poly(DMA-NAS-MAPS) as reported in *Section 4.2.1.5 of Chapter 4*, by means of a SciFlexArrayer S5 spotter from Scienion (Berlin, Germany). Both, the mouse anti-CD63 capture antibody (20 replicates) and the

rabbit anti- $\beta$ -lactoglobulin antibody (5 replicates), dissolved in PBS, were spotted at a concentration of 1 mg/mL. In the experimental conditions used, the volume of the spotted drop was 400  $\mu$ L. The chips were placed in a humid chamber immediately after the spotting and stored overnight at room temperature. After the immobilization, the residual active esters on the chip were blocked by immersing the chips in a solution of 50 mM ethanolamine in 0.1 M TRIS/HCl, pH 9, for 1 h at room temperature; the chips were then rinsed with DI water and dried with a nitrogen stream. One chip was incubated overnight in a humid chamber with AuNP-labeled anti-mouse antibody (OD = 0.05) in PBS in static incubation conditions. The chip was washed with washing buffer (Tris/HCl 50 mM pH 9, NaCl 0.25 M, Tween 20 0.05% v/v) for 10 min under stirring and finally rinsed with Milli-Q water. A second chip was incubated with the same anti-mouse antibody reacted with AuNPs in the absence of the click catalyst. Both chips were imaged with the Single Particle Interferometric Reflectance Imaging System (SP-IRIS) instrument to detect individual particles of AuNPs bound to the capture surface antibody.

## 6.2. RESULTS AND DISCUSSION

### 6.2.1 COATING OF SILICA GOLD NANOPARTICLES

In this work, 45 nm diameter gold nanoparticles, synthesized by our collaborators at Fondazione Don Gnocchi, (LABION laboratory) according to the commonly used citrate methods developed by Turkevich et al.<sup>6</sup> and Frens et al.<sup>7</sup> are employed. A silica shell is formed by condensation of sodium silicate on the surface of AuNPs, previously treated with APTES as described by Li et al.<sup>8</sup>. The parameters of the condensation reaction (time, pH and temperature) are optimized in order to form a very thin silica layer to maintain the optical properties of the nanoparticles. In fact, as already mentioned in *Chapter 1*, the distinct feature of AuNPs is the strong vibrant color of their colloidal solution that is caused by the Surface Plasmon Resonance (SPR) absorption. The different size of NPs determines the shift of SPR absorption peak to longer wavelength. This is an important parameter that can be exploited to evaluate aggregation of NPs suspension or to confirm the conjugation of biomolecules onto their surface. The AuNPs used in this work have a strong absorption peak at 545 nm which is constantly measured to control the quality of the nanoparticle suspension.

The purpose of this study is to demonstrate that a synthetic functional copolymer, poly(DMA-PMA-MAPS), recently introduced at CNR<sup>9</sup>, represents a convenient method to provide stabilization and functionalization of nanoparticles by a robust and user friendly one-step procedure. Adsorption of poly(DMA-PMA-MAPS) stabilizes the colloidal suspension, whereas the alkyne functions pending from the backbone are available for the reaction with azido modified proteins. The coating procedure is fast, user friendly, environmentally safe and produces particles that are stabilized and functionalized in a single step process.

Although the polymer has been already employed for the functionalization of different kinds of surfaces, especially for the development of glican arrays<sup>9</sup>, its use in context of nanoparticles coating is new and the results obtained very promising.

The coating procedure, schematically depicted in **Figure 27 (a)**, is performed by simply adding the clickable polymer, at low concentration (1% w/v), to the AuNPs aqueous

solution (see *Section 6.1.3, Materials and Methods*, for the details of the procedure). The process entails a simple adsorption step of the polymer onto NPs surface through the poly(DMA) segments followed by silanol condensation promoted by the MAPS monomer, which has a strong affinity for the silica shell of AuNPs. The silane monomer MAPS, reinforces the interaction between AuNPs surface and the poly(DMA) segments of the polymer chain, leading to the formation of a stable nanometric polymer layer which replaces the original citrate layer. The coating procedure, initially developed for flat silicon microarray slides, was optimized taking into account the stability of NPs. The polymer adsorption on a flat surface takes place from a concentrated ammonium sulfate solution (0.9 M). Since the salt reduces polymer solubility and forces the polymer to interact with the surface<sup>9</sup>, this process can not be immediately transferred to NPs as the use of salts causes their aggregation and precipitation during adsorption. Also the drying step, which usually increases the stability of the polymer layer, is avoided because it is incompatible with the colloidal suspension. In this work we demonstrate that the use of high salt concentration and drying are not essential to coat NPs. A coating of excellent stability is obtained also using a simplified process that does not require harsh conditions.

In the step following the polymer coating, the presence of alkyne groups on the surface allows the covalent conjugation of an azido-modified anti-mouse IgG antibody to the AuNPs surface via CuAAC click chemistry reaction (**Figure 27, b**). This step is performed by simply adding the azido-modified antibody to the alkyne-functionalized AuNPs solution in the presence of the reaction catalysts, Cu/THPTA and ascorbic acid (for the details, see *Section 6.1.5, Material and methods*).

The advantages of this kind of reaction have been already discussed in the introduction (*Chapter 2*): it is easy to perform, it works very well under mild conditions, it gives high yield with limited by-products, it is characterized by high efficiency and it provides oriented immobilization of molecules. Moreover, it is applicable to all kind of biomolecules (proteins, DNA, peptides), once properly functionalized with reactive groups that are not naturally present, but easily introduced either during their synthesis or by post-modification. DNA and peptides, can be functionalized with azide groups directly during their synthesis, whereas for proteins the insertion of clickable groups requires more efforts. To this purpose, Thermo-Fisher commercializes an

enzymatic Kit (Site-Click) which provides a simple site-selective strategy to introduce an azide group on the heavy chain *N*-linked glycans far from the antigen-binding domain. In this work, an azide-PEG-succinimidyl ester ( $N_3$ -PEG<sub>8</sub>-NHS) is employed to introduce azide functionalities on the IgG antibody, as schematically reported in **Figure 27 (b)**. Since the reaction between PEG-succinimidyl ester and protein amino groups is not regioselective, the antibody immobilization is not oriented. However, the convenience of this protocol over other types of immobilization is related to the fact that it provides the control of the degree of azide insertion thus limiting the point of contact between the protein and the surface. As a matter of fact, the molar ratio of PEG-succinimidyl ester and antibody determines the degree of substitution. This means that in the limiting case where the immobilization involves only one azido moiety, the antibody has a high degree of freedom, which is impossible to obtain when standard NHS chemistry is used for the conjugation.

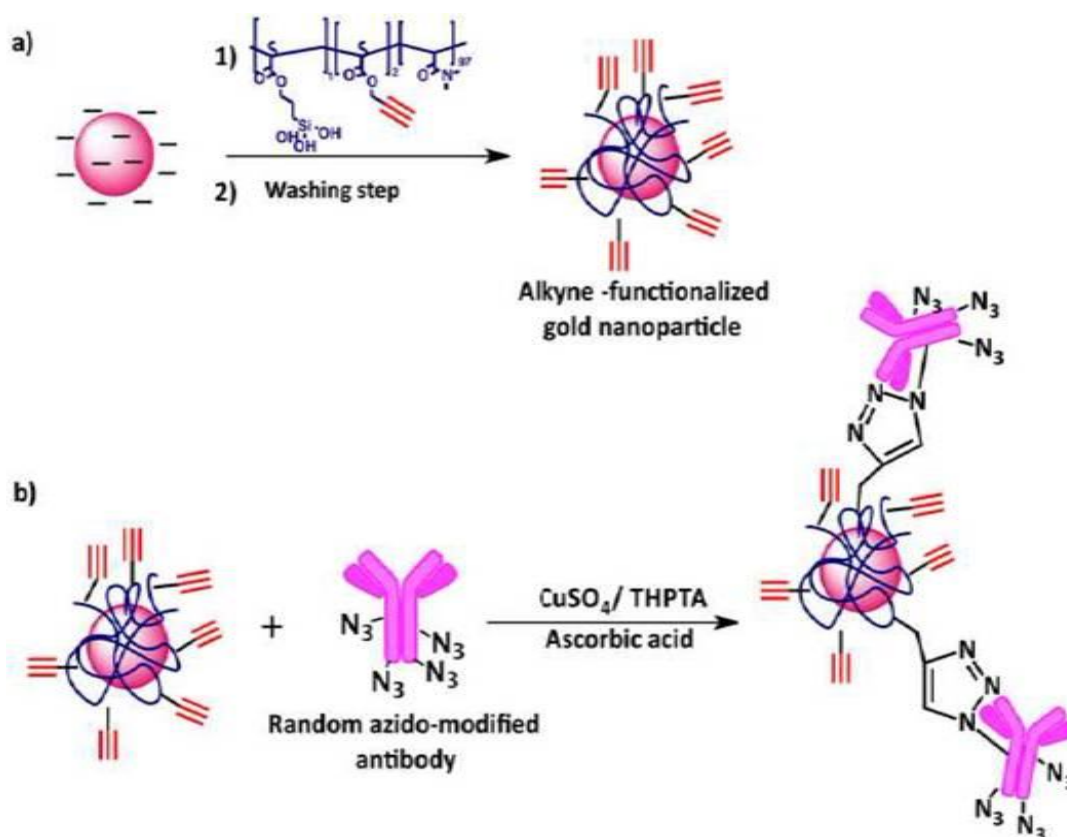


**Figure 27.** Coating process of silica AuNPs (a) with poly(DMA-NAS-MAPS) and derivatization with azido modified antibody (b)

### 6.2.2 CHARACTERIZATION OF COATED AND FUNCTIONALIZED AuNPs

A wide characterization of antibody-conjugated AuNPs (Ab linked AuNPs) is carried out at each stage of the functionalization. First of all, we confirm the presence of the polymeric coating and the antibody functionalization through electrophoresis analysis in an agarose gel (**Figure 28**). Uncoated AuNPs (**Figure 28a, lane 1**) and polymer-coated AuNPs (**Figure 28a, lane 2**), are compared: the first ones have a higher electrophoretic mobility than the second ones. This is due to the high density of negative charges on the surface of bare AuNPs, whereas the polymer shields the charges, leading to a significant mobility reduction. As illustrated in **Figure 28b**, the antibody/gold conjugation is confirmed by the different electrophoretic profile of polymer-coated AuNPs (**Figure 28b, lane 1**) and antibody-functionalized AuNPs (**Figure 28b, lane 3**). In addition, AuNPs treated with the antibody in the absence of the catalysts (THPTA/CuSO<sub>4</sub> and ascorbic acid), were used as a negative control (**lane 2**): their electrophoretic behaviour, identical to that of coated-AuNPs, proves that there is no unspecific adsorption of antibody on the NPs surface, confirming that the shift observed in **lane 3** is due to covalent binding of the antibody onto the surface.

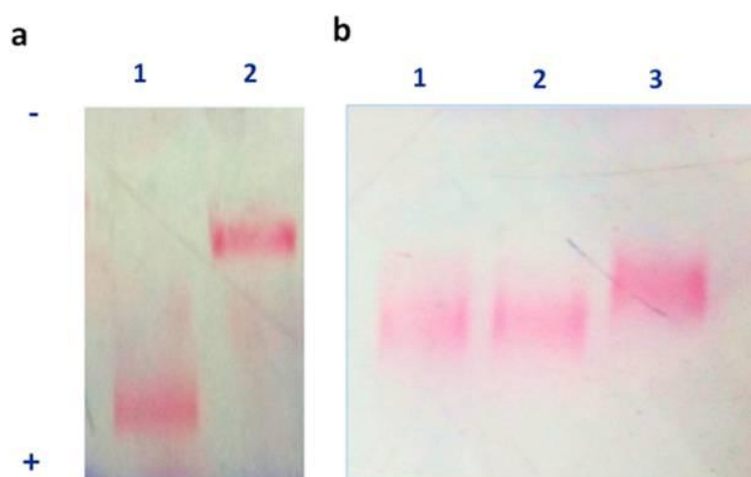


**Figure 28.** Electrophoresis of AuNPs on agarose gel. **(a) Lane 1**, uncoated AuNPs; **lane 2**, polymer-modified AuNPs. **(b) Lane 1**, polymer coated AuNPs, **lane 2**, polymer coated NPs treated with antibody in the absence of catalysts (no conjugation); **lane 3**, polymer coated particles treated with antibody and catalysts (covalent conjugation).

**Surface characterization:** UV Spectroscopy, Zeta Potential, and Dynamic Light Scattering Measurements

Several analytical techniques are employed to monitor the surface modification after each step of the process. From UV absorption spectra (**Figure 29**) a surface Plasmon band shift is appreciable after the coating process and after the conjugation with the antibody. Small changes in the refractive index of the material are caused by the deposition of each layer on the surface, resulting in a shift to longer wavelengths. Moreover, UV spectra do not show broadening, confirming absence of aggregation and thus, good quality of AuNPs suspension after each step.

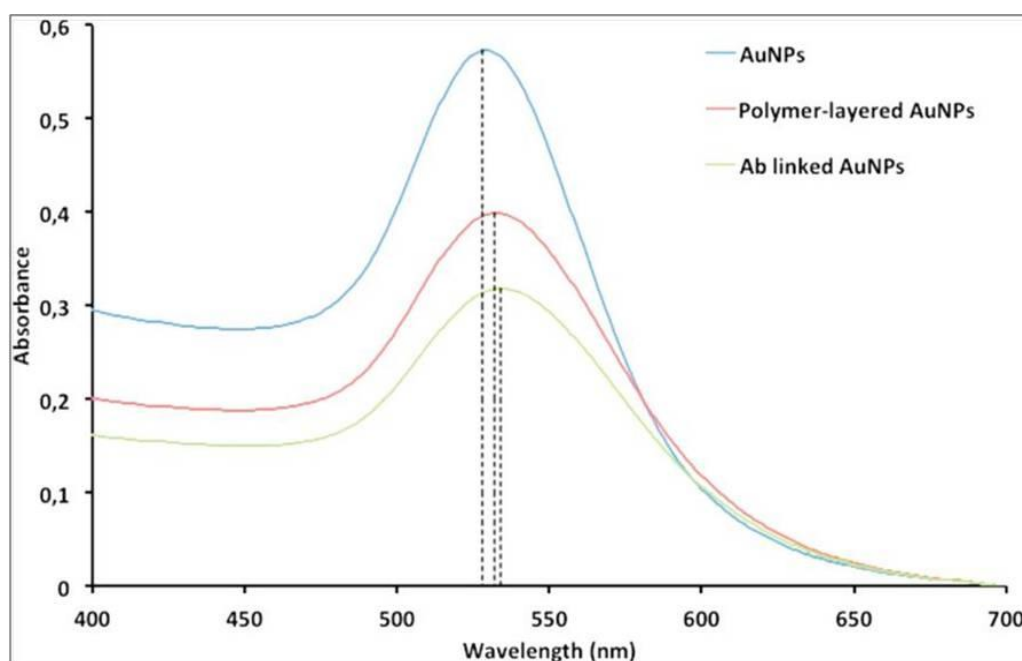


**Figure 29.** UV absorption spectra of bare AuNPs (**blue**), polymer-coated AuNPs (**red**), antibody-functionalized AuNPs (**green**)

DLS measurements are reported in **Table 2**. The hydrodynamic diameter of AuNPs becomes larger after each modification step, proving that coating and bio-functionalization are successful. Furthermore,  $\zeta$ -potential analysis confirmed the presence of polymer and antibody layers on the surface (**Table 2**). The surface charge

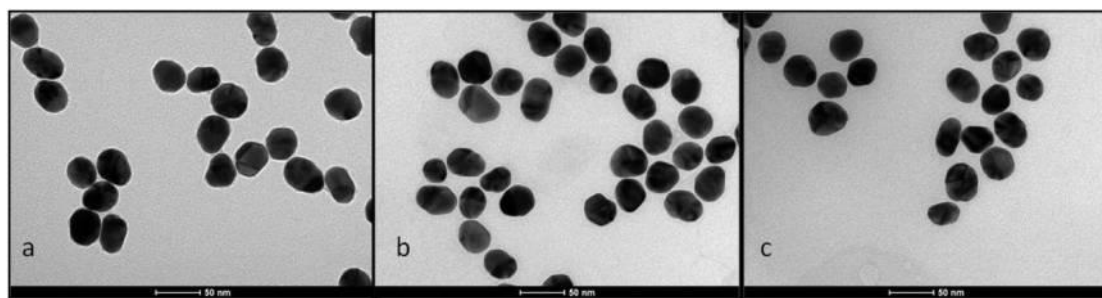
increases considerably after the addition of the polymer while a further increase occurs after bioconjugation.

Table 2. DLS measurements and Z-potential analysis after each step

<i>Sample</i>	<i>Hydrodynamic diameter (nm)</i>	<i>PDI</i>	<i>ζ-potential (mV)</i>
<b>Uncoated AuNPs</b>	47.02 ± 13.52	0.083	-25.1± 2.40
<b>Polymer coated AuNPs</b>	131.1 ± 34.93	0.071	-17.6± 0.35
<b>Ab linked AuNPs</b>	146.75 ± 87.92	0.403	-14.1± 2.26

**Stability of nanoparticles:** TEM analysis and tests for coating stability

The morphology of AuNPs is evaluated by transmission electron microscopy (TEM) and no visible aggregation is observed. As confirmed by TEM images (**Figure 30**) a homogeneous suspension is obtained after each functionalization step. The polymer coating and the antibody conjugation do not compromise AuNPs stability.



**Figure 30.** TEM images of bare AuNPs (a), polymer-coated AuNPs (b) and antibody-functionalized (c)

The effect of the coating on suspension stabilization is investigated by evaluating AuNPs stability in harsh conditions, i.e. at high and low pH values as well as at high salt concentration. The results of these simple tests show that the coating is fundamental to protect AuNPs from the pH dependent aggregation. In fact, uncoated AuNPs aggregate when the pH of the solution has either a high or low pH or high salt concentration, as demonstrated by marked colour changes (**Figure 31, left column**).

On the contrary, polymer coated nanoparticles were stable independently from solution pH and ionic strength: even when exposed at these harsh conditions, coated AuNPs maintain their original colour (**Figure 31, right column**). The extreme stability conferred by the polymer allows the employment of AuNPs in many biological contexts, especially where a high resistance to high ionic strength and pH is required.

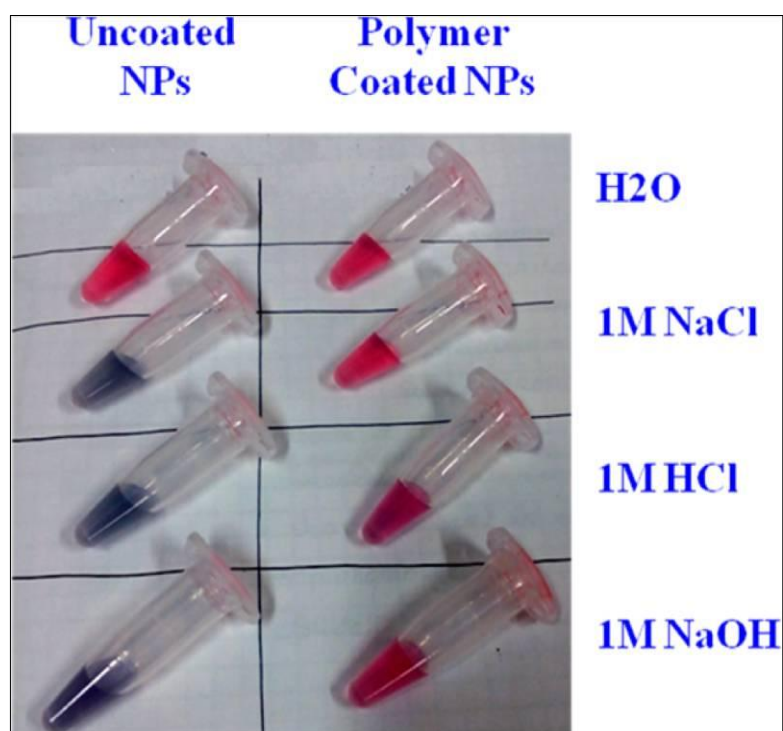


**Figure 31.** Uncoated and polymer coated AuNPs were treated with high concentration of salts or at different pH values. In these conditions, uncoated NPs are very unstable and aggregate, causing a red to blue color shift (**left column**). Nanoparticles with the clickable polymer are stable also in extreme conditions (**right column**).

### **6.2.3 APPLICATION OF ANTIBODY-LABELED NPs IN A NOVEL DIGITAL PLATFORM: Single Particle Interferometric Reflectance Imaging System (SP-IRIS)**

The development of high sensitivity methods which can detect biomarkers at very low concentrations is a hot research topic for the early diagnosis of diseases. As already mentioned in *Section 3.1*, microarray technology has a great potential in this context: current immunoassays can measure proteins at concentrations as low as  $10^{-12}$ M. However, the serum concentrations of many biomarkers at the early stages of cancer<sup>11</sup> or infections<sup>12</sup> range from  $10^{-16}$  to  $10^{-12}$ M. Therefore, detection methods which can measure these minute concentrations of biomarkers are needed. For this purpose, the new frontier in biomarker analysis is single-molecule counting or digital detection, an approach that provides high resolution and sensitivity which cannot be achieved with ensemble measurements, such as fluorescence.

To illustrate the principle of single-molecule counting digital and analogic detection modalities are compared in **Figure 32**. Fluorescence provides measurement that can be defined as an analogical signal: the intensity increases with the concentration of the species measured (**Figure 32a**). A digital detection mode allows counting individual molecules, providing measurement in discrete counts rather than averaging the intensity of many fluorophores (**Figure 32b**). Ideally, any method that can detect an event related to a single molecule enables digital detection, offering significant advantages over ensemble measurements in terms of sensitivity, down to the detection of a single molecule<sup>13</sup>.

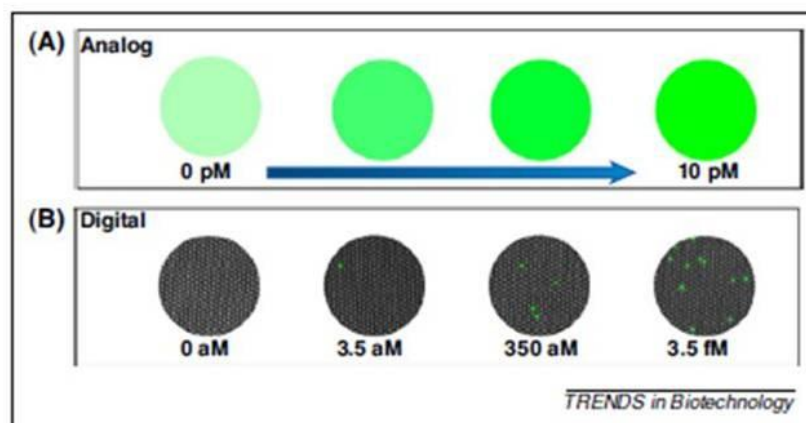


**Figure 32.** Analog and digital detection. (a) Analog detection provides an increasing intensity as the concentration increases. (b) Digital detection allows the detection of a single molecule. Reproduced with permission, from <sup>14</sup>.

The team of Prof. Selim Unlu at Boston University (MA, USA) has developed an innovative digital detection platform, called Single Particle Interferometric Reflectance Imaging Sensor<sup>15</sup>, which is an evolution of the label-free platform IRIS, described in *Section 5.3.1*. SP-IRIS is a prototype instrument for the detection of individual particles on surface and requires 100 nm silicon/silicon oxide chips in order to allow the digital detection of nanoparticles on a microarray surface.

The instrument uses one discrete LED wavelength (525 nm) to illuminate the sensor's surface using a high magnification objective to detect and count nanoparticles of known materials located on the SiO<sub>2</sub> surface; the principles are thoroughly illustrated elsewhere<sup>16</sup>. Briefly, this detection modality of SP-IRIS enhances the contrast of a single nanoparticle on a bilayered substrate by interfering the scattered field produced by the nanoparticle on the substrate surface with the reflected field generated by the buried Si-SiO<sub>2</sub> interface of the IRIS chip. The CCD camera senses the individual nanoparticles on the SP-IRIS chip as point objects, which are processed to extract size information.

Firstly, SP-IRIS was employed for direct digital detection of biological nanoparticles, such as viruses<sup>17</sup>. The direct counting of viruses by SP-IRIS simplified considerably the assay: no detection probes or labels were required for high sensitive detection.

The use of this digital platform has been extended to the detection of single biomolecules. Detecting a single molecule is more challenging than detecting a

nanoparticle such as a virus. It requires labeling the molecule to be detected with a nanoparticle. In **Figure 33** the common format of sandwich assay to detect different types of target is illustrated: specific detection probes, such as antibodies and nucleic acids, are immobilized onto the sensor support, previously coated with a functional copolymer. Target molecules in solution are recognized and bound by the immobilized probes then a secondary detection probe labeled with a nanoparticle is added in order to visualize binding events on the chip at the single molecule level.

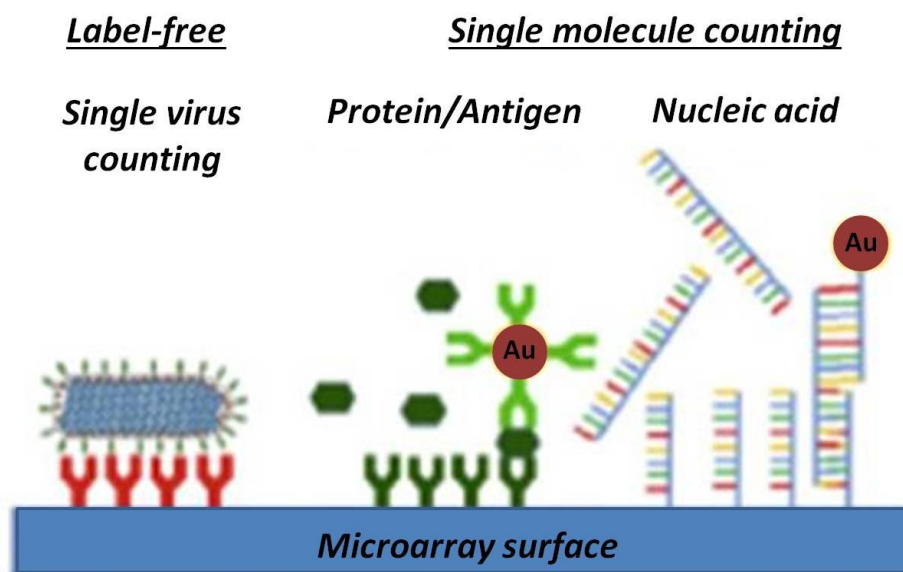


**Figure 33.** Large biological NPs, such as virus, can be visualized and counted directly. On the contrary, small targets, such as proteins and nucleic acid, require a secondary probe labeled with a NPs, which enables the digital counting.

The Si/SiO<sub>2</sub> interface of the chip generates a constructive interference with the scattered field produced by the NPs on the surface, enhancing the scattering of the light. Within this context, gold nanoparticles are used as labels thanks to their higher optical signal. Therefore, SP-IRIS utilizes small gold particles of 40nm. This AuNPs size is selected to contain steric hindrance and reduce diffusion effects.

A successful outcome of an SP-IRIS experiment is an indication of the quality of functionalized particles. When the binding between the antibody and the gold particle

occurs, individual gold particles are detected by SP-IRIS thus confirming not only that AuNPs are functional but also that they are not aggregated.

To assess the effectiveness of AuNPs conjugation to antibodies, a simple bioassay using SP-IRIS is carried out. Anti-mouse Polyclonal IgGs, tagged with AuNPs recognized specifically a mouse anti-CD 63 antibody, immobilized on the surface of an SP-IRIS chip. The gold nanoparticle tags, individually counted by the SP-IRIS software are represented by red circles (**Figure 34a, top left**). In the histogram of **Figure 34b** the number of NPs per  $\text{mm}^2$ , in different experimental conditions, is shown. When the catalysts of the click reaction (THPTA/ $\text{CuSO}_4$  and AAC) are not added during the conjugation, the anti-mouse IgG does not bind NPs (**Figure 34a, bottom left**). In this case since the AuNPs are not functional, the amount of particles counted on the surface is close to that of the negative control experiment (**Figure 34a, on the right**), in which, Rabbit-anti Bovine  $\beta$ -Lactoglobulin antibodies that are not recognized by an anti-mouse antibody are spotted on the surface. These experiments prove that gold nanoparticles are counted by SP-IRIS only when click chemistry catalysts are employed during the functionalization process, confirming that a covalent bond is formed during conjugation.

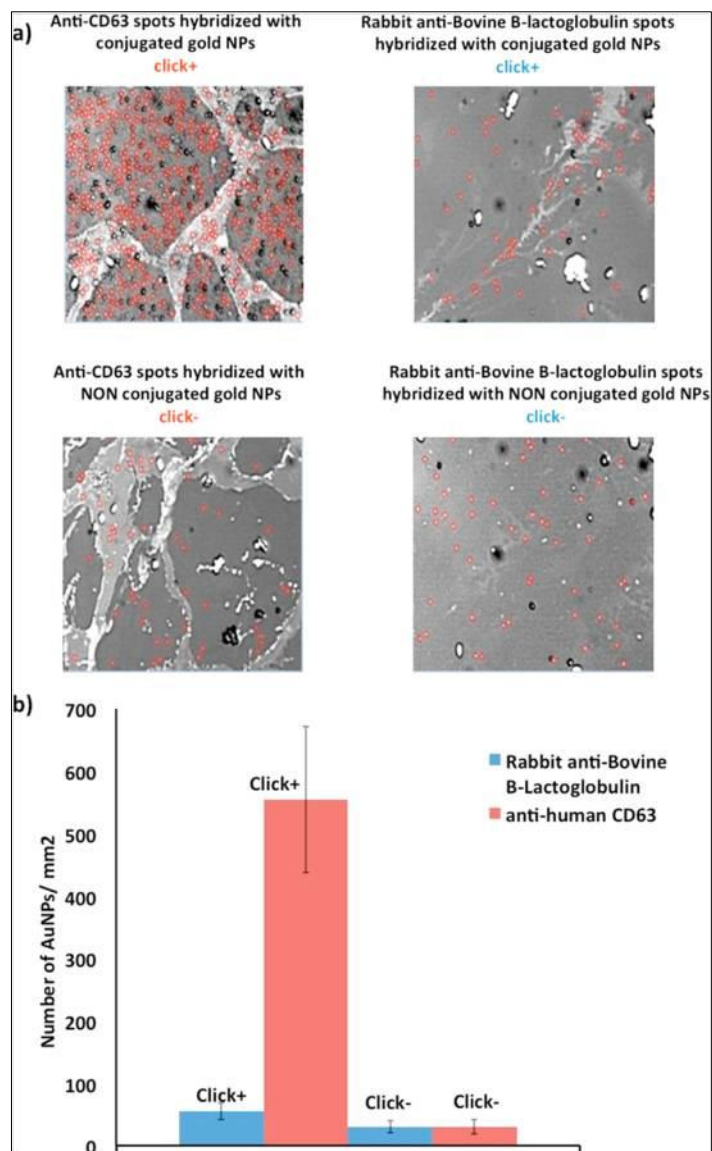


**Figure 34.** (a) SP-IRIS images of chips where different antibodies were immobilized, incubated with antibody-AuNPs in the presence (+) or in the absence (-) of catalysts. (b) histograms of the number of NPs/mm<sup>2</sup> (mean ± SD) for all the experiments

### 6.3. CONCLUSIONS

In this work, we develop a simple and robust method to coat AuNPs with a “clickable copolymer”, poly(DMA-PMA-MAPS). The use of this polymer for this purpose is new, although its application, in the field of glycan microarray, was previously reported. This approach conjugates both the simplicity and the robustness of NPs polymeric coating with the benefits of click chemistry, such as selectivity and efficiency, limited by-products and possibility to carry out the reaction under biological mild conditions. The clickable polymer confers stability to the colloidal suspension in several conditions, such as high salt concentrations and extreme pH values, and enables the functionalization with antibodies through the Cu(I)-catalyzed click reaction. Furthermore, the coated AuNPs are widely characterized and then tested in a microarray bioassay where a novel digital technology, called SP-IRIS, is employed. The proposed functionalization strategy can be extended to other kind of nanoparticles and exploited in many biological applications.

## 6.4 BIBLIOGRAPHY

- (1) Sperling, R. A.; Parak, W. J.; Ackerson, C. J.; Jadzinsky, P. D.; Kornberg, R. D.; Akerman, M. E.; Chan, W. C. W.; Laakkonen, P.; Bhatia, S. N.; Ruoslahti, E.; et al. Surface Modification, Functionalization and Bioconjugation of Colloidal Inorganic Nanoparticles. *Philos. Trans. A. Math. Phys. Eng. Sci.* **2010**, *368* (1915), 1333–1383.
- (2) Finetti, C.; Colombo, M.; Prosperi, D.; Alessio, G.; Morasso, C.; Sola, L.; Chiari, M. One-Pot Phase Transfer and Surface Modification of CdSe-ZnS Quantum Dots Using a Synthetic Functional Copolymer. *Chem. Commun.* **2014**, *50* (2), 240–242.
- (3) Finetti, C.; Sola, L.; Pezzullo, M.; Prosperi, D.; Colombo, M.; Riva, B.; Avvakumova, S.; Morasso, C.; Picciolini, S.; Chiari, M. Click Chemistry Immobilization of Antibodies on Polymer Coated Gold Nanoparticles. *Langmuir* **2016**, *32* (29), 7435–7441.
- (4) Mammen, M.; Dahmann, G.; Whitesides, G. M. Effective Inhibitors of Hemagglutination by Influenza Virus Synthesized from Polymers Having Active Ester Groups. Insight into Mechanism of Inhibition. *J. Med. Chem.* **1995**, *38* (21), 4179–4190.
- (5) Li, J. F.; Tian, X. D.; Li, S. B.; Anema, J. R.; Yang, Z. L.; Ding, Y.; Wu, Y. F.; Zeng, Y. M.; Chen, Q. Z.; Ren, B.; et al. Surface Analysis Using Shell-Isolated Nanoparticle-Enhanced Raman Spectroscopy. *Nat. Protoc.* **2013**, *8* (1), 52–65.
- (6) Turkevich, J.; Stevenson, P. C.; Hillier, J. A Study of the Nucleation and Growth Processes in the Synthesis of Colloidal Gold. *Discuss. Faraday Soc.* **1951**, *11* (0), 55.
- (7) FRENS, G.; G. Controlled Nucleation for the Regulation of the Particle Size in Monodisperse Gold Suspensions. *Nat. Phys. Sci.* **1973**, *241* (105), 20–22.
- (8) Li, J. F.; Tian, X. D.; Li, S. B.; Anema, J. R.; Yang, Z. L.; Ding, Y.; Wu, Y. F.; Zeng, Y. M.; Chen, Q. Z.; Ren, B.; et al. Surface Analysis Using Shell-Isolated Nanoparticle-Enhanced Raman Spectroscopy. *Nat. Protoc.* **2013**, *8* (1), 52–65.
- (9) Zilio, C.; Bernardi, A.; Palmioli, A.; Salina, M.; Tagliabue, G.; Buscaglia, M.; Consonni, R.; Chiari, M. New “clickable” Polymeric Coating for Glycan Microarrays. *Sensors Actuators B Chem.* **2015**, *215*, 412–420.
- (10) Giljohann, D. A.; Mirkin, C. A. Drivers of Biodiagnostic Development. *Nature* **2009**, *462* (7272), 461–464.
- (11) Srinivas, P. R.; Kramer, B. S.; Srivastava, S. Trends in Biomarker Research for

Cancer Detection. *Lancet. Oncol.* **2001**, 2 (11), 698–704.

- (12) Barletta, J. M.; Edelman, D. C.; Constantine, N. T. Lowering the Detection Limits of HIV-1 Viral Load Using Real-Time Immuno-PCR for HIV-1 p24 Antigen. *Am. J. Clin. Pathol.* **2004**, 122 (1), 20–27.
- (13) Cretich, M.; Daaboul, G. G.; Sola, L.; Ünlü, M. S.; Chiari, M. Digital Detection of Biomarkers Assisted by Nanoparticles: Application to Diagnostics. *Trends Biotechnol.* **2015**, 33 (6), 343–351.
- (14) Walt, D. R. Optical Methods for Single Molecule Detection and Analysis. *Anal. Chem.* **2013**, 85 (3), 1258–1263.
- (15) Reddington, A. P.; Trueb, J. T.; Freedman, D. S.; Tuysuzoglu, A.; Daaboul, G. G.; Lopez, C. A.; Karl, W. C.; Connor, J. H.; Fawcett, H.; Ünlü, M. S. An Interferometric Reflectance Imaging Sensor for Point of Care Viral Diagnostics. *IEEE Trans. Biomed. Eng.* **2013**, 60 (12), 3276–3283.
- (16) Yurt, A.; Daaboul, G. G.; Connor, J. H.; Goldberg, B. B.; Selim Ünlü, M.; Mazzola, L.; Whitesides, G. M.; Sperling, R. A.; Gil, P. R.; Zhang, F.; et al. Single Nanoparticle Detectors for Biological Applications. *Nanoscale* **2012**, 4 (3), 715.
- (17) Daaboul, G. G.; Lopez, C. A.; Chinnala, J.; Goldberg, B. B.; Connor, J. H.; Ünlü, M. S. Digital Sensing and Sizing of Vesicular Stomatitis Virus Pseudotypes in Complex Media: A Model for Ebola and Marburg Detection. *ACS Nano* **2014**, 8 (6), 6047–6055.



# *Part B*

## Chapter 7

# INTRODUCTION TO DNA GEL ELECTROPHORESIS

Electrophoresis is one of the most used and powerful analytical techniques employed in biochemistry and molecular biology to separate biopolymers, such as nucleic acids (DNA and RNA) and proteins. The process can be defined as the migration and separation of charged compounds in a supporting medium under the influence of an external electrical field. In fact, when charged molecules are placed in an electric field, they migrate toward either the positive or negative pole according to their charge. In contrast to proteins, which can have either a net positive or net negative charge, nucleic acids have always a net negative charge, imparted by their sugar-phosphate residues, and migrate toward the anode. Analytes are separated according to their electrophoretic mobility, an important parameter specific for each molecule and each medium that depends on the ratio between charge and frictional coefficient, which, in turn, depends on the molecular mass.

The separation of compounds, by electrophoresis, depends on the differential migration of analytes in an applied electric field. The electrophoretic migration velocity ( $u_p$ ) of an analyte towards the electrode of opposite charge is given by:

$$u_p = \mu_p \cdot E \quad (1)$$

where  $\mu_p$  is the electrophoretic mobility and  $E$  is the electric field strength. The electrophoretic mobility is proportional to the ionic charge and inversely proportional to the frictional forces acting on the migrating specie. When two species in a sample have different charge or experience different frictional forces, they will separate from one another as they migrate through a buffer solution.

The frictional forces experienced by an analyte ion depend on the viscosity ( $\eta$ ) of the medium and the size and shape of the ion. Accordingly, the electrophoretic mobility of an analyte at a given pH is given by:

$$\mu_p = \frac{z}{6\pi\eta D} \quad (2)$$

where  $z$  is the net charge of the analyte and  $r$  is the Stokes radius of the analyte which is expressed by:

$$r = \frac{k_B T}{6\pi\eta D} \quad (3)$$

where  $k_B$  is the Boltzmann constant, and  $T$  is the temperature,  $D$  is the diffusion coefficient. These equations indicate that the electrophoretic mobility of the analyte is proportional to the charge of the analyte and inversely proportional to its radius. The electrophoretic mobility can be determined experimentally from the migration time and the field strength:

$$\mu_p = \frac{L \cdot l}{t \cdot V} \quad (4)$$

where  $L$  is the total length between the two electrodes,  $l$  is the migration distance of each DNA band,  $t$  is the time required for the analyte to migrate (migration time),  $V$  is the applied voltage (field strength).

When the molecules to be separated are double stranded DNA (*dsDNA*), single-stranded DNA (*ssDNA*) or RNA the scenario is more complicated since these species, above a certain size, have a constant charge/size ratio and thus identical electrophoretic mobility in free solution. Their electric charge and friction coefficient scale linearly with their molecular weight making the size separation in buffer impossible<sup>1,2</sup>.

To overcome this problem, a sieving matrix has to be employed in order to retard the analytes in proportion to their molecular size. Hydrogels are widely employed as sieving matrices in electrophoresis to separate nucleic acids. The hydrogel has a dual role: on one hand it provides separation, thanks to the torturous path through which the DNA molecules migrate; on the other hand it acts as anti-convective medium.

In slab gel electrophoresis, the gel consists of crosslinked, hydrophilic polymers, either synthetic or extracted from living organisms, mostly vegetal. The two types of gels most commonly used are agarose and polyacrilamide (*See Section 7.3*)

## 7.1 DNA SEPARATION MECHANISM

Experimental and theoretical studies into the mechanism of DNA electrophoresis have led to the formulation of two widely accepted migration models: the *Ogston model* and the *reptation model*<sup>2</sup>. In the *Ogston model*, spherical DNA coils move through the connected pores large enough to accommodate their passage. This model is applicable only when DNA molecules have radii of gyration less than or equal to the average pore radius of the gel. However, the *Ogston model* breaks down for large molecules, whose radius of gyration exceeds the average pore radius of the gel. In this case a *reptation model* (or its variants) is most commonly applied. This model assumes that DNA deforms from its random –coil conformation to enter and migrate through the gel matrix in a "snake-like" fashion (hence "reptation"). With this "head-and-tail" character, DNA moves through the network of the gel pores.

In last years, the reptation theory has been refined to take into account the influence of higher electric field strength. This turned into a *Biased Reptation Model*<sup>3</sup>. Furthermore, when the influence of the tube length fluctuation has to be kept in consideration, the *Biased Reptation with Fluctuation* theory is applied<sup>4</sup>.

## 7.2 WHAT IS A HYDROGEL?

A hydrogel can be defined as a three dimensional network of polymers made of natural or synthetic materials, possessing elasticity and flexibility under deformation due to large water content. Even when the deformation is very slow, a hydrogel keeps a memory of its shape forever. Under physiological conditions, they are able to retain a large amount of water or biological fluids and, for this reason, they are characterized by a soft rubbery consistency similar to living tissues, making them an ideal substance for a variety of biomedical applications, including the development of DDS (drug delivery systems)<sup>5</sup> and scaffolds for tissue engineering and repair<sup>6</sup>.

Hydrogels do not disintegrate during swelling, thanks to their crosslinked structure. The nature of crosslinking is one of the most used criteria for the classification of hydrogels<sup>7</sup>. In particular, the crosslinking points can be physical or chemical. In physical gels, the crosslinking is normally achieved via physical processes such as hydrophobic association, chain aggregation, crystallization, ionic complexation, and hydrogen bonding. These features allow their solvent casting, post process bulk modification and reshaping. They are easy to fabricate, biodegradable and non-toxic, properties that lack in chemical gels, which are formed by a chemical reaction, i.e. chemical covalent crosslinking (simultaneously or post polymerization). For this reason, unlike physical hydrogels, they are permanent and irreversible.

In the absence of crosslinking points, the interactions between polymer chains are just topological. In particular, polymers, which are in dilute solutions, do not interact with each other because they are isolated, behaving as a single chain. However, when the polymer concentration increases, the chains became entangled, leading to the formation of a network. Although potentially very viscous, entangled solutions cannot be defined as gels, because the chain-chain interactions are purely temporary. The concentration at which the polymer coils start to touch each other in solution is defined "*overlap threshold concentration*" ( $c^*$ ). Solutions of long linear polyacrylamide (PAA), at a concentration above  $c^*$ , (polymerized without crosslinker) are examples of viscoelastic solutions.

## 7.3 GENERAL CHARACTERISTICS OF COMMON ELECTROPHORETIC GEL MATRICES

The separation of DNA fragments by molecular mass is determined by the characteristics of the gel matrix chosen for the separation<sup>8</sup>. The supports most frequently used as matrices in slab gel electrophoresis are agarose and polyacrylamide.

### 7.3.1 AGAROSE GELS

Agarose is a polysaccharide, composed of an alternating copolymer of 1,3-linked  $\beta$ -D-galactose and 1,4-linked 3,6-anhydro- $\alpha$ -L-galactose, rarely substituted with sulphate, carboxylate and/or pyruvate residues<sup>9</sup>, which confer to the matrix a negative charge. At high temperature, agarose molecules have a random coil structure<sup>10</sup>. Upon cooling, the formation of helical fiber bundles, linked together by hydrogen bonds, occurs. The gelation process results from hydrogen bonds that reinforce and rearrange links between the fiber bundles in "junction zone"<sup>11</sup>. Electron micrographs analysis have shown that the structure of an agarose gel matrix is a random fibrous network with irregularly branch points and many dangling ends<sup>12</sup>.

Agarose is an efficient, non-toxic medium to separate nucleic acids. Thanks to its simplicity and rapidity of preparation, agarose is widely used for the routine determination of DNA size and many other purposes, such as the purification of restriction fragments and PCR (polymerase chain reaction) products. The high strength of agarose gels allows handling of low gels percentage for the separation of moderate and large DNA molecules ranging in size from  $\sim$ 100 bp to  $\sim$ 20 kilobase pairs (kbp). The molecular sieving is strictly related to pores size, which depends on the concentration of agarose, usually referred to as a percentage of agarose to volume of buffer (w/v). In general, the higher the concentration of agarose, the smaller the pore size is. This means that a high concentration of agarose should be used if the aim is to separate small DNA fragments, on the contrary, a low concentration is recommended to separate large DNA fragments. In particular agarose concentrations ranging from 0.7% (good separation and resolution of large 5–10kbp DNA fragments) to 2% (good

resolution for small 0.2–1kbp fragments) are employed. For fragments larger than 25 kb *pulse field gel electrophoresis* is required<sup>13</sup>. This technique involves the application of alternating current from two different directions.

Hydroxyethylation can be exploited to modify agarose in order to create low melting agarose, which has a lower packing density of the agarose bundles which reduce their pore size<sup>14</sup> and thus DNA mobility. Low melting agarose is usually employed when isolation of separated DNA fragments is desired.

The non-covalent interactions between the agarose fiber bundles allow the possibility to re-melt an agarose gel after its use in an electrophoresis analysis.

However, the main limits of agarose are its high cost and the poor separation of low molecular weight samples.

### **7.3.2 POLYACRYLAMIDE GELS**

Polyacrylamide gels were first used for electrophoresis, in 1959. They are chemically cross-linked gel matrices formed by the reaction of acrylamide with a bifunctional crosslinking agent. Among the large number of cross-linking reagents, listed and compared by Righetti et al.<sup>15</sup>, *N,N'*-methylenebisacrylamide (Bis) is the most common one. The composition of the gel is controlled by %T, the total w/v concentration of acrylamide plus cross-linker, and %C, the w/w percentage of cross-linker included in %T. The gel is formed by free radical polymerization, usually catalysed by ammonium persulfate and *N,N*-tetramethylethylenediamine (TEMED). The number of chains and their length per gel are related to the initiator<sup>16</sup> and to the monomer concentration<sup>17</sup>.

The structure of polyacrylamide gels is heterogeneous due to the fact that Bis polymerizes with itself more rapidly than with acrylamide<sup>18</sup>. Comparing these gels to agarose gels, they are more difficult to handle, more toxic and more difficult to prepare. However, they have an excellent resolving power and high load capacity. As a matter of fact, with cross-linked polyacrylamide, DNA fragments smaller than 100 bp can be effectively separated.

The pore size of polyacrylamide gels typically is of few nm<sup>19</sup> and can be exactly controlled by varying the total concentration of the main monomer, acrylamide (T), and the degree of cross-linking (C): by increasing the cross-linking<sup>20</sup> or by polymerizing

diluted monomer solutions<sup>21</sup> the porosity of polyacrylamide is increased. However, there are limits to both approaches because the formation of gels does not occur below a concentration of 2%, while high concentration of the Bis monomer (20%) confers turbidity to matrices. In practice, the use of polyacrylamide is limited by the range of pore size that can be achieved (from 3 to 25 nm). This range is useful for protein separations, DNA mapping and sequencing.

Even though cross-linked polyacrylamides provide good resolution and efficiency in the separation of low molecular weight DNA fragments, a number of drawbacks limit their use and application. In fact, polyacrylamide handling is complicated by the fact that the polymerization has to be carried out under an inert atmosphere in order to prevent any free radical generation by oxygen. Moreover, the polymerization is temperature dependent and, for this reason, temperatures during gel production must be carefully controlled. However, the main limit is related to the toxicity of these gels: acrylamide is a potent neurotoxin and should be handled with care. Although polyacrylamide is considered to be non-toxic, polyacrylamide gels should also be handled with gloves due to the possible presence of free acrylamide. Lastly, since it is not possible to solubilize the gel matrix after electrophoresis, it is difficult to recover the bands from the gel.

## 7.4 ELECTROPHORESIS COMPONENTS

### 7.4.1 DNA DETECTION: FLUORESCENT DYES

Once electrophoresis has been completed, there are different approaches to make visible the DNA species separated in the gel. One of the most classical DNA-binding dye is *Ethidium Bromide* (EB), used to stain DNA in agarose and polyacrylamide gels. It intercalates itself between DNA base pairs in a concentration dependent manner. When exposed to UV light, the activation of electrons in the aromatic rings occurs, leading to the release of energy and thus an emission of fluorescence. However, agarose gels, which contain EB, have to be handled carefully because this dye is known to be mutagen and carcinogen.

Silver staining is a highly sensitive method for the visualization of nucleic acid bands after electrophoretic separation on polyacrylamide gels. Silver ions bind nucleic acids, leading visible dark bands on the gel.

Alternative stains for DNA include SYBR Gold, SYBR Green II and **SYBR Green I (SG)**. (**Figure 1**). The latter is considered a highly sensitive fluorescent nucleic acid binding dye and it is largely used thanks to its ability to enhance fluorescence up to 1,000 fold upon interaction with double stranded DNA<sup>22</sup>.

The use of these dyes in ultraviolet trans-illumination enables detection of DNA at picogram levels. The binding mechanism of the dyes to nucleic acids is believed to be different than that of the more conventional phenanthridinium intercalator dyes, such as EB, which usually can increase brightness up to 100 fold in complex with DNA, i.e. ten times less than SYBR Green.

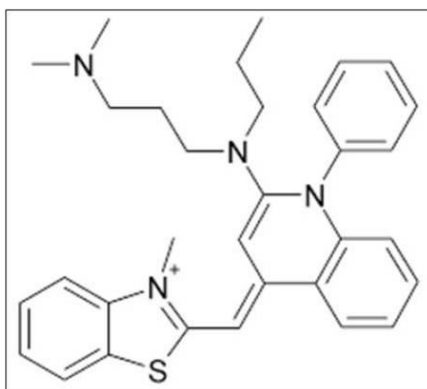


**Figure 1.** Chemical structure of SYBR Green I

The resulting DNA-SG-complex absorbs blue light ( $\lambda_{\text{max}} = 497 \text{ nm}$ ) and emits green light ( $\lambda_{\text{max}} = 520 \text{ nm}$ ). The dye binds preferentially to double-stranded DNA, but also to single-stranded DNA, and RNA even if with lower sensitivity. Dragan et al<sup>22</sup> illustrated the fluorescence properties and the mechanism of interaction between SG and DNA: the aromatic rings of the dye intercalate into DNA by van der Waals interactions. SG/DNA complex stability is promoted by a charge-charge interaction formed by the positively charged triazole group of the dye and phosphates of the DNA base pairs. The intercalation mechanism and the charge-charge interaction effectively immobilize the dye in a favourable and energetically conformation state<sup>23</sup>, leading to a dramatic enhancement of SG fluorescence.

#### 7.4.2 ELECTROPHORETIC BUFFER SYSTEMS

The buffer plays a significant role in electrophoresis because it controls the pH within the matrix, a parameter that determines the electrophoretic behaviour of nucleic acids. In addition, the ionic strength (salt content) of the buffer influences the electrophoretic mobility of DNA<sup>24</sup>. The buffer conductivity is an important characteristic, as DNA does not migrate effectively under an electric field in low conductive media, however high ionic strength buffers generate a significant amount of heat.

Depending on the purpose, different categories of buffer systems are available for electrophoresis. They can be classified as *dissociating* and *non-dissociating*, *continuous* and *discontinuous*.

Briefly, *dissociating buffer systems* are required when single-stranded DNA (ssDNA) has to be analyzed. Denaturing agents are needed to unfold the DNA or RNA and to break hydrogen bonds, which stabilize nucleic acids base pairs, to obtain single-stranded DNA (ssDNA). The most commonly *dissociating buffer* includes urea or formamide as DNA denaturants.

In the absence of denaturants, dsDNA, such as a PCR product, maintains its double helical structure, which gives it a rod-like form as it migrates through a gel. In these kinds of separation, *non-dissociating buffer system* are employed.

*In continuous buffer systems* the composition and concentration of salts are the same in the gel and in the running buffer. They are the easier to prepare and give a good resolution in many applications. Some examples of this kind of buffers are Tris-acetate (TAE) or Tris-borate (TBE) at a concentration of approximately 50mM (pH 7.5-7.8). They usually contain ethylenediaminetetraacetic acid (EDTA) (pH 8.0). However, the bands often tend to broad in these systems, leading to a poor resolution. For this reason, *discontinuous (multiphasic) systems* are used to improve band sharpness and resolution in some cases. They employ different buffers for gel and running buffer<sup>25</sup>.

#### **7.4.3 VOLTAGE/CURRENT APPLIED**

In DNA electrophoresis, a good compromise between the voltage that should be applied and the mobility of DNA fragments is required. In fact, the higher the voltage/current, the faster the DNA migrates. However, if the voltage is too high band streaking, especially for DNA  $\geq$  12-15kb, can occur. Moreover, high voltage causes a dramatic increase in buffer temperature, leading to the melting of the gel and decrease of DNA bands resolution. On the contrary, a too low voltage can reduce the mobility of DNA, causing band broadening. Therefore, it is highly recommended not to exceed 5-8 V/cm and 75 mA for standard size gels or 100 mA for minigels

#### 7.4.4 LOADING BUFFER

A buffer containing glycerol or sucrose has to be added to the DNA fragments that will be electrophoresed. The aim is to increase the density of DNA solution, promoting its entrance and migration through the gel matrix. Moreover, the loading buffer also contains tracking dyes, such as bromophenol blue or xylene cyanol, which are small molecules that indicate the progress of electrophoresis analysis.

#### 7.5 FROM SLAB GEL TO CAPILLARY ELECTROPHORESIS (CE)

As already mentioned above, DNA molecules cannot be separated by electrophoresis in free-solution; instead physical supports, such as crosslinked polyacrilamide or agarose gel matrices, are required in order to separate differently-sized DNA molecules into distinct zones. Slab gels matrices are an efficient format to provide size-based separation of DNA with a reduced diffusion of DNA molecules. This allows the separated-DNA bands to remain sharp and a good resolution can be achieved if the gel formulation and electrophoresis conditions are chosen properly.

Although slab gel electrophoresis is a widely employed technique, alternative electrophoretic formats have been developed in order to overcome its labor-intensive and time-consuming nature. Other limits are represented by the fact that it is difficult to fully automate slab gel techniques and, lastly, they are potentially hazardous to the end users because of the neurotoxic acrylamide monomers, commonly employed to formulate the gels.

All these drawbacks can be overcome or reduced when electrophoresis is performed within silica submillimeter diameter capillaries. This technique is called *Capillary electrophoresis (CE)*, a powerful analytical method, which allows the separation of both small organic/inorganic ions and large biopolymers. In CE the separation takes place within fused silica capillaries with on-line detection by fluorescence or UV absorbance. Capillaries with different diameters (about 10 to 300  $\mu\text{m}$ ) and a wide range of length are available.

The advantages of performing electrophoresis in open tubes of very small diameter are summarized in a comprehensive review in reference<sup>26</sup>. Briefly, capillary electrophoresis offers the following advantages:

- Effective heat dissipation, minimal temperature gradients and thus minimal band broadening
- Possibility of using high voltages with consequent increase in separation efficiency.
- Possibility to analyze minute amounts of sample thanks to its high sensitivity
- Stabilization of the medium against convective flow by the “wall effect”<sup>27</sup>: the small diameter of the column counteracts the convective flow allowing the use physical gels as sieving matrices

The number of theoretical plates, N, in CE is given by the following formula:

$$N = \frac{\mu V}{2D_m}$$

(5)

V is the applied voltage,  $\mu$  is the apparent mobility in the separation medium and  $D_m$  is the diffusion coefficient of the analyte. According to this equation, the efficiency of separation is only limited by diffusion and is proportional to the strength of the electric field. With CE it is possible to obtain high separation efficiency and, as a consequence, a better performance compared to slab gel systems.

It is clear that the miniaturization of the electrophoretic system offers several advantages over slab gel approaches. In particular, it reduces health risks from toxic chemicals and, due to the self-contained nature of the apparatus, it allows the use of viscoelastic fluids for the separation. Furthermore, CE is an order of magnitude faster than slab gel electrophoresis and may be completely automated.

Early efforts to apply capillary electrophoresis to the separation of nucleic acids were based on *gel-filled* capillaries. Many research groups have investigated the use of capillaries filled with crosslinked polyacrylamide gels, obtaining excellent separation of

DNA fragments<sup>28</sup>. However, gel filled capillaries have many limitations: the entire capillary must be replaced when the separation medium has degraded, the filling of the capillary requires great caution in order to avoid the introduction of air bubbles. In addition, the shrinkage of the gel during polymerization can be a source of bubbles, which are trapped by the rigid structure of the crosslinked gel, leading to band broadening and diffusion. Furthermore, the entrance of the gel receives all charged particles and impurities that contaminate the sample; as a consequence, this zone is very prone to clogging. In order to overcome the problems associated with crosslinked intracapillary separation media, uncrosslinked matrices were developed<sup>29</sup>. The replacement of the gel matrix with low viscosity polymers, e.g. linear (uncrosslinked) polyacrylamide (PAA), was a key step in the development of DNA capillary electrophoresis. In fact, polymer solutions can be easily pumped in and out of the capillary and replaced with fresh matrix without replacing the entire capillary. Since linear polymers can distort, bubbles are avoided allowing efficient DNA separations and sequencing<sup>30</sup>. High-resolution DNA separations are achieved with capillaries filled with uncrosslinked polymeric media, by using potential gradients (e.g. 300 V/cm), which would be inconceivable in a standard slab format.

Bode and co-workers<sup>31</sup> were the first to propose the use of noncrosslinked polyacrylamide for separation of biopolymers in electrophoresis. However, the use of non-crosslinked hydrogels became popular only in combination with CE, because the heat dissipation and anti-convective properties of thin capillaries allowed DNA separations in fluids without losing resolution. Guttman and co-workers<sup>32</sup> demonstrated that the crosslinking of the polymer matrix is not necessary when dsDNA separation is performed within a capillary.

One of the main advantages of employing uncrosslinked matrices for DNA separation in capillaries is the ease of their preparation and use, compared to crosslinked ones. As a matter of fact, no gelation or chemical reactions are needed for the preparation of uncrosslinked matrices, which maintain stability under the high potential gradients, routinely employed for CE.

As illustrated by Chiari et al.<sup>33</sup> and by Hebenbrock and co-workers<sup>34</sup>, PAA has proven to have an excellent sieving ability among all the other types of linear or branch polymers. However, a huge number of polymers have been used for separating DNA in

capillary electrophoresis. The matrices are prepared by simply dissolving the polymer in the buffer at the desired concentrations. The most common polymers employed are natural polymers such as agarose<sup>35</sup>, cellulose derivatives such as methylcellulose (MC)<sup>36</sup>, hydroxyethylcellulose (HEC)<sup>37</sup>, hydroxypropyl-methylcellulose (HPMC)<sup>38</sup> and glucomannan<sup>39</sup> or synthetic polymers such as linear polyacrylamide, polydimethylacrylamide, polyethylene glycol (PEG), polyethylene oxide (PEO)<sup>40</sup>. Chiari et al.<sup>41</sup> have introduced poly (*N*-acryloyl amino ethoxy ethanol) (AAEE), a polymer that is more resistant to hydrolysis compared with conventional polyacrylamides.

## 7.6 FROM CAPILLARY ELECTROPHORESIS TO MICROCHIP BASED-GEL ELECTROPHORESIS

As described in the previous section, Capillary Electrophoresis (CE) is one of the powerful tool for DNA detection and separation and, for this reason, many efforts have been directed toward extending the capabilities of CE instruments in the microscale through development of *Lab-on-a-Chip (LoC)* systems, defined as hybrid micro analytical devices, where an entire experiment can be integrated into the same miniaturized substrate, incorporating various processes. To this extent, the integration of electrophoresis capabilities on a *LoC* device is extremely useful. Miniaturization offers great promises to provide sophisticated, portable, low-cost diagnostic tools that can be immensely beneficial in both traditional clinical settings and in areas lacking of an adequate laboratory infrastructure.

A typical DNA analysis in capillary electrophoresis, involves the injection of a sample containing a mixture of fragment sizes at the inlet of a capillar separation channel, after which the fragments are transported through the sieving matrix under the action of an applied electric field. Since the migration velocity of the DNA fragments depends on their length, the mixture separates into zones containing like-size fragments that are subsequently detected at a fixed downstream location (**Figure 2a**). This finish-line detection method adapted by this technology is widely used, but it is also subjected to drawbacks including difficulty in resolving larger-sized fragments that comprise the slowest moving zones and thus require the longest time to reach the detection point. For this reason bands broadening and diffusion are often marked phenomena in systems with end-point detection. Miniaturized systems offer new opportunities to employ alternative detection schemes that can help address these issues. Roger et al.<sup>42</sup> illustrated an automated whole-gel scanning detection system that enables the progress of microchip-based gel electrophoresis of DNA to be continuously monitored along an entire microchannel (**Figure 2b**). This method offers potential advantages over conventional finish-line techniques, such as CE, including shorter analysis times because the DNA fragments no longer need to migrate through the entire length of the

separation channel to reach the detector. In fact, shorter run times provide also reduced band broadening and thus, improve separation resolution, particularly for larger sized fragments. Furthermore, thanks to the flexibility of the system, it is possible to observe smaller and faster moving fragments during the early stages of the separation before they have experienced significant diffusive broadening.

With a system like this, it is possible to directly observe the separation process in real time because a continuous and detailed picture of the electrophoresis process as it unfolds is provided, allowing to monitor rapidly and accurately fundamental physical parameters associated with DNA migration phenomena (e.g., mobility, diffusive broadening).

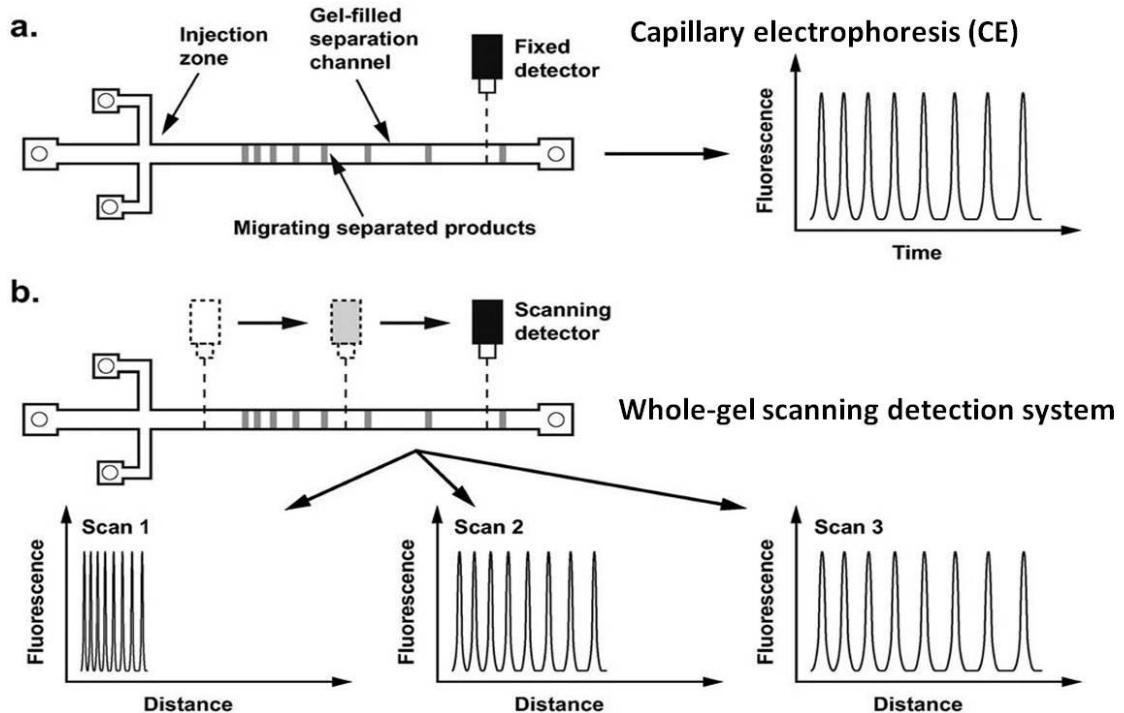


**Figure 2.** Overview of detection methods used in DNA microchip gel electrophoresis. A sample containing charged analytes (e.g., DNA, proteins) is injected into a separation channel filled with a sieving matrix. (a) Finish-line methods are predominantly employed to detect the separated products by positioning a detector at a fixed downstream distance from the injection zone (fragments are shown migrating from left to right). Capillary electrophoresis requires a system like this. (b) Scanning methods using a detector that can traverse the separation channel so that it can be continuously imaged allows the entire separation process to be observed as it unfolds in time<sup>42</sup>.

Nowadays, analytical miniaturized systems, which integrate sample separation with automated analysis, are commercially available. An example is the electrophoresis system produced by the company Agilent Technologies, called *2100 Bioanalyzer*, a chip-based capillary electrophoresis machine to analyse RNA, DNA, and proteins. This instrument was the first commercialized by this company. 2100 Bioanalyzer uses microfluidics technology for the analysis of biological samples by microchannel electrophoresis. In particular, it is widely used in RNA quality control measurements before downstream experiments like microarrays.

More recently, the same company, has developed a novel electrophoretic platform, the so-called *2200 TapeStation*, that employs precast multilane gels and microfluidics enabling semi-automated operation, simplifying sample handling and reducing assay times and costs. For these reasons TapeStation is reportedly simpler and faster than the 2100 Bioanalyzer.

The automated TapeStation platform keeps all the advantages of the miniaturized systems described above, including improved data precision and reproducibility, short analysis times and minimal sample consumption. Its whole-gel scanning detection system enables the progress of microchip-based gel electrophoresis of samples to be constantly monitored in time, providing a continuous and detailed picture of the electrophoresis process.

The 2200 TapeStation will be illustrated in detail in the next Chapter. The activity carried out in the frame of a scientific collaboration with Agilent Technologies to improve the electrophoretic separation of DNA within this work-station is the subject of the second part of this thesis work.

## 7.7 BIBLIOGRAPHY

- (1) McDonell, M. W.; Simon, M. N.; Studier, F. W. Analysis of Restriction Fragments of T7 DNA and Determination of Molecular Weights by Electrophoresis in Neutral and Alkaline Gels. *J. Mol. Biol.* **1977**, *110* (1), 119–146.
- (2) Salieb-Beugelaar, G. B.; Dorfman, K. D.; Van Den Berg, A.; Eijkel, J. C. T. Electrophoretic Separation of DNA in Gels and Nanostructures. **2009**.
- (3) Slater, G. W.; Mayer, P.; Hubert, S. J.; Drouin, G. The Biased Reptation Model of DNA Gel Electrophoresis: A User Guide for Constant Field Mobilities. *Appl. Theor. Electrophor.* **1994**, *4* (2), 71–79.
- (4) Viovy, J. L. Reptation Theories of Electrophoresis. *Mol. Biotechnol.* **1996**, *6* (1), 31–46.
- (5) Peppas, N. A. Hydrogels and Drug Delivery. *Curr. Opin. Colloid Interface Sci.* **1997**, *2* (5), 531–537.
- (6) Drury, J. L.; Mooney, D. J. Hydrogels for Tissue Engineering: Scaffold Design Variables and Applications. *Biomaterials* **2003**, *24* (24), 4337–4351.
- (7) Ullah, F.; Othman, M. B. H.; Javed, F.; Ahmad, Z.; Akil, H. M. Classification, Processing and Application of Hydrogels: A Review. *Mater. Sci. Eng. C* **2015**, *57*, 414–433.
- (8) ZEIGER, R. S.; SALOMON, R.; DINGMAN, C. W.; PEACOCK, A. C. Role of Base Composition in the Electrophoresis of Microbial and Crab DNA in Polyacrylamide Gels. *Nature, Publ. online 19 July 1972*; | doi10.1038/10.1038/newbio238065a0 **1972**, *238* (81), 65.
- (9) Stellwagen, N. C. Electrophoresis of DNA in Agarose Gels, Polyacrylamide Gels and in Free Solution. *Electrophoresis* **2009**, *30* (S1), S188–S195.
- (10) Rinaudo, M. Gelation of Polysaccharides. *J. Intell. Mater. Syst. Struct.* **1993**, *4* (2), 210–215.
- (11) Pines, E.; Prins, W. Structure-Property Relations of Thermoreversible Macromolecular Hydrogels. *Macromolecules* **1973**, *6* (6), 888–895.
- (12) Johnson, E. M.; Berk, D. A.; Jain, R. K.; Deen, W. M. Diffusion and Partitioning of Proteins in Charged Agarose Gels. *Biophys. J.* **1995**, *68* (4), 1561–1568.
- (13) *Pulse Field Gel Electrophoresis*; Jordan, K., Dalmasso, M., Eds.; Methods in Molecular Biology; Springer New York: New York, NY, 2015; Vol. 1301.
- (14) Serwer, P. Agarose Gels: Properties and Use for Electrophoresis. *Electrophoresis* **1983**, *4* (6), 375–382.
- (15) Righetti, P. G. *Isoelectric Focusing*: Theory, Methodology, and Applications; Elsevier Biomedical Press, 1984.

- (16) Nossal, R. Network Formation in Polyacrylamide Gels. *Macromolecules* **1985**, *18* (1), 49–54.
- (17) Cannon-Carlson, S.; Tang, J. Modification of the Laemmli Sodium Dodecyl Sulfate-Polyacrylamide Gel Electrophoresis Procedure to Eliminate Artifacts on Reducing and Nonreducing Gels. *Anal. Biochem.* **1997**, *246* (1), 146–148.
- (18) Johner, A.; Daoud, M. Intermediate Swelling of Gels. *J. Phys.* **1989**, *50* (15), 2147–2159.
- (19) Pato, M. The Practice of Quantitative Gel Electrophoresis. *Biochem. Educ.* **1987**, *15* (1), 52.
- (20) ORNSTEIN, L. DISC ELECTROPHORESIS. I. BACKGROUND AND THEORY. *Ann. N. Y. Acad. Sci.* **1964**, *121*, 321–349.
- (21) Zakharov, S. F.; Chrambach, A. The Relative Separation Efficiencies of Highly Concentrated, Uncrosslinked or Low-Crosslinked Polyacrylamide Gels Compared to Conventional Gels of Moderate Concentration and Crosslinking. *Electrophoresis* **1994**, *15* (1), 1101–1103.
- (22) Dragan, A. I.; Pavlovic, R.; McGivney, J. B.; Casas-Finet, J. R.; Bishop, E. S.; Strouse, R. J.; Schenerman, M. A.; Geddes, C. D. SYBR Green I: Fluorescence Properties and Interaction with DNA. *J. Fluoresc.* **2012**, *22* (4), 1189–1199.
- (23) Erkkila, K. E.; Odom, D. T.; Barton, J. K. Recognition and Reaction of Metallointercalators with DNA. *Chem. Rev.* **1999**, *99* (9), 2777–2796.
- (24) On, T. C. *The Presence of G Enetically*; 2006.
- (25) Orbán, L.; Chrambach, A. Discontinuous Buffer System for Polyacrylamide and Agarose Gel Electrophoresis of DNA Fragments. *Electrophoresis* **1991**, *12* (4), 233–240.
- (26) Jorgenson, J. W.; Lukacs, K. D. Capillary Zone Electrophoresis. *Science* **1983**, *222* (4621), 266–272.
- (27) Virtanen, R. *Zone Electrophoresis in a Narrow-Bore Tube Employing Potentiometric Detection*: A Theoretical and Experimental Study; [Finnish Academy of Technical Sciences]: Helsinki, 1974.
- (28) Nishikawa, T.; Kambara, H. Separation of Long DNA Fragments by Capillary Gel Electrophoresis with Laser-Induced Fluorescence Detection. *Electrophoresis* **1994**, *15* (2), 215–220.
- (29) Heiger, D. N.; Cohen, A. S.; Karger, B. L. Separation of DNA Restriction Fragments by High Performance Capillary Electrophoresis with Low and Zero Crosslinked Polyacrylamide Using Continuous and Pulsed Electric Fields. *J. Chromatogr.* **1990**, *516* (1), 33–48.
- (30) Fung, N.; N. *DNA Sequencing with Capillary Electrophoresis and Single Cell Analysis with Mass Spectrometry*; Ames, IA, 1998.
- (31) Bode, H. J. The Use of Liquid Polyacrylamide in Electrophoresis. I. Mixed Gels

- Composed of Agar-Agar and Liquid Polyacrylamide. *Anal. Biochem.* **1977**, *83* (1), 204–210.
- (32) Guttman, A.; Wanders, B.; Cooke, N. Enhanced Separation of DNA Restriction Fragments by Capillary Gel Electrophoresis Using Field Strength Gradients. *Anal. Chem.* **1992**, *64*, 2340–2351.
- (33) Chiari, M.; Nesi, M.; Fazio, M.; Righetti, P. G. Capillary Electrophoresis of Macromolecules in “syrupy” Solutions: Facts and Misfacts. *Electrophoresis* **1992**, *13* (1), 690–697.
- (34) Hebenbrock, K.; Schügerl, K.; Freitag, R. Analysis of Plasmid-DNA and Cell Protein of Recombinant Escherichia Coli Using Capillary Gel Electrophoresis. *Electrophoresis* **1993**, *14* (8), 753–758.
- (35) Bocek, P.; Chrambach, A. Capillary Electrophoresis in Agarose Solutions: Extension of Size Separations to DNA of 12 Kb in Length. *Electrophoresis* **1992**, *13* (1–2), 31–34.
- (36) Strege, M.; Lagu, A. Separation of DNA Restriction Fragments by Capillary Electrophoresis Using Coated Fused Silica Capillaries. *Anal. Chem.* **1991**, *63* (13), 1233–1236.
- (37) Grossman, P. D.; Soane, D. S. Experimental and Theoretical Studies of DNA Separations by Capillary Electrophoresis in Entangled Polymer Solutions. *Biopolymers* **1991**, *31* (10), 1221–1228.
- (38) Baba, Y.; Ishimaru, N.; Samata, K.; Tsuchioka, M. High-Resolution Separation of DNA Restriction Fragments by Capillary Electrophoresis in Cellulose Derivative Solutions. *J. Chromatogr. A* **1993**, *653* (2), 329–335.
- (39) Izumi, T.; Yamaguchi, M.; Yoneda, K.; Isobe, T.; Okuyama, T.; Shinoda, T. Use of Glucomannan for the Separation of DNA Fragments by Capillary Electrophoresis. *J. Chromatogr. A* **1993**, *652* (1), 41–46.
- (40) Fung, E. N.; Yeung, E. S. High-Speed DNA Sequencing by Using Mixed Poly(ethylene Oxide) Solutions in Uncoated Capillary Columns. *Anal. Chem.* **1995**, *67* (13), 1913–1919.
- (41) Chiari, M.; Micheletti, C.; Nesi, M.; Fazio, M.; Righetti, P. G. Towards New Formulations for Polyacrylamide matrices: N-Acryloylaminoethoxyethanol, a Novel Monomer Combining High Hydrophilicity with Extreme Hydrolytic Stability. *Electrophoresis* **1994**, *15* (1), 177–186.
- (42) Lo, R. C.; Ugaz, V. M. Microchip DNA Electrophoresis with Automated Whole-Gel Scanning Detection. *Lab Chip* **2008**, *8* (12), 2135.

## Chapter 8

### DEVELOPMENT OF A NOVEL SIEVING MATRIX THROUGH *CLICK CHEMISTRY* FOR HIGH PERFORMANCE DNA ELECTROPHORESIS

The work described in this chapter aimed at improving the electrophoretic performance of DNA polymer sieving matrices through the synthesis of novel hydrogels. It was carried out, in part, in the Agilent Technologies laboratories in Edinburgh, UK. Agilent has recently introduced the so-called 2200 TapeStation system, an automated platform that allows simpler, faster and more reliable electrophoresis. It consists of three elements (**Figure 3**): a consumable, credit card sized, plastic tape, called ScreenTape, (**Figure 3a**), an instrument (the 2200 TapeStation, **Figure 3b**) and an analysis software (**Figure 3c**). The system is characterized by speed, efficiency and simplicity: it consents to perform nucleic acids separations in few minutes in an semi-automated way. It just requires loading consumable, sample vials and ScreenTape into the 2200 TapeStation. A dedicated software controls sample loading and separation. At different times, images of the entire channels are acquired and processed. The part of the platform called ScreenTape is a pressure moulded polyethylene cartridge that contains multiple gel channels of miniaturized dimensions (2 cm length X 1.5 mm width) for separating DNA and RNA. This platform combines the advantages of CE in terms of miniaturization and automatization of the system with the simplicity of use of slab gel electrophoresis. In fact, the separation distance in the ScreenTape is much smaller than that of a traditional slab gel leading to shorter separation times. In addition, since the cartridge contains miniaturized pre-cast gels, its use reduces personel handling and health risks from toxic chemicals. Even though the ScreenTape cannot truly be defined as a microfluidic device for electrophoresis, its small scale format provides great advantages for rapid and cost-effective analysis. Unlike capillary electrophoresis, where the use of uncrosslinked matrices is preferred

for the reasons discussed in *Section 7.5*, the ScreenTape technology uses cross-linked gels since in millimetric size channels convective motions make impossible to use viscoelastic solutions that, otherwise, would flow out of the channel. The gel is formed within the microchannels by polymerization of monomers and cross-linkers, injected together with a foto radical initiator before polymerization. The **ScreenTape architecture** is illustrated in **Figure 3a**, in detail: the credit card-sized, disposable ScreenTape consists of multiple separation lanes for separating DNA. Each ScreenTape has 16 lanes so that several samples can be analyzed in a single run. The **buffer chamber** is located at the top of the channel and contains optimised buffers for the effective separation of nucleic acid fragments (or proteins). The integrated ink-**electrodes** apply a current across the ScreenTape and eliminate the need for any additional electrophoresis equipment. The **gel matrix** contained within ScreenTape has been developed specifically to resolve nucleic acids or proteins. Agilent has developed a number of gel formulations for a wide range of applications. However, as it will be discussed in detail in the next sections, improvement in resolution is still needed in certain size ranges.

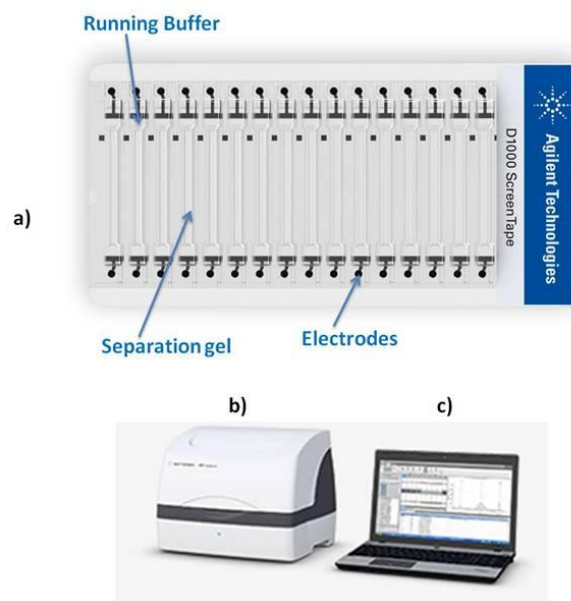


**Figure 3.** Three elements of Agilent 2200 TapeStation: an example of ScreenTape (a), the TapeStation instrument (b) and the software (c)

In the frame of the collaboration with Agilent Technologies, several existing gel matrices were considerably improved by adjusting monomer concentration or by the addition of specific additives. However, the resolution of native double stranded DNA in the 500 to 25 base pairs (bp) range was not as good as that obtained with other competing microfluidic workstations for electrophoresis, like the aforementioned 2100 Bioanalyzer.

The most relevant achievement of the work reported here is the synthesis of an innovative gel matrix for high performance DNA electrophoresis obtained by a “*click chemistry*” reaction. To the best of our knowledge, it is the first time that *click-hydrogels* have been used in this application.

Traditional approaches for the synthesis of hydrogels generally require random radical polymerization of water soluble monomers. With these radical-based uncontrolled crosslinking methods, the formation of non-uniform gels occurs and, as a consequence, such hydrogels do not have a well-defined molecular architecture. Moreover they suffer, often, from poor mechanical and structural properties. Therefore, efficient methodologies that can provide chemical stability and controllable crosslinking kinetics are needed.

The utilization of *Click chemistry*<sup>1</sup> addresses many of the above mentioned issues in the design and fabrication of functional hydrogels. In fact, as widely described in Chapter 2 of PART A of this dissertation, the well known *copper (I)-catalyzed azide-alkyne cycloaddition (CuAAC)* has enormous advantages. Reaction specificity, high yields and good functional group tolerance are the features of click chemistry that allow the preparation of hydrogel networks of complex architecture. Moreover, the efficiency of this reaction provides, under mild conditions, hydrogels with near-ideal network connectivity and improved physical properties. Additionally, the liberty to incorporate a variety of functional groups into hydrogel matrix owing to the mild and specific nature of the CuAAC reaction is very attractive since it would allow easier fabrication of various functional and responsive materials<sup>2</sup>.

Hilborn and co-workers<sup>3</sup> were the first who exploited CuAAC reaction to make hydrogels. They used poly(vinyl alcohols) (PVAs) functionalized with alkyne and azide pendant groups as hydrogel precursors. In the presence of reaction catalysts (Copper

(II) sulphate and sodium ascorbate), the modified PVA polymers were crosslinked in a few minutes in dimethylsulfoxide (DMSO) and aqueous solutions. Gelation speed and efficiency were easy to control as they depend on functional group and catalysts concentration as well as on the stoichiometry and structure of the polymeric components.

One of the most common applications of click hydrogels involves the *in vivo* studies. Chawla et al.<sup>4</sup> developed saccharide-peptide hydrogels as new synthetic extracellular matrices for regenerative medicine applications. In addition, many researchers have used hydrogels synthesized using click chemistry for the creation of supports for cell culture and proliferation<sup>5</sup>. Furthermore, click-hydrogels represent powerful tools for tissue engineering and regenerative medicine<sup>6</sup> as well as drug-delivery platform for the controlled release of entrapped bioactive materials<sup>7</sup>.

In this work, *copper (I)-catalyzed azide-alkyne cycloaddition (CuAAC)*, allowed to obtain an innovative electrophoretic gel matrix without using UV initiation and thus affording the possibility to add a fluorescent dye in the gel. In fact, one of the major focus of the work was to investigate a gel matrix formulation containing the fluorescent dye SYBR Green I for DNA and RNA detection. It is well known<sup>8</sup> that including a dye in the gel matrix improves band shape (by providing a more consistent mass to charge ratio for the analyte) and provides more fluorescence during extended electrophoresis. Suenaga et al.<sup>8</sup> compared three possible staining methodologies, using SYBR Gold as dye, for DNA detection in agarose gel electrophoresis analysis. They involve prestain, in-gel stain and poststain methods. In particular, the authors call the “pre stain method” when the dye is mixed directly with the DNA samples; this mixture is then loaded and separated in the gel matrix. The “in-gel stain method” was when DNA samples were separated through a gel matrix containing the dye, whereas the “poststain method” is when the gel, after electrophoresis, is immersed in a solution containing the dye, allowing its staining. Briefly, their experimental results show that the sensitivity of the in-gel stain method is comparable to that of poststain method, commonly employed. Furthermore, in terms of separation efficiency, in-gel stain method provide a higher efficient separation compared to that obtained with the prestain approach. In particular, the authors show that some DNA bands are clearly

separated by the in-gel stain method, whereas these bands are not separated by the poststain method.

Hydrogels obtained by radical polymerization approaches that use UV initiators, such as acrylic based hydrogels, are not compatible with in-gel stain method as the dye is not stable under UV light. Polymerization methods using red-ox initiators that would be compatible with the stain in the gel, are often difficult to control. An example is represented by the polymerization initiated by ammonium persulfate and TEMED, where temperature and oxygen play a critical role for reproducibility.

As demonstrated by this thesis, the click chemistry polymerization approach is easy to perform, reproducible and compatible with in-gel stain. Furthermore, another advantage of a gel matrix produced via click chemistry is the absence of toxic and not stable monomers, such as acrylamide, a potent neurotoxin that, in its powdered form, can be easily aerosolized with serious hazard for the users. In particular, the innovative gel matrix developed in this work is composed of two preformed polymers: a dimethylacrilamide copolymer bearing alkyne functionalities as the main gel component (**T**) and a poly(ethylene glycol) bisazide as the crosslinker (**C**). Two different dimethylacrilamide based copolymers were used in this project. One polymer was obtained by copolymerization of *N,N*-dimethylacrylamide (DMA), 3-trimethylsilyl-prop-2-ynyl methacrylate (PMA) and 3-(trimethoxysilyl)propyl methacrylate (MAPS). Copoly(DMA-PMA-MAPS), already described in *Chapter 4 (Section 4.1, PART A)* of this dissertation, was employed in the first part of this work (Section 8.2.1- Section 8.2.3 of *“Results and Discussion”*). Its characteristic is that the alkyne functionality is introduced in the polymer chain by copolymerization of an alkyne monomer. Due to the incompatibility of alkyne groups with radical polymerization, the alkyne group was protected by a 3-trimethylsilyl-propyl group, and deprotected in a second stage. The other dimethylacrilamide-based copolymer, called Copoly-Alkyne, was synthesized by a different procedure, that involves post polymerization modification of poly(DMA-NAS-MAPS). The two copolymers have similar composition and features. Copoly Alkyne, most suitable for large scale production, was employed in all the experiments (Section 8.2.4- Section 8.2.8. of *“Results and Discussion”*), carried out in the Agilent Technologies laboratories in Edinburgh (UK).

Since both polymers bear alkyne functionalities, they react with azido-groups of the crosslinker (C) through the *copper (I)-catalyzed azide-alkyne cycloaddition (CuAAC)*, leading to a novel hydrogel structure, which provides separations of DNA, superior to those usually obtained with polyacrilamide gels, that are the industry bench mark for high resolution separation of DNA and RNA.

## 8.1 MATERIAL AND METHODS

### 8.1.1 Reagents

*N,N*-Dimethylacrylamide (DMA), 3-(trimethoxysilyl)propyl methacrylate (MAPS), propargylamine, *N*-(2-aminoethyl)maleimide trifluoroacetate salt, dibenzocyclooctyne-amine, copper sulfate (CuSO<sub>4</sub>), ascorbic acid (AAC), Tris(3-hydroxypropyltriazolylmethyl)amine (THPTA),  $\alpha,\alpha'$ -Azobisisobutyronitrile (AIBN), anhydrous tetrahydrofuran (THF), SYBR Green I nucleic acid gel stain, tetrapentylammonium hydroxide (TPAOH) solution, Tris-EDTA Buffer 100X concentrate, salmon sperm DNA, poly(ethylene glycol) bisazide ( $M_w$  1,100), *N*-[Tris(hydroxymethyl)methyl]glycine (Tricine), 2,2-Bis(hydroxymethyl)-2,2',2''-nitrilotriethanol, 2-Bis(2-hydroxyethyl)amino-2-(hydroxymethyl)-1,3-propanediol, Bis(2-hydroxyethyl)amino-tris(hydroxymethyl)methane (Bis-Tris) were purchased from Sigma Aldrich (St. Louis, MO, USA). All solvents were used as received. *N*-acryloyloxysuccinimide and 3-azido-1-propylamine were synthesized as reported elsewhere<sup>9</sup>. GeneRuler 100bp DNA Ladder, 1500 bp DNA fragment, 25 bp DNA fragment were purchased from ThermoFisher. D1000 ScreenTape and the recipes of 10X Running Buffer (0,5M Bis-Tris/ 1M Tricine) and of Loading Buffer with and without SYBR Green I were provided by Agilent Technologies, Edinburgh (UK).

### 8.1.2 Synthesis of poly(DMA-PMA-MAPS) , poly(DMA-NAS-MAPS) and Copoly-Alkyne

Poly(DMA-PMA-MAPS) and poly(DMA-NAS-MAPS) were synthesized as reported in Chapter 5 of PART A of this PhD dissertation. Copoly-Alkyne has been synthesized as reported by Sola et al.<sup>10</sup> The procedure implies a post-polymerization modification reaction of the parent polymer poly(DMA-NAS-MAPS), constituted of *N,N*-dimethylacrylamide, DMA, (97% molar fraction), *N*-acryloyloxysuccinimide, NAS (2% molar fraction) and 3-(trimethoxysilyl)propyl methacrylate (MAPS, 1% molar fraction). A detailed description of the synthesis and characterization of the parent polymer are

reported elsewhere<sup>11</sup>. Briefly, after degassing anhydrous THF with helium, DMA, NAS and MAPS were added to the reaction flask so that the total monomer feed was 20% w/v and their molar ratio 97:2:1 respectively. The reaction mixture was heated to 65°C for two hours in presence of  $\alpha, \alpha'$ -azoisobutyronitrile (AIBN). The crude material was cooled to room temperature and diluted 1:1 with dry THF; the solution was then precipitated in petroleum ether (10 times the volume of the reaction mixture) to eliminate unreacted monomers. The polymer was collected by filtration as a white powder and dried under vacuum at room temperature. To introduce the new functionality (alkyne), a 20% w/v solution of the copolymer was prepared by dissolving it in dry THF and a 2.5 molar excess, respect to the moles of NAS, of the propargylamine was added to the crude material, assuming that the concentration of NAS along the polymer chain is 20 mM. The mixture was stirred for 5 h at room temperature and then diluted 1:1 with anhydrous THF. The polymer was precipitated in petroleum ether (10 times the volume of the reaction mixture), filtered on a Buckner funnel and dried under vacuum at room temperature. To further purify the obtained powder, the polymer was dissolved again in anhydrous THF to a final concentration of 10% w/v and re-precipitated in petroleum ether. The powder was finally filtered and dried again under vacuum at room temperature

### **8.1.3 Click gel preparation and polymerization conditions**

Copoly-Alkyne (T) was dissolved in 1X Running Buffer Solution (50mM BisTris-100mM Tricine) to a final concentration of 15% (w/v); to this solution, poly(ethylene glycol) bisazide (C), ( $M_w$  1.100), was added to a final concentration of 15mM. The mixture of the two polymers was stirred for few seconds at 50°C. To this solution Copper Sulfate, ( $CuSO_4$ , 2.5mM), Tris(3-hydroxypropyltriazolylmethyl)amine (THPTA 10mM), SYBR Green I (20X, from a stock of 10.000X in DMSO) were added. Lastly, ascorbic acid (12.5mM) was added to initiate the polymerization. The mixture was then stirred for few seconds. The solution was withdrawn with ultrathin Insulin Syringe 30 Gauge and empty D1000 ScreenTape were filled by making a small hole in the bottom chamber. Once the channels of the ScreenTape were filled, ScreenTape was put in a waterbath. Polymerization occurred within 9-10 minutes at 70°. 1X Running Buffer was then

added with ultrathin Insulin Syringe 30 Gauge by making a small hole in the upper chamber. The ScreenTape was kept at room temperature for 2 hours before electrophoresis.

#### **8.1.4 ScreenTape store conditions**

ScreenTape with click gels polymerized inside the channels was stored for shelf-life studies as follow: the injection sites were covered with silicon grease and then it was stored in the fridge in a box with damp paper towels at the bottom to reduce evaporation. Just in case of buffer loss, the upper chambers were refilled with 1X Running Buffer before electrophoresis analysis.

#### **8.1.5 DNA Ladder preparation**

A stock of 40ng/uL of Generuler 100bp with two additional DNA fragments was prepared as follow: 1uL of 1500bp fragment, 20uL GeneRuler 100bp DNA Ladder and 2uL 25bp fragment were added to 227uL 1XTE (Tris-EDTA Buffer)

#### **8.1.6 Preparation of DNA samples**

All reagents (Loading Buffer without or without SYBR Green I and DNA 40ng/mL stock solution) were allowed to equilibrate at room temperature; 40  $\mu$ L of this solution were added to an equal volume of Loading Buffer with or without SYBR Green I. DNA samples were placed in PCR vials (volume required: 4uL/tube) and vortexed using IKA vortexer and adaptor at 2000 rpm for 1 minute. The vials were spinned down to position the samples at the bottom of the tubes.

### **8.1.7 FT-IR spectra analyses**

FT-IR spectra were recorded using a Jasco-660 spectrometer and analyzed with Spectra Manager software 1.52 (Jasco, MD, USA). The samples were mixed with KBr and compressed to obtain a tablet. Then 32 scans were recorded over the range 4000–400  $\text{cm}^{-1}$  at a resolution of 4  $\text{cm}^{-1}$  at intervals of 1  $\text{cm}^{-1}$ . All the spectra have been analyzed after subtracting the spectrum of a blank KBr pellet.

### **8.1.8 Fluorescence assay**

A standard solution of Loading buffer 4X SYBR Green and a solution of Loading buffer 4X SYBR Green with 15% (w/v) Copoly-Alkyne as additive were prepared and stored up to one month. In a 96-well plate 3 replicates of each type of loading solution were prepared by adding 2,6  $\mu\text{L}$  of salmon sperm DNA (100ng/mL) to 10 $\mu\text{L}$  of the standard loading solution and of the loading solution with Copoly-Alkyne.

Fluorescence of each replicate was read by a fluorometer (Nanodrop 3300, excitation wavelength 488 nm, emission wavelength 535 nm) at DAY 0, DAY 1, DAY 9 and DAY 28.

### **8.1.9 Swelling test**

Four channels of a ScreenTape were filled with Click gel solution (15% T, 15mM C) and gelified as described in Section 8.1.3. 1X running buffer containing 20X SYBR Green I was added in the upper chamber and then the ScreenTape was stored as described in Section 8.1.4. Using the 2200 TapeStation Software Controller, Camera Settings parameters were set with 300 milliseconds of exposure time and images of the four channels were taken at DAY 0, DAY 1, DAY 7, DAY 13, DAY 25.

Image J software was used to display a two-dimensional graph of the fluorescence intensities along a line within the channels. The x-axis represents distance in pixel along a line of a channel and the y-axis is the fluorescence intensities (gray scale values).

#### **8.1.10 Electrophoretic conditions and Data Analysis**

Electrophoresis was performed in the 2200 TapeStation instrument, provided by Agilent Technologies. Tape Station Controller allowed setting all the electrophoretic conditions.

For our purpose, an electric field of 150 V was applied and the gels were run at 25 °C. In general, the duration of electrophoresis was 500 seconds. Extended running conditions corresponded to 1200 second maximum.

TapeStation Software Analysis provided automatically images analysis and calculation of electrophoresis parameters (resolution, area, mobility).

## 8.2 RESULTS AND DISCUSSION

### 8.2.1 DEVELOPMENT OF A NOVEL HYDROGEL WITH PREFORMED POLYMERS THROUGH CLICK CHEMISTRY

The overarching goal of this work was to develop a novel hydrogel, which could improve the performance provided by the standard acrylamide-based gel matrices in commercial use for the analysis of DNA fragments ranging from 25 to 1500 base pairs (bp). In fact, despite their efficiency, the two main limitations of acrylic-based hydrogels are: first, the employment of toxic and not stable monomers and, second, the need of radical polymerization approaches that use UV initiators, which are incompatible with prestain gel methods, as the dye is not stable under UV light. The incorporation of the dye in the gel matrix is desirable, because it is well documented that in-gel stain method provides more efficient separations of DNA fragments compared to the prestain and poststain approach<sup>8</sup>. In particular, the acrylic-based commercial formulations would greatly benefit from an increase of resolution, in size region between 500 and 25 double base pairs range.

The formation of hydrogels from preformed polymers overcomes all the limitations described above. In fact, besides the replacement of the toxic and unstable acrylamide, radical polymerization with UV initiators is avoided, permitting to introduce the dye in the matrix before gelation.

The development of functional *N,N* dimethylacrylamide-based copolymers is one of the most important field of research in the CNR laboratory. In particular, as already illustrated in the PART A of this dissertation, poly(DMA-NAS-MAPS), a copolymer made of three different monomers *N,N*-dimethylacrylamide (DMA), *N*-acryloyloxysuccinimide (NAS), and 3(trimethoxysilyl)propyl methacrylate (MAPS), introduced in 2004 has proven to be an ideal candidate to coat surfaces for microarray applications<sup>11</sup> and to functionalize nanoparticles<sup>12</sup>, thanks to the presence of *N*-acryloyloxysuccinimide (NAS), an active ester group, highly reactive towards several nucleophiles, in particular amine, which are naturally present in biomolecules like proteins or peptides. Zilio et al.<sup>13</sup> in 2014 synthesized a new copolymer similar to

poly(DMA-NAS-MAPS), with the only difference that succinimide ester was replaced by an alkyne functionality. The new copolymer, poly(*N,N*-dimethylacrylamide (DMA)-3-trimethylsilyl-prop-2-ynyl methacrylate (PMA)-3-(Trimethoxysilyl)propyl methacrylate (MAPS)), poly(DMA-PMA-MAPS), was produced by random radical copolymeration of the three monomers, by a synthetic approach similar to that used for the parent copolymer and enables the conjugation of biomolecules derivatized with azide groups that react with the alkyne monomer through the well known click reaction: *the copper-catalyzed 1,3-dipolar cycloaddition (CuAAC)*.

In the first part of this work, we utilized CuAAC reaction to form hydrogels by crosslinking poly(DMA-PMA-MAPS), the main component of the gel matrix **(T)**, synthesized as described in *Section 8.2.2*, with poly(ethylene glycol) bisazide ( $M_w$  1100), PEGN<sub>3</sub>, the crosslinker of the reaction **(C)**. The reaction affords triazoles in excellent yields with complete regioselectivity. **Figure 4** shows a schematic representation of the novel hydrogel structure.

The cycloaddition reaction between an alkyne and an azide functional group is greatly accelerated by Cu<sup>I</sup> obtained by the reduction of CuSO<sub>4</sub> (Cu<sup>II</sup>) with sodium ascorbate (AAC). The use of active Cu<sup>I</sup> catalyst in click reactions that involve biomolecules, suffers from two major drawbacks. One is the cytotoxicity of Cu<sup>I</sup>, while the second is the slow reaction rate, which hampers the quantitative reaction between alkyne and azide functional groups. The introduction of the water soluble tris-(hydroxypropyl)triazolylmethylamine (THPTA) ligand that forms a coordination complex with copper during the process improved dramatically the quality of the gel allowing a faster and more efficient gelation by blocking the bioavailability of Cu<sup>I</sup> and ameliorating the potential toxic effects while maintaining its catalytic effectiveness<sup>14</sup>. As it will be discussed in the next sections, the introduction of THPTA ligand was essential because it promoted a more efficient crosslinking between azide and alkyne functional groups, remarkably improving the performance of the novel click gel.

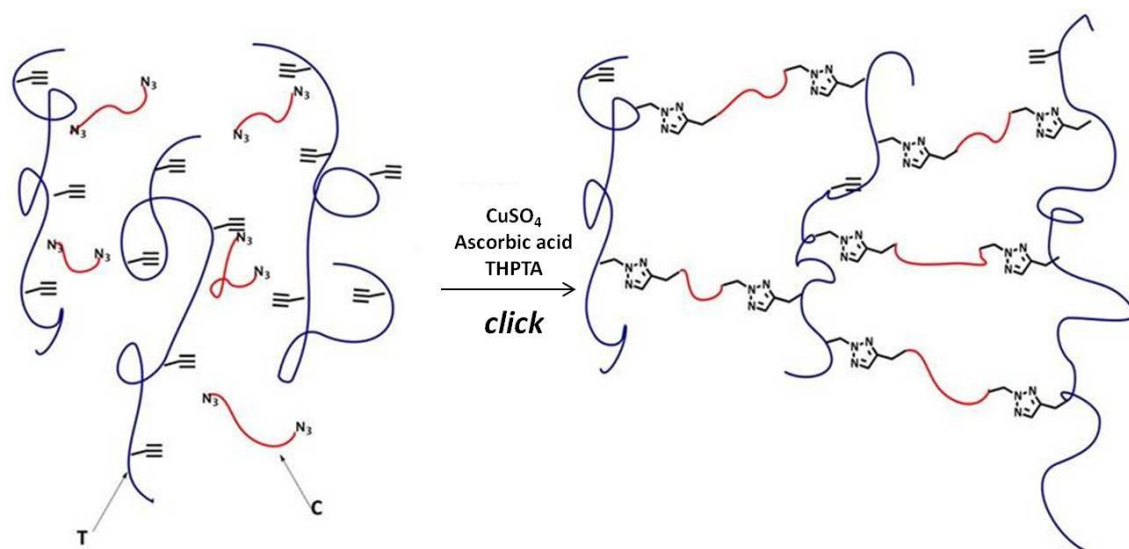


**Figure 4.** Scheme of Copoly-Alkyne (T)/ poly-ethylene glycol bisazide (C) network formation via Huisgen cycloaddition (CuAAC). The triple bonds of (T) are reactive towards the azide functionalities of (C) in the presence of the catalysts (CuSO<sub>4</sub>/AAC/THPTA) allowing the formation of stable triazoles structures.

### **8.2.2 OPTIMIZATION OF THE DYE IN THE GEL MATRIX AND THE KEY ROLE OF THPTA**

As mentioned above, the new gel provides a number of advantages over common hydrogels. The first is that its formation does not require the use of toxic and unstable monomers, such as acrylamide. The second is that, since the polymerization procedure does not require an UV initiator, a more homogeneous gel structure can be obtained. Radical polymerization reactions are sensitive to oxygen content and to UV light intensity. The different sections of the microchannel during radical polymerization were differently exposed to both oxygen and light, therefore the gel structure was dishomogeneous with serious consequences on the DNA local mobility and significant loss of efficiency. In addition, thanks to the gelation mechanism, it was possible to incorporate the dye (SYBR Green I) directly in the mixture (in-gel stain method), avoiding addition of the dye to the sample; in fact, the poststain process is not compatible with the ScreenTape format. These features of the new gel are advantageous over polyacrylamide gels, where the dye needs to be added to the sample after the gel is formed to avoid its photodegradation during polymerization.

A number of experiments, aimed at improving the performance of the click gel by optimizing the dye concentration in the gel matrix, were performed. A set of experiments was also conducted to investigate the role of the THPTA ligand. Both additives proved to be fundamental to achieve the desired performance.

Regarding the optimization of the dye concentration, increasing amounts of SYBR Green I (6X, 10X, 14X and 20X, from a commercial stock solution of 10,000X) were incorporated directly in the polymer solution, composed of 10% w/v of poly-DMA-PMA-MAPS (T) and 20mM of PEGN<sub>3</sub>, (C) in 50mM Bis-Tris, 100mM Tricine, pH 7.3. The experimental procedure used to form the gel showed to be robust and requires mild conditions. Firstly, the mixture of the two polymers was prepared in order to promote their entanglement; subsequently, the catalyst, CuSO<sub>4</sub>, and the desired dye amount were added to the solution and, lastly, the reaction was initiated by the addition of ascorbic acid. A 100bp Ladder with additional 1500 bp and 25bp double stranded DNA fragments, was the sample employed in all the experiments reported in this Chapter.

Initial formulations, lacking of THPTA, failed to provide an acceptable performance. As it is appreciable from **Figure 5**, the electrophoretic pattern was slightly improved by increasing the dye concentration (**Figure 5 a, b, c, d**); however, the bands were broad and poorly resolved at any concentration. Addition of THPTA, to the same polymer/buffer formulation (10%T, 20mM C), did not improve so much the performance but reduced significantly the gelation time (**Figure 5e**). Finally, as shown in **Figure 5f**, the best separation was obtained, by adding THPTA ligand to the polymer solutions, at the highest SYBR Green concentration (20X) by decreasing the concentration of the polymers in the mixture (7% T, 14mM C). The use of THPTA ligand blocked the bioavailability of Cu<sup>I</sup>, promoting a more efficient crosslinking between azide and alkyne functional groups, improving remarkably the performance and accelerating the gelation process.

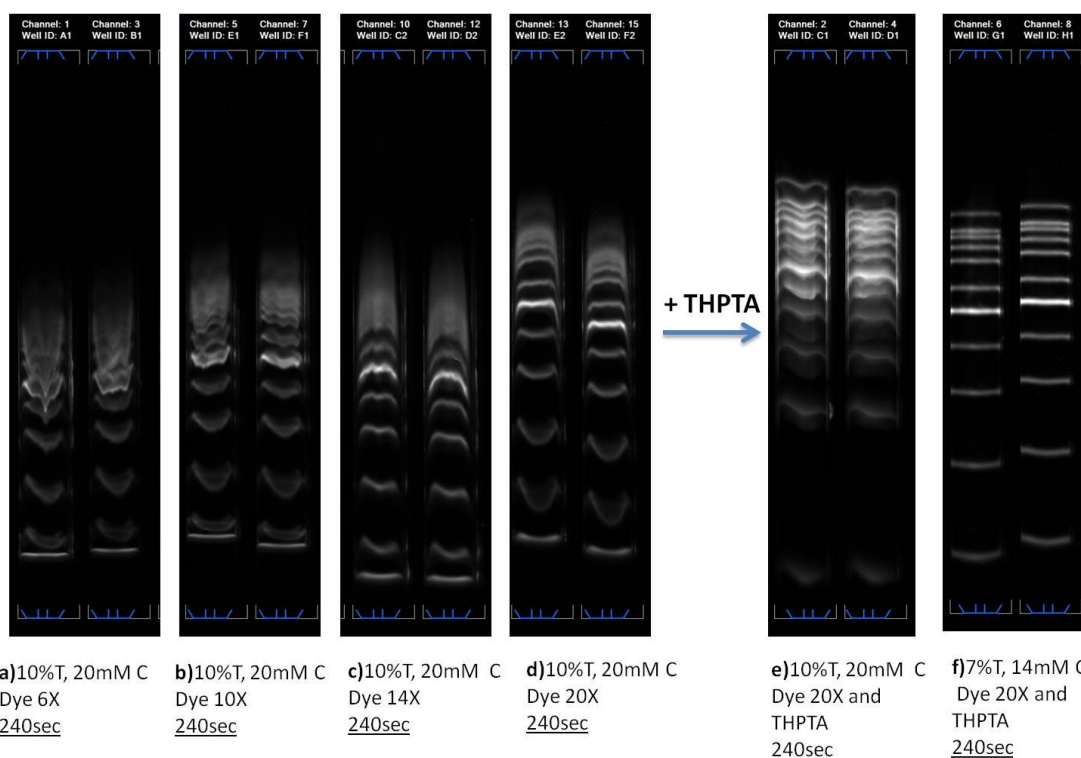


**Figure 5.** Optimization of the performance of the click hydrogel. Several dye concentrations (6X, 10X, 14X, 20X) were tested in a click gel matrix composed of 10% T and 20mM C. (**a, b, c, d**). No THPTA ligand was used. On the contrary, Figure **5e** shows a click hydrogel matrix composed of 10% T and 20mM C, where THPTA ligand was added. The gelation time was considerably reduced but the performance still needs to be improved. Just decreasing the concentrations of the polymers (7%T, 14mM C), adding THPTA ligand and maintaining 20X of the dye, an excellent performance was then obtained (Figure **5f**). The same electrophoresis time (240 seconds) was used for the comparison of all the conditions.

Since the gel must be formed within the microchannels, in view of a large scale, industrial production, it was of utmost importance to control the gelation speed to avoid clogging of the syringe during the injection of the monomer solution in the filling step. In order to obtain a proper mixing of the gel components during manufacturing, the amount of catalyst was carefully studied and optimized in order to achieve a good compromise between gelation time and performance. In particular, with 2.5mM of  $\text{CuSO}_4$ , 10mM of THPTA, and 12.5mM ascorbic acid ([Cu]:[THPTA]:[AAc]=1:4:5) gelation occurs in about 120 minutes at room temperature. In view of manufacturing of this gel matrix in an industrial context, this time was too long. Therefore, in order to reduce the time to 10 minutes, the process was further optimized: the monomer solution was introduced at room temperature in the ScreenTape, which was then heated to 70 °C.

### **8.2.3 COMPARISON BETWEEN “IN-GEL STAIN” AND “PRESTAIN” APPROACHES**

After optimization of the gel formation, two different staining approaches for DNA detection in the new hydrogel were compared to demonstrate the advantages in terms of separation performance provided by the inclusion of the dye the gel matrix. In particular, the separation achieved by directly incorporating the dye in the gel matrix (in-gel stain procedure), (**Figure6b**), was compared with that of the prestain method where the dye is added to the DNA immediately before electrophoresis (**Figure6a**). In both separations the amount of SYBR Green I used was the same (20X). The electrophoretic profile provided by the in-gel staining procedure was remarkably better than that obtained with the prestain. A better separation efficiency was achieved when the dye was incorporated in the gel matrix, leading to an excellent resolution of all the DNA fragments. The most significant improvement was observed for the low molecular weight ( $M_w$ ) DNA fragments, i.e. in the region between 500 and 100 bp, which was compressed in the prestain procedure. In fact, in the in-gel stain method the low  $M_w$  fragments had higher mobility and no band broadening occurred. On the contrary, the separation efficiency in the prestain gel was compromised by the diffusion of the bands.

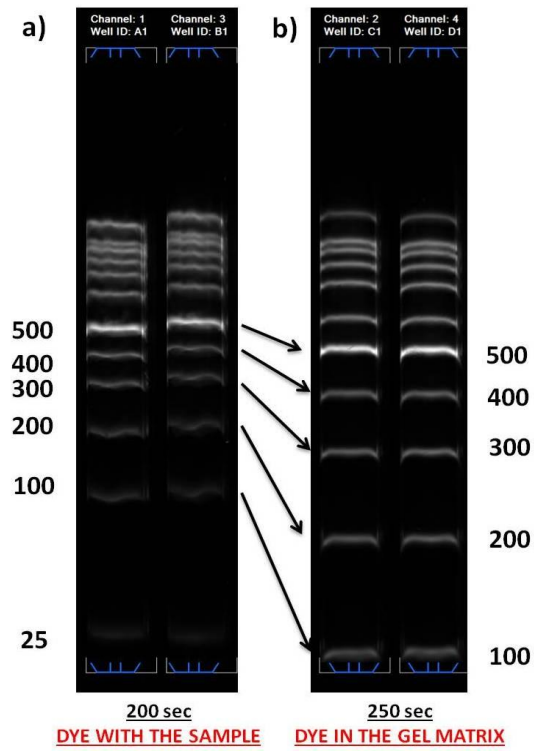


**Figure 6:** Comparison between prestain method (a) and in-gel stain approach (b). Low molecular weight fragments (500-100) are better separated in case b, thanks to the inclusion of the dye in the gel matrix.

#### **8.2.4 DEVELOPMENT OF A “CLIKABLE” POLYMER THROUGH A POST MODIFICATION**

##### **APPROACH**

Poly(DMA-PMA-MAPS), the basic component of the hydrogel, was introduced by Zilio et al.<sup>13</sup> and it was obtained through a radical polymerization process. Its synthesis required protection of the triple bond before polymerization, followed by deprotection, dialysis and lyophilization. Although the preliminary results obtained with this polymer were excellent, its use in large scale production might be problematic due to the need of a purification step through dialysis. In view of manufacturing the matrix in an industrial context, it was necessary to develop an alternative synthetic strategy for the PDMA based copolymer. Sola et al.<sup>15</sup> have recently introduced a new approach to produce a polymer similar to poly(DMA-PMA-MAPS), with the only difference that the alkyne moiety is bound to the backbone chain through an amide bond instead of an ester (see **Figure 7**). The new strategy exploited the parent poly(DMA-NAS-MAPS) polymer as scaffold to obtain, through a post-polymerization modification (PPM) approach, a family of polymers by reacting, in a quantitative way, the active esters contained in the polymer chain with bifunctional amines, bearing different functional groups. In this work we have inserted, along the polymer chain, alkyne groups, which enable click chemistry reaction with azide modified polymers. This synthesis is more suitable for large scale applications as it avoids deprotection and dialysis steps.

In all the experiments described from now on, the post-modification strategy illustrated in **Figure 7** and the copper (I)-catalyzed azide-alkyne cycloaddition (CuAAC) were used to form the gel matrix.

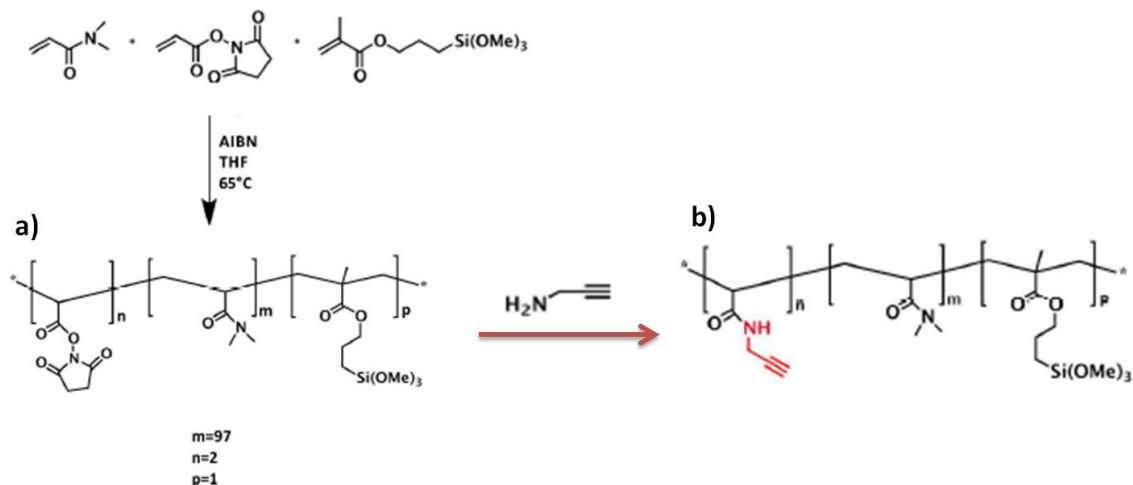


**Figure 7.** Scheme of the synthesis of poly(DMA-NAS-MAPS) (a) the precursor of Copoly Alkyne (b) obtained by post-polymerization reaction with propargil-amine.

In order to verify the efficacy of the post-polymerization reaction, the modified polymer was analyzed by Fourier Transform Infrared Spectroscopy (FTIR). **Figure 8** illustrates FTIR spectra of Copoly Alkyne (a) and of poly(DMA-NAS-MAPS) (b). In **Figure 8a** the typical signal of triple bonds stretching is evident at  $2090\text{ cm}^{-1}$ . Furthermore, the quantitative conversion of NHS ester into the alkyne functionality is demonstrated by the disappearance of the signal at  $1740\text{ cm}^{-1}$  (**Figure 8b**) that corresponds to the stretching of NHS ester carbonyl present in poly(DMA-NAS-MAPS).

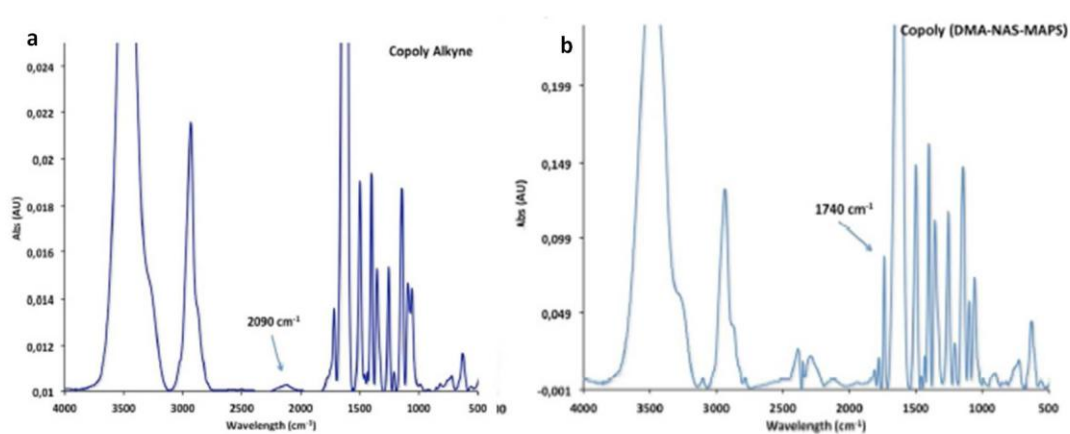


**Figure 8.** FTIR spectra of Copoly Alkyne, poly(DMA-NAS-MAPS), registered using a Jasco 660 spectrophotometer. A total of 32scans were recorded over the range 4000-400  $\text{cm}^{-1}$  at a resolution of  $4 \text{ cm}^{-1}$  at intervals of  $1 \text{ cm}^{-1}$ . The spectra are magnified to highlight the signals typical of each introduced group

To verify the equivalence of Copoly Alkyne, the copolymer obtained by PPM and poly(DMA-PMA-MAPS), the copolymer produced by direct incorporation of the alkyne monomer, hydrogels produced with the two copolymers in identical conditions were compared. **Figure 9A** shows a click hydrogel (15%T, 15mM C) containing Copoly Alkyne, while **Figure 9B** shows a click hydrogel (7% T, 14mM C) with poly(DMA-PMA-MAPS). Despite the different methods of synthesis used, the performance was comparable. However, a higher polymer concentration had to be employed in the case of Copoly Alkyne (**hydrogel B**), and, as a consequence, it was necessary to increase the electrophoresis time to allow the 1500 bp fragment, taken as a reference peak, to migrate the same distance. Increased resolution of the low  $M_w$  fragments, was detected in the new formulation. As clearly visible in **Figure 9**, relatively to the 1500 bp fragment, the mobility of DNA fragments in the region of 500-100 bp was slightly higher for Copoly Alkyne (**hydrogel B**), leading to a better separation.

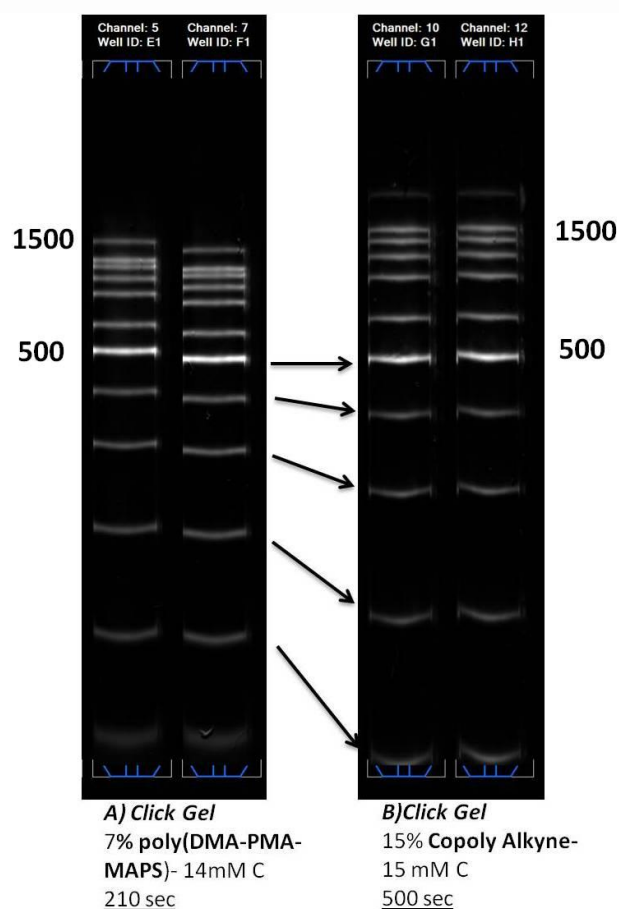


**Figure 9.** Comparison between click hydrogels obtained by CuAAC reaction between poly(DMA-PMA-MAPS) and PEGN<sub>3</sub> (**hydrogel A**), and Copoly Alkyne and PEGN<sub>3</sub> (**hydrogel b**)

### **8.2.5 COMPARISON BETWEEN CLICK HYDROGEL AND ACRYLAMIDE-BASED GEL**

The novel click hydrogel obtained was compared with the state-of-the-art acrylamide-based gel. The new gel provided excellent separations of DNA, superior to those usually obtained with the commercial gel matrix, bench mark for high resolution separations of DNA and RNA. In the images shown in **Figure 10a**, Generuler 100bp Ladder, with the addition of 1500 bp and 25bp double stranded DNA fragments, was electrophoresed on both gels, standard acrylamide-based formulation (**A**) and click hydrogel (15% T, 15mM C), (**B**). While the commercial gel required addition of the dye to the sample (pre-stain method), the click hydrogel contained the fluorescent dye in the matrix (in-gel stain). The performance of the click gel compares favourably to a standard acrylamide matrix under a fixed run distance of the 1500 bp fragment, used as reference parameter, with notable improvements in several key aspects including efficiency and selectivity. Band broadening in radical hydrogels was probably due to an effect called *lensing effects* induced by UV photoinitiation. In fact, since the microchannels of the ScreenTape have a curved geometry, their sections were differently exposed to both oxygen and light intensity, therefore the UV polymerization was affected by an uneven light intensity and oxygen content and, as a consequence, the gel structure was dishomogeneous with serious consequences on the local mobility and significant loss of efficiency. On the contrary, since the click hydrogel does not require formation of radicals, the structure of the gel is more homogeneous and independent from the channel configuration. Moreover, thanks to the inclusion of the dye in the gel matrix, a remarkable improvement of separation efficiency for fragments lower than 500 bp was achieved. The graph depicted in **Figure 10b** reports the resolution obtained in the two gels calculated by the Analysis Software of the instrument. A higher electrophoresis time was employed for the click hydrogel, but the resolution of DNA fragments ranging from 500 to 100 bp was significantly better.

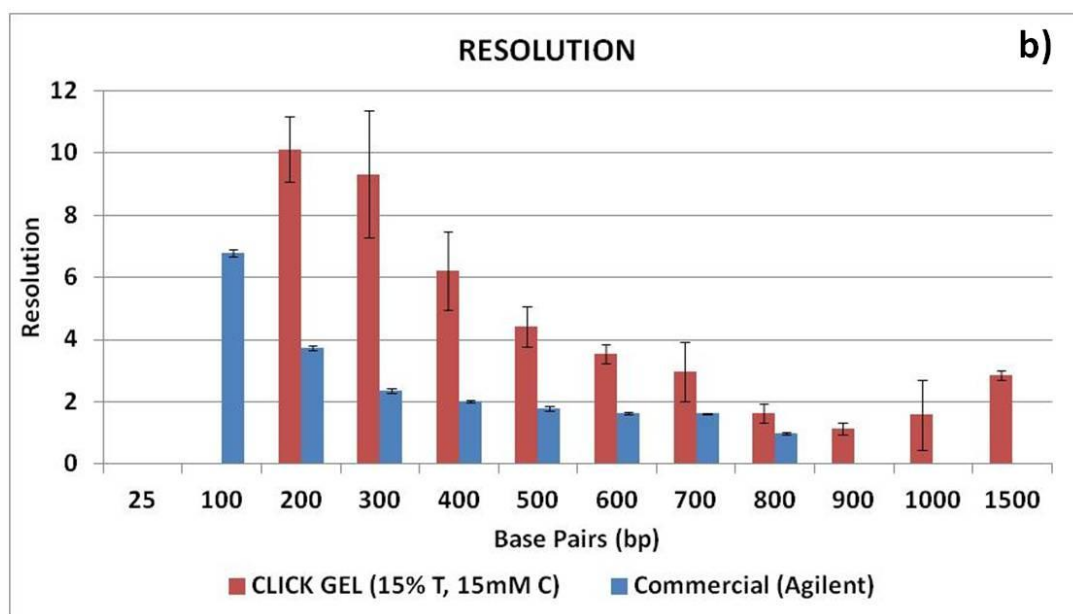
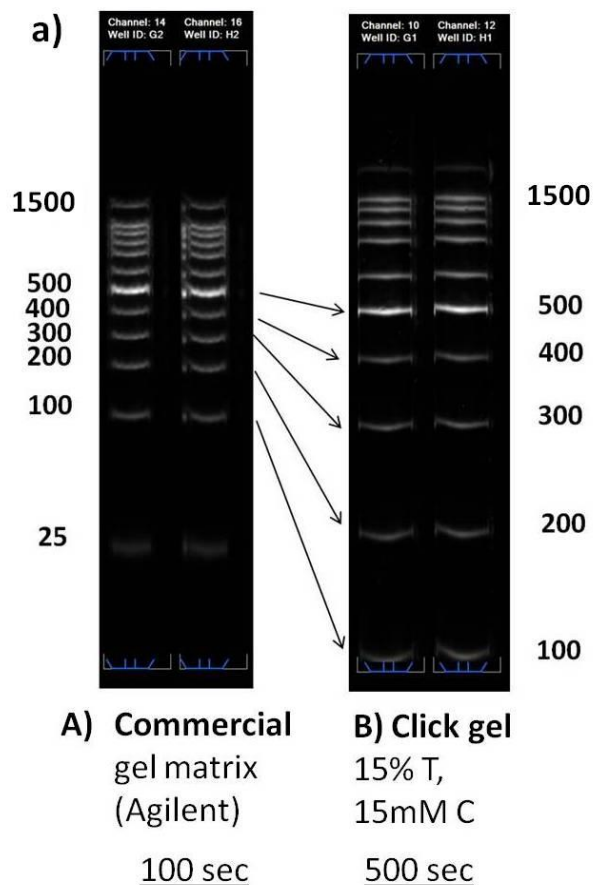


**Figure 10.** a) Comparison between the separation profile of acrylamide (A), and of click based gel (15% T 15Mm C with 20X of SYBR Green I in the matrix), (B). For the comparison, the same run distance of the highest base pairs (1500) was chosen. (b) Calculation of resolution parameter between acrylamide based gel matrix and the click one.

Furthermore, the click gel exhibits excellent band shape and fluorescence signal stability under extended running conditions (**Figure 11**). This allows for improved separation of higher molecular weight bands (up to 1500bp in this case) with minimal band dispersion or signal loss even after extensive electrophoresis time (1200 seconds)

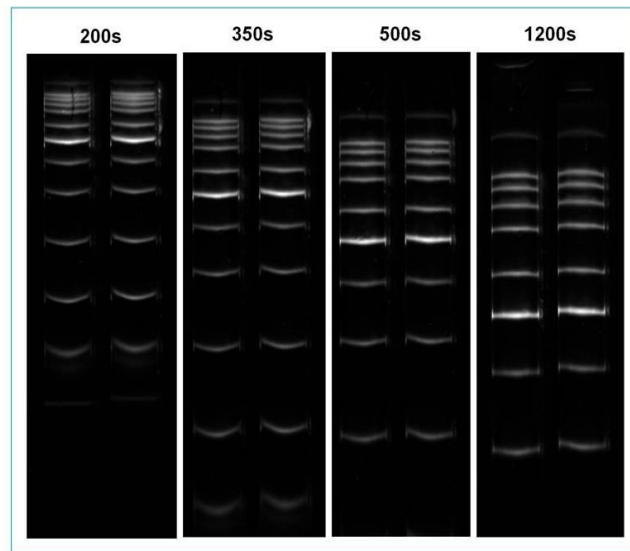


**Figure 11.** Click Gel (15% T 15Mm C): extended run time separation from 25-1500 bp. DNA large bands (high molecular weight) keep an excellent shape after extensive electrophoresis time

### 8.2.6 CLICK HYDROGEL FORMULATIONS WITH DIFFERENT POLYMER CONCENTRATIONS

Since the two preformed polymers, Copoly Alkyne (T) and Poly-ethylene glycol bisazide (C) are the main components of the click gel, the pore size of this network is determined by their concentration in the gel matrix: the higher the total copolymer and cross-linker concentration, the smaller the pore size is. Since the gelation mechanism is totally different than that of standard polyacrylamide gels, the percentage of T and C has to be optimized by carefully tuning the relative concentrations of the two polymers. In particular, considering that poly(ethylen glycol) bis azide is a bifunctional linker, the best ratio T:C is found to be 2:1. For example, all the click hydrogels shown so far have the following composition: 15% w/v T and 15mM C. The rationale behind this ratio is that a 15 % w/v Copoly Alkyne solution contains about 30 mM of alkyne groups, being the alkyne molar fraction 2%. So, in order to maintain the 2:1 ratio the concentration of the crosslinker is set at 15mM. This approach provides an efficient cross-linking between azide functionalities of C and triple bonds of T, since the bifunctional crosslinking may have the possibility to bind two different polymer chains together. Different ratios of the two polymers are either not able to form the gel or, in other cases, the obtained gel leads to poor performance electrophoresis.

Several concentrations of the two preformed polymers are tested, maintaining the ratio 2:1 constant to evaluate the minimum concentration required to form a click hydrogel offering a good separation profile. In particular, **Figure 12** illustrates formulations with decreased concentrations of the two polymers, ranging from 15% to 8.5 %T. This is the minimum concentration able to provide a homogeneous gel with good DNA resolving power. The graphs reported in **Figure 13** compare the mobility **(a)** and the resolution **(b)** in the formulations **B** (12%T, 16,6 mM C) and **D** (10%T 10mM C) illustrated in **Figure 12**, with the same parameters in a standard acrylamide-based gel matrix. Since the size dependent mobility curve of click formulations is steeper than in polyacrylamide, the resolution, in particular that of low  $M_w$  fragments, is higher in the click hydrogels.

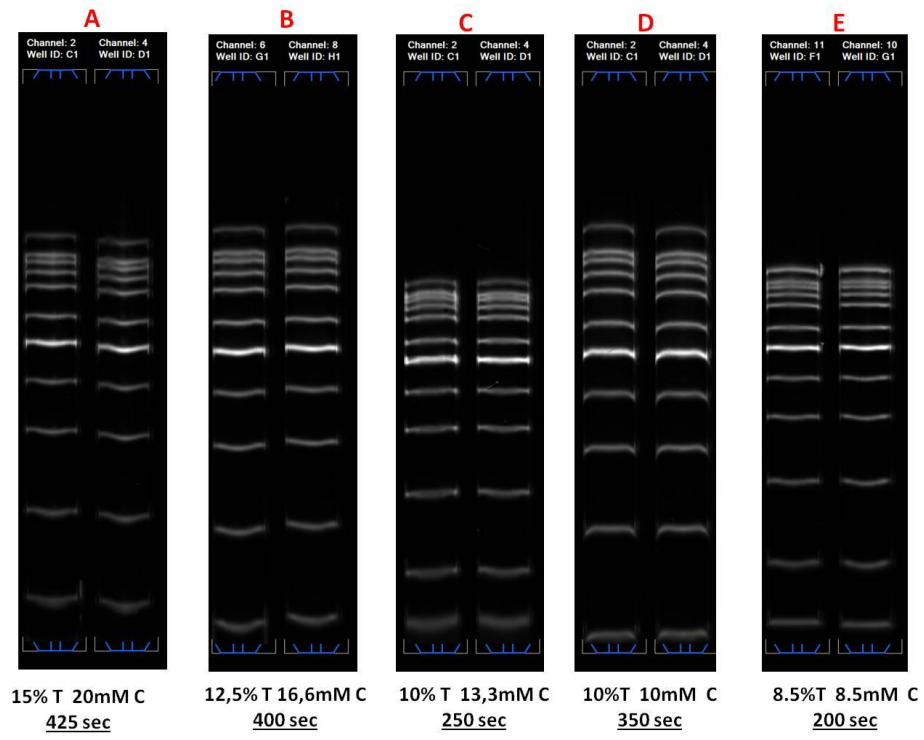


**Figure 12.** DNA separation performance with decreasing concentrations of Copoly Alkyne (T) and PEGN<sub>3</sub> (C)

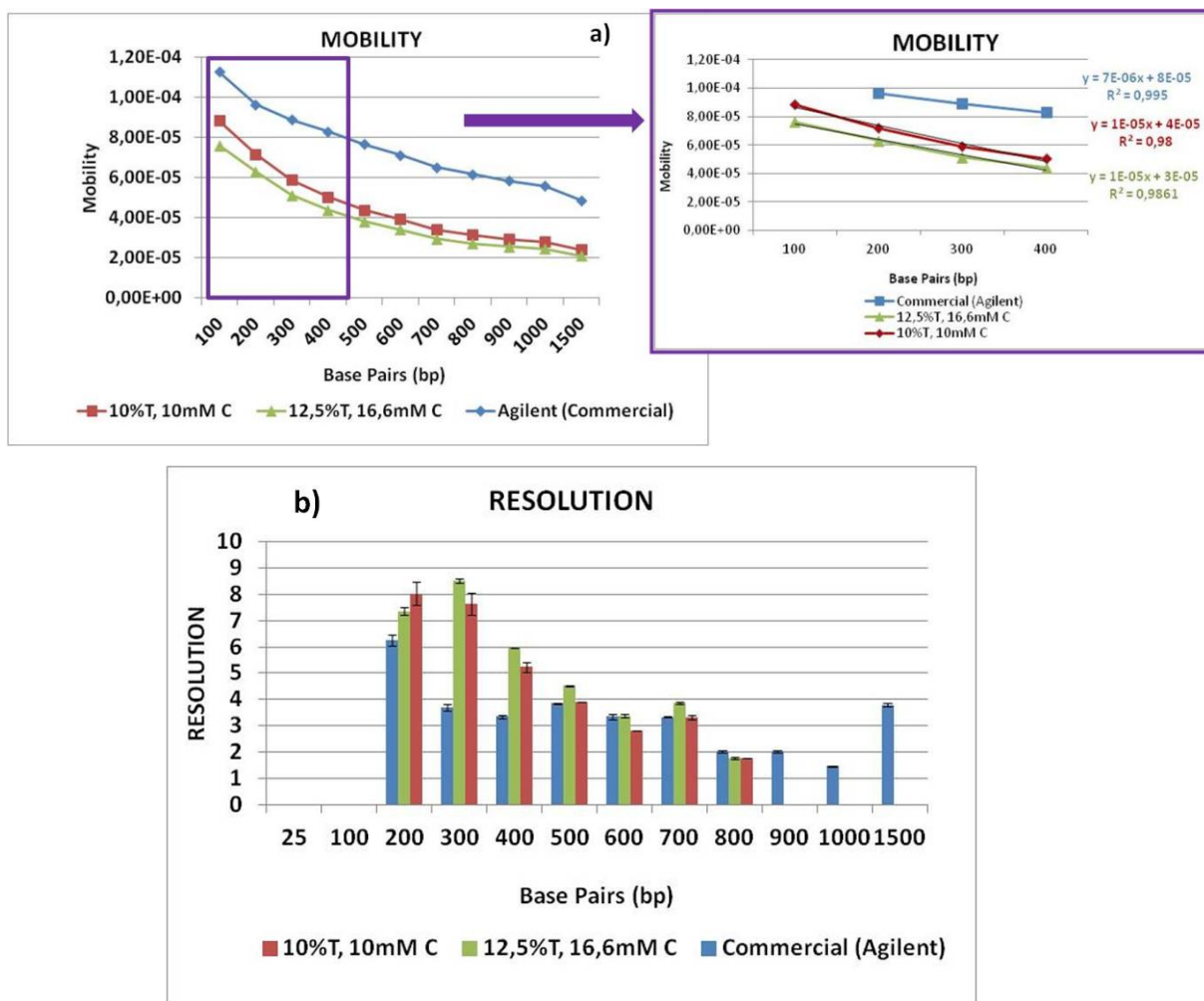


**Figure 13.** Mobility (a) and resolution (b) of **B** and **D** click hydrogels formulations (Figure 12) compared with the same parameters of an acrylamide-base gel. The slopes in the purple box confirm that click hydrogels have higher mobility than that of acrylamide-based gel. All the parameters are calculated according to the Software Analysis of 2200 TapeStation.

### **8.2.7 SHELF-LIFE STUDIES AND DYE STABILITY**

Fluorescent dyes are widely employed for the detection of nucleic acids in electrophoresis. As mentioned in *Chapter 7, Section 7.5.1*, commercial products such as SYBR<sup>®</sup> Green I, II and SYBR Gold stain have been shown to provide highly sensitive detection due to a combination of over 1000-fold fluorescence enhancement upon binding to nucleic acids and very low background in the unbound state.

Although these dyes have superior sensitivity over traditional DNA-binding dyes, such as Ethidium bromide (EB), they are not stable in aqueous solutions. Usually they are stored as stock solutions in organic solvents such as dimethyl sulfoxide and are transferred into aqueous solvents prior to electrophoresis. It is well documented that, in aqueous solvents, the fluorescence emission of these dyes for DNA detection drops to about half within 4 to 14 days of storage at room temperature<sup>16</sup>. As a result, we observe that in-gel stain, click gels has a short *shelf-life* which hampers their potential application. In particular, **Figure 14a** shows the results of a *shelf-life* study where a standard click gel (15% T, 15mM C, 20X dye in the gel matrix, pH 7.3) is stored in different channels of the same ScreenTape cartridge. GeneRuler, 100bp DNA fragments is run in different days in order to evaluate the gel performance over time.

As it is clearly observable, after 1 DAY the degradation of the dye affects the shape of the bands corresponding to the high molecular weight fragments (i.e the range between 1500 bp and 500 bp), while narrow bands are maintained up to 1 week for the low  $M_w$  (500bp-25 bp) fragments. The band broadening influences the resolution that declines significantly for some of the fragments while it remains constant for the DNA of small size. As shown in **Figure 14b**, the resolution data at DAY 1 and DAY 6 are comparable to those at DAY 0 for fragments ranging from 100-to 500 bp. Moreover, after 27 days, due to the dye degradation, no fluorescence signals are detected.

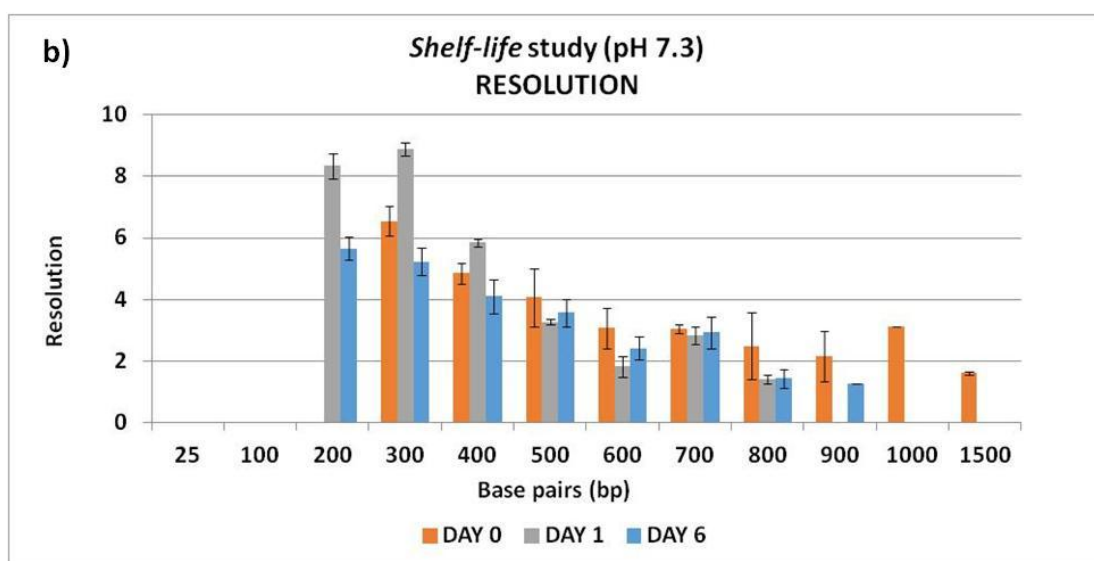
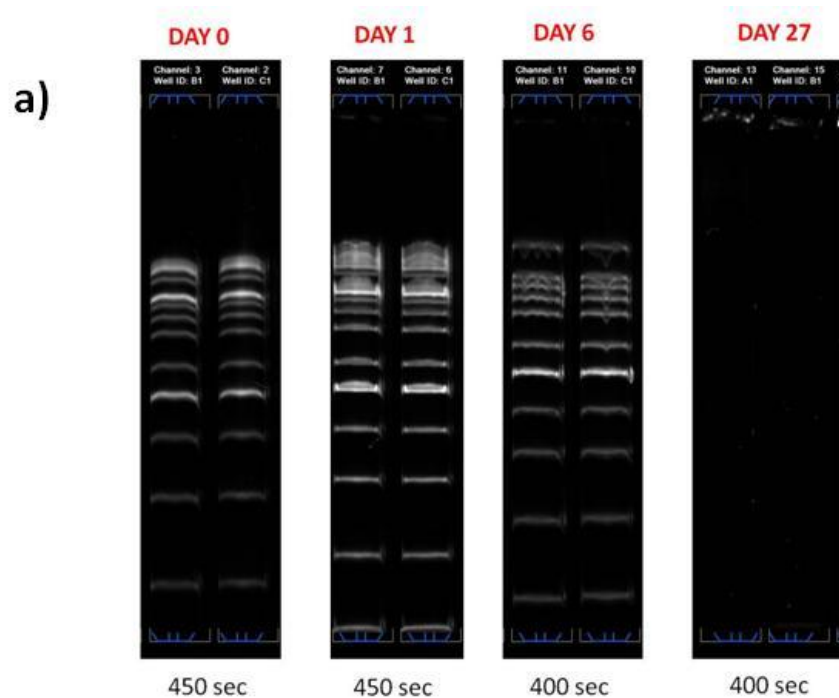


**Figure 14.** a) *Shelf-life* study of a standard Click gel (15% T 15mM C, 20X dye in the gel matrix, pH 7.3). The separation performance for high  $M_w$  bands (1500- 500) is compromised after 1 DAY, while low  $M_w$  bands (500-25 bp) keep a good separation profile. After 27 days, the performance is totally compromised due to the instability of SYBR Green I. (b) Resolution parameters: resolution data of DAY 1 and DAY 6 are compared to those of DAY 0 below 500 bp, while high  $M_w$  loses resolution in time.

In an effort to prolong the shelf-life of the new gel matrix, strategies to stabilize SYBR Green I are investigated. Detergents, such as Triton 100X and Tween 20 or compounds such as Cyclodextrins<sup>17</sup> have been used to improve the stability but their effects on dye stabilization are not sufficient in the context of our experiments. Zeng et al.<sup>18</sup> describe the use of tetrapentylammonium ion in TAPS (3-[tris(hydroxymethyl)methyl)methylamino]-1-propanesulfonic acid) buffer to increase the stability of complexes formed between DNA and bisintercalator dyes, such as SYBR Green. However, this report does not suggest that the stability of the dyes themselves is affected, nor mention the effect on SYBR Green stains.

The inventors of the US 6,365,341 B1 patent "*Stabilization of highly sensitive nucleic acid stains in aqueous solutions*"<sup>16</sup> demonstrate that quaternary compounds, in particular quaternary salts of tetramethylammonium, tetrabutylammonium and tetrapentylammonium, extend the *shelf-life* of highly sensitive nucleic acid dyes.

These compounds have the general structural formula  $R_4NX$  where  $R_4N$  is a cation and each R is independently a  $C_{1-6}$  alkyl group or a  $C_{1-6}$  alkoxy group, N is nitrogen, X is a halide anion (the preferred are bromide or chloride) or a hydroxyl anion which dissociates from the cation  $(R_4N)^+$  in an aqueous environment. When employed in nucleic acids electrophoretic separation, the useful concentration of the quaternary compound was between 5 and 20 mM.

Taking inspiration from this patent, in this work, tetrapentylammonium hydroxide (TPAOH),  $[CH_3(CH_2)_4]_4N(OH)$ , at 14mM is used as part of the buffer system. Although it slightly increases the pH of the solution (from 7.3 to 7.6), it does not affect the gel separation performance.

A *shelf-life* study is set by adding this compound to the standard buffer (50mM Bis-Tris-100mM Tricine). As in the aging study described above, the performance is evaluated over time by running 20ng of Ladder 100 bp in different days (**Figure 15a**).

The *shelf-life* of the dye is considerably improved: intense fluorescence signals are detected up to 41 days confirming the stability of the dye in these conditions. The resolution of DNA fragments at DAY 41 is compared to that obtained at DAY 0 (**Figure 15b**). Furthermore, a better resolution is achieved in the 300-400 bp range. However, as observed in the previously study, the resolution of high  $M_w$  (1500-500 bp) fragments is progressively lost.

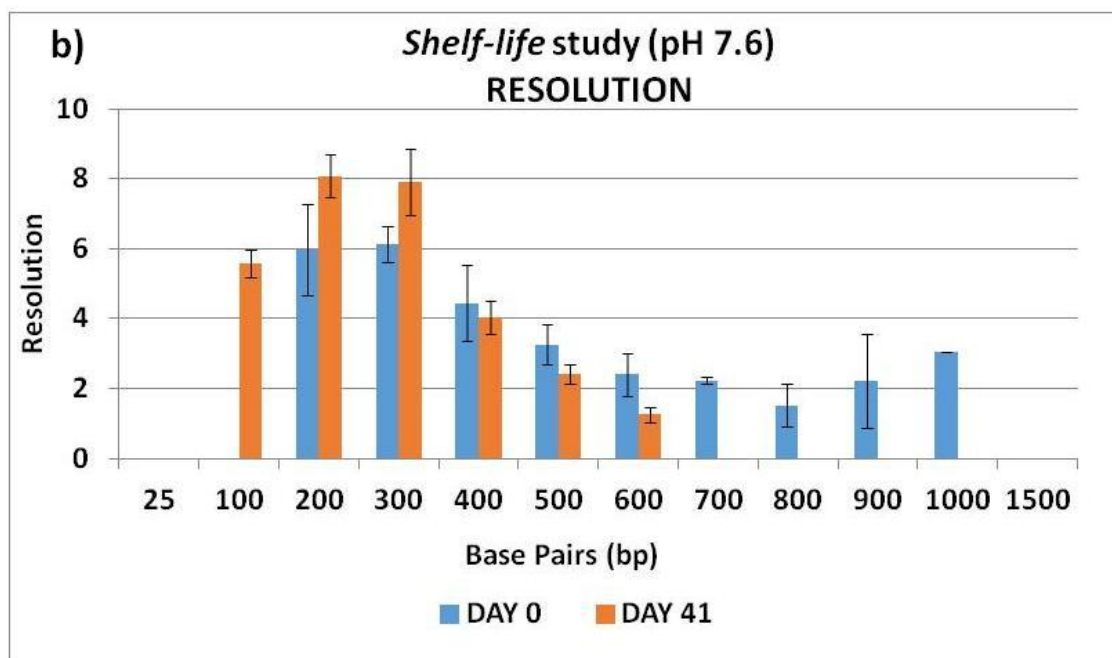
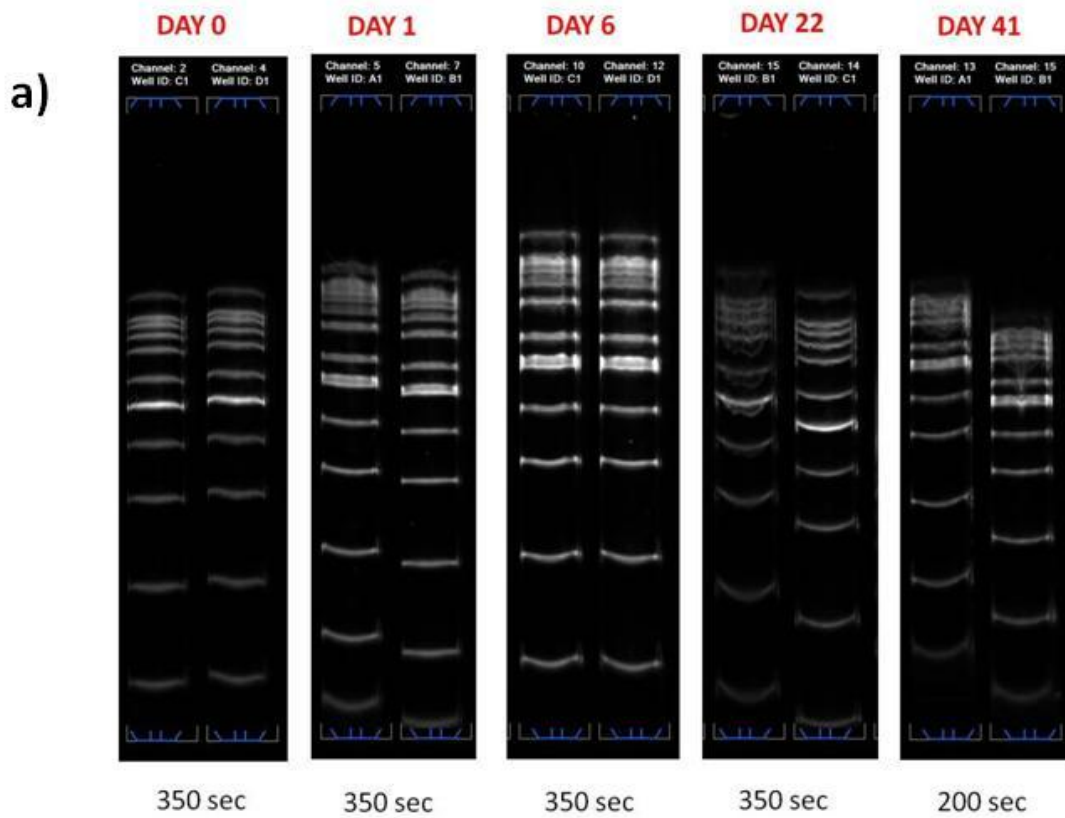


**Figure 15.** (a) *Shelf-life study* of a standard Click gel (15% T 15mM C, 20X dye in the gel matrix, pH 7.6). The stabilizer TPAOH is added to the standard buffer, allowing a remarkable improvement of the shelf-life of the dye. (b) Comparison between DAY 0 performance and DAY 41 in terms of resolution

Although the *shelf-life* of the dye is considerably improved, thanks to the employment of quaternary compounds (TPAOH) with consequent improvements in performance stability over time for the low Mw fragments, there is still a phenomenon to investigate: the broadening of bands in the 500-1500 bp range that occurs already after 1 day from the ScreenTape production. This problem hinders the commercial use of these types of gels.

Among the different strategies tested, which include optimization of buffer concentration and composition, storage conditions, dye type and concentration, the approach that provides successful results is the injection of a reduced amount of DNA so to decrease of DNA/dye concentration ratio.

**Figure 16a** shows the results of a *shelf-life* study where the efficiency of the bands, obtained in different days and at different DNA sample loads, 20 or 5 ng, is reported. A four times reduction in the amount of DNA loaded, improves dramatically the efficiency of high MW bands up to 1 month of aging. In the separation run at day 30, the resolution obtained by loading 5ng of DNA is significantly better than that obtained loading 20 ng (**Figure 16b**). In addition, the signal intensity of the bands does not change when 5 ng of DNA are injected (**Figure 17**), confirming that a good performance is kept up to 1 month.

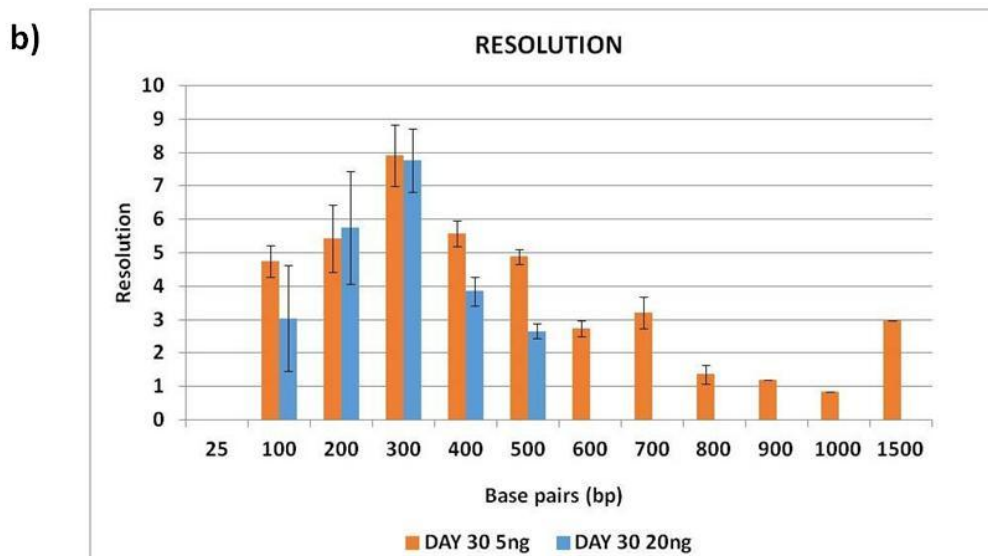
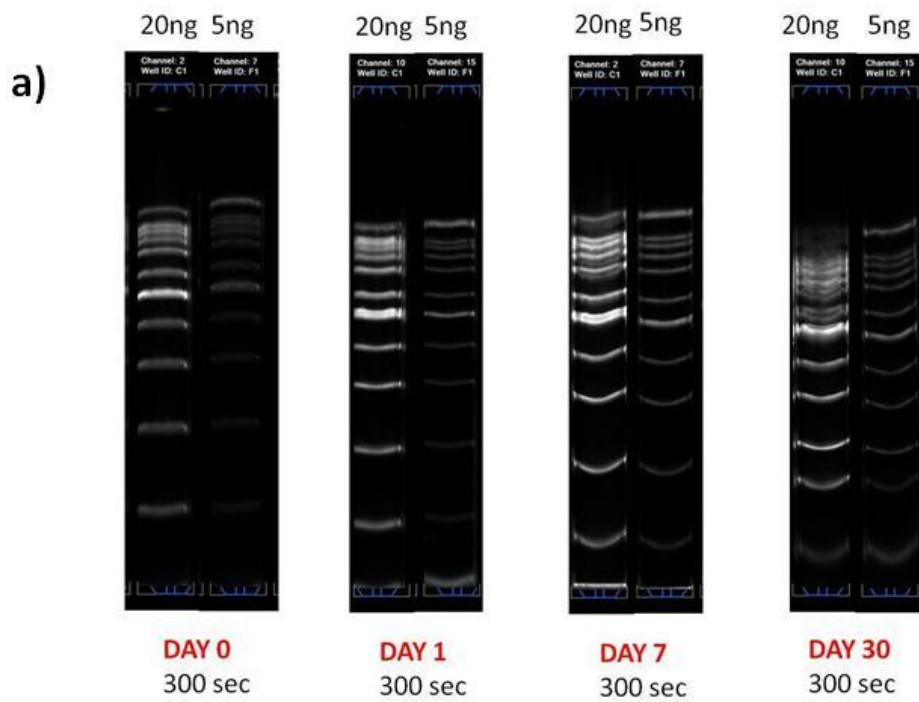


**Figure 16.** (a) Shelf-life study of a standard Click gel (15% T 15mM C, 20X dye in the gel matrix). The stabilizer TPAOH is added to the standard buffer and 20 ng and 5 ng of Generuler 100 bp are run in parallel in time. By decreasing DNA concentration the performance is remarkably improved. (b) The resolution at DAY 30, obtained by loading 5 ng of DNA, is better than that obtained loading 20 ng.

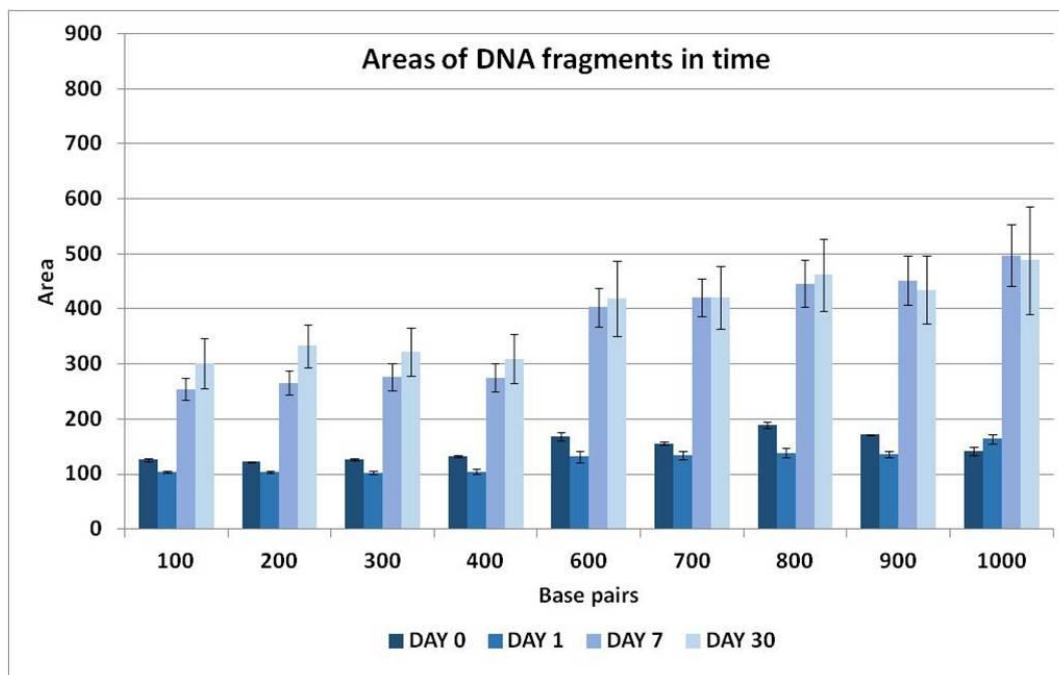


**Figure 17.** Areas values of DNA fragments when 5 ng of 100bp Ladder are loaded. The signal intensity of the bands does not change in time.

Furthermore, the performance obtained loading 5 ng of DNA exhibits excellent band shape and fluorescence signal stability under extended running conditions (**Figure 18**). This allows for improved separation of higher molecular weight bands (up to 1500bp in this case) with minimal band dispersion or signal loss even after extensive electrophoresis time (700 seconds).

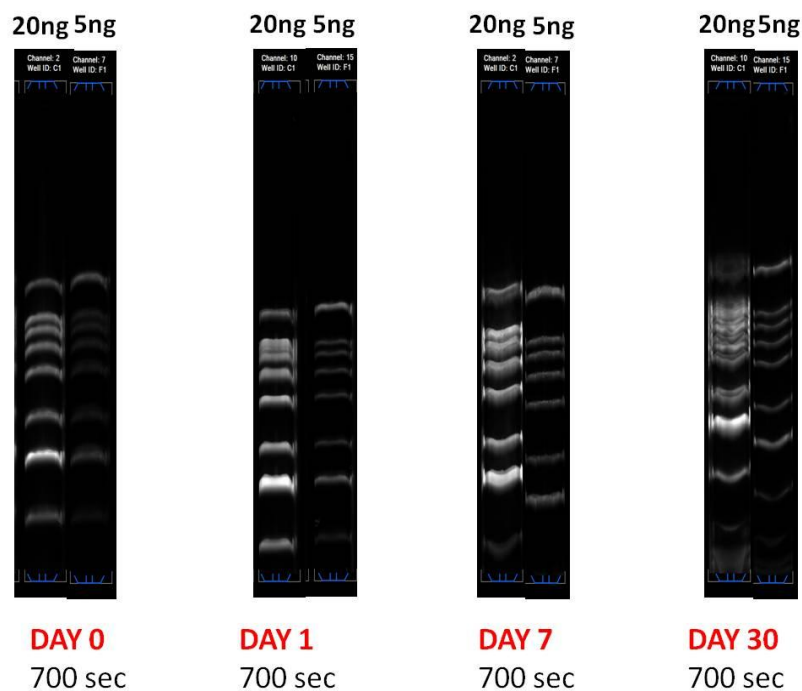


**Figure 18.** Extended runtime separation from 25-1500 bp. DNA large bands (high molecular weight) keep an excellent shape after extensive electrophoresis time when 5 ng are loaded.

The performance improvement obtained by reducing the amount of DNA injected seems to suggest that the ratio between SYBR Green/DNA plays a significant role in band broadening. In fact, although an improvement of the *shelf-life* of the dye is achieved by using the stabilizer TPAOH, the availability of dye in the gel matrix seems to decrease over time, affecting the performance of the high  $M_w$  by altering the optimal dye/DNA concentration ratio. The probable loss of SYBR Green in time appears to be compensated by decreasing the DNA concentration so to keep an optimal ratio between SYBR Green and high  $M_w$  DNA sample.

A number of experiments are devoted to understand the possible causes of in-gel dye degradation. The aim is to evaluate if the click reaction catalysts can affect dye stability. However, the phenomenon of the degradation of the high  $M_w$  bands at DAY 1 is not explained by any experimental result since none of the click reaction components, taken separately or in mixture, degrades the dye so quickly. Therefore, it is decided to investigate the influence of the main component of the click gel, the Copoly Alkyne, on SYBR Green availability/degradation. In particular, in order to evaluate the

interaction between the dye and the polymer, the dye is incubated with the polymer in the usual loading solution for an extended period of time. The following simple experiment, whose results are illustrated in **Figure 19**, is performed: a standard loading solution with SYBR Green I (**positive control**) and loading solution with SYBR Green and Copoly Alkyne (**negative control**) are prepared and stored up to 1 month. Prior to electrophoresis, the DNA samples are mixed with the two loading solutions. The separation of 20 ng of DNA samples, stained with the loading solutions with and without the polymer, is evaluated in parallel, at different time intervals, in a D1000 standard Tape. In the presence of the standard loading solution (**positive control**), the separation profile is constant up to 1 month, without any decrease of fluorescence signal. On the contrary, the performance of the DNA sample prepared with the loading solution containing the polymer (**negative control**) changes in time with a significant reduction of fluorescence signal.

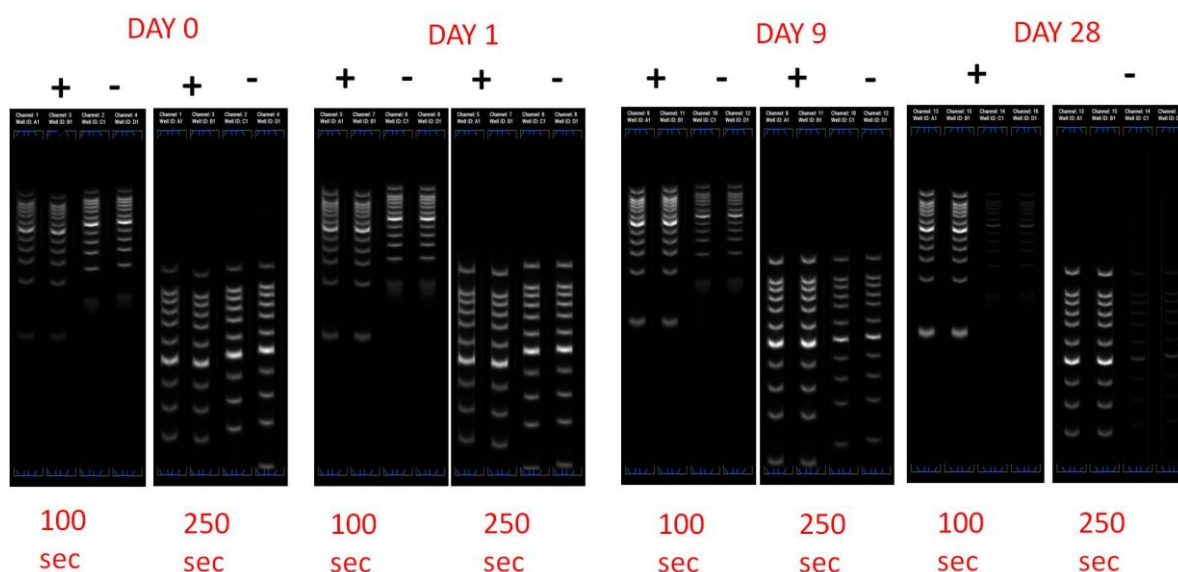


**Figure 19.** Evaluation in parallel in time of the separation of 20 ng of DNA sample stained with the loading solutions with and without the polymer. The assay is performed in a D1000 standard ScreenTape. In the presence of the standard loading solution (+), the separation profile is constant up to 1 month, without any decrease of the fluorescence signal. On the contrary, the fluorescence signal of the DNA sample prepared with the loading solution containing the polymer (-) reduces significantly.

The fluorescence intensity of the bands of two DNA samples is quantified by calculating the areas of the bands. The graph reported in **Figure 20** shows the comparison between the areas of bands of the different base pairs fragments at day 28: the DNA sample electrophoresed with the loading solution containing the polymer loses most of its fluorescence intensity, compared to the DNA prepared with the standard loading solution.

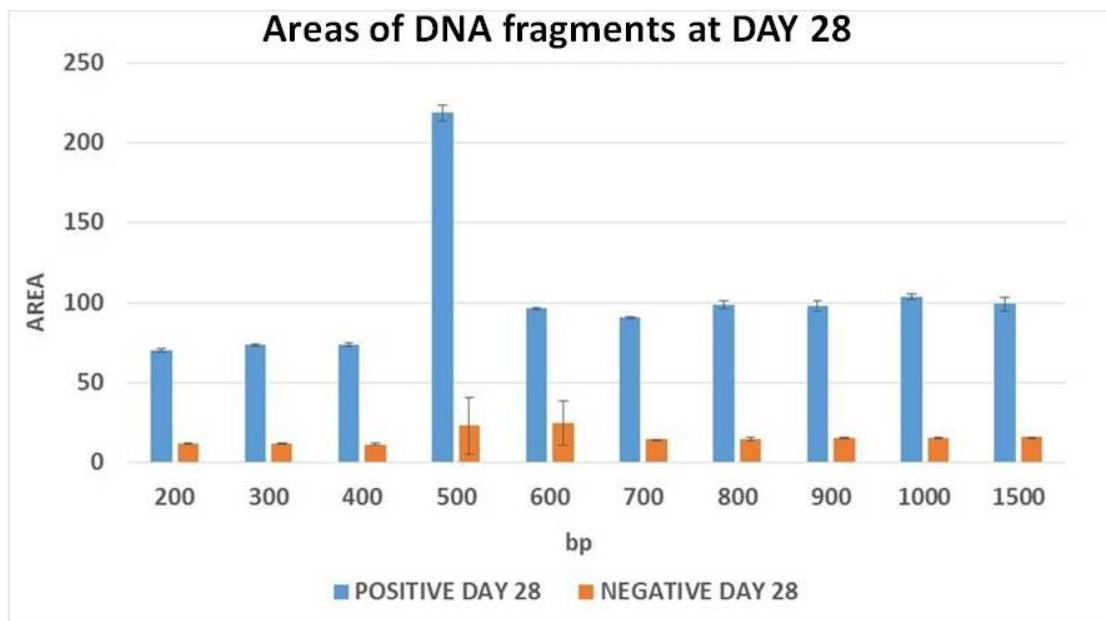


**Figure 20.** Areas of DNA base pairs at DAY 28: DNA sample prepared with loading solution containing the polymer (**negative control**, orange) loses dramatically fluorescence, in comparison to DNA sample prepared with the standard loading solution (**positive control**, blue)

At the same time, a fluorescence assay is carried out by simply measuring with a fluorimeter the fluorescence intensity, at different time intervals, of the same two loading solutions employed for the electrophoresis analysis. In particular, salmon sperm DNA is added to the two solutions before measuring the fluorescence signal whose intensity is related to the amount of functional SYBR Green, that binds with the salmon sperm DNA. As shown in the graph in **Figure 21** the loading solution containing the polymer (**orange**) loses progressively fluorescence intensity in time and at day 28 a negligible fluorescence signal is detected. On the contrary, standard loading solution (**blue**) maintains a good fluorescence signal up to 1 month. This simple experiment seems to suggest that an interaction between the polymer and the dye occurs that

reduces the availability of free dye. However, more experiments are needed to understand the interaction mechanism. One could speculate that hydrophobic bonds might be formed between the poly(dimethylacrylamide) backbone of the polymer and hydrophobic portions of SYBR Green I. Also, electrostatic interactions between the silanols of Copoly-Alkyne and the positive charges of the dye could play a significant role. Understanding the cause of performance degradation over time is mandatory to exploit commercially this new promising matrix.

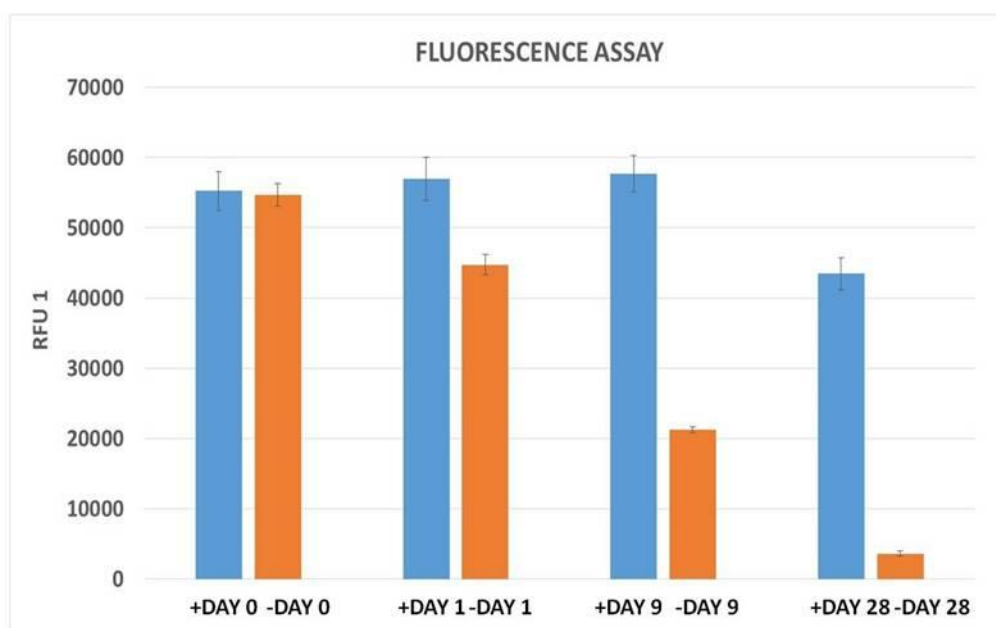


**Figure 21.** Fluorescence intensity, measured over time, of standard loading solution (**positive control, blue**), and loading solution with Copoly-Alkyne (**negative control, orange**).

### **8.2.8 CHARACTERIZATION OF CLICK GEL: SWELLING TEST**

A parameter, characteristic of hydrogels, is the *overswelling*. In a physical sense, the overswelling gives an idea of how much solvent gels can up-take. This property depends mostly on the nature of solvent and polymer chain. In general, the more solvent the gel takes up, the higher the swelling power is. This parameter has a great significance for the performance of the gel in the context of this work as the swelling can affect the *meniscus*, i.e the interface between the gel and the buffer, and, as a consequence the performance of DNA separation.

For this purpose the swelling of a standard click gel (15%T, 15mM C) is evaluated directly in the ScreenTape, by taking images of the same channel of the Tape at different time intervals. The images are taken with the camera of the TapeStation instrument up to 25 days. From the images taken in different days, it is appreciable just by naked-eye that the meniscus shape of the click gel does not change over time (**Figure 22**). For a more precise quantification of the meniscus variations, in **Figure 23** a graph of the fluorescence intensities along a channel is reported: the x-axis represents the distance in pixel along a single channel containing the gel matrix and the y-axis is the fluorescence intensity (gray scale value). For the same channel, five different profiles are obtained in order to monitor differences in time. In particular, every channel is composed of two different regions, the gel matrix and the buffer, which have two different colours. The change of colour, around 840 px (x-axis) corresponds to the interface between the gel and the buffer, that is the meniscus. This change of colour occurs always in the same position indicating that the gel does not swell. At the same time, the decrease of the fluorescence intensity (values of gray scale, x-axis) over time corresponds to a loss of fluorescence intensity of the gel matrix. In fact, despite of the use of TPAOH as stabilizer, the decrease of fluorescence intensity confirms that a certain degree of degradation of the dye occurs in the gel matrix over time.

The absence of gel swelling, observed in the experiment mentioned above, is perfectly in accordance with all the good results reported in this Chapter: since no swelling

occurs, the interface of the click gel remains constant and provides a good separation profile which is not affected by gel overswelling.

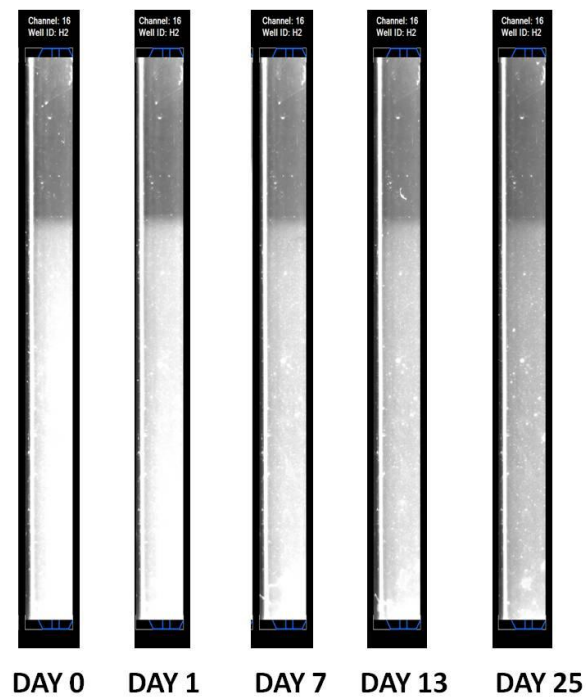


**Figure 22.** Images of the same channel of the ScreenTape, taken at different days. The more fluorescent region of the channel is the gel matrix, whereas the region less bright is the buffer. The interface between the two regions is the meniscus that does not change in time.

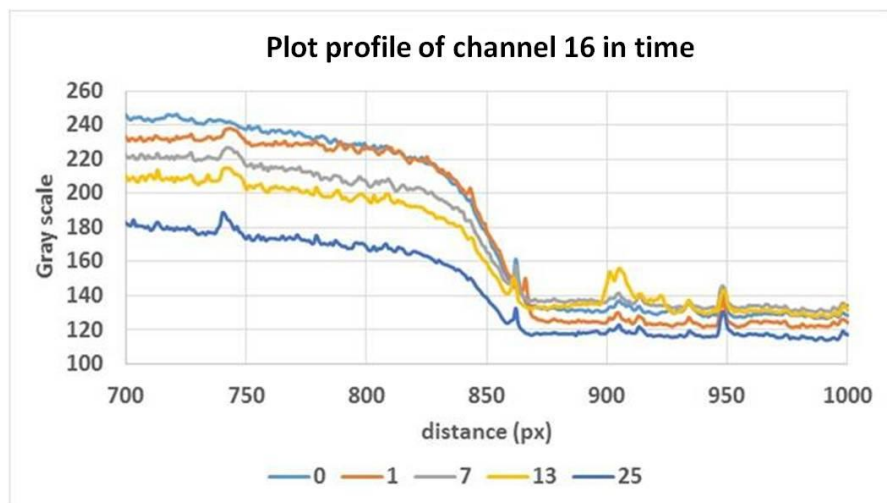


**Figure 23.** Plot profiles at different days of channel 16 of the ScreenTape, which contains click gel matrix. The fluorescence intensity (gray scale values) along the channel is reported. The value around 840 px (x-axis) corresponds to the interface between the gel and the buffer, that is the meniscus. This does not change in time, indicating that the meniscus does not change because the gel is not swelling.

### 8.3 CONCLUSIONS

This work is aimed at developing a novel sieving matrix for high performance DNA electrophoresis, using the classic *click copper (I)-catalyzed azide-alkyne cycloaddition (CuAAC)* reaction. The activity was carried out in the frame of a scientific collaboration with Agilent Technologies (UK). The new gel is used as DNA sieving matrix in the automated Agilent platform, called 2200 TapeStation, a system for high throughput, fast and automated electrophoresis. In the ScreenTape the separation occurs in plastic microchannels with great reduction of analysis time and reagents consumption.

An innovative approach is used for the synthesis of hydrogels based on a *click chemistry* reaction. The sieving matrix is formed mixing two polymers bearing reactive functional groups: poly(dimethylacrilamide) functionalized with an alkyne moiety (Copoly-Alkyne) and Poly(ethylene glycol) bis-azide bearing azido groups at both ends. The two polymers react through the well known copper (I)-catalyzed azide-alkyne cycloaddition (CuAAC), forming a novel hydrogel. The gelation process does not require UV-initiators permitting to include a fluorescent dye before gel formation. Moreover, toxic and not stable monomers, such as acrylamide, are replaced with nontoxic preformed polymers as components of the gel matrix. Excellent separations of DNA are obtained with resolution remarkably better than that provided by standard commercial acrylamide gels. In particular, a considerable improvement is found in the resolution of fragments below 500 bp thanks to the inclusion of dye in the gel matrix.

A considerable part of the activity is dedicated to extend the *shelf-life* of the novel sieving matrix. The results obtained are promising: the click gel provides excellent DNA separations up to one month with negligible swelling.

## 8.4. BIBLIOGRAPHY

- (1) Sperling, R. A.; Parak, W. J.; Ackerson, C. J.; Jadzinsky, P. D.; Kornberg, R. D.; Akerman, M. E.; Chan, W. C. W.; Laakkonen, P.; Bhatia, S. N.; Ruoslahti, E.; et al. Surface Modification, Functionalization and Bioconjugation of Colloidal Inorganic Nanoparticles. *Philos. Trans. A. Math. Phys. Eng. Sci.* **2010**, *368* (1915), 1333–1383.
- (2) Yigit, S.; Sanyal, R.; Sanyal, A. Fabrication and Functionalization of Hydrogels Through “click” chemistry. *Chem. - An Asian J.* **2011**, *6* (10), 2648–2659.
- (3) and, D. A. O.; Hilborn\*, J. Poly(vinyl Alcohol)-Based Hydrogels Formed by “Click Chemistry.” **2006**.
- (4) Chawla, K.; Yu, T.-B.; Liao, S. W.; Guan, Z. Biodegradable and Biocompatible Synthetic Saccharide-Peptide Hydrogels for Three-Dimensional Stem Cell Culture. *Biomacromolecules* **2011**, *12* (3), 560–567.
- (5) Tibbitt, M. W.; Anseth, K. S. Hydrogels as Extracellular Matrix Mimics for 3D Cell Culture. *Biotechnol. Bioeng.* **2009**, *103* (4), 655–663.
- (6) Hunt, J. A.; Chen, R.; van Veen, T.; Bryan, N.; Maldonado-Codina, C.; Efron, N.; White, J. K.; Titus, J. S.; Tanabe, H.; Aretz, H. T.; et al. Hydrogels for Tissue Engineering and Regenerative Medicine. *J. Mater. Chem. B* **2014**, *2* (33), 5319.
- (7) Peppas, N. A. Hydrogels and Drug Delivery. *Curr. Opin. Colloid Interface Sci.* **1997**, *2* (5), 531–537.
- (8) Suenaga, E.; Nakamura, H. Prestaining Method as a Useful Tool for the Agarose Gel Electrophoretic Detection of Polymerase Chain Reaction Products with a Fluorescent Dye SYBR Gold Nucleic Acid Gel Stain. *Anal. Sci.* **2005**, *21* (6), 619–623.
- (9) Mammen, M.; Dahmann, G.; Whitesides, G. M. Effective Inhibitors of Hemagglutination by Influenza Virus Synthesized from Polymers Having Active Ester Groups. Insight into Mechanism of Inhibition. *J. Med. Chem.* **1995**, *38* (21), 4179–4190.
- (10) Sola, L.; Molecolare, R. SYNTHESIS OF CLICKABLE COATING POLYMERS BY POST-POLYMERIZATION MODIFICATION: APPLICATION IN SYNTHESIS OF CLICKABLE COATING POLYMERS BY POST-POLYMERIZATION MODIFICATION: APPLICATION IN MICROARRAY TECHNOLOGY ACS Paragon Plus Environment. **2016**.
- (11) Pirri, G.; Damin, F.; Chiari, M.; Bontempi, E.; Depero, L. E. Characterization of A Polymeric Adsorbed Coating for DNA Microarray Glass Slides. *Anal. Chem.* **2004**, *76* (5), 1352–1358.
- (12) Finetti, C.; Colombo, M.; Prosperi, D.; Alessio, G.; Morasso, C.; Sola, L.; Chiari, M. One-Pot Phase Transfer and Surface Modification of CdSe-ZnS Quantum Dots Using a Synthetic Functional Copolymer. *Chem. Commun.* **2014**, *50* (2), 240–242.
- (13) Zilio, C.; Bernardi, A.; Palmioli, A.; Salina, M.; Tagliabue, G.; Buscaglia, M.; Consonni, R.; Chiari, M. New “clickable” Polymeric Coating for Glycan Microarrays. *Sensors Actuators B Chem.* **2015**, *215*, 412–420.
- (14) Uttamapinant, C.; Tangpeerachaikul, A.; Grecian, S.; Clarke, S.; Singh, U.; Slade, P.; Gee,

- K. R.; Ting, A. Y. Fast, Cell-Compatible Click Chemistry with Copper-Chelating Azides for Biomolecular Labeling. *Angew. Chem. Int. Ed. Engl.* **2012**, *51* (24), 5852–5856.
- (15) Sola, L.; Damin, F.; Gagni, P.; Consonni, R.; Chiari, M. Synthesis of Clickable Coating Polymers by Postpolymerization Modification: Applications in Microarray Technology. *Langmuir* **2016**, *32* (40), 10284–10295.
- (16) Hugh, W.; Stein, T. M. ( 12 ) United States Patent ( 10 ) Patent NO .: **2002**, *1* (12), 4–9.
- (17) Shin, J.-A.; Lim, Y.-G.; Lee, K.-H. Copper-Catalyzed Azide–Alkyne Cycloaddition Reaction in Water Using Cyclodextrin as a Phase Transfer Catalyst. *J. Org. Chem.* **2012**, *77* (8), 4117–4122.
- (18) Zeng, Z.; Clark, S. M.; Mathies, R. A.; Glazer, A. N. Improved Stability and Electrophoretic Properties of Preformed Fluorescent Cationic Dye-DNA Complexes in a Taps-Tetrapentylammonium Buffer in Agarose Slab Gels. *Anal. Biochem.* **1997**, *252* (1), 110–114.

## **Chapter 9**

### **FINAL CONCLUSIONS AND FUTURE PERSPECTIVES**

In this PhD thesis the use of hydrophilic polymers as important tools for bioanalytical applications involving nanotechnology, microarray technology and DNA gel electrophoresis has been widely illustrated. The two parts of this work, PART A and PART B, share the employment of *N,N*-dimethylacrylamide based copolymers, developed at the laboratory of Analytical Microsystems of the Institute of Chemistry for Molecular Recognition (National Research Council of Italy) where the thesis has been carried out. In particular, PART A is related to development of innovative procedures to modify the surface of gold nanoparticles (AuNPs) and quantum dots (QDs) with *N,N*-dimethylacrylamide based copolymers and their application in immunosensing via microarray technology to improve the biosensing performance. In fact, nanoparticle based, highly sensitive immunoassays for inexpensive, population-wide screening of biomarkers of different diseases is a hot research topic. For this reason, in the future, other new functionalization strategies and polymeric coatings will be introduced for the the biofunctionalization of other kinds of nanoparticles, such as magnetic nanoparticles.

In PART B of the dissertation a R&D activity carried out in collaboration with the company Agilent Technology (UK) has been presented. This section focuses on the development of a new hydrogel sieving matrix for high performance DNA electrophoresis through a *click chemistry* approach. Further investigations will be devoted to stabilize the electrophoretic performance of the new click hydrogel over time, aimed at the gel production scale-up and its further industrialization. Moreover, many studies will be dedicated to the development of other kinds of "clickable polymers", exploitable to form hydrogels with application on advanced microscale analytical technologies.

## Appendix

Research paper publications and book chapters are here reported:

✓ **Chiara Finetti** , Miriam Colombo, Davide Prosperi, Giulia Alessio, Carlo Morasso, Laura Sola and Marcella Chiari, “*One-pot phase transfer and surface modification of CdSe–ZnS quantum dots using a synthetic functional copolymer*” **Chemical Communications**, 2014, 50, 240-242

✓ **Chiara Finetti**, Lauren Plavish, Marcella Chiari, “*Use of Quantum dots as mass and fluorescence labels in microarray biosensing*”, **Talanta**, 2016, 147, 397-401

✓ **Chiara Finetti**, Laura Sola, Margherita Pezzullo, Davide Prosperi, Miriam Colombo, Benedetta Riva, Svetlana Avvakumova, Carlo Morasso, Silvia Picciolini and Marcella Chiari “*Click Chemistry immobilization of antibodies of polymer coated gold nanoparticles*”, **Langmuir**, 2016, 32, 7435-7441

✓ Laura Sola, **Chiara Finetti**, Paola Gagni, Marcella Chiari and Marina Cretich “*Surface modifications by Polymers or Biosensing Applications*”, **Biological and Pharmaceutical Applications of Nanomaterials**, Edit by P. Prokopovich, CRC Press, 2015, 347-390

✓ Laura Sola, Alessandro Gori, Marina Cretich, **Chiara Finetti**, Caterina Zilio, Marcella Chiari, “*Clickable Polymeric Coating for Oriented Peptide Immobilization*”, **Peptide Microarray**, Edit by M.Cretich and M. Chiari, Humana Press Inc, 2016, 1352, 167-182

✓ Emanuela Cova, , Simona Inghilleri, Laura Pandolfi, Monica Morosini, Sara Magni, Miriam Colombo, Davide Piloni, **Chiara Finetti**, Gabriele Ceccarelli, Gabriele, Laura Benedetti, Maria Gabriella Cusella, Manuela Agozzino, Raffaele Allevi, Mrakic-Sposta Simona, Moretti Sarah, Davide Prosperi, Davide; Federica Meloni, “*Bioengineered Gold Nanoparticles Targeted to Mesenchymal Cells from Patients with Bronchiolitis Obliterans Syndrome Does Not Rise the Inflammatory Response and Can Be Safely Inhaled by Rodents*”, **Nanotoxicology**, submitted

# One-pot phase transfer and surface modification of CdSe–ZnS quantum dots using a synthetic functional copolymer†

Cite this: *Chem. Commun.*, 2014, 50, 240

Received 9th August 2013,  
Accepted 25th October 2013

DOI: 10.1039/c3cc46086j

www.rsc.org/chemcomm

Chiara Finetti,<sup>a</sup> Miriam Colombo,<sup>b</sup> Davide Prospero,<sup>b</sup> Giulia Alessio,<sup>b</sup> Carlo Morasso,<sup>c</sup> Laura Sola<sup>a</sup> and Marcella Chiari<sup>\*a</sup>

**We present a facile, one-pot procedure for the organic-to-water phase transfer and biofunctionalization of semiconductor nanocrystals (quantum dots, or QDs) which employs a synthetic functional copolymer, namely poly(DMA-NAS-MAPS), consisting of three components: a surface interacting monomer, *N,N*-dimethylacrylamide (DMA), a chemically reactive monomer, *N*-acryloyloxysuccinimide (NAS), and a silane monomer, [3-(methacryloyloxy)-propyl]-trimethoxysilane (MAPS). The nanocrystals were transferred to water by exploiting the amphiphilic character of the copolymer backbone. Hydrolyzed MAPS units contributed to improve the solubility of QDs in water, whereas NAS exhibited reactivity toward biomolecules. A solution of streptavidin in phosphate buffer exhibited good dispersion ability leading to a clear and transparent colloidal suspension, indicative of good QD dispersion during phase transfer and purification. Unlike most of the published methods, the proposed functionalization approach does not require coupling agents and multistep reactions.**

Semiconductor nanocrystals, commonly referred to as quantum dots (QDs), are a class of inorganic fluorophores that have been the subject of intense research in the past 20 years due to their unique photophysical properties including photostability, a wide excitation band, narrow emission, spectral range and brightness.<sup>1</sup> Among the different types of QDs, CdSe–ZnS core-shell QDs, ranging in diameter from 2 nm (480 nm emission) to 8 nm (660 nm emission), are the most widely used in biological applications as fluorescent tags in cellular imaging or optical bar codes.<sup>2–4</sup> The development of methods that can manipulate QD surface chemistry while maintaining optical properties

identical to those of as-synthesized, organic-soluble QDs is a hot research topic.<sup>5</sup> In particular, controlling the surface properties of QDs allows fine tuning of size and solubility, which are key factors for their utilization as fluorophores or as multifunctional nanoscaffolds for the attachment of biomolecules or other types of molecules. In most circumstances, the resulting composite nanoparticles need to be stable in water, small, biocompatible, monodisperse and chemically reactive. An increasingly popular method for solubilizing and functionalizing QDs is to wrap their surface with an amphiphilic polymer, which has the advantage of conferring long-term colloidal stability.<sup>6–8</sup> The solubilization mechanism usually consists of interdigitation of the hydrophobic segments of the polymer with the surfactant ligands (*e.g.*, trioctylphosphine oxide –TOPO– and/or hexadecylamine –HDA–), which are frequently adopted for post-synthetic stabilization of nanocrystals, tightly bound onto the QD surface, thus leaving the polar polymer backbone exposed to the external environment with the hydrophilic groups protruding from the surface.

In this communication, we report a robust approach for the preparation of soluble and functional QDs for use as fluorescent tags in bioimaging, sensing and therapeutics. This is the first time a functional polymer, poly(DMA-NAS-MAPS) (Copoly), was exploited for the transfer of nanoparticles from an organic solvent to an aqueous phase. The polymer has recently been explored for the modification of different kinds of flat surfaces for biosensing.<sup>9,10</sup> The use of Copoly is advantageous as it does not allow the formation of micelles during the NP phase transfer process, which is likely to happen with other amphiphilic polymers.<sup>11</sup> The copolymer consists of a random assemblage of three different components: a surface interacting monomer, a chemically reactive monomer, and a silanating moiety; it exhibits good dispersion ability in water and phosphate buffer (150 mM, pH 8.5) and was exploited to functionalize QDs allowing for their phase transfer and surface derivatization by a one-pot procedure (see ESI† for details). The amphiphilic polymer was obtained by radical random polymerization of *N,N*-dimethylacrylamide (DMA), *N*-acryloyloxysuccinimide (NAS), and [3-(methacryloyl-oxy)-propyl]trimethoxy-silane (MAPS) in tetrahydrofuran (THF).<sup>12</sup>

<sup>a</sup> Istituto di Chimica del Riconoscimento Molecolare, CNR, Via Mario Bianco, 9, 20131 Milano, Italy. E-mail: marcella.chiari@icrm.cnr.it

<sup>b</sup> NanoBioLab, Dipartimento di Biotecnologie e Bioscienze, Università degli Studi di Milano-Bicocca, Piazza della Scienza 2, 20126 Milano, Italy

<sup>c</sup> Laboratory of Nanomedicine and Clinical Biophotonics, Centre for Innovation and Technology Transfer, Fondazione Don Carlo Gnocchi ONLUS, Milan, Italy

† Electronic supplementary information (ESI) available: Experimental details of particle phase transfer, TEM images, particle size and ζ-potential analyses, NanoSight analysis, PL and UV-vis spectra, gel electrophoresis, Raman spectroscopy, coating procedure and microarray experiments. See DOI: 10.1039/c3cc46086j

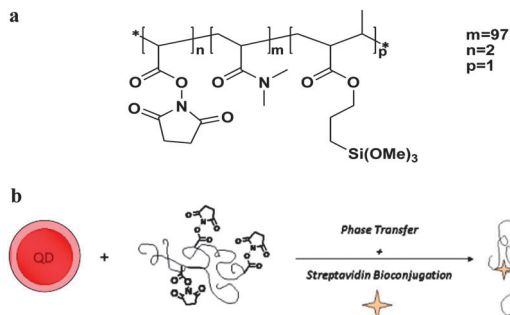


**Fig. 1** (a) Chemical structure of Copoly (DMA-NAS-MAPS). (b) Schematic representation of one-pot phase transfer of the CdSe-ZnS QDs and derivatization.

The chemical structure of Copoly and the coating procedure are provided in Fig. 1a and b. The nanocrystals were transferred to water by exploiting the amphiphilic character of the copolymer backbone that conferred solubility in both water and THF. The MAPS unit also improved the solubility of QDs in water, whereas NAS exhibited reactivity toward biomolecules. A solution of streptavidin (SAV) in phosphate buffer exhibited a good dispersion ability, leading to a clear and transparent colloidal suspension, indicative of a good QD dispersion during phase transfer and purification. During the organic-to-aqueous phase transfer, streptavidin was directly coupled to the active ester groups of the polymer. Commercial CdSe-ZnS QDs of known concentration were precipitated from decane and quantitatively dispersed in chloroform. The concentration of QDs, after various steps, was assessed using a calibration curve with nanoparticle solutions whose concentration was inferred assuming a quantitative transfer from chloroform. The validity of this assumption was confirmed from the concentration values estimated by NanoSight analysis (see NanoSight Analysis in the ESI†).

Following phase transfer, functionalization and purification, physical characterization of the CdSe-ZnS nanocrystals was carried out. The polymer-coated CdSe-ZnS QDs in water maintained high fluorescence, half of that in chloroform (see ESI,† Fig. S3a). The presence of multiple *N*-hydroxysuccinimidyl ester groups on the polymer rendered the coated QDs extremely reactive toward proteins, even under mild conditions. By exploiting the reaction between amino groups of lysine, present in most natural polypeptide chains and polymer active esters, streptavidin was efficiently immobilized on Copoly-QDs by simple incubation in phosphate buffer saline (150 mM, pH 8.5). Only minor changes in the spectral properties for QDs were observed after SAV coupling as shown in Fig. 3c. The FWHM of the emission band was  $28 \pm 2$  nm for particles emitting at 651 nm, indicating a narrow size distribution of QDs. The absorption and emission spectra of commercial CdSe-ZnS and of CdSe-ZnS coated with copoly(DMA-NAS-MAPS) (Copoly-QDs), after immobilization of SAV, were similar (see ESI,† Fig. S3b). Also there is no relevant difference in the size distribution measured using NanoSight for the streptavidin modified commercial QDs and the in-house modified QDs (see ESI,† Fig. S2). The encapsulation of QDs in this amphiphilic polymer provided extended stability, demonstrated by

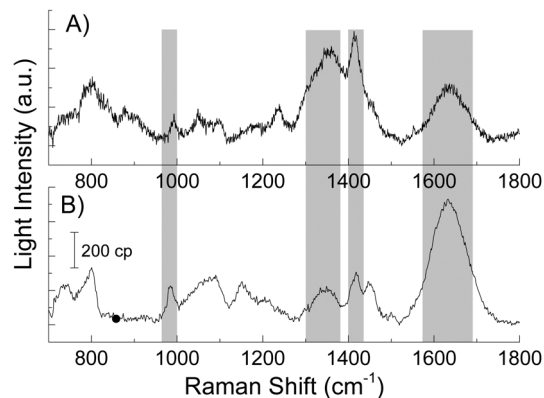


**Fig. 2** Raman spectra of Copoly QDs dispersed in water (A) and of a solution  $10 \text{ mg ml}^{-1}$  of Copoly in water (B). The bands of the chemical groups of the Copoly are shown in grey: amide I band at  $1635 \text{ cm}^{-1}$ ;  $\text{CH}_3$  stretching at  $1416 \text{ cm}^{-1}$ ; amide III band at  $1348 \text{ cm}^{-1}$  and C-C stretching at  $987 \text{ cm}^{-1}$ .

the fact that no changes in solubility or fluorescence decrease were observed over three months under storage at  $4^\circ \text{C}$ . This suggests that Copoly-QDs did not degrade over time.

The presence of Copoly on the surface of the nanocrystals dispersed in water was confirmed by Raman spectroscopy. In Fig. 2 the characteristic peaks corresponding to the chemical structure of the polymer are present in the polymer coated QD spectrum.

Transmission electron micrographs (TEM) revealed that nanocrystals have approximately a rod-like shape with an average size of about 10 nm in the longer dimension and an aspect ratio of 2 : 1 (Fig. 3a). The similarity of size and shape of QDs in aqueous solution and in organic solvent (see ESI,† Section 3.1) suggests that there is no aggregation during phase transfer. The results of the dynamic light scattering (DLS)

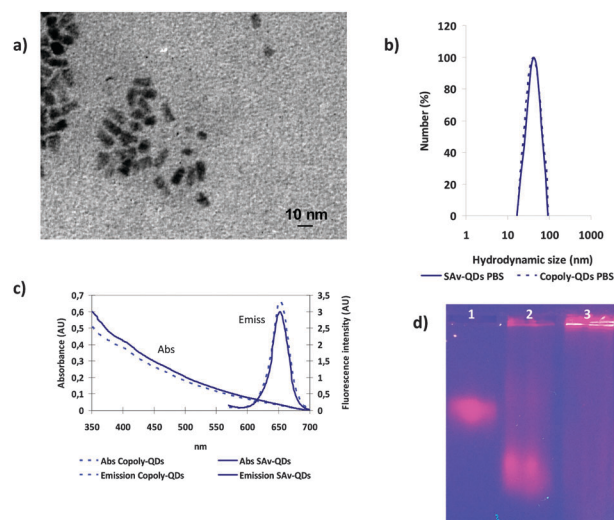


**Fig. 3** Morphology of streptavidin-QDs analyzed by TEM (a). Hydrodynamic size of QDs assessed by DLS measurement (b). Solutions were at pH 7 in water. Absorbance spectra of functionalized QDs (solid line) and not functionalized (dotted line) (c). Gel electrophoresis of 0.8% agarose (d). QDs are visualized under UV light. Lane (1): Commercial QDs; lane (2): streptavidin QDs; lane (3): non-functionalized QDs.

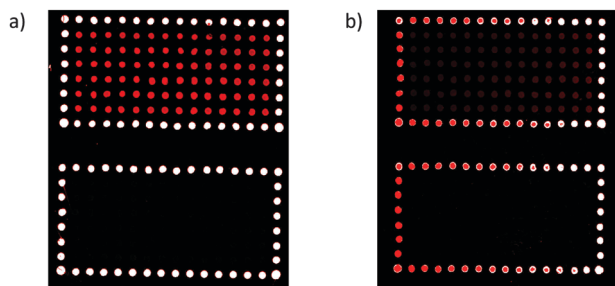


Fig. 4 Biotinylated antibody (upper subarray) and non-biotinylated antibody (lower subarray) incubated with QDs functionalized with streptavidin (a) and QDs coated with the Copoly (b). Laser power and PMT were set at 70% of their power.

measurements show a hydrodynamic diameter of  $42.7 \pm 2.9$  nm for SAV-functionalized QDs (SAV-QDs), and  $40.4 \pm 8.9$  nm for the non-functionalized Copoly-QDs (Fig. 3b). In both cases the DLS values show a narrow size distribution. DLS analysis was also used to investigate the influence of salt concentration on stability. The results indicate good stability both in buffer solution and in water (see ESI,† Fig. S1). Gel electrophoresis analysis was used to separate the nanoparticles. The overall electrophoretic mobility of the nanoparticles is due to the differences in molecular weight and/or overall surface charge. The mobility of Copoly-QDs (lane 3) was compared to that of SAV-QDs (lane 2) and to that of commercial streptavidin-QDs (lane 1) (Fig. 3d). SAV-QDs clearly migrated towards the cathode, whereas Copoly-QDs did not migrate at all. Combining these data, we concluded that the presence of the protein bound to the polymer conferred a charge, and thus an electrophoretic mobility of the QDs, leading to the formation of a sharp and pronounced band. When the band extracted from the gel was electrophoresed a second time, the same narrow band was recovered, indicating that the streptavidin was indeed irreversibly bound to the nanoparticles and not just physically adsorbed on their surface (data not shown).

The zeta potential ( $\zeta$ ) obtained at pH 7.0 was  $-15.25 \pm 6.94$  mV for SAV-QDs and  $-41.89 \pm 7.72$  mV for Copoly-QDs, likely suggesting high stability of the solution with minimal aggregation in water at this pH. The difference between  $\zeta$  values of QDs, namely those coated with the copolymer and those with streptavidin bound to the copolymer, confirmed the presence of protein molecules on their surface, which contributed to a decrease in the density of negative charges.

In order to assess the potential of our QD-functionalization strategy, Copoly-QDs were used as labels in a bioassay experiment. Biotinylated and non-biotinylated (control) Anti-Rabbit IgG antibodies were immobilized over two different subarrays on Copoly-coated silicon slides as provided in the ESI.† Fluorescence images of 84 replicates surrounded by a frame of Cy5 labeled streptavidin reference spots are shown in Fig. 4. The two chips were incubated side-by-side with SAV-QDs (Fig. 4a) and with Copoly-QDs (Fig. 4b). Both chips contain spots of a

non-biotinylated antibody (bottom frame) as additional negative controls. Only the chip incubated with SAV-QDs showed fluorescent spots of high intensity (upper frame of Fig. 4a). The specific interaction of streptavidin modified QDs with biotinylated antibodies is demonstrated by the absence of fluorescence on spots of non-biotinylated antibodies. The slide incubated with Copoly-QDs revealed a negligible fluorescence signal for both subarrays (Fig. 2b). The elimination, or at least the minimisation, of non-specific binding between the capture antibodies and QDs was important to improve the accuracy and sensitivity of microarray-based immunoassays.<sup>10,13</sup>

In conclusion, streptavidin coated CdSe core shell quantum dots were successfully phase transferred and functionalized under ambient conditions *via* a one-pot approach using copoly(DMA-NAS-MAPS). The use of this polymer with QDs is new, although its application in the fields of microarray and microfluidics was previously reported. To the best of our knowledge, none of the methods employed for the functionalization of QDs can compete with the one described here in terms of robustness and simplicity. The physical and functional characterization of the polymer/streptavidin functionalized QDs has demonstrated that they are suitable as fluorophores or as multifunctional nanoscaffolds for the attachment of biomolecules.

This work was supported by Istituto Italiano di Tecnologia, Project Seed IPG-CHIP, and Fondazione Regionale per la Ricerca Biomedica di Regione Lombardia (FRRB). We thank R.Allevi (CMENA, University of Milan) for TEM images.

## Notes and references

- 1 W. C. W. Chan and S. Nie, *Science*, 1998, **281**, 2016.
- 2 M. Bruchez, M. J. M. Moronne, P. Gin, S. Weiss and A. P. Alivisatos, *Science*, 1998, **281**, 2013.
- 3 D. R. Larson, W. R. Zipfel, R. M. Williams, S. W. Clark, M. P. Bruchez, F. W. Wise and W. W. Webb, *Science*, 2003, **300**, 1434.
- 4 M. Y. Han, X. H. Gao, J. Z. Su and S. Nie, *Nat. Biotechnol.*, 2001, **19**, 631.
- 5 L. H. Chena, H. L. Chou, C. H. Chenc and C. H. Tseng, in *Nanotechnology and Nanomaterials*, ed. S. Neralla, 2012, ISBN 978-953-51-0714-9.
- 6 T. Pellegrino, L. Manna, S. Kudera, T. Liedl, D. Koktysh, A. L. Rogach, S. Keller, J. Radler, G. Natile and W. J. Parak, *Nano Lett.*, 2004, **4**, 703.
- 7 J. C-A. A. Lin, R. A. Sperling, J. K. Li, T.-Y. Yang, P.-Y. Li, M. Zanella, W. H. Chang and W. J. Parak, *Small*, 2008, **4**, 334.
- 8 R. E. Anderson and W. C. W. Chan, *ACS Nano*, 2008, **2**, 1341.
- 9 F. Giavazzi, M. Salina, R. Cerbino, M. Bassi, D. Proserpi, E. Ceccarello, F. Damin, L. Sola, M. Rusnati, M. Chiari, B. Chini, T. Bellini and M. Buscaglia, *Proc. Natl. Acad. Sci. U. S. A.*, 2013, **110**, 9350.
- 10 P. Gagni, L. Sola, M. Cretich and M. Chiari, *Biosens. Bioelectron.*, 2013, **47C**, 490.
- 11 D. L. Nida, N. Nitin, W. W. Yu, V. L. Colvin and R. Richards-Kortum, *Nanotechnology*, 2008, **23**, 19.
- 12 G. Pirri, F. Damin, M. Chiari, E. Bontempi and L. E. Depero, *Anal. Chem.*, 2004, **76**, 1352.
- 13 M. Cretich, G. Di Carlo, R. Longhi, C. Gotti, N. Spinella, S. Coffa, C. Galati, L. Renna and M. Chiari, *Anal. Chem.*, 2009, **81**, 5197.



ELSEVIER

Contents lists available at ScienceDirect

Talanta

journal homepage: [www.elsevier.com/locate/talanta](http://www.elsevier.com/locate/talanta)

# Use of quantum dots as mass and fluorescence labels in microarray biosensing



Chiara Finetti, Lauren Plavisch, Marcella Chiari\*

Consiglio Nazionale delle Ricerche, Istituto di Chimica del Riconoscimento Molecolare, 20131 Milano, Italy

## ARTICLE INFO

### Article history:

Received 12 May 2015

Received in revised form

30 September 2015

Accepted 4 October 2015

Available online 9 October 2015

### Keywords:

Microarrays

Label-free detection

Mass label

Fluorescence detection

Quantum dots

Interferometry

## ABSTRACT

In this work, we demonstrate the efficacy of a Quantum Dot (QD) mass label strategy to enhance sensitivity in an interferometric technique called interferometric reflectance imaging sensor (IRIS). This biomass detection platform confers the advantage of absolute mass quantification and lower cost, easily implementable equipment. We discuss the advantages of this label when used in parallel with fluorescence detection. QDs represent a unique opportunity to improve sensitivity in both mass-label detection methods due to their large detectable mass, as well as in fluorescence detection, as they fluoresce without quenching. Streptavidin-conjugated QDs (SA-QDs) have been investigated as such a dual-role probe because of their large shape and mass, their 655 nm emission peak for fluorescent detection platforms, and their robust insensitivity to photobleaching and quenching. In particular we explored their dual role in a microarrays immunoassay designed to detect antibodies against  $\beta$ -lactoglobulin, a common milk allergen. The SA-QDs formed a large detectable monolayer of 6.2 ng/mm<sup>2</sup> in the saturation conditions, a mass signal corroborated by previous studies by Platt et al. [1].

© 2015 Elsevier B.V. All rights reserved.

## 1. Introduction

In the field of biosensing, the high-throughput detection of protein biomarkers has become paramount for disease detection. It is generally acknowledged that to achieve direct biomarker detection without complex preconcentration steps, analyses methods offering high selectivity and low limits of detection (LOD) in the pM–fM range are required [2]. Microarrays are a valuable way to increase throughput, but one possible issue that arises with microarrays is a need to maintain high sensitivity. Fluorescent labels are widely used as transducers in biosensing as they typically provide LODs of pM order [3,4]. However, in certain applications, label-free methods allowing direct detection of biological analytes are preferable. QDs have already been established as a fluorescent marker, but fluorescence detection is not suitable in resource limited settings or for point-of-care platforms. The large mass of QDs makes these particles suitable also for mass-based detection technologies, which is why the largest Streptavidin conjugated QD available, QD-655, were chosen. This size QD has already been demonstrated for another biomass-detection technology, dual polarization interferometry (DPI), and here we propose it as a so-called mass label for another biomass detection platform, interferometric reflectance imaging sensor (IRIS). IRIS

was originally conceived as a label-free technology, but antigens are so small that their mass is often undetectable. Adding a secondary antibody to the assay yielded large gains in sensitivity, because the mass of a large secondary antibody reveals shows an increase in mass due to the presence of an antigen, much in the same way a fluorescent secondary antibody indicates the presence of an antigen. Adding QDs as a massive tertiary particle further amplifies the mass signal, while introducing the possibility for further analysis with a fluorescence platform. Yet another advantage of QDs is that unlike organic fluorophores, QDs are inorganic semiconductor crystals unsusceptible to photobleaching or quenching.

In addition to being insensitive to photobleaching, quenching, or self-quenching, label-free methods are compatible with kinetic measurements which are not allowed by fluorescence detection. Mass measurements can be made at every step of an assay, either in wet conditions in a flow cell or in dry conditions after each step is completed. This yields hitherto unknown information about so-called sandwich and tower assays as well as spot quality and morphology. Ideally, label-free detection in a multiplex assay allows the simultaneous analysis of a number of different biomarkers captured at specific locations directly from a biological fluid. Unfortunately, in the real world, the situation is complicated by the fact that, apart from the species of interest, other species that can also bind to the biosensor are present at much higher concentrations. As a result, many of the changes at the sensor surface are due to nonspecific interactions which create a “noise

\* Corresponding author. Fax: +39 0228901239.

E-mail address: [marcella.chiari@icrm.cnr.it](mailto:marcella.chiari@icrm.cnr.it) (M. Chiari).

floor” that considerably reduces detection sensitivity. A recent review article Arlett et al. [5] comparing the limit of detection (LOD) versus the analysis time of different biosensors comes to the conclusion that the performance of a sensing platform is often limited by non-specific binding effects rather than by its intrinsic performance.

A possible solution to overcome sensitivity and specificity issues without employing expensive equipment is the use of a mass label. In this work we demonstrate the efficacy of a mass label strategy to enhance sensitivity based on quantum dots (QDs). These nanoparticles have already been established as a fluorescent marker, but in addition, their large mass makes them suitable also for mass-based detection technologies. QDs have been demonstrated for one such technology, dual polarization interferometry (DPI) [1], and here we propose them as a so-called mass label for another biomass detection platform, the interferometric reflectance imaging sensor (IRIS) [6].

IRIS is a simple reflective interferometric platform for multiplexed label-free detection of biomolecular interaction on bilayered Si/SiO<sub>2</sub> substrates. Samples are illuminated at different wavelengths using a tunable laser and reflections from this surface are detected as intensity variations by a CCD camera. Layered substrates demonstrate characteristic spectral reflectance due to the interference of reflected light from the Si–SiO<sub>2</sub> and SiO<sub>2</sub>–air interfaces. It was originally conceived of as a label-free technology, as it assumes that an observed increase in mass is due to the capturing of the target analyte. However, some captured particles, such as antigens, are so small that their mass is often undetectable. In an effort to overcome the lack of sensitivity and specificity of label-free methods, Ahn et al. [7] have obtained a 7-fold sensitivity enhancement in cytokine detection on the IRIS sensing platform. The authors achieved this signal enhancement by adding secondary detection antibodies that recognize a different epitope of the cytokine. The authors demonstrated that these secondary detection antibodies, which they call “mass tags,” allowed successful detection of IL-6 in cell culture medium. Reaching this level of sensitivity without specifically enhancing the mass of the captured target would have been impossible. The addition of biomass in the case of an antibody mass label can be very small, especially as the authors saw a loss of mass during the study. In fact, the achievement of these high-sensitivity measurements relied on a careful study of protein desorption and mass loss [7].

In this work we demonstrate the advantages of a QD mass label strategy to enhance sensitivity in mass detection and their further usefulness in conjunction with fluorescence detection. Streptavidin-conjugated QDs have been investigated as such a dual-role probe in an example assay, and their binding capacity to a biotin-conjugated protein has been explored in model systems. Their minimum detectability as a mass label has been evaluated *vis-à-vis* their sensitivity as a fluorescent label. The same chip can be used in both detection platforms, extending the dynamic range of detection and providing an opportunity for point-of-care screening unavailable with traditional fluorophores. Although with a mass label, the method can no longer be considered truly label-free, the use of a mass label provides sensitivity close to that of fluorescence without any of the drawbacks of fluorescence detection, combined with simple hardware components typical of the label-free IRIS platform [8].

## 2. Materials and methods

### 2.1. Reagents

Phosphate-buffered saline (PBS), Trizma base (Tris), HCl, ethanolamine, sodium chloride, potassium chloride, calcium chloride,

magnesium chloride 6-hydrate, sodium bicarbonate, sodium phosphate, bovine serum albumin (BSA), biotin-labeled bovine serum albumin (Bio-BSA), Tween 20, ammonium sulfate, N-dimethylacrylamide (DMA), 3-(trimethoxysilyl)propyl methacrylate (MAPS), azoisobutyronitrile (AIBN),  $\beta$ -lactoglobulin from bovine milk,  $\alpha$ -lactalbumin from bovine milk, and streptavidin from *Streptomyces avidinii* (lyophilized powder) were all purchased from Sigma-Aldrich (St. Louis, MO, USA). N-acryloyloxysuccinimide (NAS) was synthesized as reported elsewhere [9]. 655 ITK TM Organic Quantum Dots (QD-655) were purchased from Life Technologies.  $\alpha$ -Lactalbumin antibody, bovine  $\beta$ -lactoglobulin antibody, biotin-SP-conjugated AffiniPure Goat Anti-Rabbit IgG, AffiniPure Goat Anti-Rabbit IgG, and Cyanine 3-labeled streptavidin (SA-Cy3), were all obtained from Jackson ImmunoResearch (West Grove, PA, USA).

Silicon oxide chips with a 100 nm thermal oxide layer were bought from Silicon Valley Microelectronics (Santa Clara, CA, USA), and IRIS chips patterned with four 500 nm thermal oxide layer subregions were a kind gift from Prof. Selim M. Unlu, Boston University.

### 2.2. Detection setup

The LED-based interferometric reflectance imaging sensor (IRIS) has been well described as a method to detect accumulated biomass using the shift in spectral reflectance [6]. In summary, the spectral reflectance of biomass on an SiO<sub>2</sub> surface is sequentially sampled at four specific wavelengths, illuminated by an ACULED VHL surface-mount LED package (Perkin-Elmer), which has four independently driven LEDs with peak emission wavelengths of 455 nm, 518 nm, 598 nm, and 635 nm. At each wavelength, intensity of reflected light is measured pixel by pixel from images taken with a CCD camera (Retiga 2000R from QImaging). The position of each LED's emission peak at key positions along the specified SiO<sub>2</sub> reflectance curve (which is thickness-dependent) is critical for detecting a shift in this curve due to a change in the thickness, i.e. added material. After acquiring images of the substrate for each of the four wavelengths, each pixel of the CCD image has a measurement of the reflective interference intensity at all four wavelengths. Pixels from the entire sensor are then fitted to a curve derived using the Fresnel equations, which describe the reflection and refraction of light through layers with different refractive index [10]. Fluctuations in light intensity are monitored with an on-chip reference region. Here it is bare silicon, a non-interfering surface [8]. After fitting every pixel in the image, the surface topography of the sensor's surface is presented in a grey-scale image, where brighter regions indicate greater thickness on the surface. To determine optical spot heights, the average value from pixels in a background region around the spot is subtracted from the average value of pixels inside the spot. To eliminate dirt and other particles from averages, pixels more than one standard deviation were automatically eliminated from the calculations [7]. This optical spot height has been calibrated for several common microarray materials to convert the data into a surface density. Previously reported values correlate 1 nm of optical thickness to 1.21 ng/mm<sup>2</sup> of BSA, 1.28 ng/mm<sup>2</sup> of IgG, and 0.8 ng/mm<sup>2</sup> of DNA [11].

### 2.3. Coating of microarray slides with poly(DMA–NAS–MAPS)

To functionalize the surface of silicon slides, a thin film of N,N-dimethylacrylamide (DMA)–acryloyloxysuccinimide (NAS)–3(trimethoxysilyl)–propylmethacrylate (MAPS) copolymer.

–poly(DMA–NAS–MAPS)– was applied as previously described [9]. Briefly, silicon chips were immersed prepared for treatment with oxygen plasma and then immerse in a poly(DMA–NAS–

MAPS) solution (1% w/v in 0.9 M  $(\text{NH}_4)_2\text{SO}_4$ ) for 30 min. The chips were then rinsed with distilled water, dried under nitrogen gas, and cured under vacuum at 80 °C for 15 min. Copoly(DMA–NAS–MAPS) was chosen for its easy, reproducible coating procedure, its resistance to nonspecific binding, and because it can functionalize silicon without altering its optical properties [12].

For the label-free IRIS imaging and fluorescence detection, all proteins were printed on 15 mm square Si chips patterned with four 500 nm  $\text{SiO}_2$  subregions, each 50  $\mu\text{m}$  square subregions, spotted by a SciFlexArrayer S5 spotter from Scienion (Berlin, Germany). 400  $\mu\text{L}$  of each species was spotted from recommended buffers with at least 7 replicates on each chip. Ahn et al. [13] recommend PBS sensitive mass measurements, as it promotes protein binding while minimizing etching to the  $\text{SiO}_2$  surface. For oligomer spots, the authors recommend 150 mM phosphate buffer. Printed chips were placed in a humid chamber and incubated at room temperature overnight. The chips were then blocked with 50 mM ethanolamine solution in 1 M tris/HCl pH 9 for 1 h, rinsed with distilled water, and dried under a stream of nitrogen gas.

#### 2.4. $\beta$ -Lactoglobulin assays

$\beta$ -Lactoglobulin,  $\alpha$ -lactalbumin (negative control), both at 1 mg/mL, and Cyanine 3-labeled streptavidin at 2  $\mu\text{g}/\text{mL}$  concentration were patterned as described above with 14 spot replicates per protein. The chips were then incubated with anti bovine  $\beta$ -lactoglobulin antibody at varying concentrations in incubation buffer (Tris/HCl 0.05 M pH 7.6, NaCl 0.15 M, Tween 20 0.02%). For detection limit experiments, 6 chips were incubated for 2 h in dynamic conditions with anti- $\beta$ -lactoglobulin antibody at 10, 5, 2, 1, 0.5 and 0 ng/mL in incubation buffer (Tris/HCl 0.05 M pH 7.6, NaCl 0.15 M, Tween 20 0.02%) with 1% (w/v) BSA.

After the primary incubation, chips were washed with washing buffer (0.05 M Tris/HCl pH 9, 0.25 M NaCl, 0.05% v/v Tween 20) for 10 min on a lab shaker, rinsed with water, and incubated with the biotin-labeled secondary antibody (biotin-SP-conjugated AffiniPure Goat Anti-Rabbit IgG) at 1  $\mu\text{g}/\text{mL}$  in PBS for 1 h. Chips were then washed with PBS (pH 7.2) and water for 10 min each and then incubated for 2 h in dynamic conditions. Finally, the chips were incubated with 100  $\mu\text{L}$  of 15 nm SA-QDs in PBS. Chips were washed again with PBS for 10 min each then dip rinsed in water and dried under  $\text{N}_2$  gas.

Fluorescence was determined by a ProScanArray scanner (PerkinElmer, Boston, MA), and silicon chips were analyzed with a 633 nm laser at constant laser power and photomultiplier gain. The fluorescence intensities as well as the mass signals of 14 replicate spots were averaged.

IRIS images were acquired and fitted with Zoiray Acquire software. For each protein, signals from 6 to 14 replicate spots were averaged using MGrid spot finding software provided as a kind gift from the laboratory of Prof. Selim Ünlü.

In order to determine the limit of detection (LOD), the concentrations of antibody used were plotted versus the intensities of the corresponding detected fluorescence and mass signal, respectively. The values were fitted with a linear regression and the limit of detection (LOD) was taken to be three standard deviations above the blank signal, i.e. at zero analyte concentration. The corresponding analyte concentration was interpolated from the slope of the linear regression corresponding to this value. *T*-test and Anova were performed to confirm the linear regression.

### 3. Results and discussion

#### 3.1. QDs as a mass label

IRIS as an optical technique relies on surface accumulation of mass. In microarray experiments mass accumulation is limited by available binding sites, so it is desirable for each binding event to capture a large mass. Platt et al. [1] demonstrated the efficacy of streptavidin-conjugated QD-655 nanoparticles as a mass label in the detection of biomolecules using a commercial platform called Analight Bio200 (Farfield, UK) based on dual polarization interferometry (DPI), which also exploits differences in refractive index to detect accumulating layers of mass [14]. QD-655 nanoparticles are 8 nm  $\times$  15 nm ellipsoids in shape, but with their protein coating, their overall diameter is about 20 nm. QDs are promising labels for their dual action of having a large detectable mass as well as a fluorescent emission peak at 655 nm [15]. Their use in microarrays has been advocated to extend the dynamic range of the technique and increase assay sensitivity [16,17]. In this study, the use of SA-QDs as high-powered labels in an immunoassay microarray designed to study the interaction between  $\beta$ -lactoglobulin, a common milk allergen, and an anti  $\beta$ -lactoglobulin polyclonal antibody was explored. In particular, the efficacy of QDs to enhance sensitivity in interferometric reflectance imaging sensor (IRIS) techniques was studied and the advantages of this label when used with an interferometric detection platform as well as in fluorescence detection was investigated. We chose an immunoassay microarrays designed to detect antibodies against  $\beta$ -Lactoglobulin (Fig. 1), a common milk allergen.

Toward this end,  $\beta$ -lactoglobulin and  $\alpha$ -lactalbumin (control) were immobilized on Copoly (DMA–NAS–MAPS) coated silicon slides of 500 nm, and the chips were blocked as described in Section 2. IRIS images were taken after each step of the assay, as shown in Fig. 2. The spotted chip was first incubated with varying concentrations of the primary antibody (anti  $\beta$ -lactoglobulin IgG), then with a secondary antibody (biotinylated anti-IgG) and, lastly with SA-QDs. IRIS allows calculation of the mass increase due to the specific binding response of antibodies to the surface immobilized allergen  $\beta$ -lactoglobulin. The specificity was demonstrated by the absence of a mass increase signal on the  $\alpha$ -

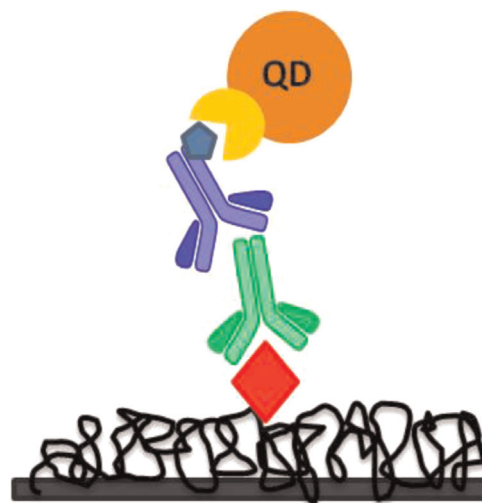


**Fig. 1.** The  $\beta$ -Lactoglobulin assay was carried out as follows.  $\beta$ -Lactoglobulin (red) is spotted on IRIS coated chip (black). Then, the chip was then incubated with the antibody against  $\beta$ -lactoglobulin (primary antibody, Ab 1°, green). The incubation of the Ab 1° was followed by an incubation with a secondary biotinylated antibody (Ab 2°, blue) and finally with streptavidin-conjugated QDs (SA-QDs, orange). (For interpretation of the references to color in this figure legend, the reader is referred to the web version of this article.)

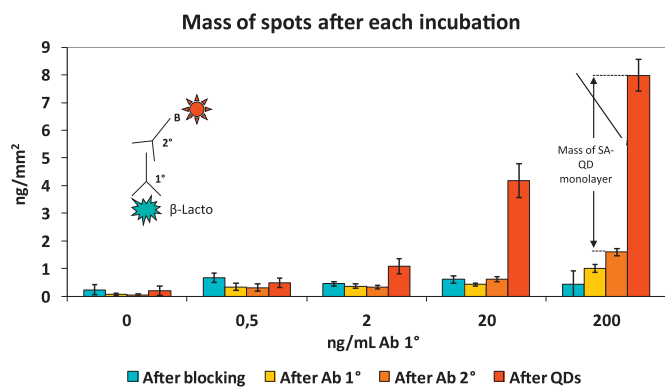


**Fig. 2.** Several concentrations of the primary antibody were tested. IRIS images were taken after each incubation step, and each addition of biomass was recorded. The mass of the SA-QD layer is taken as the difference between the mass after the secondary antibody and the mass after SA-QD incubation. Schematic representation of SA-QDs as mass tag (inset).

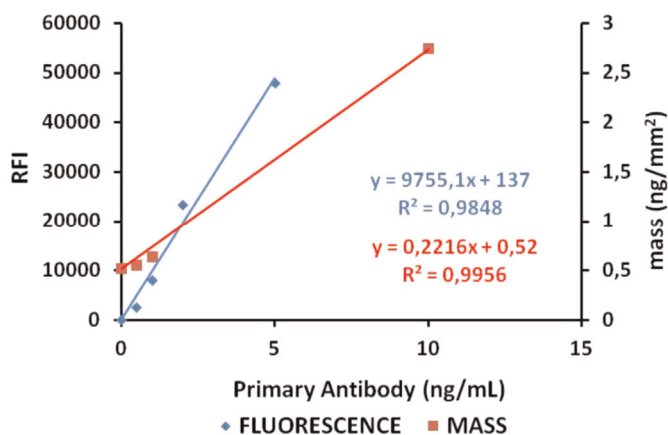


**Fig. 3.** Dose response curves of fluorescence and IRIS immunoassay used to extrapolate the LODs in mass and fluorescence detection modes.

lactalbumin antigen used as a control (not shown). In the experiment described in Fig. 2, the immobilized allergen was incubated with four concentrations of the same antibody between 0.5 ng/mL and 200 ng/mL control with no anti- $\beta$  lactoglobulin antibody (0 ng/mL) and. As shown in Fig. 2, the assay response was significantly amplified by the addition of the further component, SA-QDs, which bind to the biotinylated secondary IgG. For certain concentrations of target, a 4-fold increase in mass captured on the surface was obtained, compared to the negligible enhancement due to the biotinylated antibody. In our experimental conditions, the mass of the secondary antibody is not sufficient to provide the desired increase in sensitivity as clearly shown in Fig. 2. At 2 ng/mL of target concentration the mass increase becomes detectable only after the QD incubation.

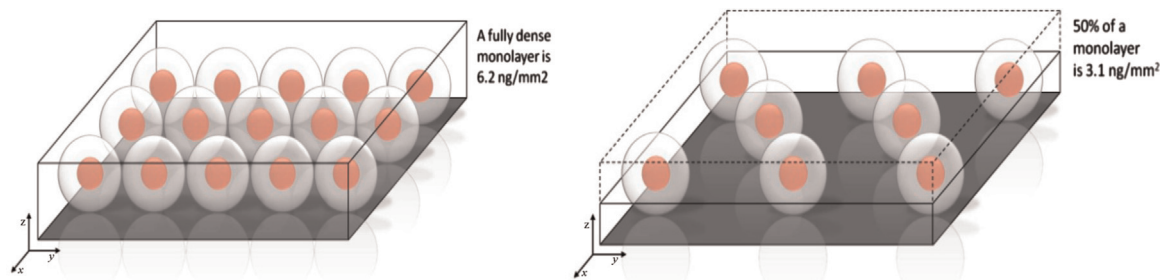


**Fig. 4.** At high concentrations of analyte, SA-QDs saturate the surface, creating a monolayer with a surface density of 6.2 ng/mm<sup>2</sup>. At lower concentrations, we can calculate a percentage of a monolayer.

This SA-QDs amplification step significantly reduces the LOD (limit of detection) of the primary antibody in this assay. An additional advantage of this approach is that QDs are fluorescent even when excited by a wavelength (633 nm) less than the ideal violet or ultraviolet wavelength. This confers a second to this type of label an additional advantage over other types of mass tag: the dual detection mode of these particles. Fig. 3 reports the calibrations curves of the studied immunoassay obtained with mass and fluorescence labels. Detected mass and fluorescence signals were plotted versus antibody concentration (10, 5, 2, 1, 0.5 and 0 ng/mL). The values were fitted with a linear regression and the limits of detection (LOD) were calculated. An LOD of 10.6 ng/mL was obtained in label-free conditions; this value was reduced to 0.81 ng/mL with SA-QD when their mass was measured and to 0.020 ng/mL when the fluorescence was detected.

The advantage in gained sensitivity of using QDs, both as mass or fluorescent tags, over only a secondary antibody is clearly demonstrated. In some situations, secondary antibodies alone are sufficient to enhance the mass signal. Ahn et al. [7] have been able to achieve high sensitivity in the detection of cytokines with only a secondary antibody as a mass tag. Because that work was conducted in real time in a flow cell, the authors were able to arrive at highly accurate measurements by accounting for mass loss due to desorption, normalizing each spot density to its original mass. In end point measurements that are the majority of microarray platform one cannot establish desorption kinetics, because measurements are carried at single points in time in dry conditions. Here we found that the QDs, acting as a larger detectable mass tag with a dual role as a fluorophore, allowed us to avoid elaborate desorption calculations, making the particles attractive for their reproducibility. In addition, by combining the two modes one can expand the dynamic range of this assay from 0.02 ng/mL to 10 ng/mL.

Platt et al. [1], in their similar assay using DPI, report that the surface density of a saturated monolayer of SA-QDs is 6.19 ng/mm<sup>2</sup> and a saturated monolayer of bare streptavidin is 2.30 ng/mm<sup>2</sup>. Since the nanoparticles do not deform, a monolayer with a surface density below that of the monolayer is an open structure, less dense than a contiguous monolayer across the surface. From these figures, we can calculate a percentage of a monolayer for each surface density measured. This concept is shown schematically in Fig. 4, where a 50% decrease in surface accumulation yields 50%, i.e. half of a SA-QD monolayer. From the mass accumulation due to QDs, a density was calculated for each concentration. At saturation concentration of target (200 ng/mL), a surface density of 6.40 ng/mm<sup>2</sup> was found, closely agreeing with Platt et al.'s measurement. It is worth noting that, although these methods are based on similar principals, DPI measures biomass accumulation in wet conditions, whereas the conditions reported here are the dry mass, which corroborates the two techniques.

#### 4. Conclusions

This paper exploits the dual role of QDs as both a mass tag and fluorophore. Platt et al. [1], also investigated these particles using another instrument based on an optical interferometric principle called Dual Polarization Interferometry (DPI), which simultaneously measures the mass and thickness of biomass accumulating on a surface [14]. In this case, Platt et al. measured the surface density of a fully saturated monolayer of SA-QDs of the same size to be 6.19 ng/mm<sup>2</sup>. In the case of IRIS, a measurement at every pixel is averaged across the entire spot to yield a surface density in units mass per area. From the reported density of the SA-QD layer and this surface density, we calculated a fraction of a monolayer. The results indicate that the maximum enhancement in mass that be reached in IRIS is 6.2 ng/mm<sup>2</sup>, a value that corresponds to the mass of a monolayer of SA-QDs.

#### Acknowledgments

This work was supported by POR-FESR Regione Lombardia & Cariplo Foundation (Project MINER ID 42708181, ID 2013-1738).

#### References

- [1] G.W. Platt, F. Damin, M.J. Swann, I. Metton, G. Skorski, M. Cretich, M. Chiari, Allergen immobilization and signal amplification by quantum dots for use in a biosensor assay of IgE in serum, *Biosens. Bioelectron.* 52 (2014) 82–88.
- [2] P.R. Srinivas, M. Verma, Y.M. Zhao, S. Srivastava, Proteomics for cancer biomarker discovery, *Clin. Chem.* 48 (2002) 1160–1169.
- [3] B. Schweitzer, S.F. Kingsmore, Measuring proteins on microarrays, *Curr. Opin. Biotechnol.* 13 (2002) 14–19.
- [4] D.A. Lashkari, J.L. DeRisi, J.H. McCusker, A.F. Namath, C. Gentile, S.Y. Hwang, P. O. Brown, R.W. Davis, Yeast microarrays for genome wide parallel genetic and gene expression analysis, *Proc. Natl. Acad. Sci. USA* 94 (1997) 13057–13062.
- [5] J.L. Arlett, E.B. Myers, M.L. Roukes, Comparative advantages of mechanical biosensors, *Nat. Nanotechnol.* 6 (2011) 203–215.
- [6] G.G. Daaboul, R.S. Vedula, S. Ahn, C. Lopez, A. Reddington, E. Özkumur, M. S. Ünlü, LED-based interferometric reflectance imaging sensor for quantitative dynamic monitoring of biomolecular interactions, *Biosens. Bioelectron.* 26 (2011) 2221–2227.
- [7] S. Ahn, D.S. Freedman, P. Massari, M. Cabodi, M.S. Ünlü, A. Mass-Tagging, Approach for enhanced sensitivity of dynamic cytokine detection using a label-free biosensor, *Langmuir* 29 (2013) 5369–5376.
- [8] R.S. Vedula, G.G. Daaboul, A. Reddington, E. Özkumur, D.A. Bergstein, M. S. Ünlü, Self-referencing substrates for optical interferometric biosensors, *J. Mod. Opt.* 57 (2010) 1564–1569.
- [9] G. Pirri, F. Damin, M. Chiari, E. Bontempi, L. Depero, Characterization of a polymeric adsorbed coating for DNA microarray glass slides, *Anal. Chem.* 76 (2004) 1352–1358.
- [10] V. Özkumur, J.W. Needham, D.A. Bergstein, R. Gonzalez, M. Cabodi, J. M. Gershoni, B.B. Goldberg, M.S. Ünlü, Label-free and dynamic detection of biomolecular interactions for high-throughput microarray applications, *PNAS* 105 (2008) 7988–7992.
- [11] E. Özkumur, A. Yalçın, M. Cretich, C.A. Lopez, D.A. Bergstein, B.B. Goldberg, M. Chiari, M.S. Ünlü, Quantification of DNA and protein adsorption by optical phase shift, *Biosens. Bioelectron.* 25 (2009) 167–172.
- [12] M. Cretich, G. Di Carlo, R. Longhi, C. Gotti, N. Spinella, S. Coffa, C. Galati, L. Renna, M. Chiari, High sensitivity protein assays on microarray silicon slides, *Anal. Chem.* 81 (2009) 5197–5203.
- [13] S. Ahn, P.S. Spuhler, M. Chiari, M. Cabodi, M.S. Ünlü, Quantification of surface etching by common buffers and implications on the accuracy of label-free biological assays, *Biosens. Bioelectron.* 36 (2012) 222–229.
- [14] M. Swann, L.L. Peel, S. Carrington, N.J. Freeman, Dual polarization interferometry: an analytical techniques to measure changes in protein structure in real time, to determine the stoichiometry of binding events, and to differentiate between specific and non specific interaction, *Anal. Biochem.* 329 (2004) 190–198.
- [15] (a) I.L. Medintz, H.T. Uyeda, E.R. Goldman, H. Mattoussi, Quantum dot bioconjugates for imaging, labeling and sensing, *Nat. Mater* 4 (2005) 435–446;  
(b) Whaley, P., Invitrogen company literature. (<http://tools.lifetechnologies.com/content/sfs/manuals/mp19000.pdf>), Page 1.
- [16] E. Morales-Narvaez, H. Monton, A. Fomicheva, A. Merkoci, Signal enhancement in antibody microarrays using quantum dots nanocrystals: application to potential Alzheimer's disease biomarker screening, *Anal. Chem.* 84 (2012) 6821–6827.
- [17] S.K.J. Ludwig, C. Tokarski, S.N. Lang, H.Y. Zhu LA. van Ginkel, A. Ozcan, M.W. F. Nielsen, Calling biomarkers in milk using a protein microarray on your smartphone, *PLOS One* 10 (2015), Article Number: e0134360.

# Click Chemistry Immobilization of Antibodies on Polymer Coated Gold Nanoparticles

Chiara Finetti,<sup>†,||</sup> Laura Sola,<sup>†</sup> Margherita Pezzullo, Davide Proserpi,<sup>‡</sup> Miriam Colombo,<sup>‡</sup> Benedetta Riva,<sup>‡</sup> Svetlana Avvakumova,<sup>‡</sup> Carlo Morasso,<sup>§</sup> Silvia Picciolini,<sup>§</sup> and Marcella Chiari<sup>\*,†</sup>

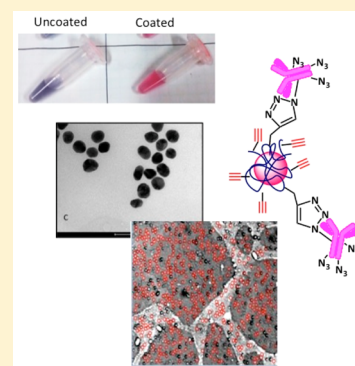
<sup>†</sup>Istituto di Chimica del Riconoscimento Molecolare, CNR, Via Mario Bianco 9, 20131 Milano, Italy

<sup>‡</sup>NanobioLab, Dipartimento di Biotecnologie e Bioscienze, Università degli Studi di Milano-Bicocca, Piazza della Scienza 2, 20126 Milano, Italy

<sup>§</sup>Laboratory of Nanomedicine and Clinical Biophotonics, Centre for Innovation and Technology Transfer, Fondazione Don Carlo Gnocchi ONLUS, 20121 Milano, Italy

<sup>||</sup>Dipartimento di Scienze Farmaceutiche, Università degli Studi di Milano, Via Mangiagalli 25, 20133 Milano, Italy

**ABSTRACT:** The goal of this work is to develop an innovative approach for the coating of gold nanoparticles (AuNPs) with a synthetic functional copolymer. This stable coating with a thickness of few nanometers provides, at the same time, stabilization and functionalization of the particles. The polymeric coating consists of a backbone of polydimethylacrylamide (DMA) functionalized with an alkyne monomer that allows the binding of azido modified molecules by Cu(I)-catalyzed azide/alkyne 1,3-dipolar cycloaddition (CuAAC, click chemistry). The thin polymer layer on the surface stabilizes the colloidal suspension whereas the alkyne functions pending from the backbone are available for the reaction with azido-modified proteins. The reactivity of the coating is demonstrated by immobilizing an azido modified anti-mouse IgG antibody on the particle surface. This approach for the covalent binding of antibody to a gold-NPs is applied to the development of gold labels in biosensing techniques.



## 1. INTRODUCTION

In the past decade, the use of nanoparticles in biomedical research has significantly expanded.<sup>1</sup> Their application in diagnosis and therapeutics, including, among others, chemical sensors,<sup>2</sup> magnetic resonance imaging contrast agents,<sup>3</sup> drug/gene delivery systems,<sup>4</sup> and cancer treatment,<sup>5</sup> have been extensively reviewed. The immobilization of proteins, DNA, or organic molecules on nanoparticles allows the formation of hybrid materials with interesting characteristics.<sup>6</sup>

Biomolecules can be immobilized on a nanoparticle either passively through hydrophobic or ionic interactions (physical adsorption), or covalently by a chemical reaction with an activated surface group. Covalent immobilization provides important advantages over physical adsorption, the most important being the higher stability of the bioconjugate.<sup>7</sup> Commonly used strategy for protein immobilization implies the activation of the nanoparticle with a chemical group that reacts with primary amines or carboxylic acids present on the surface of any protein. However, the coating of nanosized objects is sometimes difficult due to poor stability of the nanoparticles in suspension during and after the coating process. A convenient way to functionalize the surface of nanoparticles employs functional polymers that, in addition to providing anchoring points to the surface, stabilizing the colloidal suspension.

The purpose of this study is to demonstrate that a synthetic functional copolymer, copoly(DMA-PMA-MAPS), recently introduced by our group<sup>8</sup> represents a convenient method to

provide stabilization and functionalization of nanoparticles by a robust and user-friendly one-step procedure. The polymer belongs to a family of copolymers which have been successfully employed to produce various surface coatings. The key of their success in forming stable coatings of few nanometers is the combination, on the same chain, of two monomers: *N,N*-dimethylacrylamide (DMA) and  $\gamma$ -methacryloxypropyltrimethoxysilane (MAPS). Furthermore, a number of functional monomers can be introduced by random radical polymerization into this basic structure to confer to the coating specific binding properties. In the version presented here, one of such functional monomers bears an alkyne functionality that promotes the binding of azido modified molecules by Cu(I)-catalyzed azide/alkyne 1,3-dipolar cycloaddition (CuAAC, click chemistry). In this work, the polymer was used for the modification of gold nanoparticles surrounded by a thin silicon oxide layer. The polymer coating stabilizes the colloidal suspension, whereas the alkyne functions pending from the backbone are available for the reaction with azido modified proteins. To demonstrate the functionality of the modified nanoparticles, an anti-mouse IgG antibody, modified with azido groups, was covalently linked to the nanoparticle surface. This surface modification approach is of general applicability in

**Received:** March 29, 2016

**Revised:** June 30, 2016

**Published:** July 1, 2016

different fields spanning from the functionalization of antibodies, whose use is widespread from clinical diagnosis or disease treatment,<sup>9,10</sup> to the development of labels in biosensing techniques<sup>11,12</sup>

## 2. MATERIALS AND METHODS

**2.1. Materials.** Phosphate-buffered saline (PBS), tris-(hydroxymethyl)aminomethane (Tris), HCl, sodium hydroxide (NaOH), ethanolamine, *N,N*-dimethylformamide (DMF), sodium chloride (NaCl), sodium phosphate (Na phosphate), bovine serum albumin (BSA), copper(II) sulfate pentahydrate (CuSO<sub>4</sub>), L-ascorbic acid (AAC), tris(3-hydroxypropyltriazolymethyl)amine (THPTA), agarose low gelling temperature, ethylenediaminetetraacetic acid (EDTA), boric acid, Tween20, ammonium sulfate ((NH<sub>4</sub>)<sub>2</sub>SO<sub>4</sub>), *N,N*-dimethylacrylamide (DMA),  $\gamma$ -methacryloxypropyltrimethoxysilane (MAPS), azoisobutyronitrile (AIBN), and goat anti-mouse polyclonal IgG (whole molecule) antibody were all purchased from Sigma-Aldrich (St. Louis, MO). *N*-Acryloyloxy-succinimide (NAS) and 3-trimethylsilyl-prop-2-ynyl methacrylate (protected PMA) were synthesized as reported elsewhere.<sup>13,14</sup> Rabbit anti-bovine beta-lactalbumin was purchased from Jackson Immuno Research (West-Grove, PA); purified anti-mouse CD63 was purchased from BioLegend; azido-PEG<sub>8</sub>-*N*-hydroxysuccinimide (N<sub>3</sub>-PEG-NHS) ester was purchased from Jena Bioscience (Jena, Germany). Silicon oxide chips with a 100 nm thermal oxide layer were bought from Silicon Valley Microelectronics (Santa Clara, CA); 30 kDa centrifugal filters were purchased from Amicon.

**2.2. Synthesis of Poly(DMA-NAS-MAPS) and Poly(DMA-PMA-MAPS).** The polymers, poly(DMA-NAS-MAPS) and poly(DMA-PMA-MAPS), were synthesized as reported in refs 15 and 8. The copolymers were obtained by free radical polymerization of DMA and MAPS with NAS or protected PMA. The total monomer concentration in the feed was 20% w/v, while the molar fraction of the three monomers was, in both polymer, 97%, 1% for DMA and MAPS and 2% for NAS or protected PMA.

Briefly, for the synthesis of poly(DMA-NAS-MAPS), the three monomers were diluted in anhydrous tetrahydrofuran, together with a thermocatalyst (AIBN); the reaction flask was heated to 65 °C to initiate the polymerization process, and after 2 h the polymer was precipitated in petroleum ether and collected as a white powder.

The synthetic process of poly(DMA-PMA-MAPS) required two separate steps: (a) the synthesis of polymer which contains 3-trimethylsilyl-prop-2-ynyl methacrylate, a protected form of prop-2-ynyl prop-2-enoate (PMA) and (b) removal of the protective trimethylsilyl groups. The first step was similar to that used for the synthesis of poly(DMA-NAS-MAPS), while the deprotection was achieved by dissolving the polymer in a basic solution containing potassium carbonate. After a 3 h reaction, the polymer was dialyzed and lyophilized.<sup>8</sup>

**2.3. Synthesis of Silica Gold Nanoparticles.** A solution (200 mL) of tetrachloroauric(III) acid (0.01% w/v) in water was heated to reflux. Next, 700  $\mu$ L of trisodium citrate (2%) was added to the solution and left under stirring at 100 °C for a few minutes until the appearance of a deep red color indicated the formation of the nanoparticles. The suspension was left under stirring at 100 °C for further 20 min and then slowly cooled down to room temperature.

A very thin layer of silicon oxide was grown on the surface according to the protocol described by Li et al.<sup>16</sup> A volume of 30 mL of a gold nanoparticles suspension was mixed with 400  $\mu$ L of APTEs (1 mM) and left under stirring. After 15 min, 3.2 mL of a sodium silicate solution (0.54% w/v) acidified until the pH was <11 was added to the gold nanoparticles. The suspension was left under stirring for 3 min at room temperature and for 35 min in a water bath at 70 °C.

To stop the reaction, the gold nanoparticles were moved in a bath of water at 4 °C. At last, gold nanoparticles were centrifuged at 3000g for 20 min at 15 °C and resuspended in water.

**2.4. Nanoparticles Coating.** Poly(DMA-PMA-MAPS) was dissolved in DI water to a final concentration of 1%; to this solution, a suspension of AuNPs (0.1 mg/mL) was added and the mixture was

gently stirred for 1 h in the dark on a shaker. To remove the polymer excess, the AuNPs suspension was washed two times with DI water by centrifugation (10 min at 7000 rpm). After the second washing cycle, the supernatant was discarded and replaced by sodium phosphate buffer (pH 7.4, 50 mM) and the suspension stored at 4 °C.

**2.5. Antibody Derivatization.** An anti-mouse IgG antibody was dissolved in PBS to a final concentration of 5 mg/mL; to this solution, azido-PEG<sub>8</sub>-NHS ester was added to a final concentration of 0.5 mM. The mixture was stirred for 2 h at room temperature. Once the reaction was completed, the azido modified IgG was washed three times by centrifugation on 30 kDa centrifugal filters (10 min at 7000 rpm) to remove residual traces of unreacted azido ester.

**2.6. Functionalization of Gold Nanoparticles.** Polymer coated AuNPs were spun down and resuspended in Na phosphate buffer (50 mM pH 7.4); to this suspension, the azido modified antibody (1 mg/mL), CuSO<sub>4</sub> (100  $\mu$ M), THPTA (400  $\mu$ M), and ascorbic acid (6.25 mM) were added. The mixture was then stirred overnight. The antibody-AuNPs suspension was washed three times by centrifugation (10 min at 7000 rpm) to remove residual traces of unreacted azido antibody. To prove that the covalent binding was promoted by the CuSO<sub>4</sub>/THPTA/AAC assisted click reaction, the same procedure was performed without addition of the click catalysts. In this case, the anti-mouse antibody could only be adsorbed on the polymer coated AuNPs.

**2.7. Nanoparticles Characterization.** **2.7.1. Morphology.** Transmission electron microscopy (TEM) images of AuNPs were obtained on a "FEI Tecnai G" Spirit BioTWIN microscope (Hillsboro, OR) operating at 120 kV. The samples were prepared by evaporating a drop of nanoparticles onto carbon-coated copper grid (200 mesh) and allowing it to dry on the air. Nanoparticles were sonicated prior to analysis. The histograms of the particle size distribution and the average particle diameter were obtained by measuring about 150–200 particles by using Measure IT Olympus Software.

**2.7.2. Particle Size and  $\zeta$ -Potential Analyses.** Dynamic light scattering (DLS) measurements were performed at 173° with a Zetasizer Nano ZS ZEN3600 from Malvern Instruments Ltd. (Worcestershire, UK) working at 4 mW of a He–Ne laser ( $\lambda$  = 632.8 nm). A disposable cuvette with 1 cm optical path length was used for the measurements. The samples were prepared by dilution with Milli-Q water containing 1 mM citrate. Each sample was allowed to equilibrate for 30 s prior to starting measurement. The measurements were performed at 25 °C. The calculations of hydrodynamic diameter were performed using Mie scattering theory, considering absolute viscosity and refractive index values of the medium to be 0.8872 cP and 1.334, respectively. The results are reported in Intensity.  $\zeta$ -Potential measurements were elaborated on the same instrument by electrophoretic light scattering;  $\zeta$ -potential values were automatically calculated from electrophoretic mobility using Zetasizer Software (Malvern Instruments Ltd., Malvern, UK). A viscosity of 0.8872 cP, a dielectric constant of 78.5, and a Henry function of 1.5 were used for the calculations. All measurements were performed in triplicate, and the average values were calculated.

**2.7.3. Gel Electrophoresis.** In order to characterize the particles after each derivatization step, 100  $\mu$ L of functionalized and nonfunctionalized gold NPs were loaded on a 0.7% agarose gel in 0.5× Tris-borate-EDTA buffer pH 8.8 (TBE: 67 mM tris-(hydroxymethyl)aminomethane, 37 mM boric acid, 1.6 mM EDTA). The separation was run for 60 min at a constant voltage of 100 V.

**2.7.4. Optical Properties.** The optical properties of AuNPs, polymer coated AuNPs, and AuNPs functionalized with antibody were assessed by UV–visible spectrometry (spectrophotometer VP-650, Jasco). Before collecting UV–vis spectra (400–700 nm), all sample solutions were sonicated for few seconds in order to minimize aggregation. The plasmon band shift due to the polymer layers deposited on AuNPs and to the subsequent antibody linking was evaluated keeping in consideration the maximum absorption peak of bare AuNPs is 525 nm. The concentration of the AuNPs suspension is expressed in optical density (OD), measured at the maximum absorption peak (525 nm).

**2.8. Bioassay.** **2.8.1. Glass Slide Coating Procedure.** The coating procedure of a glass slide with poly(DMA-NAS-MAPS) is described elsewhere.<sup>17</sup> Briefly, silicon slides bearing a 100 nm oxide layer were activated by an oxygen plasma treatment and then immersed in a 0.8 M ammonium sulfate solution containing poly(DMA-NAS-MAPS) at 1% w/v concentration for 30 min. The chips were rinsed with water, dried with a nitrogen stream, and finally cured under vacuum at 80 °C.

**2.8.2. Microarray Experiments.** To demonstrate the binding between the antibody and AuNPs, an anti-CD63 mouse antibody, and an anti- $\beta$ -lactoglobulin rabbit antibody (negative control) were patterned on two silicon chips coated with poly(DMA-NAS-MAPS) by means of a SciFlexArrayer S5 spotter from Scienion (Berlin, Germany). Both, the mouse anti-CD63 capture antibody (20 replicates) and the rabbit anti- $\beta$ -lactoglobulin antibody (5 replicates), dissolved in PBS, were spotted at a concentration of 1 mg/mL. In the experimental conditions used, the volume of the spotted drop was 400 pL. The chips were placed in a humid chamber immediately after the spotting and stored overnight at room temperature. After the immobilization, the residual active esters on the chip were blocked by immersing the chips in a solution of 50 mM ethanolamine in 0.1 M TRIS/HCl, pH 9, for 1 h at room temperature; the chips were then rinsed with DI water and dried with a nitrogen stream.

One chip was incubated overnight in a humid chamber with a AuNP-labeled anti-mouse antibody (OD = 0.05) in PBS in static incubation conditions. The chip was washed with the washing buffer (Tris/HCl 50 mM pH 9, NaCl 0.25 M, Tween 20 0.05% v/v) for 10 min under stirring and finally rinsed with Milli-Q water. A second chip was incubated with the same anti-mouse antibody reacted with AuNPs in the absence of the click catalyst. Both chips were imaged with the SP-IRIS instrument to detect individual particles of AuNPs bound to the capture surface antibody.

**2.8.3. Optical Detection.** The Single Particle Interferometric Reflectance Imaging System (SP-IRIS) instrument (NexGen Arrays) is a prototype instrument for the detection of individual particles on surface. The instrument uses one discrete LED wavelength (525 nm) to illuminate the sensor's surface using a high magnification objective to detect and count nanoparticles of known materials located on the SiO<sub>2</sub> surface; the principles are thoroughly illustrated elsewhere.<sup>17,18</sup> Briefly, this modality of IRIS enhances the contrast of a single nanoparticle on a bilayered substrate by interfering the scattered field produced by the nanoparticle on the substrate surface with the reflected field generated by the buried Si-SiO<sub>2</sub> interface of the IRIS chip. The CCD camera senses the individual nanoparticles on the IRIS chip as point objects, which are processed to extract size information.

### 3. RESULTS AND DISCUSSION

**3.1. Coating Procedure.** The attachment of proteins, and other biomolecules, to nanoparticles is of critical interest in the development of medical products and biosensors using nanoparticles. Different strategies of surface GNP modification and functionalization are reviewed in.<sup>19</sup> Among the various approaches, thiolated PEGs, modified with a carboxyl group and activated via EDC/NHS reaction, are widely used for the immobilization of proteins. The coating strategy, based on the adsorption of these polymers, is simple and effective in suppressing particles aggregation, however it suffers from some drawbacks. The procedure requires two steps: polymer adsorption and activation of carboxyl group to provide *N*-hydroxysuccinimide (NHS) ester terminal group. PEG chains have only one functional group per chain, making it difficult to achieve a high immobilization density. Most importantly, the coupling reaction is often performed in buffered aqueous solutions near physiological pH (pH 6–9). Under these conditions, the hydrolysis of the ester group competes with the amidization process, potentially degrading the efficiency of the coupling chemistry.<sup>20</sup> Last but not least, the reaction between active esters and amino groups is not regiospecific and does not

allow the controlled and oriented immobilization of the protein. To overcome most of these drawbacks while maintaining the robustness and easy operation of the coating process, a polymeric coating that allows immobilization of chemically modified proteins by click chemistry is used in this work. Recently, we have introduced a copolymer with an alkyne functional monomer. This copolymer made of *N,N*-dimethylacrylamide (DMA), [3-(methacryloyl-oxy) propyl] trimethoxysilyl (MAPS), and prop-2-ynyl prop-2-enoate (PMA) was designed to bind azido modified biomolecules via copper(I) catalyzed Huisgen 1,3-dipolar cycloaddition (CuAAC, click chemistry) and was successfully used for the immobilization of glycans in microarray.<sup>8</sup>

Our group has a long tradition in the development of DMA based copolymers. The first polymer of the series, the poly(DMA-NAS-MAPS), copolymerized with *N*-acryloyloxy succinimide (NAS) and MAPS, was introduced to form, in few minutes, a stable functional coating on microarray glass slides.<sup>15</sup> This polymer is extremely versatile, and a wide number of functional monomers can be added to the basic structure of poly(DMA-MAPS) by random radical polymerization, in order to confer to it specific properties; examples of various monomers that have been used include active ester, oxyrane,<sup>21</sup> and ionizable groups.<sup>22</sup> The members of this polymer family adhere to a variety of different materials including glass, silicon oxide,<sup>17</sup> gold,<sup>23</sup> PDMS, and thermoplastics<sup>24</sup> by a combination of a chemi- and physisorption mechanism. Thanks to the MAPS monomer that promotes silanol condensation with hydroxyl groups introduced onto the surface by an oxygen plasma treatment, the weak noncovalent interactions between the AuNPs surface and the DMA segment are reinforced leading to the formation of an extremely stable nanometric layer. We demonstrate that one of the members of this polymer family, the poly(DMA-PMA-MAPS), coats 45 nm gold nanoparticles, prepared according to the commonly used citrate methods developed by Turkevich et al.<sup>25</sup> and Frens.<sup>26</sup> In order to promote a better adhesion of the polymer, a very thin layer of silica has been grown on top of gold. The silica shell has been obtained thanks to the condensation of sodium silicate on the surface of gold nanoparticles previously treated with APTES as described by Li et al.<sup>16</sup> A careful study of the reaction parameters (time, pH and temperature) was required to keep the silica layer very thin to not compromise the optical properties of the nanoparticles. We selected an alkyne polymer to allow bioconjugation via click chemistry to particles that are stabilized and functionalized by a single-step process. Although the polymer is not new, its use in the context of nanoparticles poses new challenges. Given the mechanism of coating formation, which entails an adsorption step followed by silanol condensation, the polymer adsorption is usually performed in highly concentrated ammonium sulfate solution to reduce polymer solubility and force its interaction with the surface. The use of salts is incompatible with nanoparticles which would aggregate and precipitate during the coating. Also the condensation step at high temperature, which normally increases the binding strength of the polymer film, is incompatible with a colloidal suspension. We demonstrate in this work that the functional PDMA copolymer has a strong affinity to the inorganic core and quickly and effectively replaces the original citrate molecules. Even when the coating process is carried out in suboptimal conditions the polymer chains wrap around the particles, forming a film dense enough to confer high stability to the colloidal solution.

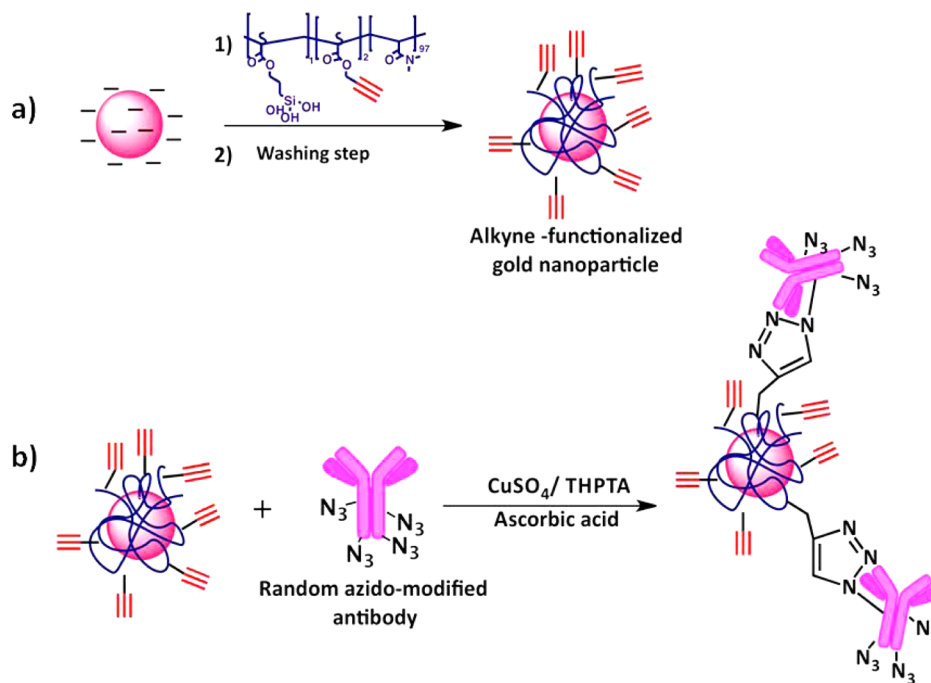


**Figure 1.** Schematic representation of the surface modification of AuNPs with a functional polymer and consequent derivatization of the polymer with an azido modified antibody.

The derivatization process is depicted in Figure 1. In the first step, AuNPs with a silica shell are coated with the linear polymer copoly(DMA-PMA-MAPS) simply by adding the copolymer to the aqueous particle suspension, as detailed in section 5 (Figure 1a). The presence of alkyne functionalities on the external polymer layer allows the covalent binding of azido-PEG modified IgGs on the AuNPs surface via CuAAC reaction. The CuAAC process is an example of a click chemistry reaction that is easy to perform, giving rise to the intended products in very high yields with little or no byproducts: it works well under many conditions, and is not affected by the presence of functional groups other than those being connected to each other. Since the conjugation requires the presence on the biomolecules of functional groups that are not naturally present, the process works well for DNA or peptides that are easily functionalized during their synthesis. For proteins, the introduction of clickable functionalities is more challenging. An enzymatic approach, commercialized under the trade name of Site-Click by Thermo-Fisher, allows simple site-selective attachment of an azido moiety to the heavy chain N-linked glycans—far from the antigen-binding domain. If used in conjunction with our alkyne modified polymer, this approach provides an effective means of orienting antibodies on the surface of gold nanoparticles. In this work, the amino groups of an anti-mouse IgG antibody are reacted with an Azido-PEG<sub>8</sub>-NHS ester, in order to introduce clickable functionalities on the antibody, as schematically reported in Figure 1. The molar ratio of PEG-ester and antibody determines the degree of substitution. Even though we cannot claim that the immobilization is oriented as the reaction between PEG-succinimidyl ester and protein amino groups is not regioselective, still the process is advantageous over other types of immobilization since it allows to control the degree of azide insertion thus limiting the point of contact between the protein and the surface. In the limiting case, the immobilization may involve only one azido group, leaving the antibody

accessible to the antigen in solution. This would never be possible with standard NHS chemistry.

The successful formation of the coating was confirmed by subjecting to electrophoresis samples of AuNPs, at each stage of the functionalization, in an agarose gel. Uncoated gold nanoparticles (Figure 2a, lane 1) have a different mobility

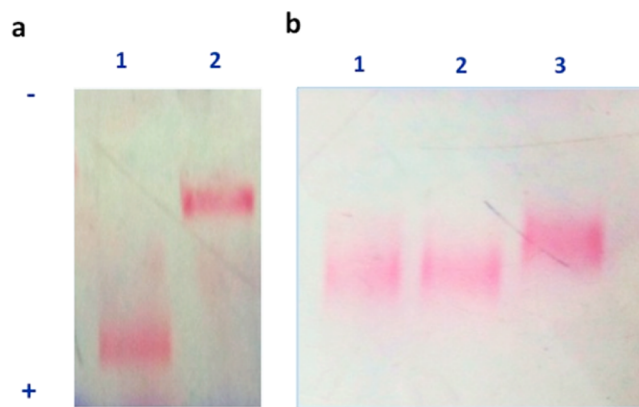


**Figure 2.** Agarose gel electrophoresis of gold nanoparticles: (a) Lane 1, uncoated nanoparticles; lane 2, polymer-modified gold nanoparticles. (b) Lane 1, polymer coated NPs (no conjugation); lane 2, polymer coated NPs treated with antibody in the absence of THPTA/CuSO<sub>4</sub> and ascorbic acid (no conjugation); lane 3, polymer coated particles treated with antibody, THPTA/CuSO<sub>4</sub>, and ascorbic acid (conjugation).

compared to polymer-modified particles (lane 2). The higher electrophoretic mobility of uncoated gold NPs is due to the high density of negative charges on their surface. On the contrary, the charges on the coated particles are shielded by the polymer layer, causing a significant mobility reduction. The antibody functionalization of AuNPs was confirmed by the difference of electrophoretic profile of polymer coated NPs

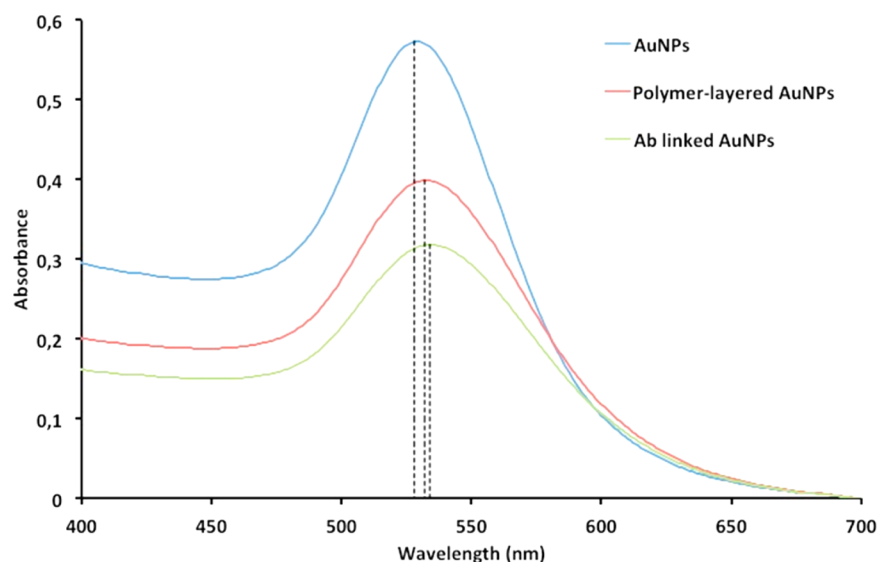


**Figure 3.** Plasmon band shift due to the polymer and antibody layers deposited on AuNPs.

(Figure 2b, lane 1) and antibody coated NPs (Figure 2b, lane 3). The covalent binding of the antibody to the surface was confirmed by the electrophoretic behavior of AuNPs incubated with the antibody in the absence of the click chemistry reagents (THPTA/CuSO<sub>4</sub> and ascorbic acid). In this case, as shown in Figure 2b, lane 2, no mobility shift was observed, indicating that no immobilization of antibody was obtained and confirming that the shift observed in lane 3 is not due to nonspecific antibody adsorption onto the nanoparticle surface.

**3.2. Surface Characterization.** The surface modification was monitored after each step with a number of state-of-the-art analytical techniques including UV spectroscopy, dynamic light scattering (DLS), zeta potential measurements, transmission electron microscopy (TEM), as well as with functional tests on particles behavior.

**3.2.1. UV Spectroscopy, Zeta Potential, and Dynamic Light Scattering Measurements.** In the UV spectra of Figure 3, surface plasmon band shifts resulting from the formation of copolymer and antibody layers are shown. The deposition of each layer on the surface causes small changes in the local refractive index of the material that induce shifts of the plasmon band.

Furthermore,  $\zeta$ -potential measurements of coated AuNPs confirmed the presence of the polymer layer. As shown in Table 1, a marked change of  $\zeta$ -potential was found for particles coated with the copolymer compared to that of naked ones.

The AuNPs hydrodynamic diameter was measured after polymer and antibody functionalization by means of DLS analyses (Table 1). Also in this case, significant changes in the hydrodynamic diameter were detected after each modification step, demonstrating the success of the functionalization.

**Table 1. Hydrodynamic Diameter and  $\zeta$ -Potential Values for Uncoated, Polymer Coated, and Ab-Linked AuNPs**

sample	hydrodynamic diameter (nm)	PDI	$\zeta$ -potential (mV)
uncoated AuNPs	47.02 ± 13.52	0.083	-25.1 ± 2.40
polymer coated AuNPs	131.1 ± 34.93	0.071	-17.6 ± 0.35
ab linked AuNPs	146.75 ± 87.92	0.403	-14.1 ± 2.26

**3.2.2. Stability of the Nanoparticles.** The transmission electron microscopy (TEM) images reported in Figure 4 show that the nanoparticle quality and morphology is maintained after each step of the functionalization: nanoparticles stability is not compromised either by polymer coating or by the binding of the antibody.

We have investigated the stability of Ab coated AuNPs and the results show that the coating is essential to protect nanoparticles from the pH dependent aggregation. The stabilization is due to steric stabilization rather than electrostatic repulsion. In fact, when AuNPs are uncoated, a marked color change, indicative of aggregation, is clearly detectable at high and low pH values as well as at high salt concentration. On the contrary, when the polymer is grafted on AuNPs surface, the pH and ionic strength do not affect the suspension stability and the original color is maintained (Figure 5). The protection induced by the polymer coating makes AuNPs more suitable for biological applications, where high ionic strength and pH changes are currently present.

**3.2.3. Application of Antibody Labeled Nanoparticles in Biosensing.** The new functionalization approach described here might find application in several research fields including therapeutic drug delivery, diagnostics and photodynamic therapy. However, we focused mostly on application in biosensing. In this work, we have tested the activity of gold immobilized antibodies in an innovative biosensing technology, called Interferometric Reflectance Imaging System (IRIS). This technology is based on well-known principles of light interference, and it was previously applied for rapid detection of large virus particles.<sup>17</sup> This platform is also suitable for detection of single molecules in a sandwich assay format. The sensor surface, coated with a functional polymer and arrayed with specific detection probes (i.e antibodies, aptamers, and nucleic acid oligos), captures one or more targets from the solution. The surface immobilized target is then recognized by a secondary probe labeled with a gold nanoparticle of 40 nm. Gold nanoparticle labels with their high optical signal are individually counted by the SP-IRIS. A successful outcome of an SP-IRIS experiment not only indicates that the particles are properly functionalized with active antibodies but also that they are not aggregated. In particular, we have immobilized on

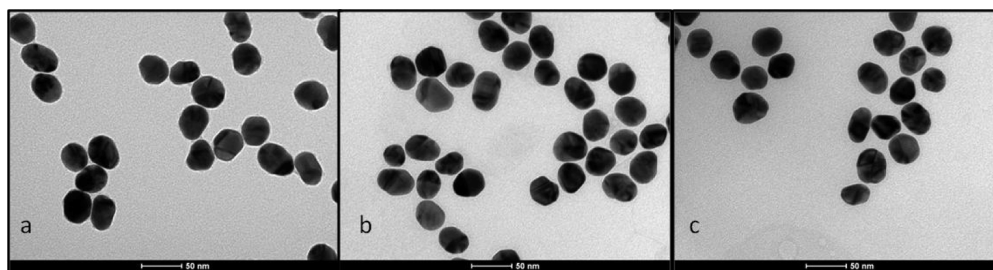


**Figure 4.** Transmission electron microscopy of individual AuNPs: (a) before, (b) after coating with copoly(DMA-PMA-MAPS), and (c) after immobilization of IgG.

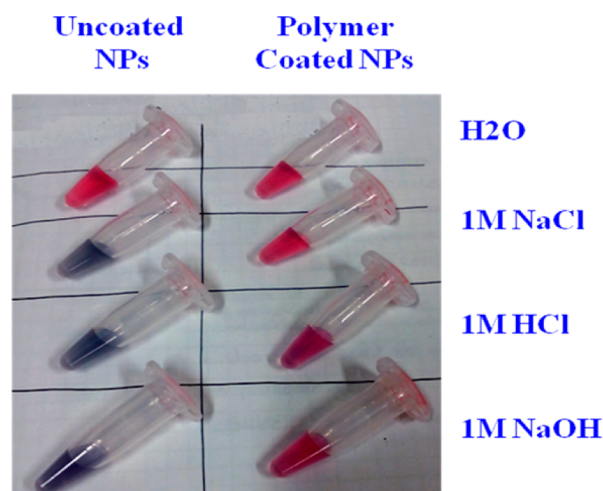


**Figure 5.** Uncoated and polymer coated AuNPs were treated with NaCl, HCl or NaOH. In these conditions, uncoated NPs are very unstable and aggregate, causing a red to blue color change (left column). Nanoparticles with the poly(DMA-PMA-MAPS) coating are stable also in harsh conditions (right column).

the surface an anti-CD63 antibody, which was specifically recognized by an AuNP labeled anti-mouse polyclonal IgG. In Figure 6a (top right), the gold particles counted by the SP-IRIS software are shown as red circles. The histogram in Figure 6b reports the number of particles per  $\text{mm}^2$  found in different sensing experiments. In the absence of THPTA/ $\text{CuSO}_4$  and ascorbic acid during AuNPs functionalization, the click chemistry reaction does not occur and, as a consequence, the secondary antibody is not labeled. In fact, the density of particles detected by SP-IRIS in this case (bottom right) is close to that of the control experiment where a noncorrelated antibody (images on the right) is spotted. These experiments confirm that the particles are detected on the surface only when the conjugation reaction is carried out in the presence of click chemistry catalysts demonstrating the covalent character of the conjugation.

#### 4. CONCLUSIONS

In this study, we described a simple and reliable method to coat AuNPs with a copolymer which stabilizes the colloidal suspension of nanoparticles in several conditions and facilitates the coupling with antibodies by means of a Cu(I)-catalyzed click reaction. The nanoparticles coating has been characterized by different complementary techniques. A gold coated anti-CD63 antibody was used as label in an innovative bioassay based on single particle counting. The successful binding of the anti-mouse-IgG antibody shows that the labeled antibody is

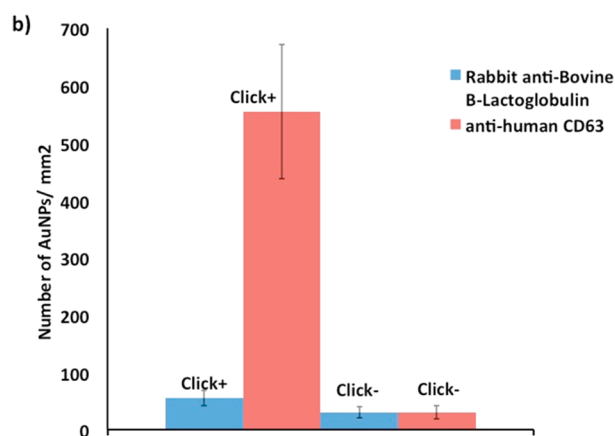
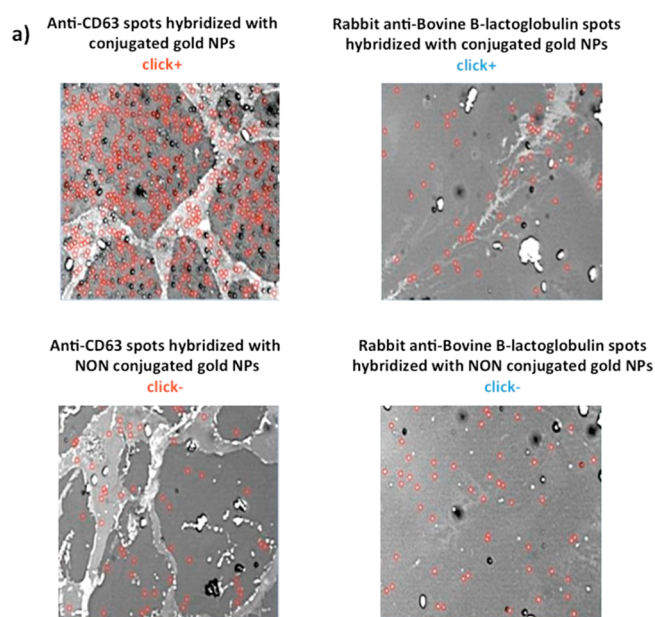


**Figure 6.** (a) SP-IRIS images of surfaces functionalized with different antibodies, incubated with an anti-mouse antibody conjugated with gold nanoparticles in the presence (+) or in the absence (–) of THPTA/ $\text{CuSO}_4$  and ascorbic acid. (b) SP-IRIS response (mean  $\pm$  SD;  $n = 20$  of particle number/ $\text{mm}^2$ ) of anti-mouse IgG linked or adsorbed on polymer coated AuNPs.

fully functional. The proposed method can be used to label antibodies in a number of different applications.

#### AUTHOR INFORMATION

##### Corresponding Author

\*E-mail: [marcella.chiari@icrm.cnr.it](mailto:marcella.chiari@icrm.cnr.it). Phone +390228500035.

## Notes

The authors declare no competing financial interest.

## ACKNOWLEDGMENTS

This work was partially supported by Regione Lombardia & Fondazione Cariplo through POR-FESR, project MINER (ID 46875467).

## REFERENCES

- (1) Bawarski, W. E.; Chidlow, E.; Bharali, D. J.; Mousa, S. A. Emerging Nanopharmaceuticals. *Nanomedicine* **2008**, *4*, 273–282.
- (2) Howes, P. D.; Chandrawati, R.; Stevens, M. M. Bionanotechnology. Colloidal Nanoparticles as Advanced Biological Sensors. *Science* **2014**, *346* (6205), 1247390.
- (3) Artemov, D.; Mori, N.; Okollie, B.; Bhujwalla, Z. M. MR Molecular Imaging of the Her-2/neu Receptor in Breast Cancer Cells Using Targeted Iron Oxide Nanoparticles. *Magn. Reson. Med.* **2003**, *49*, 403–408.
- (4) Forbes, Z. G.; Yellen, B. B.; Barbee, K. A.; Friedman, G. An Approach to Targeted Drug Delivery Based on Uniform Magnetic Fields. *IEEE Trans. Magn.* **2003**, *39*, 3372.
- (5) Fortina, P.; Kricka, L. J.; Graves, D. J.; Park, J.; Hyslop, T.; Tam, F.; Halas, N.; Surrey, S.; Waldman, S. A. Applications of Nanoparticles to Diagnostics and Therapeutics in Colorectal Cancer. *Trends Biotechnol.* **2007**, *25* (4), 145–152.
- (6) Katz, E.; Willner, I. Integrated Nanoparticle-Biomolecule Hybrid Systems: Synthesis, Properties, and Applications. *Angew. Chem., Int. Ed.* **2004**, *43* (45), 6042–6108.
- (7) Wilson, D. S.; Nock, S. Functional Protein Microarrays. *Curr. Opin. Chem. Biol.* **2002**, *6*, 81–85.
- (8) Zilio, C.; Bernardi, A.; Palmioli, A.; Salina, M.; Tagliabue, G.; Buscaglia, M.; Consonni, R.; Chiari, M. New “clickable” Polymeric Coating for Glycan Microarrays. *Sens. Actuators, B* **2015**, *215*, 412–420.
- (9) Maggon, K. Monoclonal Antibody “Gold Rush. *Curr. Med. Chem.* **2007**, *14*, 1978–1987.
- (10) Baptista, P.; Pereira, E.; Eaton, P.; Doria, G.; Miranda, A.; Gomes, I.; Quaresma, P.; Franco, R. Gold Nanoparticles for the Development of Clinical Diagnosis Methods. *Anal. Bioanal. Chem.* **2008**, *391*, 943–950.
- (11) Buijs, J.; Lichtenbelt, J. W. T.; Norde, W.; Lyklema, J. Adsorption of Monoclonal IgGs and Their F(ab')<sub>2</sub> Fragments onto Polymeric Surfaces. *Colloids Surf., B* **1995**, *5*, 11–23.
- (12) Radwan, S. H.; Azzazy, H. M. E. Gold Nanoparticles for Molecular Diagnostics. *Expert Rev. Mol. Diagn.* **2009**, *9*, 511–524.
- (13) Mammen, M.; Dahmann, G.; Whitesides, G. M. Effective Inhibitors of Hemagglutination by Influenza Virus Synthesized from Polymers Having Active Ester Groups. Insight into Mechanism of Inhibition. *J. Med. Chem.* **1995**, *38* (21), 4179–4190.
- (14) Ladmiral, V.; Mantovani, G.; Clarkson, G. J.; Cauet, S.; Irwin, J. L.; Haddleton, D. M. Synthesis of Neoglycopolymers by a Combination of “Click Chemistry” and Living Radical Polymerization. *J. Am. Chem. Soc.* **2006**, *128* (14), 4823–4830.
- (15) Pirri, G.; Damin, F.; Chiari, M.; Bontempi, E.; Depero, L. E. Characterization of A Polymeric Adsorbed Coating for DNA Microarray Glass Slides. *Anal. Chem.* **2004**, *76* (5), 1352–1358.
- (16) Li, J. F.; Tian, X. D.; Li, S. B.; Anema, J. R.; Yang, Z. L.; Ding, Y.; Wu, Y. F.; Zeng, Y. M.; Chen, Q. Z.; Ren, B.; Wang, Z. L.; Tian, Z. Q. Surface Analysis Using Shell-Isolated Nanoparticle-Enhanced Raman Spectroscopy. *Nat. Protoc.* **2013**, *8* (1), 52–65.
- (17) Daaboul, G. G.; Yurt, A.; Zhang, X.; Hwang, G. M.; Goldberg, B. B.; Ünlü, M. S. High-Throughput Detection and Sizing of Individual Low-Index Nanoparticles and Viruses for Pathogen Identification. *Nano Lett.* **2010**, *10*, 4727–4731.
- (18) Yurt, A.; Daaboul, G. G.; Connor, J. H.; Goldberg, B. B.; Selim Ünlü, M. Single Nanoparticle Detectors for Biological Applications. *Nanoscale* **2012**, *4*, 715.
- (19) Sperl, R. A.; Parak, W. J. Surface Modification, Functionalization and Bioconjugation of Colloidal Inorganic Nanoparticles. *Philos. Trans. R. Soc., A* **2010**, *368* (1915), 1333–1383.
- (20) Lim, C. Y.; Owens, N. A.; Wampler, R. D.; Ying, Y.; Granger, J. H.; Porter, M. D.; Takahashi, M.; Shimazu, K. Succinimidyl Ester Surface Chemistry: Implications of the Competition between Aminolysis and Hydrolysis on Covalent Protein Immobilization. *Langmuir* **2014**, *30* (43), 12868–12878.
- (21) Sola, L.; Chiari, M. Modulation of Electroosmotic Flow in Capillary Electrophoresis Using Functional Polymer Coatings. *J. Chromatogr. A* **2012**, *1270*, 324–329.
- (22) Sola, L.; Chiari, M. Tuning Capillary Surface Properties by Charged Polymeric Coatings. *J. Chromatogr. A* **2015**, *1414*, 173–181.
- (23) Petti, D.; Torti, A.; Damin, F.; Sola, L.; Rusnati, M.; Albisetti, E.; Bugatti, A.; Bertacco, R.; Chiari, M. Functionalization of Gold Surfaces with copoly(DMA-NAS-MAPS) by Dip Coating: Surface Characterization and Hybridization Tests. *Sens. Actuators, B* **2014**, *190*, 234–242.
- (24) Zilio, C.; Sola, L.; Damin, F.; Faggioni, L.; Chiari, M. Universal Hydrophilic Coating of Thermoplastic Polymers Currently Used in Microfluidics. *Biomed. Microdevices* **2014**, *16* (1), 107–114.
- (25) Turkevich, J.; Stevenson, P. C.; Hillier, J. A Study of the Nucleation and Growth Processes in the Synthesis of Colloidal Gold. *Discuss. Faraday Soc.* **1951**, *11*, 55.
- (26) Frens, G. Controlled Nucleation for the Regulation of the Particle Size in Monodisperse Gold Suspensions. *Nature, Phys. Sci.* **1973**, *241* (105), 20–22.